3D Imaging in Endodontics

A New Era in Diagnosis and Treatment

Mohamed Fayad
Bradford R. Johnson
Editors

Springer

Highdent laboratory

مرکز تخصصی پروتزهای دندانی

های دنت

طراحی و ساخت انواع پروتزهای دندانی بویژه ایمپلنت

برگزار کننده دوره های آموزشی تخصصی وجامع دندانسازی و...

با ما همراه باشید...

WWW.HIGHDENTlab.com

3D Imaging in Endodontics

Mohamed Fayad • Bradford R. Johnson
Editors

3D Imaging in Endodontics

A New Era in Diagnosis and Treatment

Springer

Editors
Mohamed Fayad
University of Illinois at Chicago
Chicago, Illinois
USA

Bradford R. Johnson
University of Illinois at Chicago
Chicago, Illinois
USA

ISBN 978-3-319-31464-8 ISBN 978-3-319-31466-2 (eBook)
DOI 10.1007/978-3-319-31466-2

Library of Congress Control Number: 2016942098

Printed on acid-free paper

This Springer imprint is published by Springer Nature
The registered company is Springer International Publishing AG Switzerland

Preface and Acknowledgments

New radiographic imaging systems have recently become available for use in dentistry and have transformed the way we diagnose and treat oral disease. Among these new imaging technologies are medical computed tomography (CT), cone beam computed tomography (CBCT), and magnetic resonance imaging (MRI). These imaging technologies benefit from advancements in other technologies such as high-speed computer processors and sophisticated software.

The subject of this book, CBCT, allows for the precise visualization and evaluation of teeth and surrounding structures. CBCT has great potential to become an essential diagnostic and treatment planning tool in the modern endodontic practice. However, like any new technology, we need to carefully consider appropriate indications for use, to maximize patient benefit and minimize potential risk.

Chapter 1 provides a basic understanding of CBCT from an oral radiologist's perspective. This includes imaging basics, CBCT image acquisition, rendering, viewing, and manipulation.

Chapter 2 addresses utilization of CBCT in the diagnosis and management of periapical pathosis, diagnosis of pain, cracked teeth and vertical root fractures, internal and external resorptive defects, and traumatic injuries. These are all challenging diagnostic problems that are frequently encountered in clinical practice.

Chapter 3 addresses the impact of CBCT technology on endodontic nonsurgical and surgical treatment planning. This chapter will review and compare the relative value of preoperative 2D periapical radiographs and CBCT in the decision-making process.

Chapter 4 focuses on the value of CBCT in understanding tooth anatomy prior to nonsurgical and surgical root canal therapy. The primary objective of root canal therapy is the treatment and/or prevention of apical periodontitis. A successful result requires that the operator understands and appreciates the internal anatomy and morphology of the root canal system.

Chapter 5 addresses the clinical applications of CBCT in nonsurgical endodontic retreatment. This chapter will provide an overview of how to analyze cases by viewing selected fields, coupled with a 3D-rendered perspective of the jaw segment which enables the clinician to perform a "virtual analysis" of the case prior to treatment.

Chapter 6 reviews the different applications of CBCT in diagnosis, treatment planning, and long-term outcome evaluation of periradicular surgery. In this

chapter, cases will be presented to demonstrate the value of CBCT in presurgical assessment, case selection, and treatment planning in endodontic microsurgery, including the use of CBCT to identify and manage teeth in close proximity to important anatomical structures.

Chapter 7 reviews the application of CBCT for detection, classification, localization, and differentiation of internal and external resorptive defects.

We would like to offer our sincere thanks to the contributors and co-authors of this book who have generously shared their time, expertise, and case materials.

Dr. Mohamed Fayad: I would like to dedicate this book to my father Dr. Ibrahim M. Fayad who was an instrumental figure in my life. I would like to thank my parents for all the guidance, support, and the opportunities they gave me to be who I am.

I would like to thank my wife Marilia and my children Nagi, Lila, and Zachary for their love and support they gave me over the years.

Brad Johnson thanks his wife, Liza, and three adult children, Jason, Chris, and Leah, for their support and encouragement over many years.

Both Mohamed and Brad would like to acknowledge and thank their fellow faculty, mentors, and students in the University of Illinois at Chicago Department of Endodontics, who have encouraged us and given us the time and resources to pursue this project.

Chicago, IL, USA

Mohamed Fayad
Bradford R. Johnson

Contents

Principles of Cone Beam Computed Tomography

1

Sanjay M. Mallya

1.1 Introduction

Radiographic examination is an essential component of the overall endodontic diagnosis and treatment planning process. For decades, periapical and panoramic imaging has provided this radiological information. Although these imaging modalities provide valuable information, they are limited by their inherent 2-dimensional nature. Superimpositions from adjacent structures can potentially mask anatomical variations or pathological lesions. The introduction of cone beam computed tomography (CBCT) in dentistry provided us with a diagnostic tool that overcomes this basic limitation of conventional radiographic techniques. Over the last 15 years, CBCT technology has grown rapidly to allow clinicians to acquire high-resolution images of the teeth and craniofacial bones, using relatively low radiation doses. CBCT imaging has several applications in dento-maxillofacial diagnosis including endodontic diagnosis and treatment planning, implant treatment planning, surgical and orthodontic treatment planning, evaluation of the paranasal sinuses, temporomandibular joints, intraosseous pathology, impacted teeth, etc. Clinicians who use CBCT imaging should be familiar with the basic principles of CBCT image acquisition. This chapter provides the reader with basic principles of computed tomography, and the relevant hardware and software components of a CBCT system, with a focus on their impact on image quality. It discusses radiation dose considerations in using this x-ray-based imaging modality, approaches to communicate radiation risks to the patient, and methods to minimize patient radiation exposure.

S.M. Mallya
Los Angeles, CA, USA
e-mail: smallya@ucla.edu

M. Fayad, B.R. Johnson (eds.), *3D Imaging in Endodontics*,
DOI 10.1007/978-3-319-31466-2_1

1.1.1 What Is Computed Tomography?

Computed tomography (CT) is a radiographic modality used to generate cross-sectional images of the body. In this technique an x-ray source and a radiation detector array rotate around the patient, sequentially making two-dimensional projections at hundreds of different angles along the rotational arc. At each angle, the projection represents a map of x-ray attenuation by objects along the path of the x-ray beam. Sophisticated mathematical algorithms are applied to this attenuation data to spatially reconstruct the locations of the structures within the imaged volume. Both multi-detector CT (MDCT), an imaging modality widely used in medicine, and dental CBCT use these basic physical and computational processes. Although MDCT and CBCT share similarities in the principles of image formation, there are important differences between these two technologies.

- In MDCT the x-ray source is collimated to a narrow fan-shaped beam. In contrast, in CBCT imaging, the radiation source is collimated to a cone or pyramidical beam that fully encompasses the region to be imaged. Due to the narrowly collimated beam in MDCT, the amount of scatter radiation that reaches the detector is lower, and thus, the contrast-to-noise ratio (CNR) of MDCT is higher than that of CBCT. Thus, MDCT provides much better contrast resolution than CBCT.
- The detectors used in CBCT enable a spatial resolution that is typically higher than that of MDCT images. Thus, CBCT is better suited for high-resolution diagnostic tasks, such as evaluation of teeth and periapical structures.
- An important difference between MDCT and CBCT is the radiation dose—typically MDCT protocols use much higher doses of radiation than that used for CBCT imaging.

1.2 CBCT Image Acquisition

Current dental CBCT units offer users with a variety of features that range from differences in design and footprint, technical specifications of the detectors, selectable fields of view (FOV), and the extent of the source-detector rotation during image acquisition. Many of these technical parameters influence the image quality as well as the radiation dose to the patient [1]. Clinicians should be familiar with these parameters to design patient-specific CBCT examinations that provide adequate diagnostic information, with the least possible radiation exposure to the patient.

1.2.1 X-Ray Source and Exposure Settings

As with all x-ray-based imaging modalities, an x-ray tube serves as the source of x-radiation. X-ray tubes used in dental CBCT units may have either stationary or

rotating anodes. Most dental CBCT units will allow the operator to adjust the x-ray tube voltage (peak kilovoltage, kVp) and/or the tube current (milliamperes, mA). Similar to other radiographic techniques, the kVp and mA should ideally be adjusted for each patient, taking into account the density of the structures to be imaged and the patient's size. This is important to make a diagnostically optimal radiographic image, while minimizing the patient's radiation exposure. Some CBCT units have fixed exposure parameters that cannot be modulated by the operator. Some CBCT units, for example, the NewTom 5G unit, use an automatic exposure control mechanism that customizes the mA on a patient-specific basis. Such features provide the ability to automatically maintain low radiation dose exposure during CBCT imaging.

1.2.2 Image Detector

During the rotation of the x-ray source-detector assembly, the image detector captures x-ray photons to produce a two-dimensional x-ray transmission image or a basis projection. The basis projections acquired at the different rotational angles constitute the raw data for CT reconstruction. Most currently available dental CBCT units use a flat-panel detector (FPD). In this digital detector, a phosphor screen of gadolinium oxysulfide or cesium iodide converts x-ray photons to light photons, which are then detected using a thin-film transistor array [2]. Another detector type used in dental CBCT units is the image intensifier. In this detector system, x-rays strike a fluorescent screen to produce visible light photons, which are converted by a photocathode into electrons to amplify the initial signal [3]. The electrons are accelerated and strike an output phosphor screen to produce a visible image that is captured by a CCD camera. The assembly of these various components makes the design of an image intensifier bulky. FPD provides significant advantages over image intensifier-based units. FPD is more sensitive to x-rays. Compared with image intensifiers, FPD generates images with higher contrast resolution and spatial resolution. Another disadvantage of image intensifier-based systems is the decreasing image quality over the lifetime of the unit as the phosphor screen ages.

1.2.3 Number of Basis Projections

As described above, the first step in CBCT imaging is acquisition of two-dimensional images during rotation of the x-ray source-detector assembly around the patient. The number of basis projections acquired differs between CBCT units and depends on the frame rate, the time of rotation, and the extent of the rotational arc. In general, a CBCT scan acquired with a higher number of basis projections produces an image with a higher spatial and contrast resolution. However, with a higher number of projections, the radiation dose to the patient is higher. Many CBCT

manufacturers have incorporated preset scan modes that alter the number of basis projections to either enhance image quality or lower the patient radiation dose.

1.2.3.1 Extent of the Rotation Arc (180° vs. 360°)

In many CBCT units, the basis projections are acquired during an entire 360° rotation around the patient's head. For some CBCT units, the x-ray source-detector assembly rotates around the patient for approximately 180°. In some versatile units, the operator can set the length of the rotation arc (180° vs. 360°). When a partial arc is used, fewer basis projections are acquired. This has the advantage of not only reducing the patient's radiation exposure but also decreasing scan time, thereby decreasing artifacts due to patient motion. The partial arc imaging yields a CBCT scan with lower spatial and contrast resolution [4]. However, this reduction in image quality does not always compromise the diagnostic utility of the scan. For example, the accuracy of linear measurements made for implant treatment planning is not compromised by a 180° scan mode [5]. In contrast, partial arc imaging decreases the visibility of pulp canals and increases the number of false positives when detecting vertical fractures [6]. It should be emphasized that the effect of partial arc rotation on the diagnostic efficacy is strongly dependent on the diagnostic task at hand and remains to be fully studied.

1.2.3.2 "Quick Scan" and "Fast Scan" Imaging Modes

Some CBCT units incorporate a selectable scan mode that is designed to substantially lower radiation doses. This is accomplished by requiring fewer basis projections, thereby decreasing both the scan time and the radiation dose. With these modes, the contrast-to-noise ratio is considerably lower and, thus, decreases image quality. Despite this decreased image quality, some diagnostic assessments can be adequately made, such as evaluation of root parallelism during orthodontic treatment. However, it is likely that the decreased image quality will impact certain high-resolution diagnostic tasks such as evaluation of the periodontal ligament space, root resorption, and subtle areas of bony erosion. The impact of the scan modes on the accuracy of such diagnostic tasks remains to be critically evaluated.

1.2.3.3 "High-Resolution" Scan Mode

Many CBCT units feature a selectable "high-resolution" scan mode, where the number of basis projections is increased to yield images with a higher resolution. Clinicians should use caution when using this scan mode. Importantly, such scan protocols require longer scan times and expose the patient to higher doses of radiation. The radiation exposure with this scan mode is approximately twofold higher than that in the standard scan mode. For some units the scan time with a high-resolution scan mode is as long as 40 s, thereby increasing the potential for patient motion during scan acquisition. Clinicians should be aware that a high-resolution scan mode does not always yield an image that is diagnostically superior. Standard resolution acquisitions (typically the manufacturer's default setting) are adequate

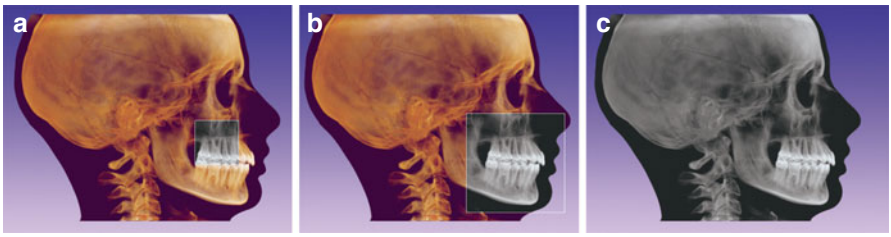

Fig. 1.1 Schematic representations of the approximate anatomical coverage provided by different fields of view of a CBCT unit. (**a**) Small FOV, (**b**) medium FOV, and (**c**) large FOV

for most diagnostic tasks and the use of a high-resolution scan mode may not add any additional diagnostically useful information.

1.2.3.4 Field of View (FOV)

The FOV is a critical parameter that must be optimized for individual CBCT imaging examinations. When selecting a specific FOV, the CBCT unit collimates the x-ray beam to a predetermined image volume size. Although there are no formal definitions, the FOV is categorized as large (maximum dimension greater than 15 cm), medium (approximately 8–15 cm), or limited/small (maximum dimension less than 8 cm diameter, Fig. 1.1). As a general rule, the smallest FOV that provides adequate anatomic coverage for the diagnostic task at hand should be selected. In some basic CBCT units, the FOV is fixed and cannot be changed by the operator. Most CBCT units are versatile, and the FOV can be selected through a range of limited to medium to full FOV coverage. Selection of the appropriate FOV is particularly important—it determines the extent of anatomic coverage and also impacts image quality and patient radiation dose. For most endodontic diagnostic tasks, a limited FOV scan will likely provide adequate anatomic coverage.

In almost all units, a smaller FOV scan is acquired using a smaller voxel size, thus yielding images with higher spatial resolution. Furthermore, a smaller FOV also reduces scattered radiation, decreasing image noise and contributing to improved image quality. This is particularly important given that many of the endodontic diagnostic applications require higher resolution, for example, evaluation of the periodontal ligament space and lamina dura. Selection of the appropriate FOV should be made considering not only the anatomic coverage but also the image resolution required for the diagnostic task. For example, in a patient with atypical odontogenic pain, all the teeth in a selected quadrant may need to be imaged to rule out an odontogenic cause for the pain. Such patients may possibly benefit from two adjacent limited FOV scans, rather than a single medium or large FOV scan. In this scenario, the lower image resolution with the medium/large FOV scan is likely to compromise critical evaluation of the apical periodontal structures.

1.2.3.5 Voxel Size

The smallest three-dimensional data unit on a CBCT image volume is the voxel. The voxel size depends on the size of the detector pixels, which in current CBCT systems ranges from 0.07 to 0.4 mm. In general, a CBCT scan acquired with a smaller pixel size produces an image with higher spatial resolution. Nevertheless, the detector pixel size is not the only determinant of image resolution. Several other machine-specific parameters such as CT reconstruction algorithms and image processing "filters" modulate the signal-to-noise ratio and image resolution.

In many CBCT units, the voxel size is predetermined for a specific FOV. Typically, smaller FOVs are imaged using a smaller pixel size. In some CBCT units, the operator can manipulate the pixel size for a given FOV. For these protocols, imaging at a smaller pixel size is accomplished by either increasing the number of basis projections or increasing the radiation exposure factors. Clinicians must be aware that these protocols will deliver a higher patient radiation exposure, compared with the standard protocol.

1.3 CBCT Artifacts

The CBCT imaging process starts by making sequential two-dimensional projections along hundreds of angles around the area of interest. Each projection represents a map of x-ray attenuation by objects along the path of the x-ray beam. Mathematical algorithms are applied to this attenuation data to spatially reconstruct the locations of the structures within the imaged volume. There are several factors that influence the accuracy of the reconstructed data. These include discretization of the imaged object, geometrical projection issues, detector noise, and the assumptions in mathematical modeling. Discrepancies between the reconstructed data and the physical state of the actual object may be evident in the image and are termed artifacts. There are several different artifacts described in CT imaging. These include beam hardening artifacts, photon starvation artifacts, cupping artifacts, and partial volume averaging. Schulze et al. [7] provide an excellent description of the physical basis for and the appearances of these various artifacts.

Beam hardening artifacts are noted around dense bony structures and around radiopaque restorations and endodontic filling materials. Clinicians who use CBCT must be aware of the appearances of such artifacts and not confuse them with pathological changes. For example, metallic restorations will result in dark bands and streaks (Figs. 1.2, 1.3, and 1.4). The dark bands which extend to the region around the restoration and to the crowns of the adjacent teeth may be interpreted as caries. When these bands appear on the crowns or roots of adjacent teeth, they may be misinterpreted as caries or root fractures. Likewise, the region around metallic posts and gutta-percha yields dark bands, which may compromise the ability to detect fractures or resorption of the adjacent root structure.

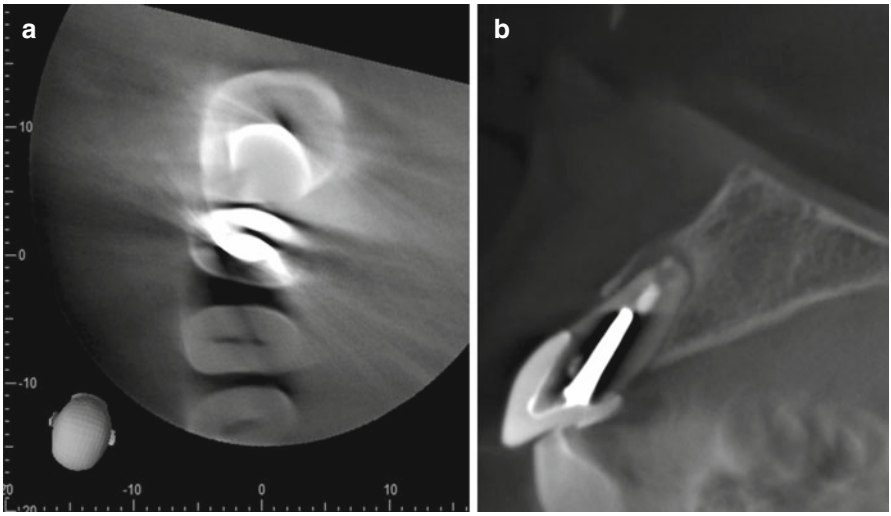

Fig. 1.2 (**a**) Axial slice demonstrating metallic restorations in the second premolar and first molar teeth. Note the radiating pattern of dark bands and streaks. Note how linear artifacts are evident on the root of the adjacent first premolar. (**b**) Sagittal CBCT section through the maxillary central incisor. Note the dark zone around the metallic post

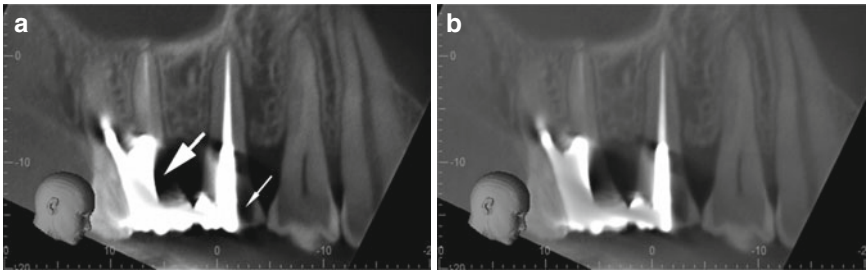

Fig. 1.3 (**a**) Sagittal slice demonstrating metallic restorations in the second premolar and first molar teeth. Note the dark bands on the molar crown (*big arrow*) and the crown of the second premolar (*small arrow*). (**b**) Same section as in panel A. Note how adjusting the density and contrast allows for better visualization of the crown and root surfaces in the regions of the dark bands, further confirming their artifactual nature

1.4 Radiation Dose Considerations

The basic premise of diagnostic radiographic imaging is that the benefits from the examination far outweigh the risks associated with ionizing radiation exposure. The principles of radiation risk and safety that apply to conventional periapical and panoramic radiography also apply to CBCT imaging. CBCT users should be familiar with the doses delivered by various CBCT imaging protocols, the risks

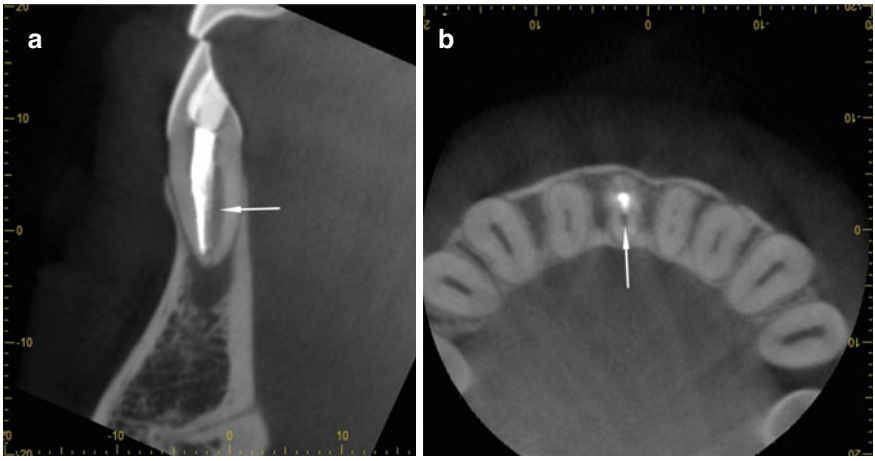

Fig. 1.4 (**a**) Sagittal and (**b**) axial slices through the mandibular anterior region. Note the presence of an unfilled canal in the central incisor (*arrows*). This additional canal should not be confused with artifacts from the radiopaque gutta-percha

associated with radiation exposure in this range, and the methods to minimize patient radiation exposure.

1.4.1 Risks from Diagnostic Radiation

X-rays are ionizing radiations. Interaction of x-ray photons with biological molecules, predominantly water, produce reactive radicals that cause ionization and potential biological damage which may manifest as radiation-induced effects. The effects depend on the specific tissues exposed and the dose and dose rate of radiation. There are two types of radiation-induced effects—deterministic and stochastic.

1.4.1.1 Deterministic Effects

Deterministic effects occur when the radiation absorption in a tissue or organ exceeds a threshold level. This threshold is dependent on the specific tissue or organ that is exposed. When the radiation dose is higher than the threshold level, the effect is induced. Further increasing the radiation dose increases the severity of this effect. Examples of deterministic effects include radiation-induced cataracts, decrease in salivary gland function, osteoradionecrosis, and radiation-induced fibrosis. Radiation doses from dento-maxillofacial radiographic imaging are orders of magnitude lower than the threshold levels for deterministic effects in the various tissues exposed. Thus, the risk of inducing such deterministic effects by maxillofacial imaging is essentially zero.

1.4.1.2 Stochastic Effects

In contrast to deterministic effects, there is no minimum threshold dose for causing stochastic effects. This implies that even low levels of radiation exposure could

trigger stochastic effects. The probability of causing stochastic effects decreases with decreasing radiation dose, and this is the basis of dose minimization in diagnostic radiology. Examples of stochastic effects include radiation-induced neoplasia and heritable effects of radiation.

The principal risk from diagnostic maxillofacial CBCT imaging is the risk of radiation-induced neoplasia. The association between radiation exposure and cancer has been firmly established both by animal studies and by studies of human populations that were exposed to ionizing radiation, either intentionally or by accident. These studies have demonstrated some basic concepts that have important implications in radiation safety and protection:

- There is a latent period between the exposure and the occurrence of cancer, which may vary from a few years to several decades.
- Certain tissues are more sensitive to the carcinogenic effects of x-radiation. In the craniofacial region these include the thyroid gland, the red bone marrow, the brain, the salivary glands, and the parathyroid glands.
- Age at the time of exposure is a strong modifier of radiation-induced cancer risk. It is estimated that radiation-induced cancer risks are at least three- to fivefold higher in children [8]. This is attributed to increased organ sensitivity to radiation-induced carcinogenesis and longer life expectancy, which allows time for neoplastic development.

It is currently accepted that ionizing radiation-caused DNA damage is the initial trigger for radiation-induced cancer. Even a single photon can produce radicals to cause DNA damage, and this explains the stochastic nature of radiation-induced neoplasia. The number of radicals produced increases with dose, and thus, the likelihood and extent of radiation-induced DNA damage increases with radiation dose. The current model for estimating radiation-induced cancer risks is based on the linear no-threshold hypothesis (LNT), which assumes that the risk of radiation-induced cancer increases linearly with increasing radiation dose. This hypothesis is based on scientific data that demonstrate such a linear dose response, although at doses typically above 100 milliGray (mGy). The nature of the risk at doses in the order of a few tens of mGy has not been experimentally established. Nevertheless, the assumptions of the LNT model have not been disproven, and thus, regulatory agencies continue to use this model to conservatively estimate risk and develop policy guidelines on radiation exposure to occupationally exposed individuals and members of the public.

1.4.2 Estimating Radiation Doses from Dento-maxillofacial CBCT

Radiation doses from diagnostic radiographic examinations are conveyed as effective dose—a radiation unit that estimates the detriment from radiation exposure. Effective dose is typically determined using dosimeters placed at multiple sites in a tissue-equivalent anthropomorphic phantom to measure absorbed doses at specific organ sites. The measured organ and tissue doses are then used to calculate the effective dose from an examination. The effective dose, expressed in the units of sieverts (Sv), accounts for the differential sensitivity of tissues to radiation-induced

Table 1.1 Relative radiation levels (RRL) designations

Relative radiation level		Effective dose range (μSv)	
		Adult	Pediatric
☢	Minimal	<100	<30
☢☢	Low	100–1000	30–300
☢☢☢	Medium	1000–10,000	300–3000

Adapted from Cody et al. [9]

stochastic effects. Thus, effective doses are used to convey the relative magnitude of radiation detriment from different radiographic examinations. It can be used to compare risks from different radiographic procedures and imaging protocols and provide an estimate of the dose that a patient is likely to receive from a specific radiographic procedure. However, effective dose does not consider the influences of age, gender, and other patient-specific risk modulators such as genetics thus, it cannot be used to accurately specify risks to an individual patient.

Dentists must be familiar with the effective doses from various maxillofacial radiographic examinations, including CBCT. To provide healthcare professionals with guidance on dose categorization, the American College of Radiology developed relative radiation level (RRL) designations, an ordinal scale of radiation doses from diagnostic procedures [9]. This scale allows clinicians to consider various procedural doses in the context of relative dose and risk. Table 1.1 lists the RRL designations for radiation dose ranges for maxillofacial radiographic examinations. Given the increased sensitivity of children to radiation-induced cancer, the limits of the dose ranges are lower for pediatric radiographic examinations.

The adult and child effective doses from common maxillofacial radiographic examinations are shown in Fig. 1.5. Notably, the reported dose ranges for CBCT examinations are broad. This variation represents differences between CBCT units, different imaging protocols, and exposure settings—all parameters that influence the radiation dose delivered to the patient, as described in Sect. 2 of this chapter. In adult patients, doses from conventional and CBCT examinations are in the minimal and low RRL ranges. Importantly, doses from the same procedures in pediatric patients extend considerably through the low RRL and potentially into the medium RRL range. This implies that the risks from the same procedures are higher in children and underscores the need to carefully consider risk-benefit determinations and to "child-size" exposure settings.

1.4.3 Conveying Radiation Risks to Patients

Often, patients ask their dentist questions regarding the dose and risks associated with imaging examinations. One approach is to convey these to patients in the context of its equivalent of background radiation exposure. In our daily lives, we are continuously exposed to radiation from natural sources. These include space radiation (cosmic rays and solar energetic particles), terrestrial radiation from radioactive elements in rocks and soil, and internal radiation from radionuclides that are ingested through food and water or inhaled through air. The average

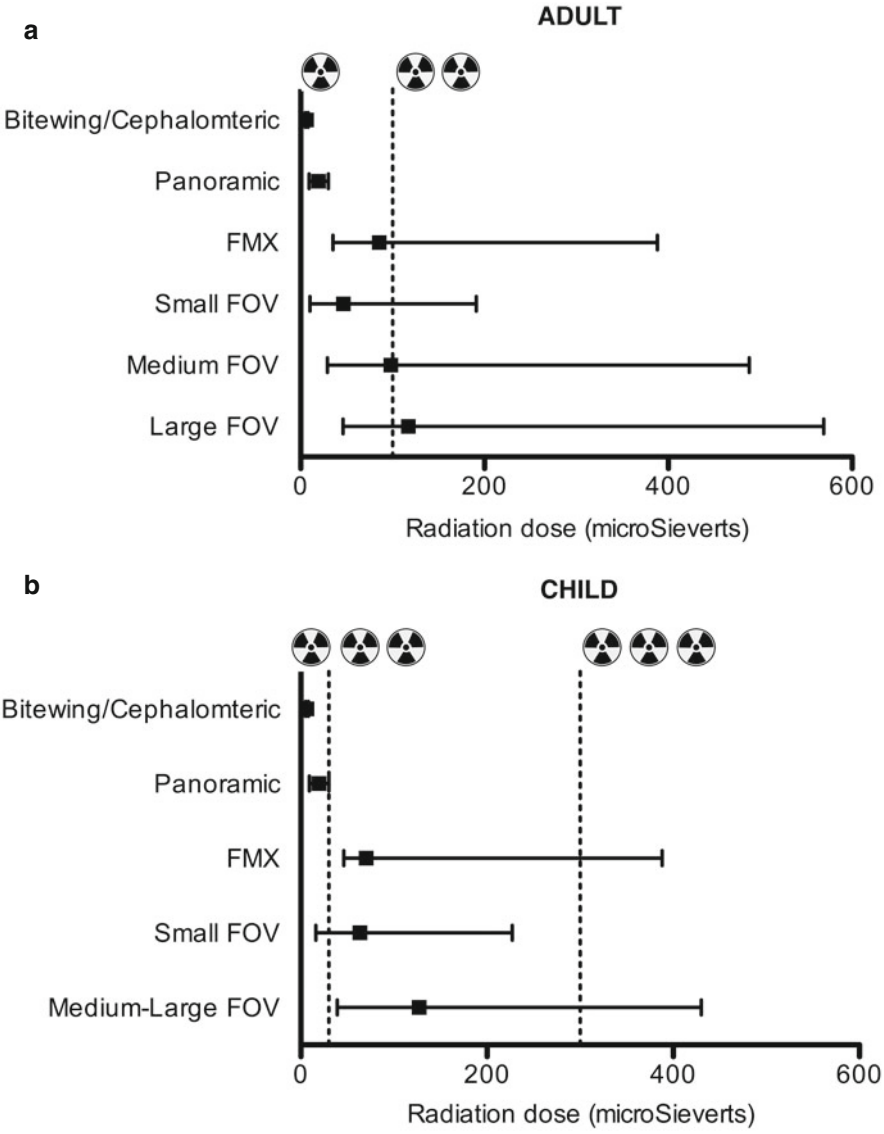

Fig. 1.5 (**a**) Effective doses for common maxillofacial radiographic examinations estimated for (**a**) adult and (**b**) child. The symbols represent median effective doses for standard exposure protocols. Data on CBCT doses was derived from Ludlow et al. [11]. The ACR RRL designations are indicated at the top of each graph. The dotted lines represent the upper and lower limits of the dose ranges that define the RRLs

annual effective dose from background radiation exposure in the United States is approximately 3.1 mSv. The number of days of background radiation is often used as basis to convey the magnitude of radiation risks from diagnostic radiological examinations.

Table 1.2 Effective doses from selected maxillofacial radiographic examinations

Radiographic procedure	Effective dose (μSv)[a]	Equivalent background radiation (days)[b]
Panoramic	20	2
Full mouth series	177	11
CBCT: small FOV (<8 cm)	47	6
CBCT: medium FOV (8–15 cm)	98	12
CBCT: large FOV (>15 cm)	117	14
MDCT, maxillofacial	913	107
MDCT, abdomen	6000	706

[a]Median effective doses for standard exposure protocols were derived from the meta-analysis of several reports, as summarized by Ludlow et al. [11]
[b]Calculation of background equivalent days is based on an annual exposure of 3.1 mSv. The background equivalent days are rounded to the nearest whole number

Table 1.2 lists typical doses from maxillofacial radiographic examinations, and the dose for these procedures is expressed as number of background days equivalent. Dentists may use this information to provide patients with an estimate of the dose that they are likely to receive. Additionally, it is also useful to provide similar data for commonly used dental and medical radiographic procedures to provide a further perspective on the relative magnitude of the dose.

1.4.4 Methods to Minimize Patient Radiation Exposure from CBCT Examinations

Overall, the cancer risks from maxillofacial radiographic imaging are small. Given the stochastic nature of radiation-induced cancer, it is important that patient exposure be minimized to the greatest extent possible. This is consistent with the principle of "ALARA"—"as low as reasonably achievable." Methods to achieve dose reduction during CBCT imaging are summarized below.

1.4.4.1 Selection Criteria

An important approach to prevent unnecessary patient radiation exposure is to select the most suitable procedure for the diagnostic task. For most endodontic tasks, intraoral radiography is the modality of choice for an initial patient evaluation. The dentist should determine whether CBCT imaging is likely to add additional information that is needed for diagnosis and/or treatment planning. The American Academy of Endodontists (AAE) and the American Academy of Oral and Maxillofacial Radiology (AAOMR) recently updated a joint position statement on the use of CBCT imaging in endodontics [10]. This statement provides several recommendations on clinical conditions that would benefit from CBCT imaging. These recommendations address diverse clinical situations that are managed by nonsurgical and surgical treatments. Dentists who use CBCT for endodontic diagnosis and treatment planning must be familiar with its advantages and limitations. Most

importantly, the decision to prescribe CBCT examination should be based on the patient's history and clinical findings, with a high likelihood that the CBCT findings will influence the diagnostic and treatment planning process. CBCT should not be used in lieu of lower dose intraoral or panoramic imaging. Furthermore, there is no evidence to justify CBCT use for routine endodontic diagnosis or for screening of asymptomatic patients.

1.4.4.2 Optimization of Imaging Protocols

In endodontics the anatomic region of interest is typically limited to a few contiguous teeth. Thus, small FOV scans generally provide adequate anatomic coverage. Restricting the field of view to the diagnostic area of interest is an important step in customizing the imaging protocol to individual patients and is an effective method to achieve dose reduction. Selecting the exposure settings based on the patient's size and tissue thickness is another approach to minimize dose to levels needed to provide a diagnostically adequate image. The use of "high-resolution" settings should be carefully considered as these significantly increase patient exposure.

Dentists who operate CBCT units in their clinics should be trained on the imaging protocol features and settings of their CBCT equipment. Procedures for periodic quality assurance of machine technical factors and operator technique should be implemented and followed.

1.4.4.3 Protective Aprons and Thyroid Collars

Maxillofacial CT examinations expose the thyroid gland, either directly by photons in the primary beam or by Compton scatter photons. The thyroid gland is highly sensitive to radiation-induced cancer, especially in children. A thyroid collar may be used to decrease the dose to the thyroid gland from the primary beam. However, it is important to ensure that the thyroid collar is not in the path of the primary beam—this would lead to significant artifacts that may compromise the diagnostic quality of the image.

The dose to the gonads from maxillofacial imaging is negligible. If the above dose reduction procedures are followed, lead aprons may not be needed during the CBCT exam. However, dentists should follow the local or regional radiation safety regulations. For example, some states in the United States require the use of lead (or lead-equivalent) aprons for all dento-maxillofacial radiographic examinations.

References

1. Pauwels R, Beinsberger J, Stamatakis H, Tsiklakis K, Walker A, Bosmans H, Bogaerts R, Jacobs R, Horner K, Consortium SP. Comparison of spatial and contrast resolution for cone-beam computed tomography scanners. Oral Surg Oral Med Oral Pathol Oral Radiol. 2012;114(1):127–35. doi:10.1016/j.oooo.2012.01.020.
2. Seibert JA. Flat-panel detectors: how much better are they? Pediatr Radiol. 2006;36 Suppl 14:173–81.

3. Wang J, Blackburn TJ. The AAPM/RSNA physics tutorial for residents: X-ray image intensifiers for fluoroscopy. Radiographics. 2000;20(5):1471–7.
4. Bechara B, McMahan CA, Moore WS, Noujeim M, Geha H, Teixeira FB. Contrast-to-noise ratio difference in small field of view cone beam computed tomography machines. J Oral Sci. 2012;54(3):227–32.
5. Neves FS, Vasconcelos TV, Campos PS, Haiter-Neto F, Freitas DQ. Influence of scan mode (180 degrees/360 degrees) of the cone beam computed tomography for preoperative dental implant measurements. Clin Oral Implants Res. 2014;25(2):e155–8. doi:10.1111/clr.12080.
6. Hassan BA, Payam J, Juyanda B, van der Stelt P, Wesselink PR. Influence of scan setting selections on root canal visibility with cone beam CT. Dentomaxillofac Radiol. 2012;41(8):645–8. doi:10.1259/dmfr/27670911.
7. Schulze R, Heil U, Groβ D, Bruellmann DD, Dranischnikow E, Schwanecke U, Schoemer E. Artefacts in CBCT: a review. Dentomaxillofac Radiol. 2011;40(5):265–73. doi:10.1259/dmfr/30642039.
8. The 2007 Recommendations of the International Commission on Radiological Protection. ICRP publication 103. Ann ICRP. 2007;37(2–4):1–332. doi:10.1016/j.icrp.2007.10.003 S0146-6453(07)00031-0 [pii].
9. Cody DD, Brateman LF, Favinger J, Geise RA, Kritzman ML, Rosen MP, Rybicki FJ, Schueler BA, Strauss KJ. ACR Appropriateness Criteria® Radiation Dose Assessment Introduction. 2015. http://www.acr.org/~/media/a27a29133302408bb86888eafd460a1f.pdf. Accessed 2 Aug 2015.
10. AAE and AAOMR Joint Position Statement: Use of Cone Beam Computed Tomography in Endodontics 2015 Update. (2015). http://www.aae.org/uploadedfiles/clinical_resources/guidelines_and_position_statements/cbctstatement_2015update.pdf. Accessed 2 Aug 2015.
11. Ludlow JB, Timothy R, Walker C, Hunter R, Benavides E, Samuelson DB, Scheske MJ. Effective dose of dental CBCT-a meta analysis of published data and additional data for nine CBCT units. Dentomaxillofac Radiol. 2015;44(1):20140197. doi:10.1259/dmfr.20140197.

Utilization of Cone Beam Computed Tomography in Endodontic Diagnosis

2

Mohamed I. Fayad and Bradford R. Johnson

Abstract

Endodontic diagnosis is dependent upon evaluation of the patient's chief complaint, medical and dental history, and clinical and radiographic examination. A clinical examination must be performed before considering any radiographic examination. Imaging is an essential part of endodontic practice, from diagnosis and treatment planning to outcome assessment. Intraoral radiographs have inherent limitations due to the compression of three-dimensional (3D) structures in a two-dimensional (2D) image. Superimposition of anatomic structures and image noise results in distortion of the area of interest. The use of cone beam computed tomography (CBCT) could overcome these issues by visualizing the dentition and the relationship of anatomic structures in three dimensions. CBCT units reconstruct the projection data to provide interrelational images in three orthogonal planes (axial, sagittal, and coronal). For most endodontic applications, limited or focused field of view (FOV) CBCT is preferred over large volume CBCT. This chapter will review the utilization of CBCT in endodontic diagnosis and management of periapical pathosis, diagnosis of pain, cracked teeth and vertical root fractures, internal and external resorptive defects, and traumatic injuries.

2.1 Introduction

Radiographic interpretation is a critical component in diagnosis, treatment, and evaluation of healing. Interpreting the film-based radiograph or digital image continues to be a somewhat subjective process. Goldman et al. [1] showed that the

M.I. Fayad, DDS, MS, PhD (✉) • B.R. Johnson, DDS, MHPE
Department of Endodontics, University of Illinois at Chicago, Chicago, IL, USA
e-mail: mfayad1@uic.edu; bjohnson@uic.edu

M. Fayad, B.R. Johnson (eds.), *3D Imaging in Endodontics*,
DOI 10.1007/978-3-319-31466-2_2

agreement between six examiners was only 47 % when evaluating healing of periapical lesions using 2D periapical radiographs. In a follow-up study, Goldman et al. [2] also reported that when examiners evaluated the same films at two different times, they only had 19–80 % agreement with their previous interpretations. In a more recent study, interobserver and intra-observer reliability in detecting periradicular radiolucencies by using a digital radiograph system was evaluated. Agreement among all six observers for all radiographs was less than 25 %, and agreement for five of six observers was approximately 50 % [3].

2.2 Detection of Periapical Lesions

CBCT imaging has the ability to detect small areas of periapical pathosis prior to being apparent on 2D radiographs [4], as well as differentiating larger, indistinct periapical radiolucent areas from normal variations in bone density (Fig. 2.1). This finding was validated in clinical studies in which periapical periodontitis detected in

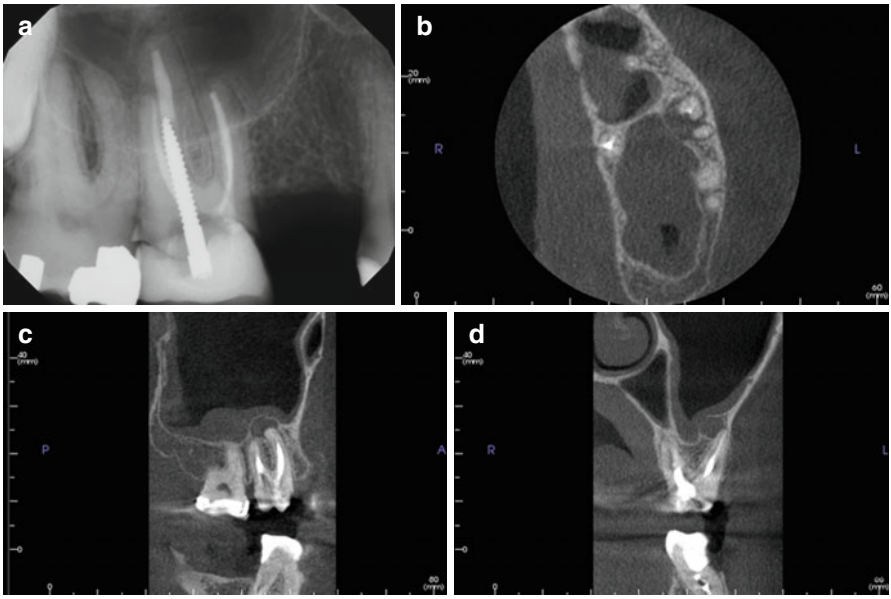

Fig. 2.1 A 49-year-old male was referred for evaluation of tooth number 3 prior to fabrication of a new crown. The root canal treatment was completed approximately 15 years ago and the tooth is currently asymptomatic, periodontal probing depths are WNL, and the tooth is negative to percussion, palpation, and bite stress testing. The referring dentist wants to know if this tooth should have treatment revision or surgery prior to a new crown. The periapical radiograph (**a**) shows possible widening of the apical PDL on all three roots but the extent, or even definitive presence, of apical pathosis is uncertain. CBCT (**b**, **c**, and **d**) reveals a distinct 5.0×8.0-mm periapical lesion with elevation of the sinus floor and inflammatory sinus mucositis (**b** axial view; **c** sagittal view; **d** coronal view)

intraoral radiographs and CBCT was 20 % and 48 %, respectively [5]. In a 1-year posttreatment study by the same authors, absence of a periapical radiolucency was found in 93 % of the cases when evaluated by 2D radiographs, but only 74 % when using CBCT [6]. Ex vivo studies in which simulated periapical lesions were created showed similar findings [7, 8].

However, some caution is warranted in the interpretation of CBCT periapical findings since the CBCT-PAI score is commonly greater than the 2D PAI score, and some teeth with healthy pulps may demonstrate a widened apical PDL space on CBCT [9].

2.3 Differential Diagnosis of Pain When Etiology Is Unclear and Identification of Unusual Anatomical Relationships

Diagnosis of orofacial pain can be a challenging process for the clinician prior to and after endodontic treatment. In challenging diagnostic pain cases, the clinical and radiographic findings are often inconclusive. Inability to determine the true source of pain can be attributed in part to limitations in both pulp sensibility testing and 2D intraoral radiographic imaging (Figs. 2.2, 2.3, 2.4, 2.5, 2.6, 2.7, and 2.8).

Persistent pain following root canal therapy or other therapeutic dental interventions can present a diagnostic challenge. Atypical odontalgia (AO), atypical facial pain (AFP), and persistent dentoalveolar pain (PDAP) are often used interchangeably to describe orofacial pain of uncertain etiology, although PDAP seems to be emerging as the preferred term [10, 11]. The diagnostic yield of intraoral radiographs and CBCT was evaluated in the differentiation between patients presenting with apical periodontitis and suspected PDAP without the evidence of periapical bone destruction. CBCT imaging detected 17 % more teeth with apical bone loss (apical periodontitis) than intraoral radiographs [12].

Fig. 2.2 A 14-year-old male was referred for consultation for tooth number 31. The panoramic radiograph revealed a radiolucency related to tooth number 31. The tooth responded positively to pulp sensibility tests, and periodontal probings were WNL except an 8-mm pocket on the mid-buccal surface. The patient was previously seen by two other dental specialists, and extraction of number 31 had been recommended by both

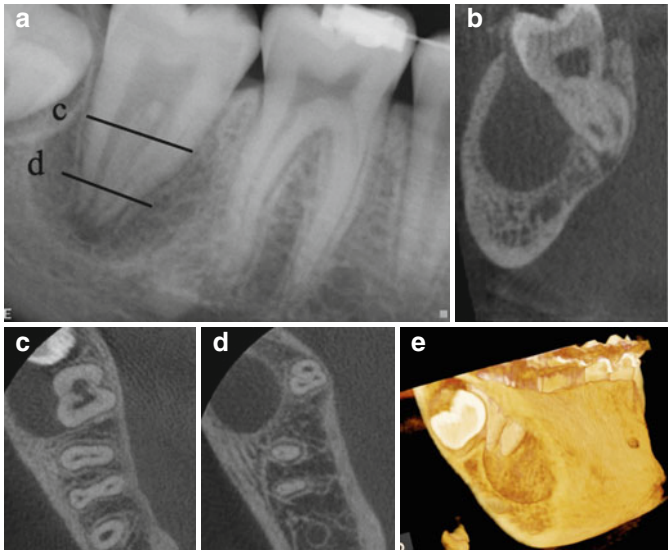

Fig. 2.3 Continuation of case from Fig. 2.2. (**a**) Periapical radiograph of tooth number 31. (**b**) Coronal view showing the buccal location of the periapical radiolucency in relation to tooth number 31. Notice the apical 1/3 of the root is surrounded by bone which explains the positive response to cold and EPT. The *lines* on the periapical radiograph correspond to the axial section views *c* and *d*. Axial sections **c** and **d** demonstrate the origin pf, the lesion as tooth number 32. 3D reconstruction (**e**) demonstrates the buccal location of the lesion and explains the isolated deep periodontal probing on the buccal aspect of tooth number 31

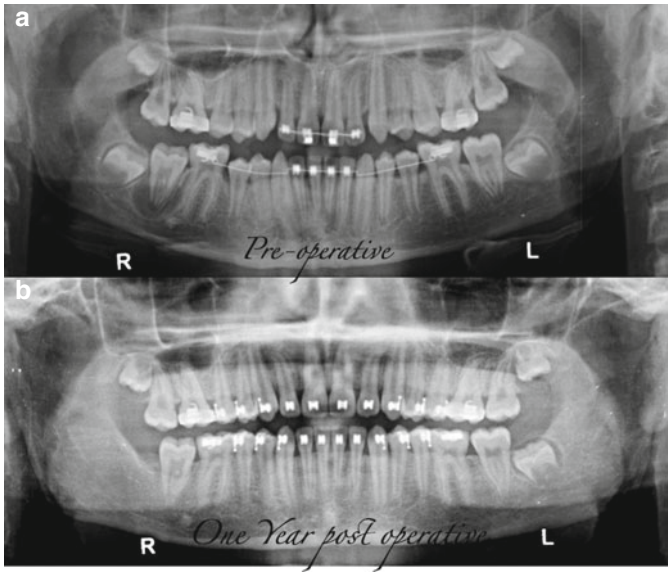

Fig. 2.4 Continuation of case from Fig. 2.2. Tooth number 32 was extracted and the lesion was submitted for biopsy. The biopsy result was a dentigerous cyst. Panoramic images (**a**) and (**b**) are preoperative and 1-year recall, respectively. Good bony healing around number 31 is evident

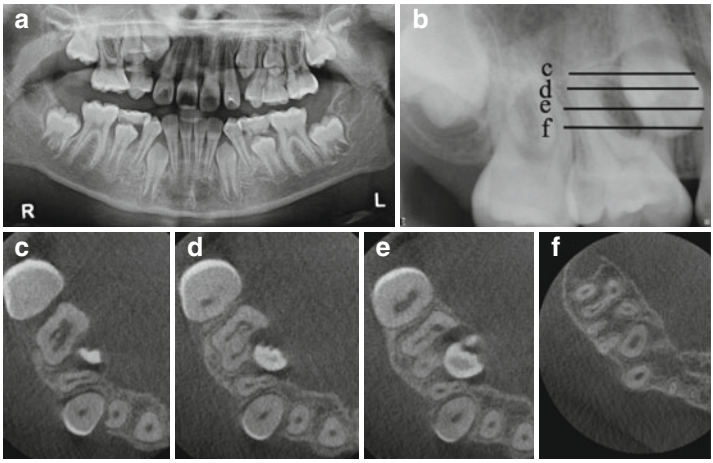

Fig. 2.5 (**a**) Panoramic radiograph of a 9-year-old patient that was referred to evaluate the path of eruption of tooth number 4 as part of orthodontic treatment planning. (**b**) Periapical radiograph of tooth number 4. The *lines* on the periapical radiograph correspond to the axial section views *c*, *d*, *e*, and *f*. (**c**–**e**) are the different coronal-apical cross section levels demonstrating the ectopic resorption of the mesio-palatal aspect of tooth number 3 by the cusp tip of tooth number 4. The resorptive pattern seen on the CBCT axial images cannot be detected on either the panoramic or periapical radiographs. (**f**) The most apical cross section showing no resorption at that level

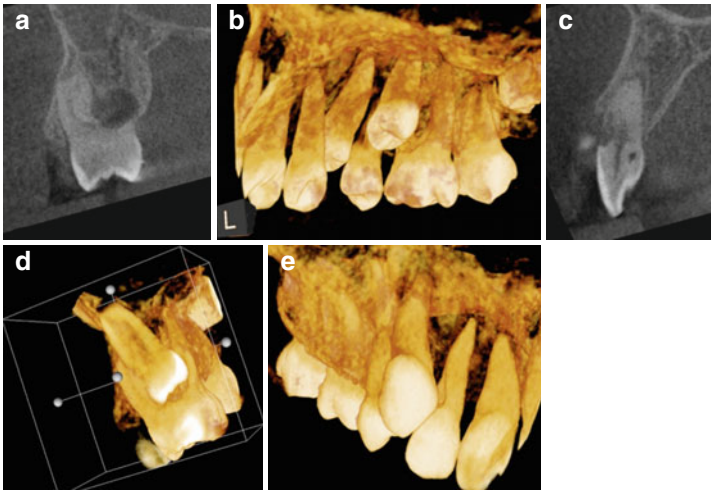

Fig. 2.6 Continuation of case from Fig. 2.5. (**a**) Coronal view of the mesial furcation of tooth number 3 demonstrating the resorptive defect in the furcation and mesio-palatal aspect. (**b**, **d**) are 3D reconstructions demonstrating the same pattern from the palatal and mesial views, respectively. (**c**) Sagittal view of tooth number 7 demonstrating resorption caused by the ectopic eruption of tooth number 6. (**e**) 3D reconstruction demonstrating the relationship between teeth numbers 6 and 7. The information obtained from this CBCT scan will have a significant impact on orthodontic treatment planning

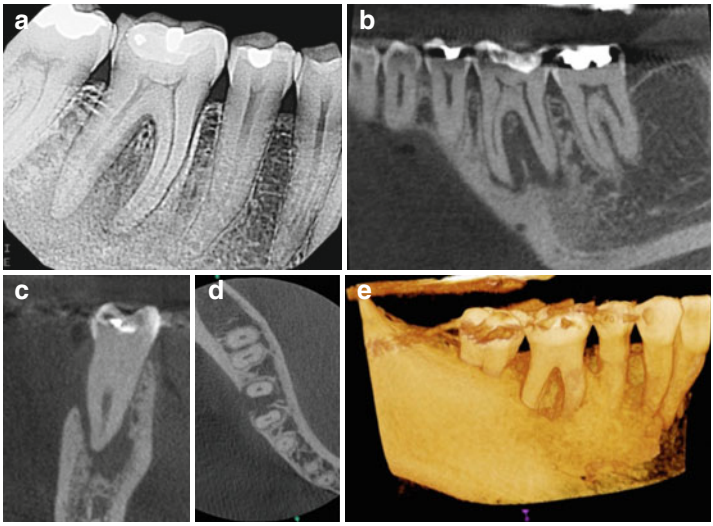

Fig. 2.7 A patient was referred for evaluation and treatment of tooth number 30. Patient presented with pain to percussion and no response to cold testing. Periodontal probing depths were WNL. Root canal therapy was indicated based on 2D radiographic findings and clinical tests. (**a**) Periapical radiograph of tooth number 30. (**b**) is a sagittal view of tooth number 30. A periapical radiolucency involving both mesial and distal roots as well as the furcation was detected. The lingual bone is still intact which gives the impression of greater bone volume and density in the furcation in the periapical (2D) radiograph than is actually present. (**c**) Coronal view of the distal root demonstrating complete loss of buccal bone. Due to the tight gingival attachment, periodontal probing was WNL. (**d**) Axial view demonstrating buccal plate perforation that cannot be detected from the 2D radiograph. (**e**) 3D reconstruction demonstrating the actual endo-perio defect. Considering the unfavorable prognosis for resolution of the extensive endo-perio lesion, extraction was recommended

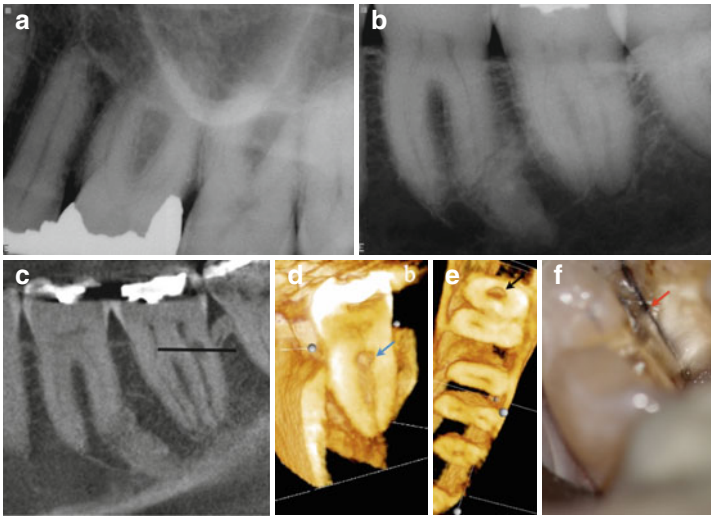

2.4 Detection of Cracked Teeth and Root Fractures

Two-dimensional radiographs (2D) are of limited value for the diagnosis of vertical root fractures (VRF) and usually only provide indirect evidence of the presence of a VRF. The three-dimensional nature of complex tooth anatomy and surrounding structures can make interpretation of 2D images challenging and unreliable (Figs. 2.9, 2.10, 2.11, 2.12, 2.13, 2.14, and 2.15).

Several studies have demonstrated the value of CBCT as an aid in the detection of VRF. In a comparative study evaluating the sensitivity and specificity of CBCT and periapical radiographs (PR) in detecting VRF, sensitivity and specificity for VRF detection of CBCT were 79.4 % and 92.5 % and for PR were 37.1 % and 95 %, respectively. In the same study, it was reported that the specificity of CBCT was reduced in the presence of root canal filling material [13]. Higher sensitivity and specificity were observed in a clinical study where the definitive diagnosis of vertical root fracture was confirmed at the time of surgery to validate CBCT findings, with sensitivity being 88 % and specificity 75 % [14]. Several case series studies have concluded that CBCT is a useful tool for the diagnosis of vertical root fractures. In vivo and laboratory studies [15, 16] evaluating CBCT in the detection of vertical root fractures agreed that sensitivity, specificity, and accuracy of CBCT were generally higher and reproducible. The detection of fractures was significantly higher for all CBCT systems when compared to intraoral radiographs. However, these results should be interpreted with caution because detection of vertical root fracture is dependent on the size of the fracture, presence of artifacts caused by obturation materials and posts, and the spatial resolution of the CBCT. In a recent study, the diagnostic ability of CBCT to assess longitudinal root fractures in endodontically treated and restored teeth was evaluated [17]. The presence of gutta-percha or cast-gold posts reduced the overall sensitivity and specificity. This was attributed to star-shaped streak artifacts that mimic fracture lines in the axial spatial view. One significant problem, which can affect the image diagnostic quality and accuracy of CBCT images, is the scatter and beam hardening caused by high-density neighboring structures, such as enamel, metal posts, and restorations. If this scatter and beam hardening is associated with or close to the tooth being assessed, the overall sensitivity and specificity are dramatically reduced.

Fig. 2.8 Patient presented for diagnosis of non-localized pain on the left side. (**a**, **b**) Periapical radiographs of the maxillary and mandibular posterior quadrants were inconclusive. All vitality, periodontal, and palpation tests were WNL. Tooth number 14 was slightly tender to percussion. A local anesthetic test was performed by administering 1.7 ml of 2 % lidocaine with 1:100,000 epinephrine via buccal infiltration to tooth number 14. The pain was not relieved. CBCTs were taken for both maxillary and mandibular quadrants. (**c**) Sagittal view of tooth number 18 demonstrating an internal resorptive defect in the distal root. The *horizontal black line* in (**c**) represents the axial section in (**e**). 3D reconstruction of the cropped distal root showing the extent of the resorptive defect in a coronal view (**d** - *arrow*) and axial view (**e** - *arrow*). (**f**) Clinical image of a crack (*arrow*) that extends into the distal canal

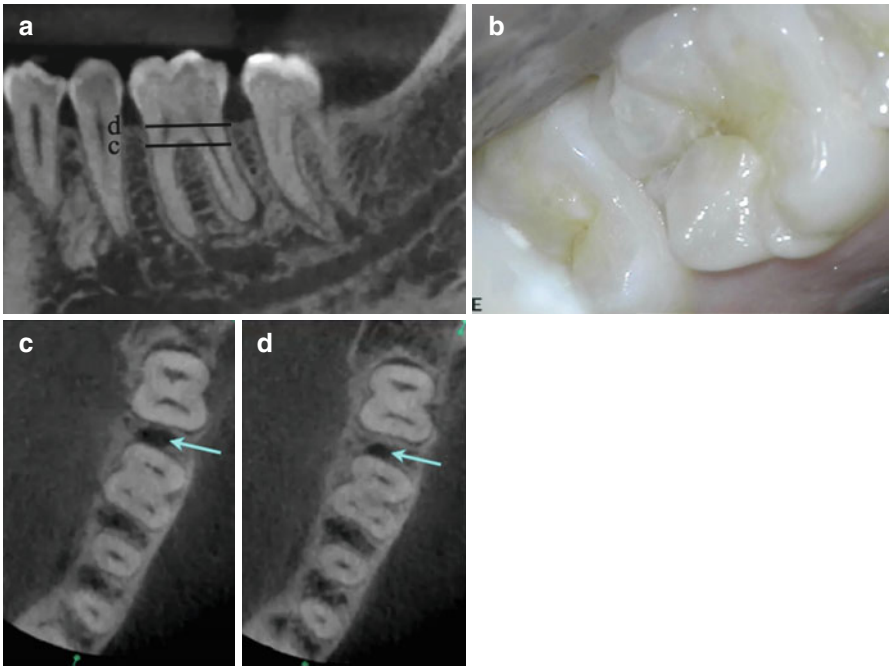

Fig. 2.9 Patient presented for evaluation and treatment of tooth number 19. The chief complaint was pain on biting and sensitivity to hot drinks. Clinical findings: no response to cold and positive response to bite stress testing. A diagnosis of a necrotic pulp and symptomatic apical periodontitis was established. The presumed etiology was extension of a distal marginal ridge crack. (**a**) Sagittal view of tooth number 19 showing a distal root periapical radiolucency. The *lines* on the sagittal view correspond to the axial section views (*c*) and (*d*). (**b**) Clinical image (occlusal view) demonstrating the distal marginal ridge crack. Axial views (**c**) and (**d**) demonstrate the distal bone loss associated with the fracture (*blue arrows*) and unfavorable prognosis

Due in part to the common presence of imaging artifacts, several investigators have questioned the superiority of CBCT in the diagnosis of VRF and urge caution in relying solely on CBCT for diagnosis of VRF [18, 19]. While we agree that caution may be warranted when using only one diagnostic test or finding, we believe that the preponderance of the evidence currently available supports the value of CBCT as an aid in the diagnosis of VFR [20, 21], and CBCT may be particularly useful in the diagnosis of horizontal and oblique fractures commonly associated with dental trauma [22] (Fig. 2.16). In particular, the CBCT sagittal view provides diagnostic information for traumatized anterior teeth that is not available with 2D periapical imaging.

Clinically, a thorough dental history and classic clinical and radiographic signs and symptoms such as pain, swelling, presence of a sinus tract, and/or presence of an isolated deep periodontal pocket can be helpful hints to suggest the presence of a VRF. Radiographically, a combination of periapical and lateral root radiolucency "halo" appearance is valuable information indicating the possible presence of

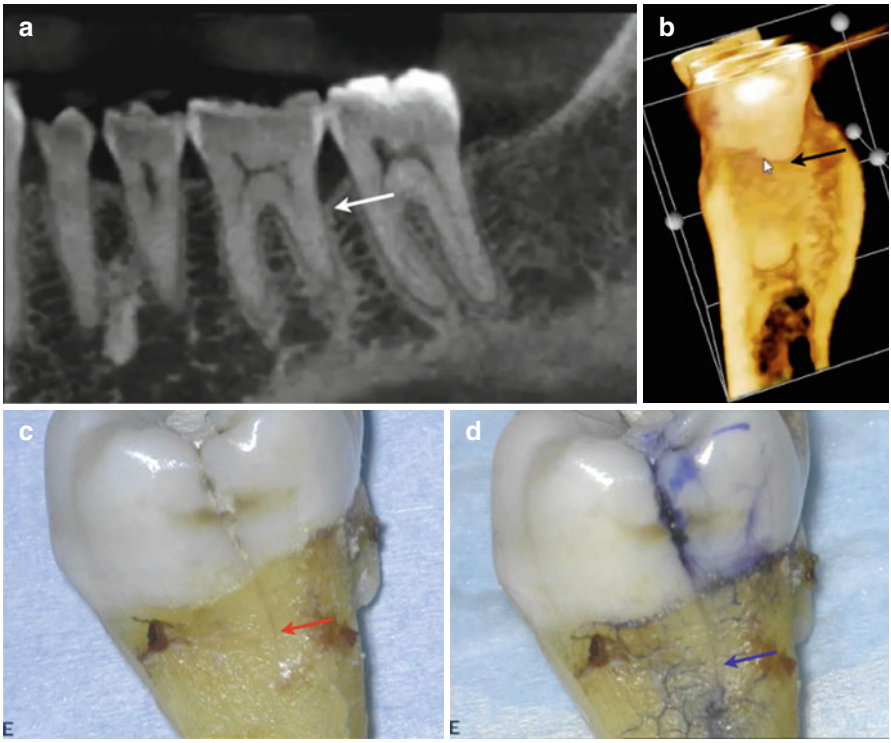

Fig. 2.10 Continuation of case from Fig. 2.9. (**a**) Sagittal view demonstrating an angled distal bony defect (*white arrow*). (**b**) 3D reconstruction view demonstrating the angled distal bony defect seen in (**a**) (*black arrow*). (**c**, **d**) show the extracted tooth before and after staining the longitudinal distal root fracture (*red and blue arrows*)

VRF. Several of the previously mentioned clinical and radiographic elements have to align to establish a presumptive diagnosis of VFR [23]; however, direct visual examination, usually requiring surgical exposure, is still the reference standard for diagnosis of VRF.

In a case series, the following five findings on CBCT exam were consistent with confirmed VRF [24]:

1. Loss of bone in the mid-root area with intact bone coronal and apical to the defect (Figs. 2.12 and 2.13)
2. Absence of the entire buccal plate of bone in axial, coronal, and/or 3D reconstruction
3. Radiolucency around a root where a post terminates (Fig. 2.14)
4. Space between the buccal/lingual plate of bone and fractured root surface (Fig. 2.15)
5. Visualization of the VRF on the CBCT spatial projection views

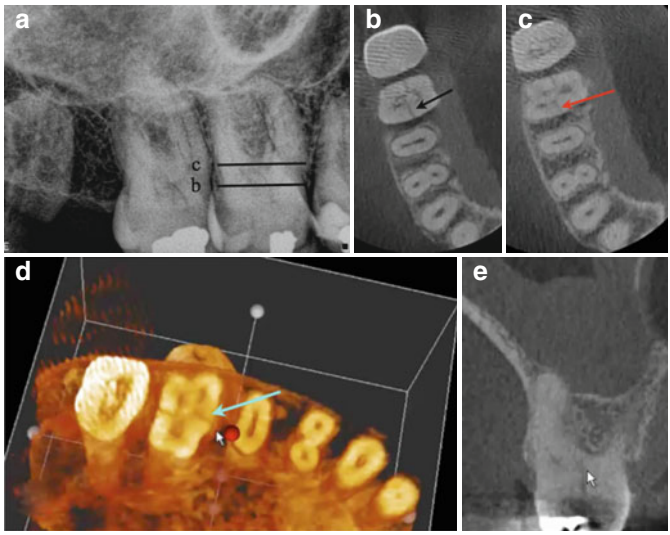

Fig. 2.11 (**a**) Periapical radiograph of tooth number 3. The patient presented complaining of pain to cold and biting. Periodontal probing depths were WNL. *Lines* correspond to the axial sections in (*b*) and (*c*). (**b**) and (**c**) are axial views showing the extent of the fracture (*black and red arrows* in (**b**) and (**c**), respectively). (**d**) 3D reconstruction, axial view of (**c**) showing the mesial-distal crack (*blue arrow*). (**e**) A coronal view demonstrating extension of the fracture into the furcation

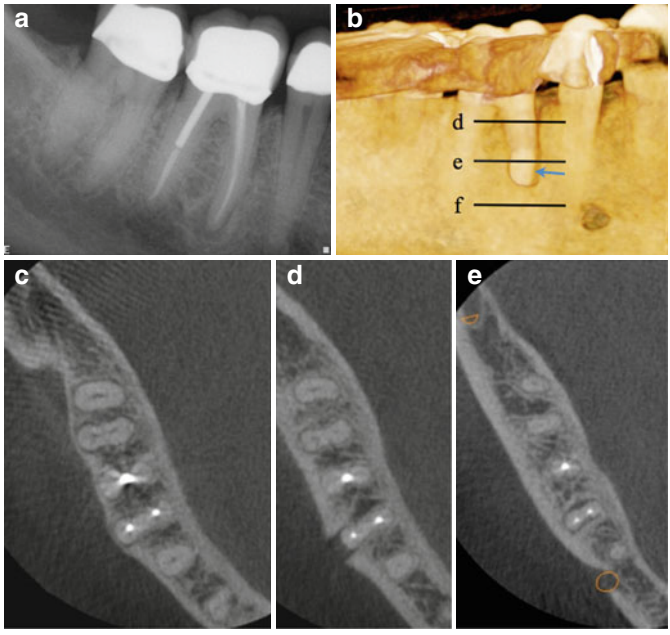

Fig. 2.12 (**a**) Periapical radiograph of tooth number 30. (**b**) 3D reconstruction demonstrating the mid-root buccal defect (*arrow*). *Lines* correspond to the axial section views (**c**), (**d**), and (**e**). Note axial view demonstrating the mid-root buccal bone loss in (**d**)

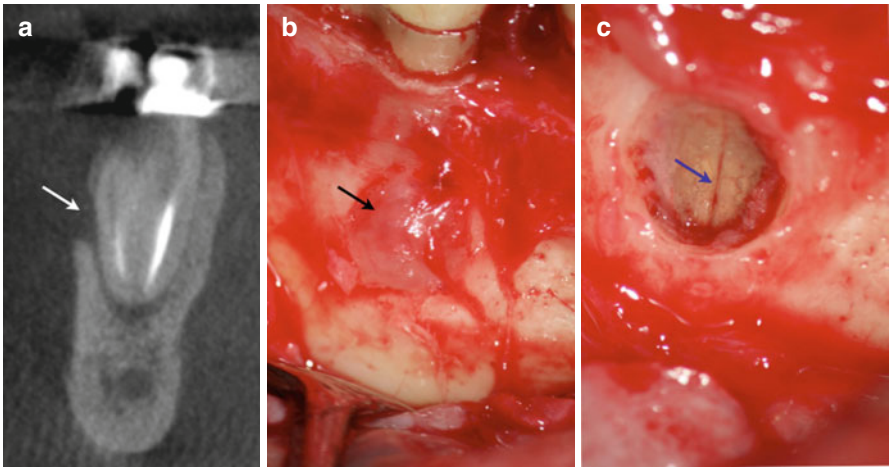

Fig. 2.13 Continuation of case in Fig. 2.12. (**a**) Coronal view demonstrating the mid-root buccal bone loss (*arrow*). Surgical exploration was performed to confirm the presence of a vertical root fracture. (**b**) Note the granulation tissue at mid-root level (*arrow*). (**c**) Surgical degranulation of the defect demonstrating the vertical root fracture in the mesial root (*arrow*)

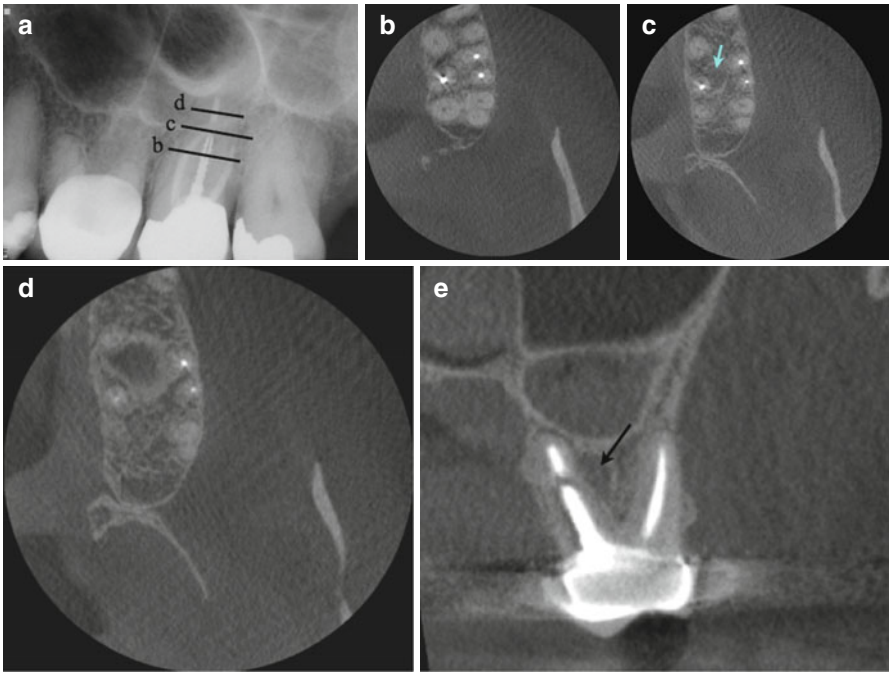

Fig. 2.14 (**a**) Periapical radiograph of tooth number 14. The three *lines* correspond to the axial section views in (*b*), (*c*), and (*d*). Note mid-root radiolucency (**c**) in relation to the palatal root at the apical level of the post (*blue arrow*). Intact palatal bone was observed coronal and apical to the mid-root level (**b**, **d**). (**e**) Coronal view showing the distal-buccal and palatal roots of number 14. The *arrow* demonstrates the lateral radiolucency in relation to the palatal root. Vertical root fracture of the palatal root was determined and patient was referred for extraction

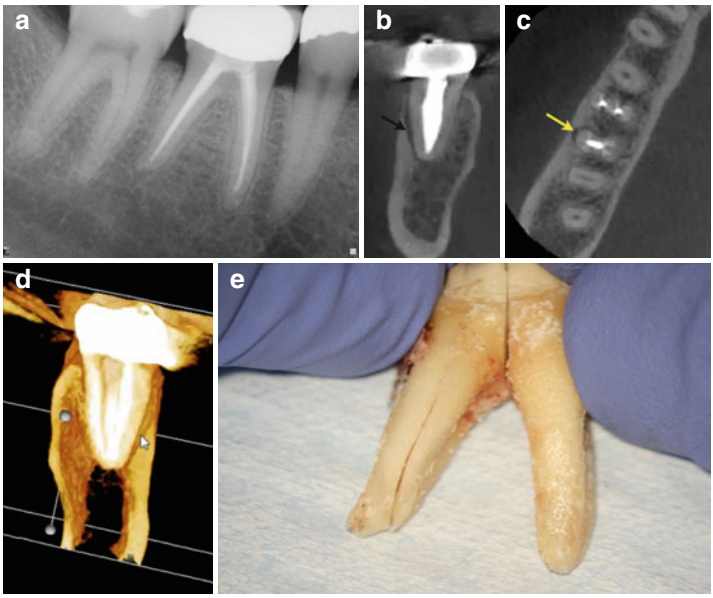

Fig. 2.15 (**a**) Periapical radiograph of tooth number 30. (**b**) Coronal view of the distal root demonstrating the space between the distal root and the buccal cortical plate (*black arrow*). (**c**) Axial view of the distal root demonstrating the space between the distal root and the buccal cortical plate (*yellow arrow*). (**d**) 3D reconstruction of the distal root demonstrating the space between the distal root and the buccal cortical plate. (**e**) Clinical image after surgical sectioning and extraction and confirmation of distal root vertical fracture

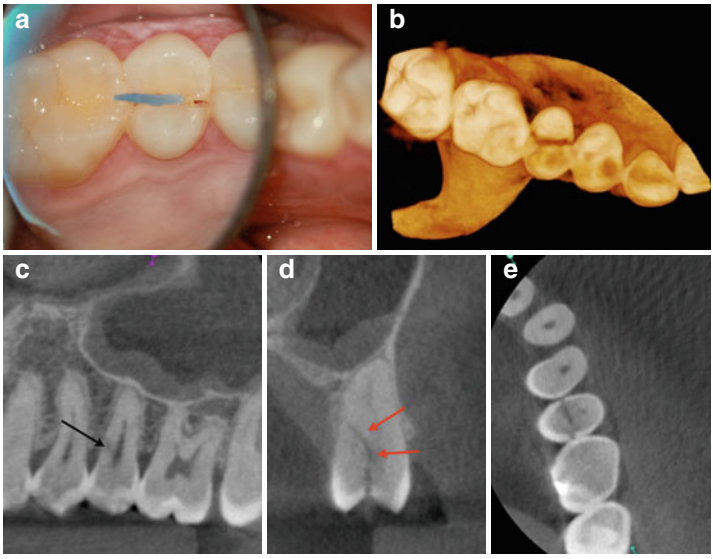

2.5 Detection and Diagnosis of Inflammatory Resorptive Defects

Diagnosis of root resorption is often challenging due to the typically quiescent onset and varying clinical presentation (Figs. 2.17 and 2.18). Definitive diagnosis and treatment planning is ultimately dependent on the radiographic representation of the disease. 2D imaging offers limited diagnostic potential when compared to 3D imaging [25, 26]. Chapter 7 will explore diagnosis and treatment of resorptive defects in greater detail.

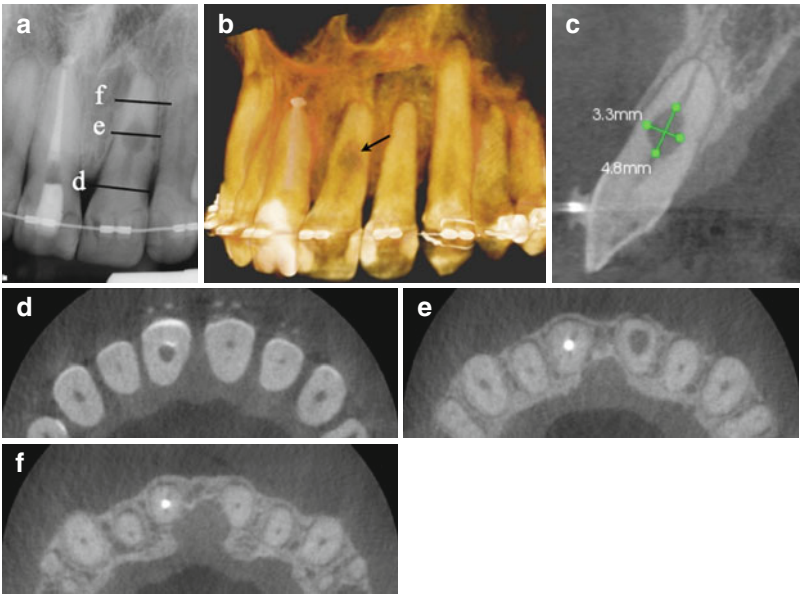

Fig. 2.17 Patient was referred for evaluation and treatment of an internal resorptive defect on tooth number 9. (**a**) Periapical radiograph of tooth number 9. The 3 lines correspond to the axial section views in (*d*), (*e*), and (*f*). (**b**) 3D reconstruction of maxillary anterior teeth demonstrating the internal resorptive defect (*black arrow*). (**c**) Sagittal view of tooth number 9 with the 3.3×4.8 mm measurement of the defect. (**d**), (**e**), and (**f**) are axial views of tooth number 9. Note the normal canal anatomy coronal and apical to the defect (**d**, **f**). The maximum width of the defect is demonstrated in axial view (**e**)

Fig. 2.16 Patient presented for evaluation of a mesial-distal fracture, tooth number 13. In order to determine restorability and the extent of the palatal cusp fracture, a CBCT was recommended. (**a**) Clinical picture with a wedge slightly separating the buccal and palatal cusps. (**b**) 3D reconstruction of the split tooth after placing the wedge. (**c**) Sagittal view of tooth number 13 demonstrating the sub-osseous extent of the fracture (*black arrow*). (**d**) Coronal view demonstrating the palatal extent of the fracture (*red arrow*). (**e**) Axial view demonstrating the split nature of both cusps. Tooth number 13 was determined to be non-restorable and extraction was recommended

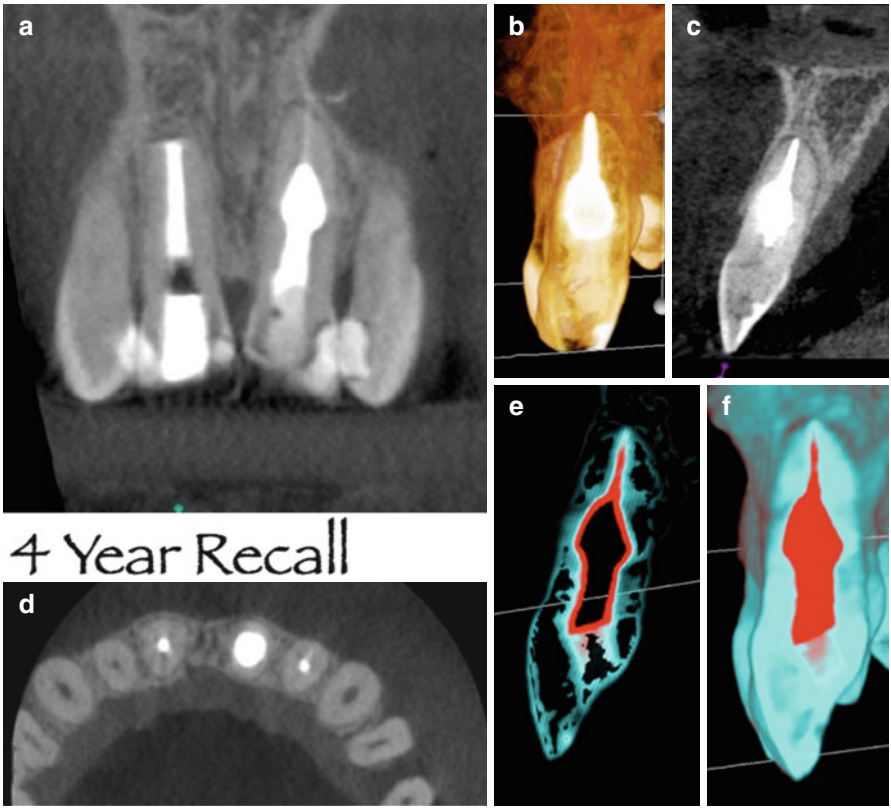

Fig. 2.18 Continuation of case in Fig. 2.17: (**a**) Coronal view, 4-year recall of tooth number 9 and healing of previous periapical surgery on tooth number 8. (**b**, **e**, and **f**) are 3D reconstructions of tooth number 9. (**e**) and (**f**) are 3D templates constructed to determine the interface and adaptability of the root canal filling to the resorptive defect canal walls. (**c**) is a sagittal view and (**d**) is an axial view through the widest section of the resorptive defect

2.6 Traumatic Dental Injuries (TDI)

Traumatic dental injuries present a clinical challenge with regard to diagnosis, treatment planning, and prognosis. Radiographic assessment is important to identify the location, type, and severity of TDI (Figs. 2.19 and 2.20). According to the 2012 International Association of Dental Traumatology guidelines [27], a series of periapical radiographs from different angulations and an occlusal film are recommended for evaluation of TDI. CBCT was recommended as well for the visualization of TDI, particularly root fractures and lateral luxations, monitoring of healing, and complications.

Unfortunately, 2D imaging has limitations in the diagnosis and detection of TDI due to projection geometry, magnification, superimposition of anatomic structures, distortion, and processing errors.

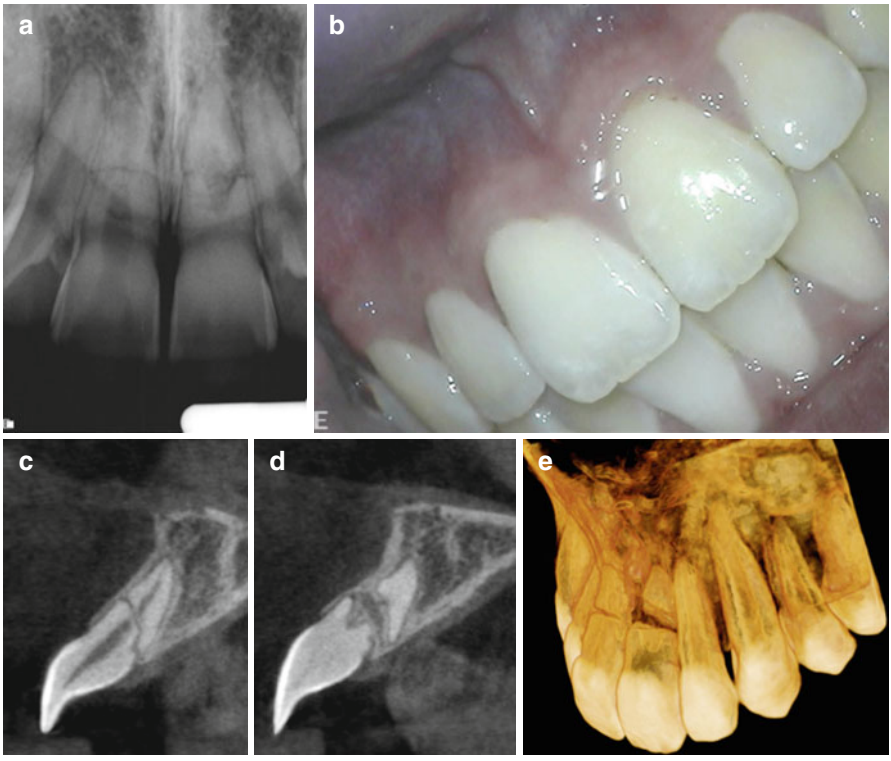

Fig. 2.19 A 15-year-old patient with history of trauma to the anterior maxilla was referred for consultation for teeth numbers 8 and 9. Tooth number 8 had a grade I mobility and tooth number 9 had a grade II + mobility. (**a**) Periapical radiograph for teeth numbers 8 and 9. Horizontal root fractures can be seen mid-root in both teeth. (**b**) Clinical picture of teeth #8 and 9. Periodontal probing depths were WNL. Marginal and attached gingiva demonstrated normal color and architecture. (**c**, **d**) are the sagittal views of teeth numbers 8 and 9, respectively. Note the oblique nature of the root fractures and bone fill between the coronal and apical segments in (**d**). (**e**) 3D reconstruction demonstrating the dislocation of the fractured segments. Since the patient was asymptomatic and CBCT revealed no periradicular pathosis, a palatal splint was suggested to address the mobility but no endodontic intervention was recommended at this time

In the diagnosis of horizontal root fractures (HRF) utilizing 2D imaging, the fracture line will only be detected if the X-ray beam passes directly through it. The 2D nature limits the accuracy in the diagnosis of the location, severity, and extent of HRF. The risk of misdiagnosis of the location and extent of the fracture by using only 2D intraoral radiography could lead to improper treatment and an unfavorable outcome. Because of the limitations of intraoral radiography, CBCT was suggested as the preferred imaging modality for diagnosis of HRF [28].

CBCT overcomes several of the limitations of 2D imaging by providing a considerable amount of 3D information about the nature and extent of the HRF. The significant difference in the nature of HRF when assessed with 2D radiographs

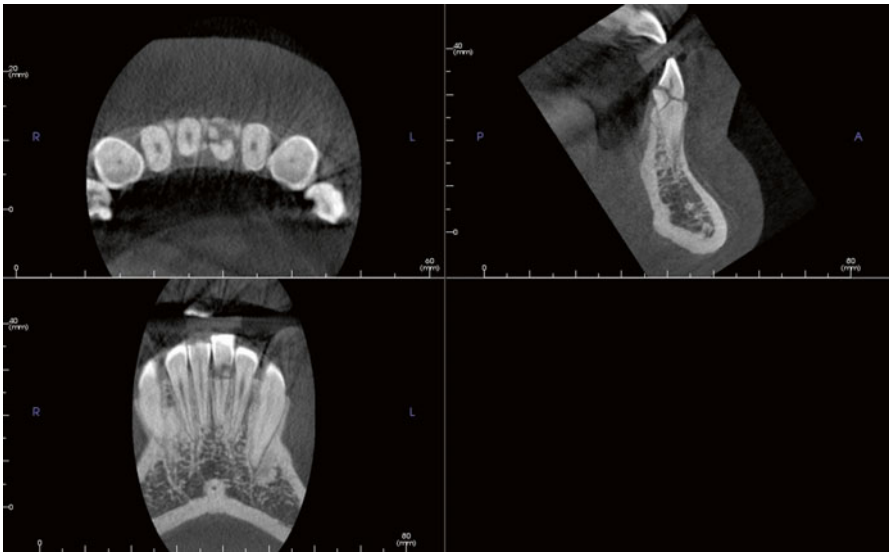

Fig. 2.20 A 13-year-old male presented approximately 2 weeks after trauma to his mandibular anterior teeth that occurred while he was playing basketball. His primary concern was the looseness of tooth number 25. A CBCT scan was taken to evaluate the extent of the fracture. The original treatment plan (extraction) was modified after viewing the CBCT, since the buccal bone was very thin and likely to be lost during a surgical extraction. The treatment plan was changed to include root canal therapy, root submergence, and eventual slow extrusion of the tooth to maintain bone for a future implant

compared to CBCT has been reported [29]. Limited FOV CBCT imaging seems to be generally advantageous in the diagnosis, assessment of prognosis, treatment planning, and treatment follow-up of HRF cases.

In pediatric patients with TDI, it should be considered that children are at greater risk than adults from a given dose of radiation both because they are inherently more radiosensitive and because they have more remaining years of life during which a radiation-induced neoplasm could develop [30].

Conclusion

CBCT is a valuable adjunct to assist in the diagnosis of periapical hard tissue changes, root fractures, traumatic dental injuries, inflammatory root resorption, and orofacial pain with no clear etiology. Conventional 2D radiography and CBCT both record structural changes in the bone. However, CBCT imaging has the ability to detect periapical pathosis prior to being apparent on 2D radiographs. Preoperative factors such as the presence and true size of a periapical lesion play an important role in endodontic treatment outcome. Success, when measured by radiographic criteria, is higher when teeth are endodontically treated before radiographic signs of periapical disease are detected.

According to the 2015 joint statement from the American Association of Endodontists and American Academy of Oral and Maxillofacial Radiology, CBCT is the imaging modality of choice for the following diagnostic situations [31]:

1. Patients presenting with contradictory or nonspecific clinical signs and symptoms associated with untreated or previously endodontically treated teeth
2. Diagnosis and management of limited dentoalveolar trauma, root fractures, luxation, and/or displacement of teeth and localized alveolar fractures, in the absence of other maxillofacial or soft tissue injury that require other advanced imaging modalities.
3. Localization and differentiation of external and internal resorptive defects and the determination of appropriate treatment and prognosis
4. If clinical examination and 2D intraoral radiography are inconclusive in the detection of vertical root fracture (VRF)

References

1. Goldman M, Pearson AH, Darzenta N. Endodontic success: who's reading the radiograph? Oral Surg Oral Med Oral Pathol. 1972;33:432–7.
2. Goldman M, Pearson AH, Darzenta N. Reliability of radiographic interpretation. Oral Surg Oral Med Oral Pathol. 1974;38:287–93.
3. Tewary S, Luzzo J, Hartwell G. Endodontic radiography: who is reading the digital radiograph? J Endod. 2011;37:919–21.
4. De Paula-Silva FW, Wu MK, Leonardo MR, da Silva LA, Wesselink PR. Accuracy of periapical radiography and cone-beam computed tomography scans in diagnosing apical periodontitis using histopathological findings as a gold standard. J Endod. 2009;35(7):1009–12.
5. Patel S, Wilson R, Dawood A, Mannocci F. The detection of periapical pathosis using periapical radiography and cone beam computed tomography – part 1: preoperative status. Int Endod J. 2012;45(8):702–10.
6. Patel S, Wilson R, Dawood A, Mannocci F. The detection of periapical pathosis using periapical radiography and cone beam computed tomography – part 2: a 1-year post-treatment follow-up. Int Endod J. 2012;45(8):711–23.
7. Sogur E, Grondahl H, Bakst G, Mert A. Does a combination of two radiographs increase accuracy in detecting acid-induced periapical lesions and does it approach the accuracy of cone-beam computed tomography scanning. J Endod. 2012;38(2):131–6.
8. Patel S, Dawood A, Mannocci F, Wilson R, Pitt Ford T. Detection of periapical bone defects in human jaws using cone beam computed tomography and intraoral radiography. Int Endod J. 2009;42(6):507–15.
9. Pope O, Sathorn C, Parashos P. A comparative investigation of cone-beam computed tomography and periapical radiography in the diagnosis of a healthy periapex. J Endod. 2014;40(3):360–5.
10. Nixdorf D, Moana-Filho E. Persistent dento-alveolar pain disorder (PDAP): working towards a better understanding. Rev Pain. 2011;5(4):18–27.
11. Nixdorf DR, et al. Differential diagnosis for persistent pain after root canal treatment: a study in the National Dental Practice-based Research Network. J Endod. 2015;41:457–63.
12. Pigg M, List T, Petersson K, Lindh C, Petersson A. Diagnostic yield of conventional radiographic and cone-beam computed tomographic images in patients with atypical odontalgia. Int Endod J. 2011;44(12):1365–2591.

13. Hassan B, Metska ME, Ozok AR, van der Stelt P, Wesselink PR. Detection of vertical root fractures in endodontically treated teeth by a cone beam computed tomography scan. J Endod. 2009;35:719–22.
14. Edlund M, Nair MK, Nair UP. Detection of vertical root fractures by using cone-beam computed tomography: a clinical study. J Endod. 2011;37(6):768–72.
15. Metska ME, Aartman IH, Wesselink PR, Özok AR. Detection of vertical root fracture in vivo in endodontically treated teeth by cone-beam computed tomography scans. J Endod. 2012;38(10):1344–7.
16. Brady E, Mannocci F, Wilson R, Brown J, Patel S. A comparison of CBCT and periapical radiography for the detection of vertical root fractures in non-endodontically treated teeth. Int Endod J. 2014;47(8):735–46.
17. Melo SLS, Bortoluzzi EA, Abreu M, Correa LR, Correa M. Diagnostic ability of a cone-beam computed tomography scan to assess longitudinal root fractures in prosthetically treated teeth. J Endod. 2010;36:1879–82.
18. Corbella S, Del Fabbro M, Tamse A, Rosen E, Tsesis I, Taschieri S. Cone beam computed tomography for the diagnosis of vertical root fractures: a systematic review of the literature and meta-analysis. Oral Surg Oral Med Oral Pathol Oral Radiol. 2014;118(5):593–602.
19. Rosen E, Taschieri S, Del Fabbro M, Beitlitum I, Tsesis I. The diagnostic efficacy of cone-beam computed tomography in endodontics: a systematic review and analysis by a hierarchical model of efficacy. J Endod. 2015;41(7):1008–14.
20. Long H, Zhou Y, Ye N, Liao L, Jian F, Wang Y, Lai W. Diagnostic accuracy of CBCT for tooth fractures: a meta-analysis. J Dent. 2014;42(3):240–8.
21. Ma RH, Ge ZP, Li G. Detection accuracy of root fractures in cone-beam computed tomography images: a systematic review and meta-analysis. Int Endod J 2015; published online ahead of print: July 17, 2015.
22. Avsever H, Gunduz K, Orhan K, Uzun I, Ozmen B, Egrioglu E, Midilli M. Comparison of intraoral radiography and cone-beam computed tomography for the detection of horizontal root fractures: an in vitro study. Clin Oral Investig. 2014;18(1):285–92.
23. Tsesis I, Rosen E, Tamse A, Taschieri S, Kfir A. Diagnosis of vertical root fractures in endodontically treated teeth based on clinical and radiographic indices: a systematic review. J Endod. 2010;36:1455–8.
24. Fayad MI, Ashkenaz PJ, Johnson BR. Different representations of vertical root fractures detected by cone-beam volumetric tomography: a case series report. J Endod. 2012;10: 1435–42.
25. Estrela C, Bueno MR, De Alencar AH, Mattar R, Valladares Neto J, Azevedo BC, De Araújo Estrela CR. Method to evaluate inflammatory root resorption by using cone beam computed tomography. J Endod. 2009;35(11):1491–7.
26. Durack C, Patel S, Davies J, Wilson R, Mannocci F. Diagnostic accuracy of small volume cone beam computed tomography and intraoral periapical radiography for the detection of simulated external inflammatory root resorption. Int Endod J. 2011;44(2):136–47.
27. Diangelis AJ, Andreasen JO, Ebeleseder KA, et al. International Association of Dental Traumatology guidelines for the management of traumatic dental injuries: 1—fractures and luxations of permanent teeth. Dent Traumatol. 2012;28:2–12.
28. May JJ, Cohenca N, Peters OA. Contemporary management of horizontal root fractures to the permanent dentition: diagnosis – radiologic assessment to include cone-beam computed tomography. J Endod. 2013;39(3 Suppl):S20–5.
29. Iikubo M, Kobayashi K, Mishima A, et al. Accuracy of intraoral radiography, multidetector helical CT, and limited cone-beam CT for the detection of horizontal tooth root fracture. Oral Surg Oral Med Oral Pathol Oral Radiol Endod. 2009;108:e70–4.
30. Scarfe WC. All that glitters is not gold: standards for cone-beam computerized tomographic imaging. Oral Surg Oral Med Oral Pathol Oral Radiol Endod. 2011;111:402–8.
31. AAE and AAOMR Joint Position Statement. Use of Cone Beam Computed Tomography in Endodontics. J Endod 2015;41(9):1393–96.

3 The Impact of Cone Beam Computed Tomography in Nonsurgical and Surgical Treatment Planning

Mohamed I. Fayad and Bradford R. Johnson

Abstract

Development of an appropriate treatment plan follows diagnosis and could be considered the foundation of a successful outcome. Until the recent introduction of cone beam computed tomography (CBCT) for dental uses, two-dimensional radiographic imaging has been the standard for dental treatment planning. In endodontics, subjective history, clinical findings, and diagnostic imaging are all essential components of the preoperative diagnosis and treatment plan (Reit and Petersson Diagnosis of pulpal and periradicular disease. In: Bergenholtz G, Horsted-Bindslev P, Reit C, eds. Textbook of Endodontology. 2nd ed. Chichester/ West Sussex: Wiley-Blackwell; 2010. p. 235–53). Conventional two-dimensional radiographs provide a cost-effective, high-resolution image, which continues to be the most popular method of imaging today. However, the diagnostic potential of periapical radiographs is limited. Information may be difficult to interpret, especially when the anatomy and background pattern is complex (Kundel and Revesz, Am J Roentgenol 126:1233–1238; 1976). Recently, CBCT has been demonstrated to be a useful tool in a number of endodontic applications. The aim of this chapter is to compare the relative value of preoperative periapical radiographs and CBCT in the decision-making process in nonsurgical and surgical endodontic treatment planning.

M.I. Fayad, DDS, MS, PhD (✉) • B.R. Johnson, DDS, MHPE
Department of Endodontics, University of Illinois at Chicago, Chicago, IL, USA
e-mail: mfayad1@uic.edu; bjohnson@uic.edu

M. Fayad, B.R. Johnson (eds.), *3D Imaging in Endodontics*,
DOI 10.1007/978-3-319-31466-2_3

3.1 Introduction

Cone beam computed tomography (CBCT) is a diagnostic imaging modality which provides a three-dimensional image of the maxillofacial region and is capable of providing images at a relatively low radiation dose (please refer to Chap. 1) and with sufficient spatial resolution for applications in endodontic diagnosis and treatment planning. CBCT overcomes many limitations with conventional radiography such as early detection of invasive cervical resorption lesions, vertical root fractures, and three-dimensional evaluation of the root canal space and surrounding anatomy [3–10]. Diagnostic information directly influences treatment planning and clinical decisions. Accurate data leads to better treatment decisions and potentially more predictable outcomes [11]. While conventional periapical radiography has been used for many years as a diagnostic aid in endodontics, some studies now demonstrate the inferiority of periapical radiographs in detecting periradicular pathosis when compared to CBCT [12–16]. CBCT has been successfully used in endodontics and several recent studies have demonstrated the advantages of CBCT over periapical radiographs [17–21]. The effective radiation dose when using CBCT is higher than conventional two-dimensional radiography, and the benefit to the patient must therefore outweigh any potential risks of the additional radiation exposure. Radiation dose should be kept as low as reasonably achievable (ALARA) [22, 23]. The value of CBCT for endodontic diagnosis and treatment planning should be determined on an individual basis to assure that the benefit/risk assessment supports the use of CBCT.

Ee et al. (2014) compared differences in endodontic treatment planning decisions using either CBCT or periapical radiographs [24]. Thirty endodontic cases completed in a private endodontic practice were randomly selected to be included in this study. Each case was required to have a preoperative digital periapical radiograph and a CBCT scan. Three board-certified endodontists reviewed the 30 preoperative periapical radiographs. The evaluators were not involved in the initial diagnosis or treatment of these 30 cases. Two weeks later, the CBCT volumes were reviewed in random order by the same evaluators. The evaluators were asked to select a preliminary diagnosis and treatment plan based solely on interpretation of the periapical and CBCT images. Diagnosis and treatment planning choices were then compared to determine if there was a change in decision-making from viewing just the periapical radiograph to the CBCT scan. In addition, both decisions were compared to the reference standard (known diagnosis confirmed during nonsurgical treatment and/or surgical exploration or extraction). A difference in treatment plan between the two imaging modalities was recorded in 19 out of 30 cases (63.3 %) ($P = 0.001$) for examiner #1, 17 out of 30 cases (56.6 %) ($P = 0.012$) for examiner #2, and 20 out of 30 cases (66.7 %) ($P = 0.008$) for examiner #3 (Fig. 3.1). The problem of incorrect, delayed, or inadequate endodontic diagnosis and treatment planning places the patient at risk and could result in unnecessary or inappropriate treatment.

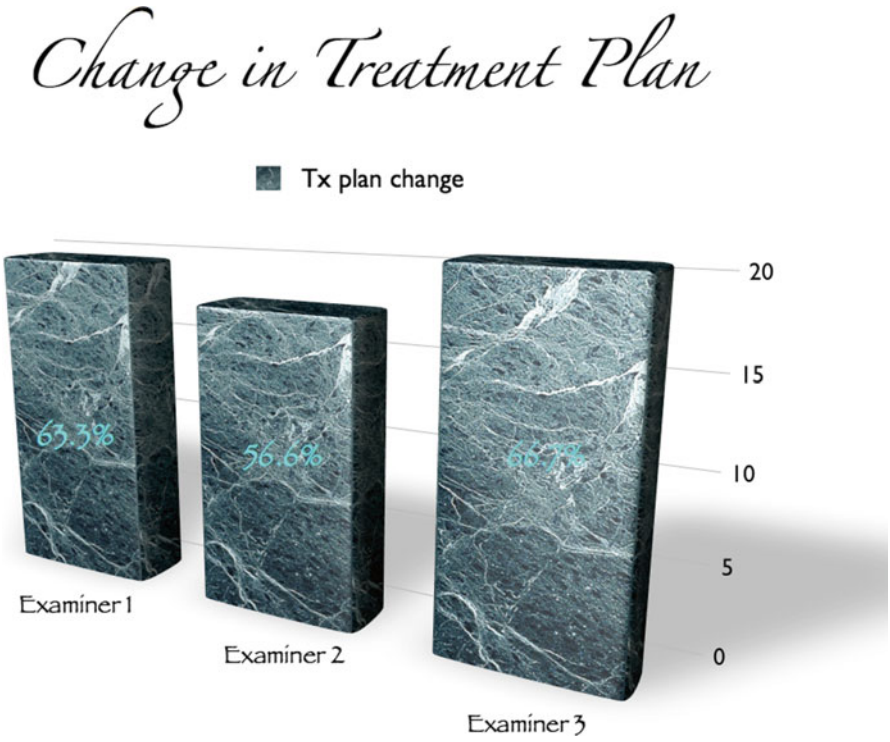

Fig. 3.1 Percentage of treatment plans changed by each of the three examiners after reviewing the CBCT

3.2 Implications for Clinical Practice

Under the conditions of the previous study [24], CBCT was a more accurate imaging modality for diagnosis of tooth anatomy and periradicular pathosis when compared to diagnosis using only periapical radiographs. An accurate diagnosis was reached in 36.6–40 % of the cases when using periapical radiographs compared to an accurate diagnosis in 76.6–83.3 % of the cases when using CBCT (Fig. 3.2). This high level of misdiagnosis is potentially clinically relevant, especially in cases of invasive cervical root resorption and vertical root fracture where a lack of early detection could lead to unsuccessful treatment and tooth loss. The previous study also demonstrates that the treatment plan may be directly influenced by information gained from a CBCT scan as the examiners altered their treatment plan after viewing the CBCT scan in 62.2 % of the cases overall (range from 56.6 to 66.7 %). This high number indicates that CBCT had a significant influence on the examiners' treatment plan.

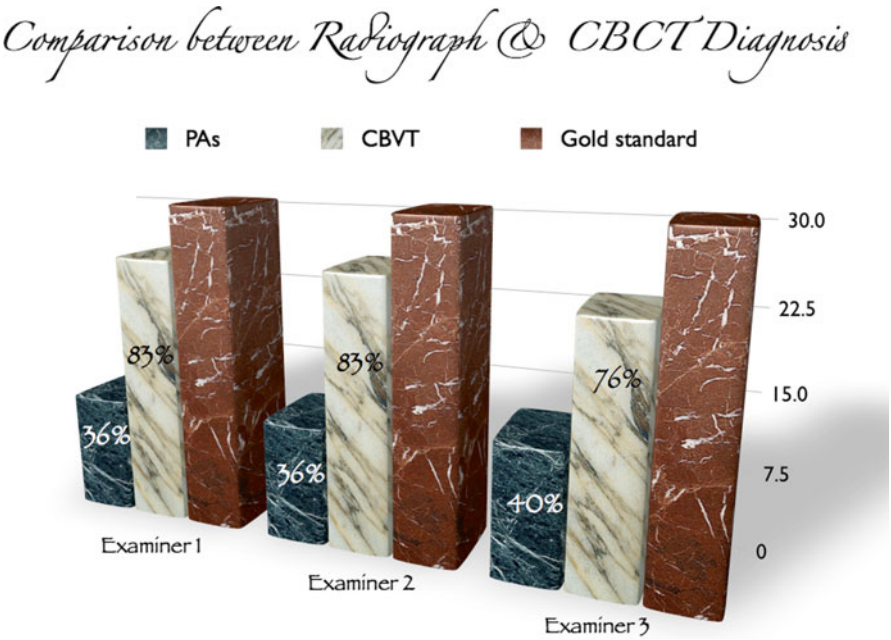

Fig. 3.2 Comparison between diagnosis after viewing a periapical radiograph vs. diagnosis after viewing CBCT for examiners 1, 2, and 3

It can be concluded that a preoperative CBCT scan provides more diagnostic information than a preoperative periapical radiograph and that this information can directly influence a clinician's treatment plan. Although imaging is a very important diagnostic tool in endodontics, it should always be used as an adjunct to the clinical exam. The addition of subjective and objective clinical findings to CBCT should allow for an even more accurate clinical diagnosis and appropriate treatment plan. Future studies may explore the potential added value of CBCT when provided along with relevant history and clinical findings.

Conclusion

Cone beam computed tomography overcomes many of the limitations of periapical radiography. The increased diagnostic information provided by the CBCT scan should result in more accurate diagnosis and improved decision-making for the management of complex endodontic problems. CBCT is a desirable addition to the endodontist's armamentarium. Examples of cases where CBCT made a significant difference in the treatment planning process are presented in Figs. 3.3, 3.4, 3.5, 3.6, 3.7, 3.8, 3.9, 3.10, 3.11, 3.12, 3.13, 3.14, 3.15, and 3.16.

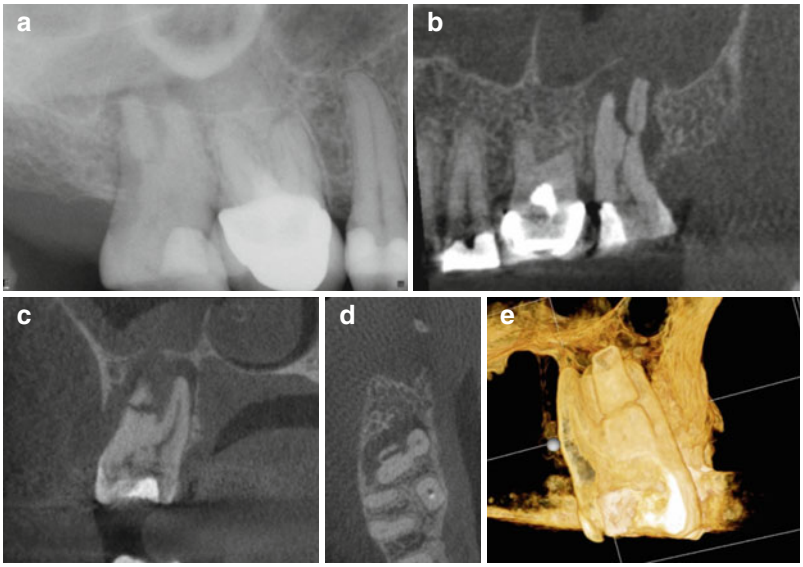

Fig. 3.3 (**a**) Periapical radiograph of tooth #2. The patient was referred for nonsurgical root canal treatment with a diagnosis of pulp necrosis and asymptomatic apical periodontitis. (**b**) Sagittal view showing the distobuccal root fracture. (**c**) Coronal view showing the unusual horizontal fracture of the distobuccal root. (**d**) Axial view of the apical one third showing a vertical buccopalatal root fracture. (**e**) 3D reconstruction showing the extent of the distobuccal root fracture

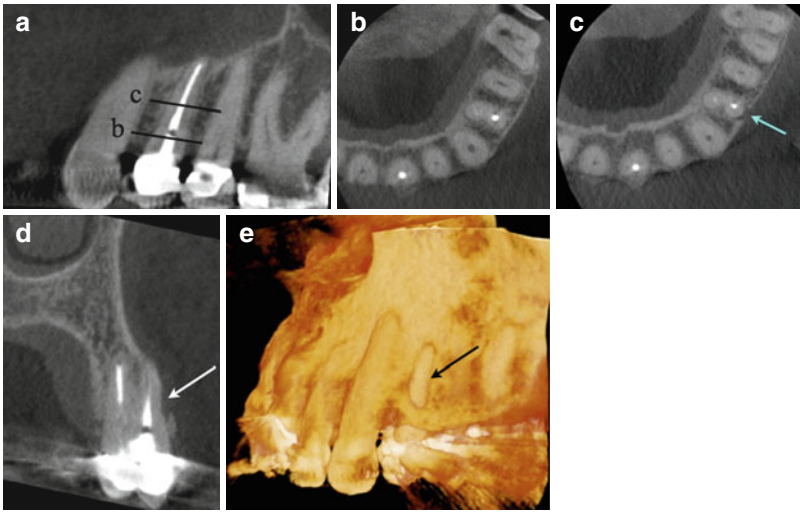

Fig. 3.4 Patient was referred for evaluation of pain to biting related to tooth #12. (**a**) Tooth # 12 had previous root canal treatment. Periodontal probing depths were WNL. The two *lines* correspond to the axial section views in (*b* and *c*). (**c**) demonstrates buccal loss of bone mid-root which is a pattern of bone loss (*blue arrow*) that is suggestive of VRF. (**d**) Coronal view of tooth #12 demonstrating mid-root buccal bone loss (*black arrow*). The intact collar of marginal bone has a tight periodontal fiber attachment, which explains why many roots with VRF do not probe in the early stages. (**e**) 3D reconstruction demonstrating the intact marginal bone and loss of buccal bone (*black arrow*). The buccal bone loss is usually adjacent to the VRF site

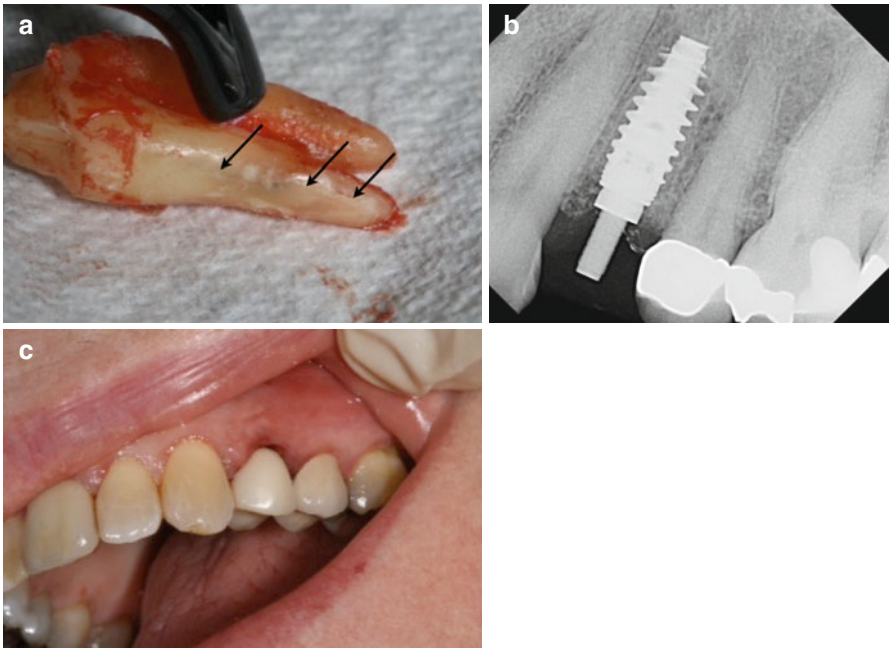

Fig. 3.5 Continuation of case in Fig. 3.4: (**a**) Tooth #12 after surgical extraction. The *black arrows* are the VRF which corresponds to the area of buccal bone loss in the CBCT. (**b**) An immediate implant was placed after the extraction. (**c**) Temporary restoration in place without loading the implant

Fig. 3.6 (**a**) Periapical radiograph of tooth #14. Symptoms included spontaneous pain and abnormal sensitivity to cold. After clinical examination and testing, the diagnosis was symptomatic irreversible pulpitis with symptomatic apical periodontitis. (**b**) CBCT sagittal view of tooth #14 showing an invasive cervical resorptive defect (ICR – Heithersay Class IV) that cannot be detected on the periapical radiograph. (**c**) Axial view demonstrating the palatal and mesial location of the defect. (**d**) Coronal view demonstrating the internal aspect of the ICR defect, rendering tooth #14 non-restorable. A change in treatment plan was made and the patient was referred for extraction

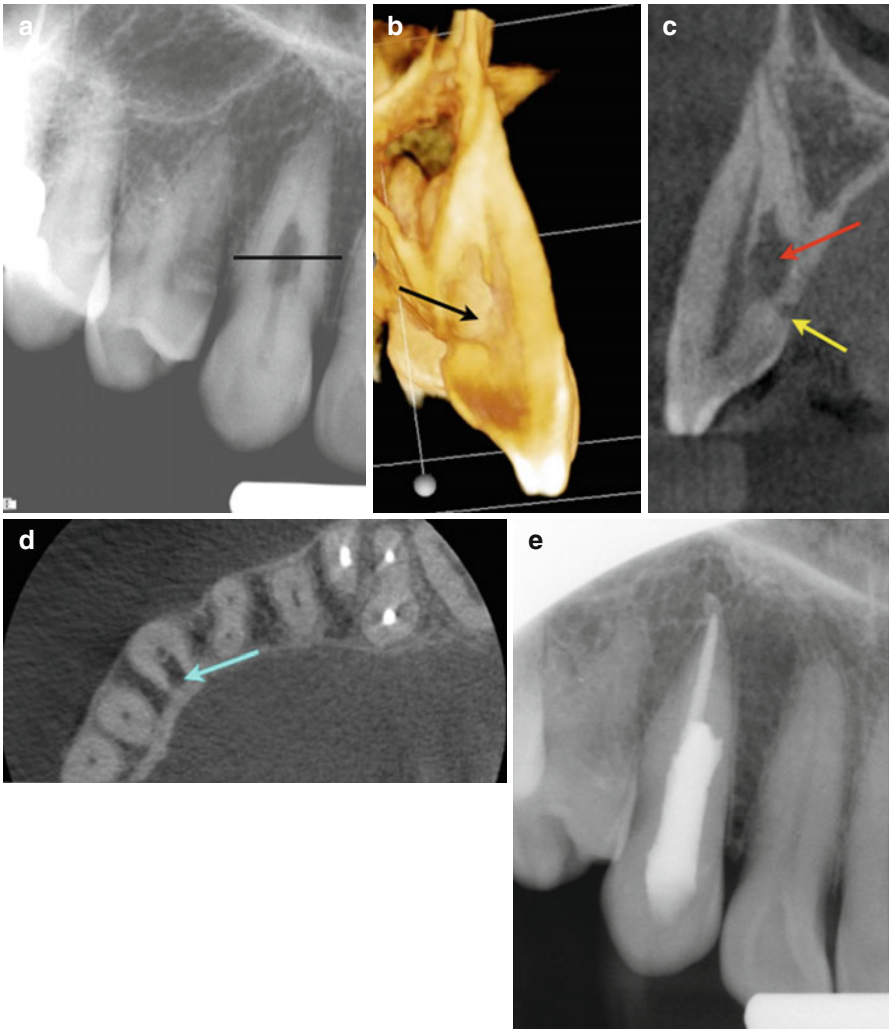

Fig. 3.7 (**a**) Periapical radiograph of tooth #6. The patient was referred for evaluation and treatment of an internal resorptive defect. The *line* corresponds to the axial section view in (**d**). (**b**) 3D reconstruction of the resorptive defect (*black arrow*). (**c**) Sagittal view of tooth #6 demonstrating the internal resorptive defect (*red arrow*), and confirming that the defect is an external ICR defect with initial entry at the cemento-enamel junction (*yellow arrow*). (**d**) Axial view demonstrating the ICR nature of the defect. Note in (**c**, **d**) that the pulp was not involved. (**e**) Postoperative radiograph of tooth #6 after root canal therapy and repair of the resorptive defect

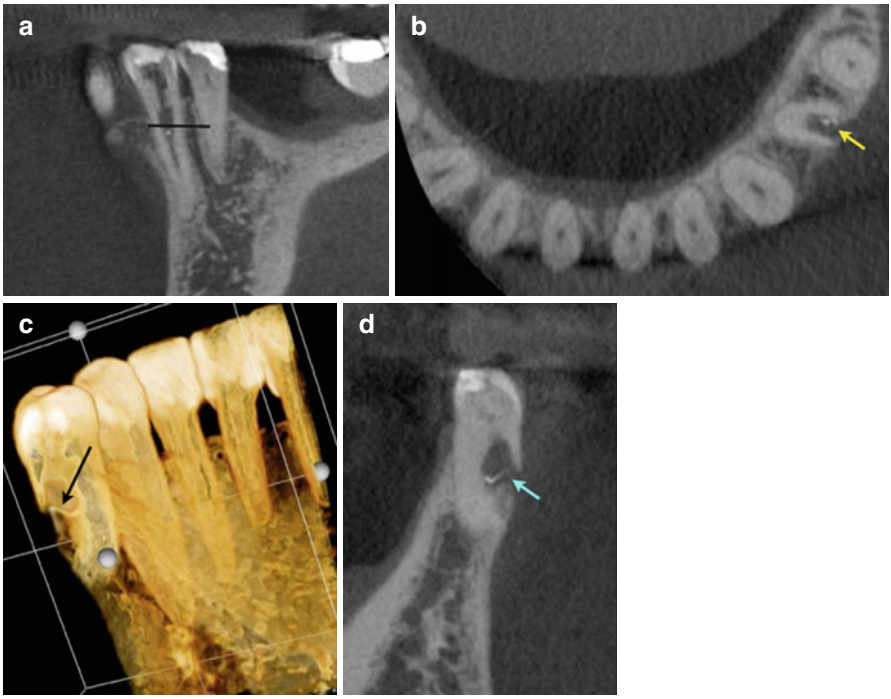

Fig. 3.8 (**a**) Periapical radiograph of tooth #21. The patient was referred for evaluation and treatment of an internal resorptive defect. The line corresponds to the axial section view in (**b**). (**b**) Axial view demonstrating the ICR nature of the defect (*yellow arrow*). (**c**) 3D reconstruction of the resorptive defect (*black arrow*). (**d**) Coronal view of tooth #21 demonstrating the external/internal resorptive defect (*blue arrow*). Note in (**b**, **c**, and **d**) the perforated root on the buccal aspect renders tooth #21 non-restorable. The treatment plan changed after reviewing the CBCT images

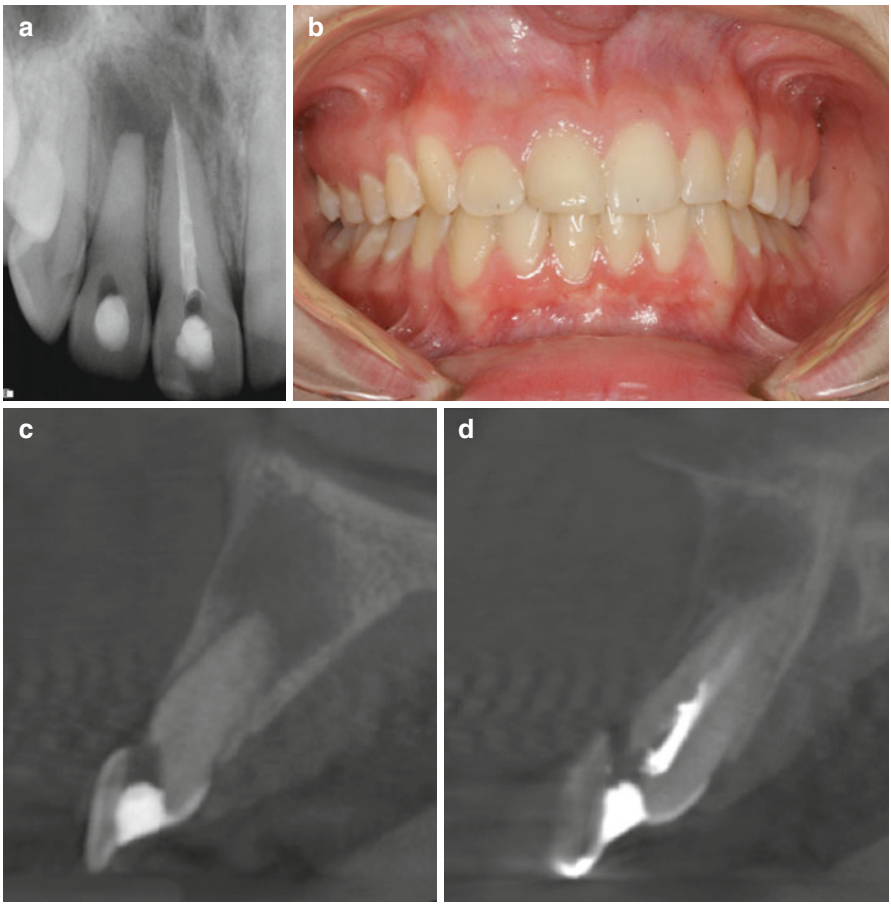

Fig. 3.9 (**a**) Periapical radiograph of teeth #7 and 8. Treatment was initiated on both teeth before referral to an endodontist. (**b**) Clinical picture showing normal soft tissue color and architecture. (**c**, **d**) are sagittal CBCT images showing facial perforations on teeth #7 and 8, respectively

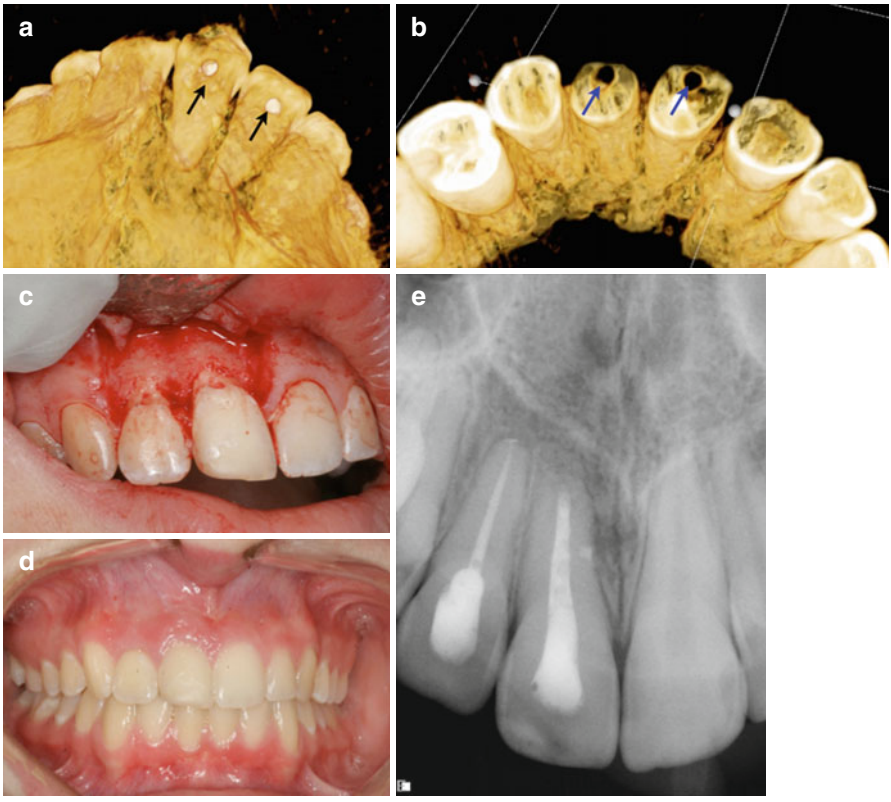

Fig. 3.10 Continuation of case in Fig. 3.9. (**a**, **b**) are 3D reconstructions showing the facial perforations (*black* and *blue arrows*) on teeth #7 and 8. (**c**) Reflection of a full-thickness mucoperiosteal flap confirmed the presence of perforations on both teeth. The perforations were repaired with Geristore™ (DenMat, Lompoc, CA). Both teeth were then treated via an orthograde approach with subsequent surgical root-end resection and filling of tooth #8. (**d**, **e**) One-year recall radiograph demonstrating soft and hard tissue healing

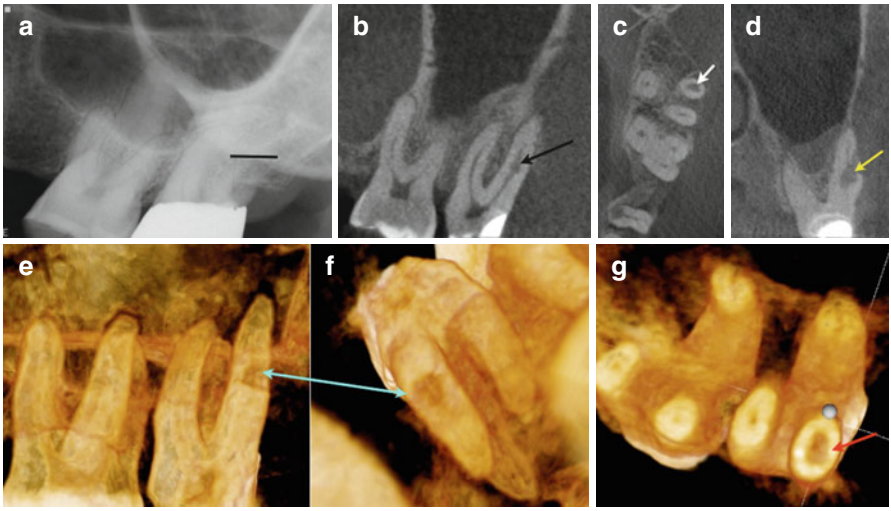

Fig. 3.11 (**a**) Periapical radiograph of tooth #15. The *line* corresponds to the axial section view in (**c**). Tooth #15 presented with pain on biting. The tooth was nonresponsive to cold, and periodontal probing depths were WNL. A diagnosis of necrotic pulp and symptomatic apical periodontitis was established. (**b**) Sagittal view of tooth #15 demonstrating an internal resorptive defect in mid-root of the distobuccal root (*black arrow*). (**c**) Axial view demonstrating the internal resorptive defect (*white arrow*). (**d**) Sagittal view demonstrating the internal resorptive defect and distobuccal root fracture (*yellow arrow*). (**e**, **f** and **g**) are 3D reconstructions of tooth #15 demonstrating the internal resorptive defect from different views (*blue and red arrows*)

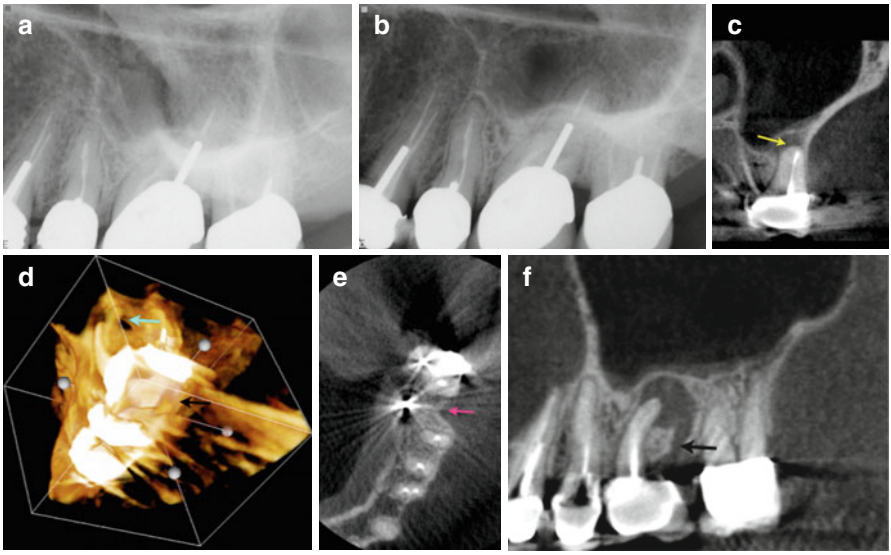

Fig. 3.12 Patient was referred for consultation and treatment of a previously treated tooth #14. Patient presented with a sinus tract related to tooth #14. (**a**, **b**) Periapical radiographs of tooth #14, mesial and distal angles, respectively. (**c**) Coronal view of the mesiobuccal root showing a missed mesiobuccal canal (*yellow arrow*). (**d**) 3D reconstruction showing a crestal bone defect (*blue arrow*). (**e**) Axial view showing a previous distobuccal root amputation site (*purple arrow*) that was not obvious on the periapical radiographs. (**f**) Sagittal CBCT view showing the crestal defect communicating with the periapical lesion (*black arrow*) and elevating the floor of the maxillary sinus with no evidence of sinus perforation

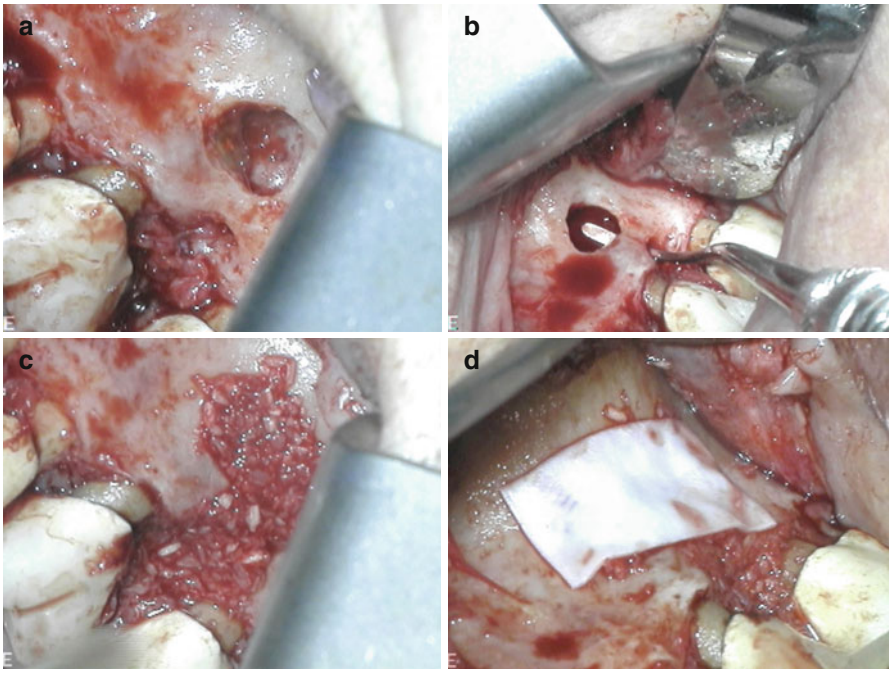

Fig. 3.13 Continuation of case in Fig. 3.12 (**a**) Clinical picture after flap reflection showing both crestal and periapical lesions. (**b**) Communication between both defects. (**c**) Both defects grafted with an EnCore™ combination allograft (Osteogenics Biomedical, Lubbock, TX). (**d**) CopiOs pericardium membrane (Zimmer, Warsaw, IN)

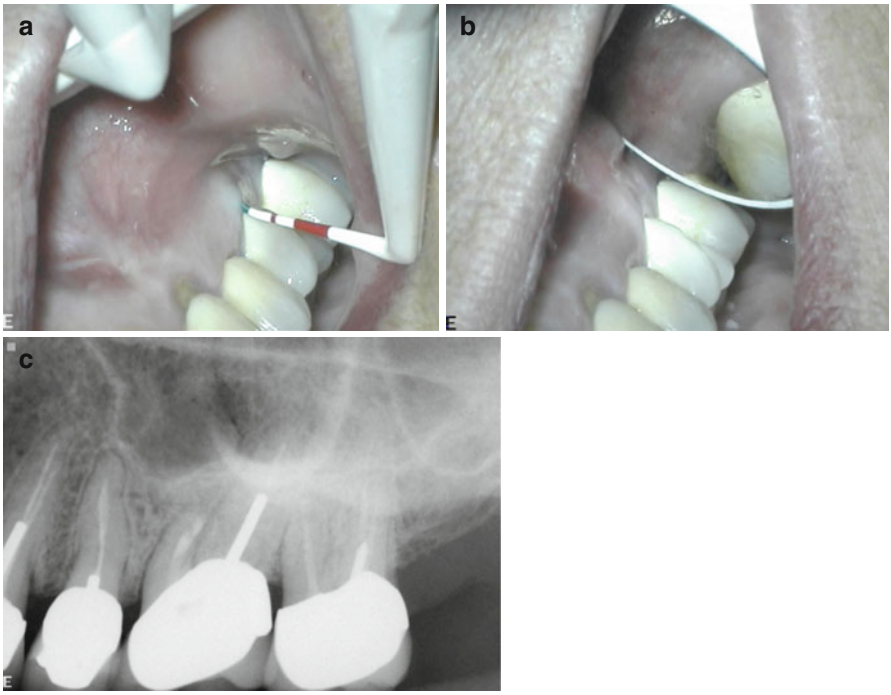

Fig. 3.14 Continuation of case in Figs. 3.12 and 3.13. (**a**, **b**) are clinical images of soft tissue healing after 1-year recall. (**c**) One-year recall radiograph

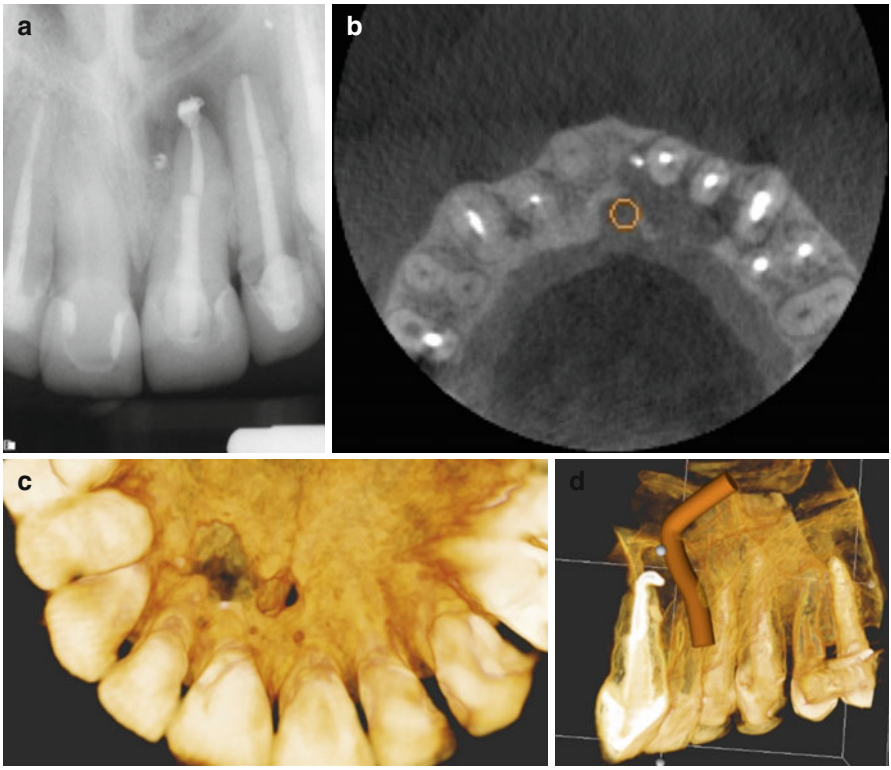

Fig. 3.15 (**a**) Periapical radiograph of the maxillary anterior region showing a periapical lesion associated with tooth #9. (**b**) Axial view showing the extent of the lesion, palatal plate perforation, and relationship of the nasopalatine neurovascular bundle to the periapical lesion. (**c**) Palatal view of the 3D reconstruction showing perforation of the palatal plate. (**d**) 3D reconstruction showing the nasopalatine bundle

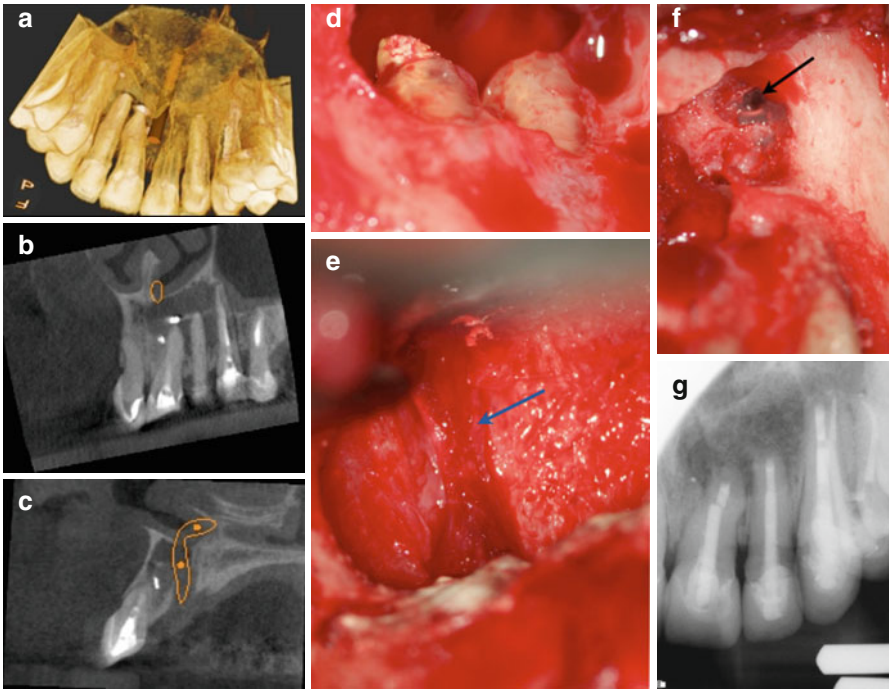

Fig. 3.16 Continuation of case in Fig. 13.15. (**a**) Palatal view CBCT reconstruction showing the exit of the nasopalatine bundle from the incisive canal. (**b**) Sagittal view showing periapical radiolucency involving teeth #9, 10, and 11. (**c**) Coronal view of the exit of the nasopalatine bundle from the incisive canal. (**d**) Periapical defect after degranulation showing the apices of teeth #9 and 10 before resection. (**e**) Clinical picture of the intact nasopalatine neurovascular bundle after degranulation (*blue arrow*). (**f**) Lateral wall of the maxillary sinus distal to tooth #11 (*black arrow*). (**g**) An immediate postoperative radiograph after grafting the through-and-through defect with Puros™ allograft (Zimmer Dental, Warsaw, IN) material and CopiOs™ membrane

References

1. Reit C, Petersson K. Diagnosis of pulpal and periradicular disease. In: Bergenholtz G, Horsted-Bindslev P, Reit C, editors. Textbook of endodontology. 2nd ed. Chichester/West Sussex: Wiley-Blackwell; 2010. p. 235–53.
2. Kundel HL, Revesz G. Lesion conspicuity, structured noise, and film reader error. Am J Roentgenol. 1976;126:1233–8.
3. Maini A, Durning P, Drage N. Resorption: within or without? The benefit of cone-beam computed tomography when diagnosing a case of an internal/external resorption defect. Br Dent J. 2008;9:135–7.
4. Patel S, Ricucci D, Durak C, Tay F. Internal root resorption: a review. J Endod. 2010;36:1107–21.
5. Estrela C, Bueno M, De Alencar AH, et al. Method to evaluate inflammatory root resorption by using cone beam computed tomography. J Endod. 2009;35:1491–7.
6. Hassan B, Metska ME, Ozok AR, et al. Detection of vertical root fractures in endodontically treated teeth by a cone beam computed tomography scan. J Endod. 2009;35:719–22.
7. Bernardes RA, de Moraes IG, Húngaro Duarte MA, et al. Use of cone-beam volumetric tomography in the diagnosis of root fractures. Oral Surg Oral Med Oral Pathol Oral Radiol Endod. 2009;108:270–7.
8. Edlund M, Nair MK, Nair UP. Detection of vertical root fractures by using cone-beam computed tomography: a clinical study. J Endod. 2011;37:768–72.
9. Fayad MI, Ashkenaz PJ, Johnson BR. Different representations of vertical root fractures detected by cone-beam volumetric tomography: a case series report. J Endod. 2012;38:1435–42.
10. Michetti J, Maret D, Mallet JP, Diemer F. Validation of cone beam computed tomography as a tool to explore root canal anatomy. J Endod. 2010;36:1187–90.
11. Liang YH, Li G, Wesselink PR, Wu MK. Endodontic outcome predictors identified with periapical radiographs and cone-beam computed tomography scans. J Endod. 2011;37:326–31.
12. de Paula-Silva FW, Wu MK, Leonardo MR, et al. Accuracy of periapical radiography and cone-beam computed tomography scans in diagnosing apical periodontitis using histopathological findings as a gold standard. J Endod. 2009;35:1009–12.
13. Velvart P, Hecker H, Tillinger G. Detection of the apical lesion and the mandibular canal in conventional radiography and computed tomography. Oral Surg Oral Med Oral Pathol Oral Radiol Endod. 2001;92:682–8.
14. Stavropoulos A, Wenzel A. Accuracy of cone beam dental CT, intraoral digital and conventional film radiography for the detection of periapical lesions: an ex vivo study in pig jaws. Clin Oral Investig. 2007;11:101–6.
15. Nakata K, Naitoh M, Izumi M, et al. Effectiveness of dental computed tomography in diagnostic imaging of periradicular lesion of each root of a multirooted tooth: a case report. J Endod. 2006;32:583–7.
16. Lofthag-Hansen S, Huumonen S, Grondahl K, Grondahl HG. Limited cone-bean CT and intraoral radiography for the diagnosis of periapical pathology. Oral Surg Oral Med Oral Pathol Oral Radiol Endod. 2007;103:114–9.
17. Cotton TP, Geisler TM, Holden DT, et al. Endodontic applications of cone-beam volumetric tomography. J Endod. 2007;33:1121–32.
18. Patel S, Dawood A, Whaites E, Pitt FT. New dimensions in endodontic imaging: part 1. Conventional and alternative radiographic systems. Int Endod J. 2009;42:447–62.
19. Patel S. New dimensions in endodontic imaging: part 2. Cone beam computed tomography. Int Endod J. 2009;42:463–75.
20. Scarfe WC, Farman AG, Sukovic P. Clinical applications of cone-beam computed tomography in dental practice. J Can Dent Assoc. 2006;72:75–80.
21. Nair MK, Nair UP. Digital and advanced imaging in endodontics: a review. J Endod. 2007;33:1–6.

22. Farman AG, Farman TT. A comparison of 18 different x-ray detectors currently used in dentistry. Oral Surg Oral Med Oral Pathol Oral Radiol Endod. 2005;99:66–71.
23. Farman AG. ALARA still applies. Oral Surg Oral Med Oral Pathol Oral Radiol Endod. 2005;100:395–7. aminers 1, 2 and 3 respectively.
24. Ee J, Fayad MI, Johnson BR. Comparison of endodontic diagnosis and treatment planning decisions using cone-beam volumetric tomography versus periapical radiography. J Endod. 2014;40:910–6.

Three-Dimensional Evaluation of Internal Tooth Anatomy

4

William J. Nudera

Abstract

The study of human tooth anatomy is fundamental to clinical endodontics. Several histologic methods used to evaluate tooth anatomy have been described for the purpose of identification and categorization of various root and root canal types. In addition, multiple articles have attempted to classify root and root canal configuration as it relates to tooth type, tooth location, root type, gender, geographic location, and ethnic background. For decades, two-dimensional radiographic images captured at various horizontal and vertical angulations have been the primary method for clinical evaluation of tooth anatomy prior to endodontic treatment. Attempting to evaluate multidimensional anatomy from planar imaging has significant limitations. Technological advancements in three-dimensional tomographic imaging have given rise to a more accurate method for the clinical evaluation of tooth anatomy. Cone beam computed tomography (CBCT) provides a nondestructive real-time capture of three-dimensional anatomic and morphologic information. A short acquisition time and a level of detail equivalent to that of in vitro tooth sectioning make CBCT imaging the first, and currently only, practical method available for the accurate, undistorted, chairside evaluation of tooth anatomy in three spatial planes prior to root canal therapy.

4.1 Introduction

A thorough knowledge of root anatomy and morphology is essential in clinical endodontics and a requirement for a successful endodontic outcome. Improper working knowledge of root anatomy has been said to rank second only to errors in diagnosis

W.J. Nudera, DDS, MS
Department of Endodontics, Clinical Faculty at the University of Illinois at Chicago, Collage of Dentistry, Chicago, IL, USA
e-mail: nudera@comcast.net

M. Fayad, B.R. Johnson (eds.), *3D Imaging in Endodontics*,
DOI 10.1007/978-3-319-31466-2_4

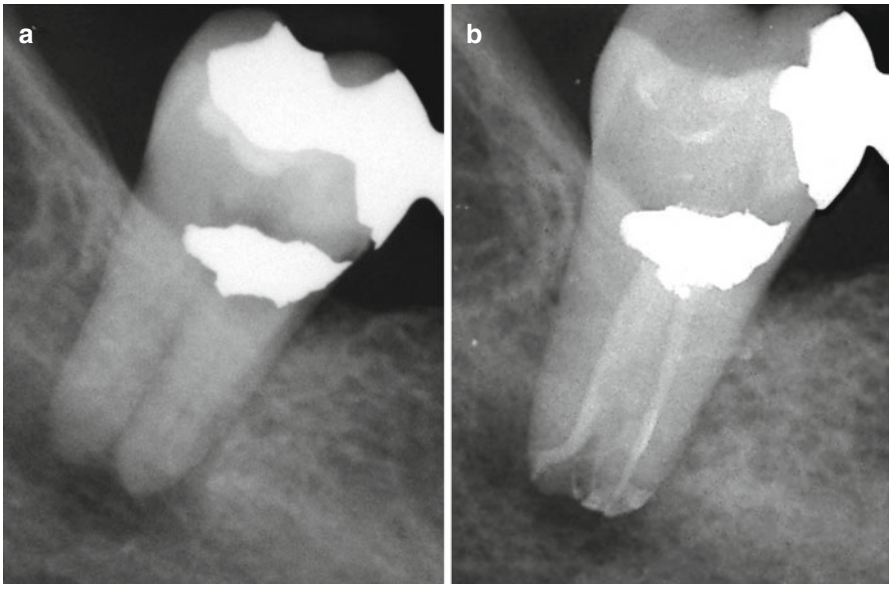

Fig. 4.1 Periapical radiograph of a right mandibular second molar with associated apical pathosis (**a**) and the post-endodontic periapical radiograph with obturation material demonstrating the complex nature of the root canal system (**b**)

and treatment planning as a cause of persistent apical pathosis [1]. The clinical application of CBCT imaging has impacted virtually every aspect of endodontics. The ability to three-dimensionally visualize a tooth prior to endodontic treatment is a reality with this technology. The complexity of the root canal system has been well documented over the last century (example of complex root anatomy: Fig. 4.1). A detailed description of the complex anatomical structure first appeared in the German dental literature in 1917 and later translated for republication in the *Journal of the American Dental Association* in 1921 [2]. In this classic publication, Walter Hess cites the independent observations of Preiswerk followed by Fischer who indicated a "wide differentiation" in canal configurations and root forms of specific teeth. Hess was the first to describe the relationship of the dental pulp and its conformity with the external roots, suggesting a wide variety in the number and form of root canal systems, "thus complicating the picture greatly" [2].

4.2 Methods for Studying Tooth Anatomy

Methods used to evaluate tooth and root anatomy can be categorized as in vitro or in vivo. In vitro methods allow for detailed microscopic and histologic examination of teeth in all dimensions and include demineralization, clearing, sectioning, modeling, scanning electron microscopy, and micro-computed tomography [3]. In vivo methods have more clinical implications and consist of traditional radiography, spiral computed tomography, optical coherence tomography, tuned aperture computed tomography,

cone beam computed tomography, ultrasound, and magnetic resonance imaging. In vitro histologic evaluation via canal staining and tooth clearing is considered to be the gold standard when evaluating root canal anatomy and morphology [4, 5]. However, these methods are destructive and limited to ex vivo ("bench top") examination. The accuracy of CBCT has been reported to be equivalent to that of histologic sectioning and staining for practical clinical purposes (i.e., identifying canals and unusual anatomy). A study directly comparing tomographic scans to that of the histologic sectioning of 152 maxillary molar teeth found identical canal configurations using the two methods [6]. A 2010 study of 233 tooth sections found a "strong to very strong correlation" between CBCT imaging and histologic sections [7]. Neelakantan et al. compared the efficacy of six different imaging methods to that of canal staining and clearing. CBCT scanning was reported to be as accurate in the identification of root canal systems as the modified staining and clearing techniques and significantly more accurate than conventional radiographic methods [8]. In another study comparing traditional radiographic techniques to that of CBCT scanning and clinical sectioning, Blattner et al. reported that CBCT scanning was a reliable method for canal detection and represents a highly accurate, in vivo method for the evaluation of tooth anatomy equivalent to that of the histologic gold standard [9] (Fig. 4.2).

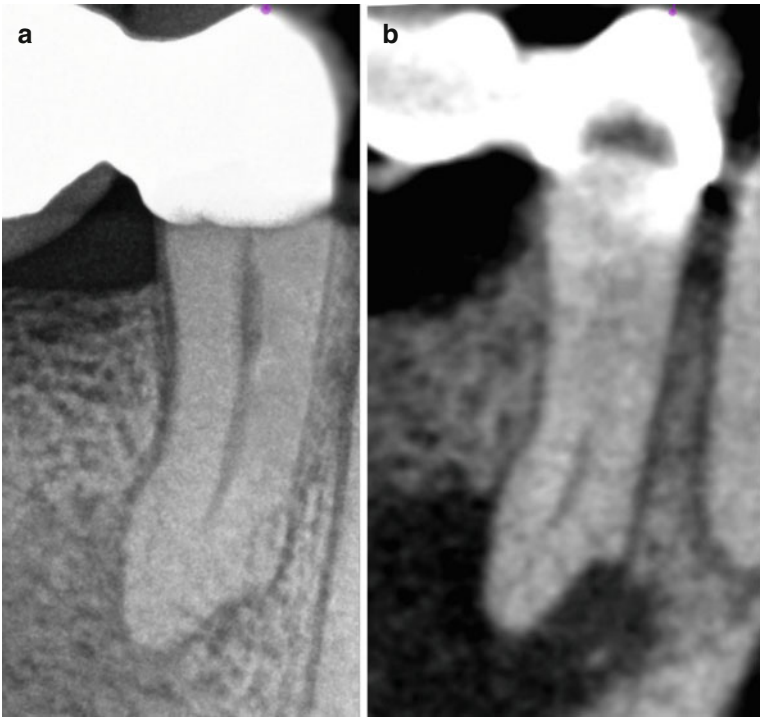

Fig. 4.2 Periapical radiograph of a right mandibular first premolar (**a**) with a corresponding sagittal CBCT slice demonstrating visible complex internal anatomy in the apical third of the root canal system (**b**)

4.3 Clinical Methods for the Evaluation of Tooth Anatomy

4.3.1 Common Tooth Forms and Anatomical Landmarks

The collective information gained from numerous anatomic and morphologic studies can be applied clinically by establishing a thorough knowledge of commonly known root variations. Average statistics for permanent human teeth with respect to type and location as well as common canal configurations can be found in many published endodontic texts. In addition, several studies have classified various canal configurations identified within a single root [3, 10]. Studies have also attempted to identify common morphologic and anatomic features of roots and root canal systems as they relate to gender, ethnicity, and geographic location [11, 12].

A study examining external landmarks of teeth and their association with internal anatomic features found specific observable patterns relating the pulp chamber to the clinical crown as well as the canal orifices to the pulp chamber floor. Seven distinct features were observed on the pulpal floor that provide clues as to the location of the canal orifices. The authors of this study proposed nine "laws" to assist in the identification root canal anatomy during endodontic treatment [13].

Studies that attempt to categorize tooth anatomy and morphology can only provide clinical treatment recommendations and guidelines as they relate to general circumstances. These guidelines are based on weighted averages and common observations. Averages are useful when studying characteristics of populations, but of limited predictive value for treatment of the individual patient. CBCT can capture information, which previously required multiple radiographs, in a more precise way than is possible with two-dimensional radiographs.

CBCT imaging overcomes several limitations found with conventional radiographic methods. Dimensionally accurate image acquisition and viewing in all three spatial planes eliminates superimposition of multiple roots and/or surrounding anatomic structures and provides more sensitivity with regard to the detection of periradicular pathosis, root resorption, and root fractures [14]. Visualization of multidimensional root curvature allows for precision treatment planning and predictable canal management [15] (Fig. 4.3). Geometrically accurate measurement capabilities assist in the determination of root length as well as establish precise intra- and inter-canal distance relationships [16]. Additionally, information obtained from a cone beam scan prior to endodontic treatment has been reported to improve diagnostic capabilities and prompt endodontic treatment plan changes [17, 18].

A preoperative CBCT scan provides an undistorted reconstruction of a tooth's internal and external morphologic features. The ability to detect more roots and root canals with greater accuracy and higher frequency when a CBCT scan is available has been reported [19] (Fig. 4.4). Figure 4.5 represents the periapical radiographs of two different maxillary second molars and their corresponding axial CBCT slices (below). Although both teeth appear radiographically similar, the corresponding axial CBCT slices reveal two very different morphologic root features and canal configurations.

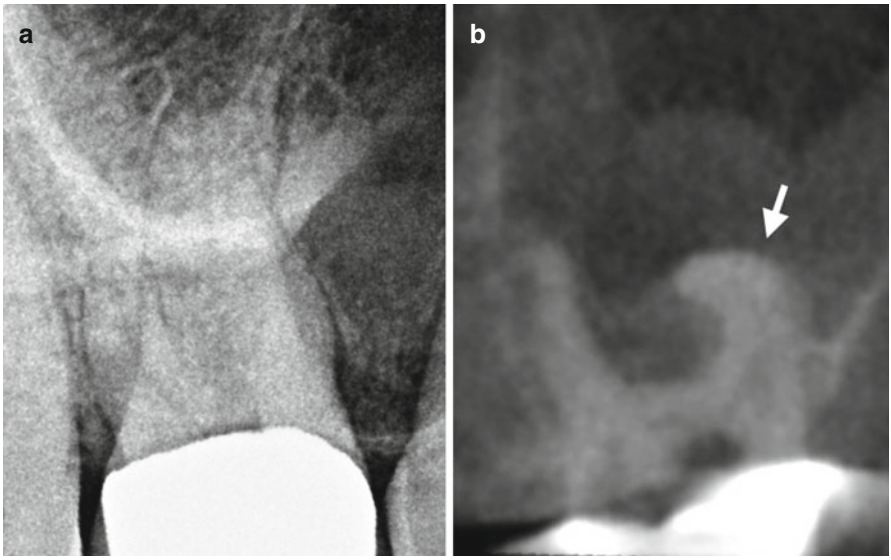

Fig. 4.3 Periapical radiograph of a maxillary right first molar (**a**) with a corresponding coronal CBCT slice demonstrating a significant curvature of the mesiobuccal root in the buccopalatal plane (*white arrow*) (**b**)

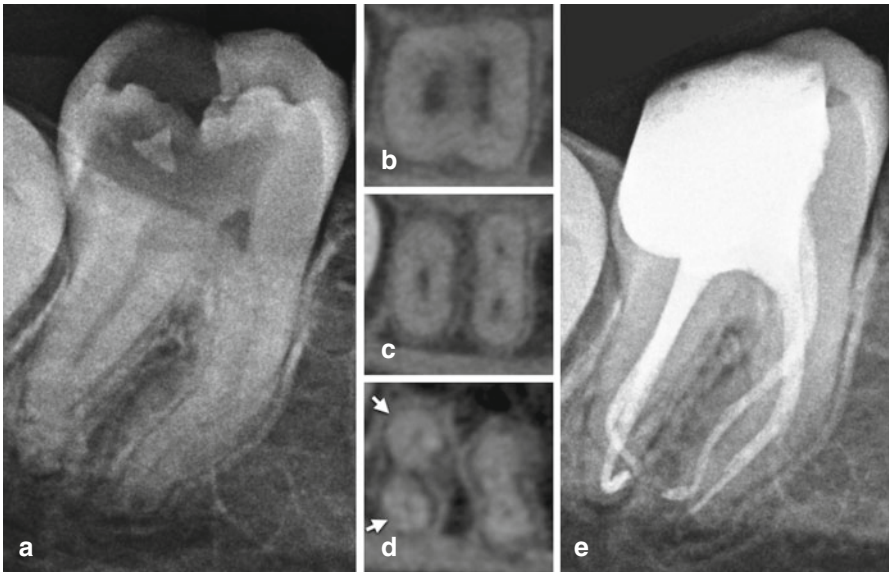

Fig. 4.4 Preoperative periapical radiograph of a right mandibular second molar (**a**) with corresponding axial CBCT slices captured from the coronal third (**b**), mid-root (**c**), and apical third (**d**). The axial CBCT slices demonstrate two distinct mesial canals as well as a division of the distal root in the apical third (*white arrows*). The post-endodontic radiograph demonstrates all identified root canals treated (**e**)

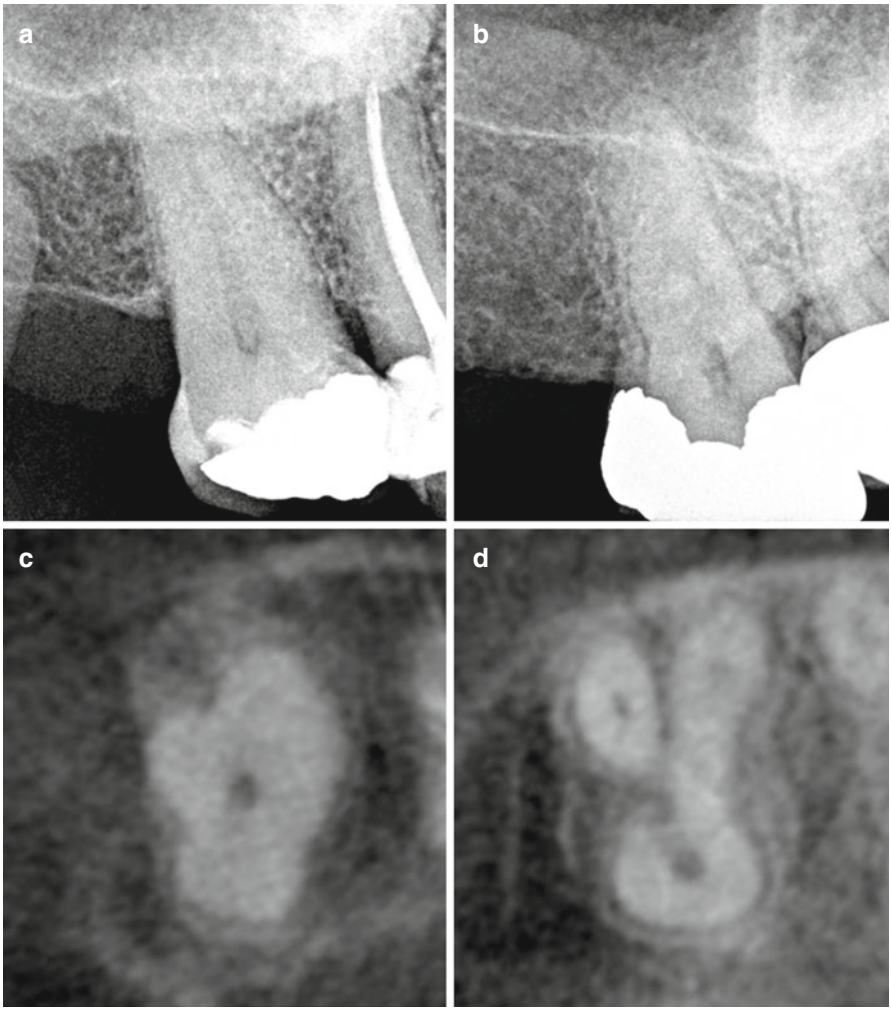

Fig. 4.5 Preoperative periapical radiographs of two different right maxillary second molars with conically shaped roots (**a**, **b**) and their corresponding axial CBCT slices (*below*) demonstrating different external root forms and different internal canal configurations (**c**, **d**)

4.3.2 Endodontic Access Design

Gaining access to the pulp chamber to facilitate the identification of all canal orifices represents the first technical step in root canal treatment that irreversibly alters tooth structure. Traditional access designs tend to be somewhat standardized per tooth type and are typically depicted in most texts with easily identifiable canal orifices at the base of a large pulpal floor. Many teeth requiring endodontic treatment present with pulp chambers that have significant alterations in volumetric space and shape due to excess deposits of tertiary dentin in response caries,

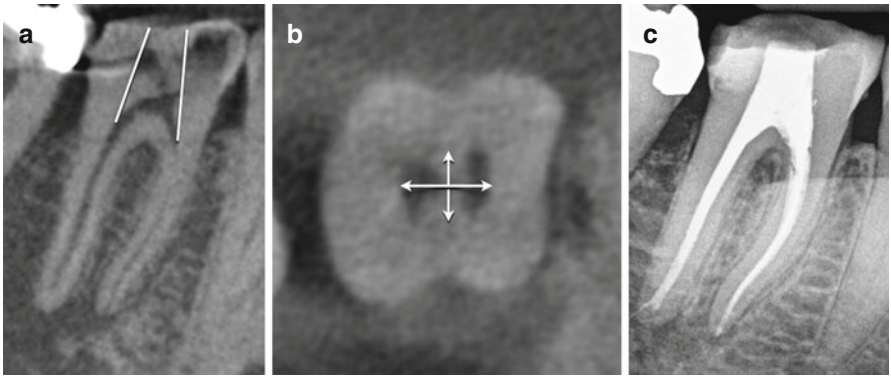

Fig. 4.6 Treatment plan for a conservative access design of a mandibular right first molar based on the exact pulp chamber morphology as determined via the CBCT scan. The sagittal CBCT slice demonstrates the planned minimum mesial/distal outline form (*white lines*) (**a**), and the axial CBCT slice captured at the level of the canal orifices demonstrates the planned mesial, distal, buccal, and lingual access extensions (**b**). The post-endodontic radiograph demonstrates a minimal access preparation and appropriate root canal system management (**c**)

bacterial ingress, dental procedures, and/or surface tooth loss over time. The integration of modern endodontic techniques and technology can assist in shaping the endodontic access based on the specific pulp chamber morphology of the tooth being treated.

Traditional access designs are treatment planned from parallel periapical and bitewing radiographs as well as clinical anatomic landmarks. This limits radiographic access design to a single plane and creates reliance upon the suggested access design standardizations. A more conservative and customized endodontic access can be designed from the anatomical information available on the CBCT volume. Precision vertical depth measurements can be determined from the occlusal plane to multiple levels within the pulp chamber in both the coronal and sagittal planes. Additionally, the lateral extension of the access as it relates to the occlusal surface can be determined from measurements available in the axial plane (Fig. 4.6). Maintaining a conservative endodontic access minimizes the unnecessary removal of tooth structure and may improve overall fracture resistance [20].

4.3.3 Evaluation of Complex Roots and Root Canal Variations

Many anatomic and morphologic variations in tooth anatomy exist within the global population. A detailed description of common statistical anatomic averages per tooth type can be found in previously published endodontic texts. In vivo identification of more complex anatomical root forms and root canal configurations can be best observed using CBCT imaging. Some variations have been reported to occur at higher frequencies and have been associated with specific geographic populations and/or ethnic heritage [11]. Multiple published case reports demonstrate the

significant advantages of CBCT over traditional radiographic imaging for the detection and management of a wide variety of anatomic and morphologic tooth and root variations [21].

4.4 Maxillary Molar Teeth

4.4.1 The Mesiobuccal Root Complex

The mesiobuccal root complex of the maxillary first permanent molar is one of the most well-documented and studied root canal systems in the endodontic literature. It is generally broad buccolingually with prominent depressions on the mesial and distal surfaces and usually contains two canals. One ex vivo study reported the presence of two mesiobuccal canals in the coronal half of maxillary first molars to be as high as 95.2 % with 71 % having separate apical portals of exit [22]. Similar variations occur in the maxillary second molars, although with less reported frequency [23]. The clinical detection and treatment of second mesiobuccal canals (MB2) can be enhanced with the acquisition of a CBCT scan [19]. The presence of an additional root and/or root canal can often be detected by studying the buccopalatal extent of the mesiobuccal root complex in the axial and coronal planes (Fig. 4.7).

4.4.2 Multiple Palatal Roots and Canals

A maxillary permanent molar with four roots and/or four root canals is not unusual when the additional root or root canal is located within the mesiobuccal root complex, but occasionally an additional root or root canal can be associated with the palatal root (Figs. 4.8 and 4.9). This morphologic variation has been suggested to occur more frequently in maxillary second molars with a reported frequency of 0.4–1.4 % [28, 29]. A CBCT scan can aid in the recognition of this rare anatomical variation as well as determine the exact location of the additional canal orifice for maximum conservation of tooth structure during endodontic access preparation.

4.5 Mandibular Molar Teeth

4.5.1 Radix Entomolaris and Radix Paramolaris

Mandibular permanent molars will occasionally present with an additional separate root located either to the lingual (radix entomolaris) or to the buccal (radix paramolaris). The literature suggests that the highest incidence of these morphologic variations is present in populations with Mongoloid ancestry (such as Chinese, Eskimo, and Native Americans) and occurs at a frequency of 5–40 % [24]. Although traditional two-dimensional imaging at various angles can reveal clues as to the presence of these additional roots, exposing the anatomic location of the additional canal

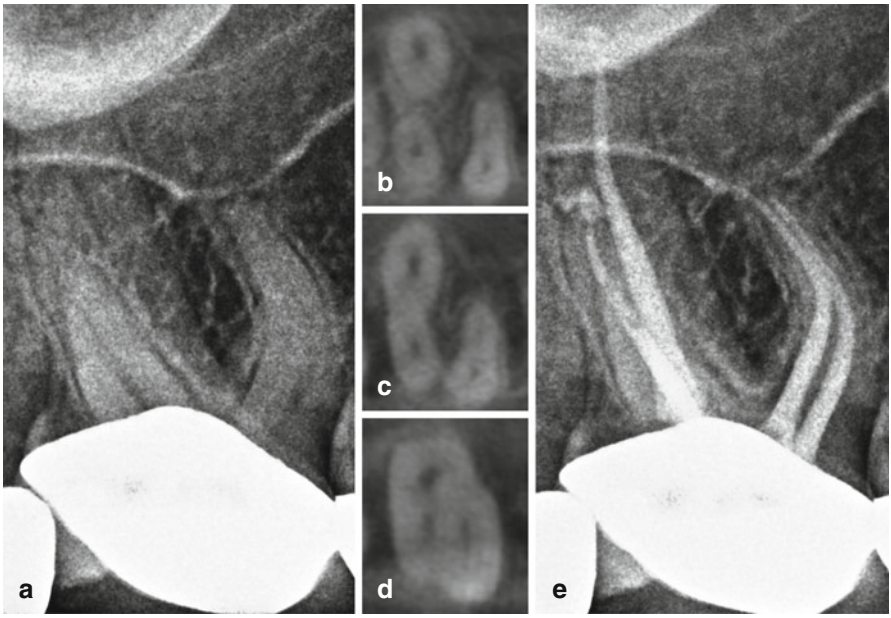

Fig. 4.7 Preoperative periapical radiograph of a maxillary right first molar (**a**) with corresponding axial CBCT slices captured from the apical third (**b**), mid-root (**c**), and coronal third (**d**) demonstrating a mesiobuccal root with two identifiable root canal systems. The post-endodontic periapical radiograph demonstrates all identified root canals treated (**e**)

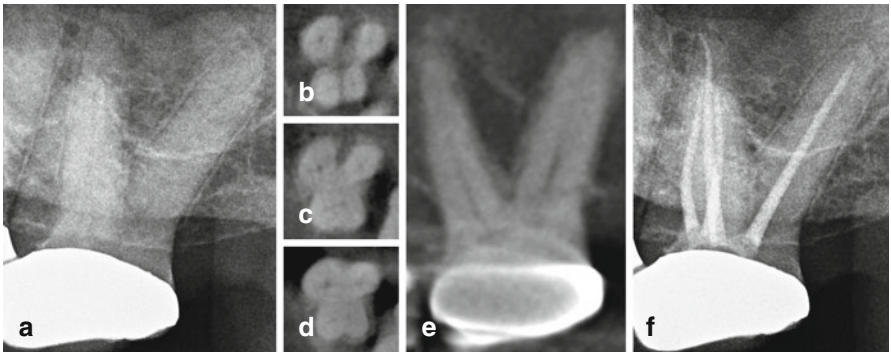

Fig. 4.8 Preoperative periapical radiograph of a maxillary left second molar (**a**), with corresponding axial CBCT slices captured from the apical third (**b**), mid-root (**c**), and coronal third (**d**) demonstrating four separate canals and a morphologic root division into four separate roots. The sagittal CBCT slice demonstrates two separate palatal roots (**e**). The post-endodontic periapical radiograph demonstrates all identified root canal systems treated (**f**)

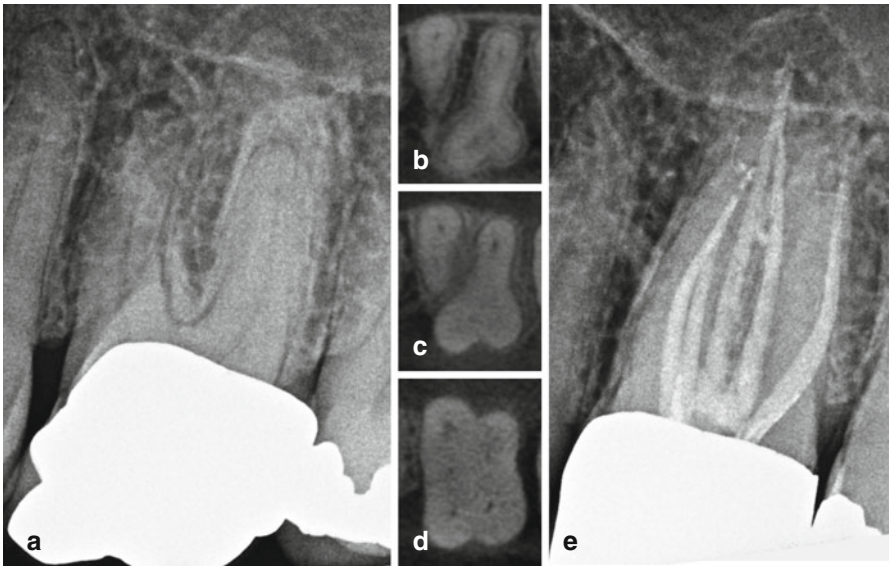

Fig. 4.9 Preoperative periapical radiograph of a maxillary left first molar (**a**) with corresponding axial CBCT slices captured from the apical third (**b**), mid-root (**c**), and coronal third (**d**) demonstrating five separate root canal systems (two canals in the mesiobuccal root and two canals in the palatal root). The post-endodontic periapical radiograph demonstrates all identified root canal systems treated (**e**)

orifice during endodontic access can pose a clinical challenge. A CBCT scan will not only confirm the presence of these additional roots but also assist in determining the exact location of the canal orifice so that a proper access design can be planned (Fig. 4.10).

4.5.2 C-Shaped Canal

A "C-shaped" root canal system is considered to be a variation in root morphology that causes the root to take on the shape of the letter "C" when viewed in cross section. The canals may or may not be separate. C-shaped canal configurations vary greatly among different ethnicities and have been reported to be as high as 30 % among individuals of Asian descent. This variation occurs most often in mandibular second molars (Fig. 4.11), but has also been documented in maxillary first molars (Fig. 4.12), mandibular first and third molars, and mandibular premolars [25].

4.5.3 Isthmus Canals

An isthmus is often present between the buccal and lingual canals in mesial and/or distal roots of mandibular permanent molar teeth. Occasionally, an additional canal

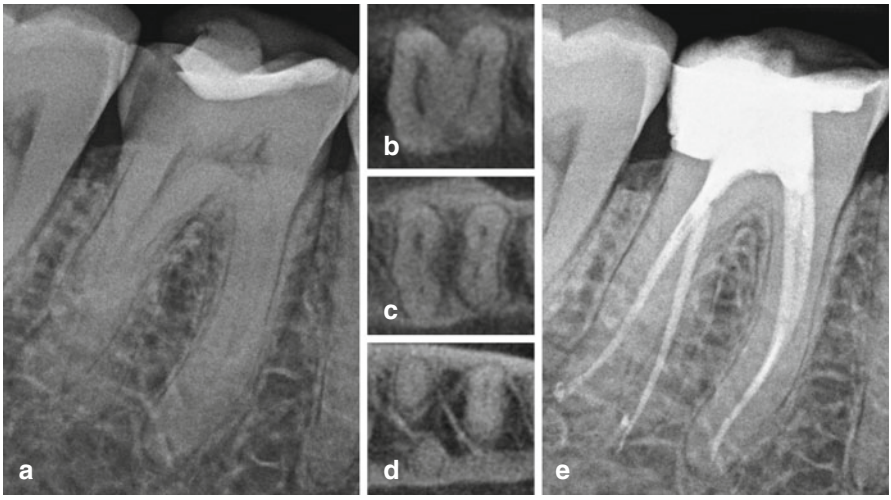

Fig. 4.10 Preoperative periapical radiograph of a mandibular right first molar with an anatomical presentation consistent with radix entomolaris (**a**). Axial CBCT slices captured from the coronal third (**b**), mid-root (**c**), and apical third (**d**) confirm the presence of a separate root positioned to the lingual. Post-endodontic periapical radiograph demonstrates all identified root canal systems treated (**e**)

can be identified and treated within this isthmus space. When present, these canals are referred to as middle mesial and/or middle distal canals. Middle mesial canals have been reported to occur at rate as high as 15 %, with 6.7 % being identified as independent (Fig. 4.13). The incidence of a middle distal canal is reported to be much less, with the highest frequency reported at 3 % (Fig. 4.14). The usefulness of CBCT imaging to identify and manage such canals has been reported in the literature [26, 27].

4.6 Maxillary Premolar Teeth

Maxillary permanent premolar teeth are generally broad buccolingually and narrow mesiodistally. They can present with two separate roots containing one canal per root or one broad root containing one or multiple canals. When one broad root is present, the corresponding internal anatomy can consist of a single ribbon-shaped canal or one of several documented multiple canal classifications with various levels of canal division and separate apical foramina. On occasion these teeth can present with a third root and/or third root canal. The frequency for this anatomic variation has been reported to be as high as 6 % for maxillary permanent first premolars and 3 % for maxillary permanent second premolars [28]. The addition of a CBCT scan can help determine the class of canal division, the presence of bifidity or trifidity, and the exact level at which the canal division(s) occurs (Fig. 4.15).

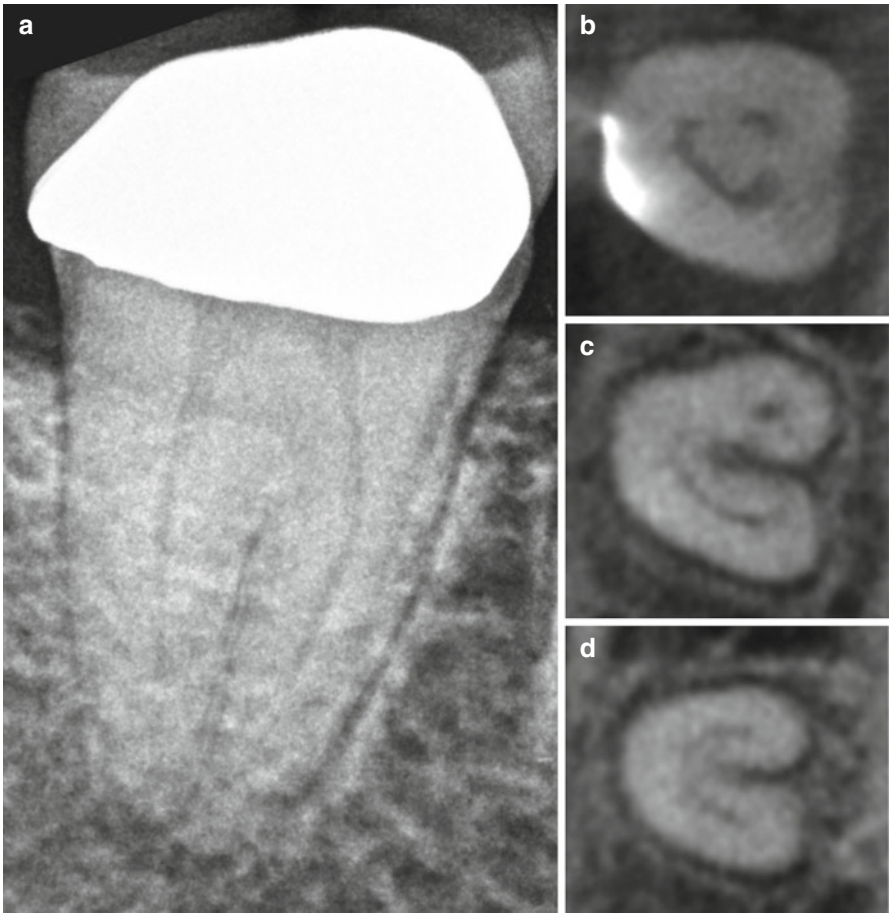

Fig. 4.11 Preoperative periapical radiograph of a mandibular right second molar (**a**) with corresponding axial CBCT slices captured from the coronal third (**b**), mid-root (**c**), and apical third (**d**) demonstrating a C-shaped external root form and C-shaped internal root canal configuration

4.7 Mandibular Premolar Teeth

Mandibular permanent first premolar teeth are reported to have one canal 74 % of the time, two canals 25.5 % of the time, and three canals 0.5 % of the time, whereas mandibular permanent second premolar teeth are reported to have one canal 88 % of the time and a second or third canal only 12 % of the time [29]. Just as in maxillary permanent premolar teeth, the traditional radiographic presence of a "fast break" generally indicates a canal division. CBCT imaging can help further determine the presence of multiple canals at the level of the suspected canal division (Figs. 4.16 and 4.17).

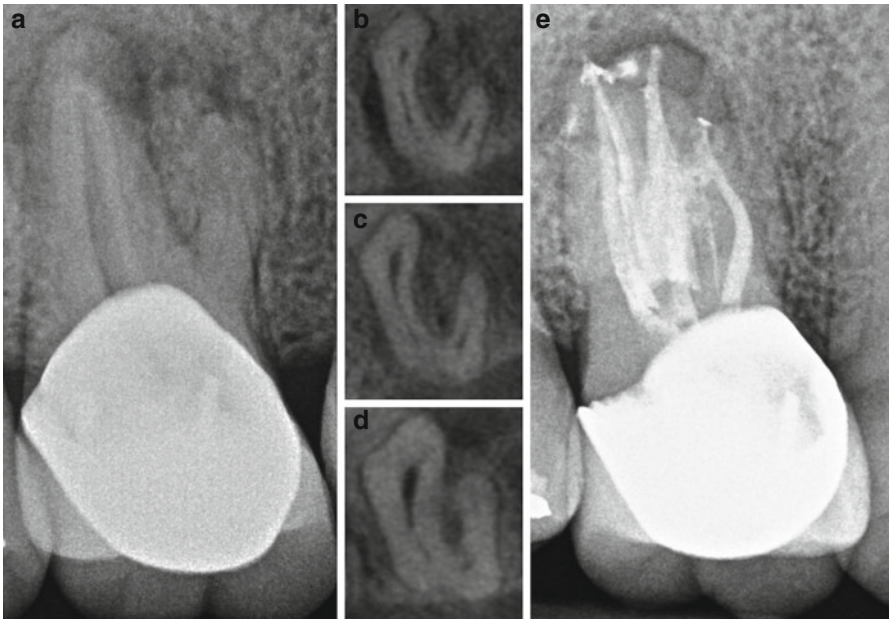

Fig. 4.12 Preoperative periapical radiograph of a maxillary right first molar (**a**) with corresponding axial CBCT slices captured from the apical third (**b**), mid-root (**c**), and coronal third (**d**) demonstrating a C-shaped external root form and confluent root canal configuration. The post-endodontic radiograph demonstrates proper management of the C-shaped internal root canal anatomy (**e**) (Case courtesy of Dr. Hong Chon, Specialized Endodontic Solutions, Bloomingdale, IL)

4.8 Mandibular Incisor Teeth

Mandibular permanent central and lateral incisors are narrow mesiodistally and broad buccolingually with corresponding ribbon-shaped root canal systems. Although most mandibular incisors are reported to have only one canal, the incidence of two canals has been reported to range from 12.4 to 53%. A more recent publication reported that the frequency of two canals in mandibular incisors is 36.25%, with 1.3% of these canals having separate foramina [30]. The anatomic positioning of these teeth in the dental arch makes access to the lingual extent of the root canal system challenging. A cone beam scan can be studied in the sagittal and axial plane to determine the presence or absence of an additional canal as well as aid in the creation of an endodontic access designed for maximum visualization and minimal removal of tooth structure (Fig. 4.18).

4.9 Additional Anatomic and Morphologic Considerations

4.9.1 Dens Invaginatus

Dens invaginatus is a developmental anomaly resulting from infolding of the enamel organ during tooth development. It is most commonly observed on maxillary lateral incisors and presents with varying degrees of severity and complexity [31]. CBCT

imaging demonstrates the unique internal features of this anomaly as well as the challenges associated with endodontic therapy (Fig. 4.19).

4.9.2 Accessory Canals

Multiple communications exist between the dental pulp and the surrounding periodontium via the apical foramen and accessory (lateral) canals. The distribution of accessory canals has been documented to occur at various levels throughout the root canal system as well as the floor of the pulp chamber, with the greatest number of

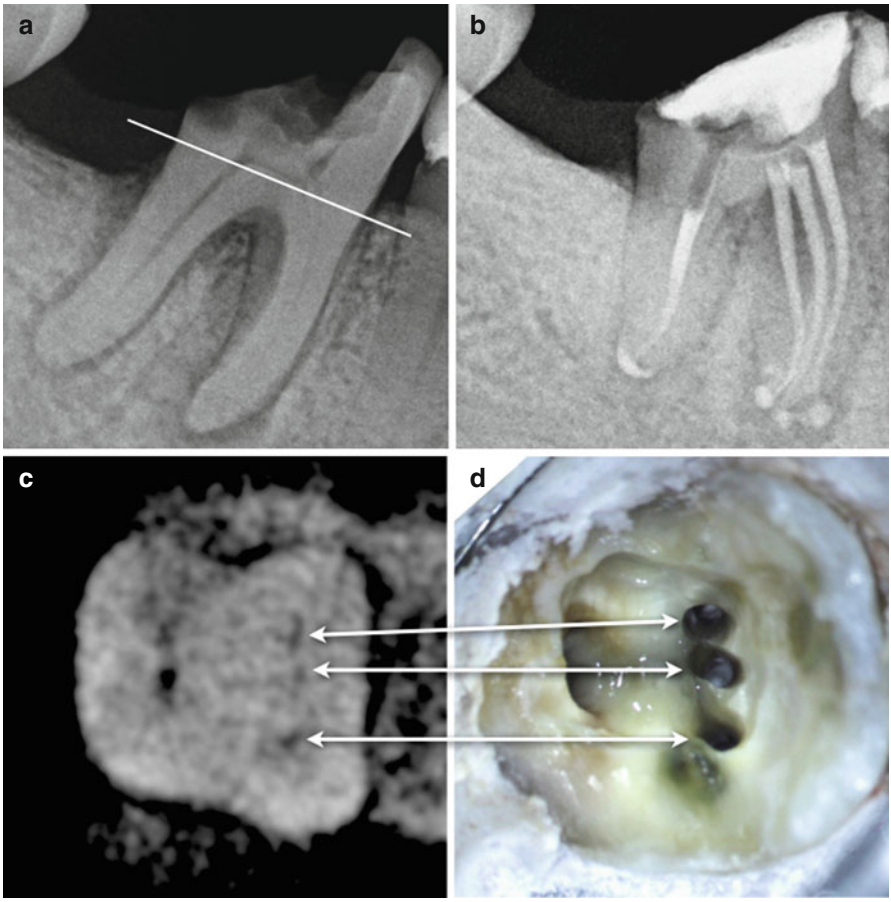

Fig. 4.13 Preoperative periapical radiograph of a mandibular right first molar (*white line* represents level of the axial CBCT slice [below]) (**a**). Postoperative periapical radiograph demonstrating three mesial canals with separate apical foramina (**b**). Axial CBCT slice demonstrating three identifiable mesial canals (**c**). Clinical photo demonstrating three instrumented mesial canals in the exact location shown in the preoperative axial CBCT slice (*arrows*) (**d**)

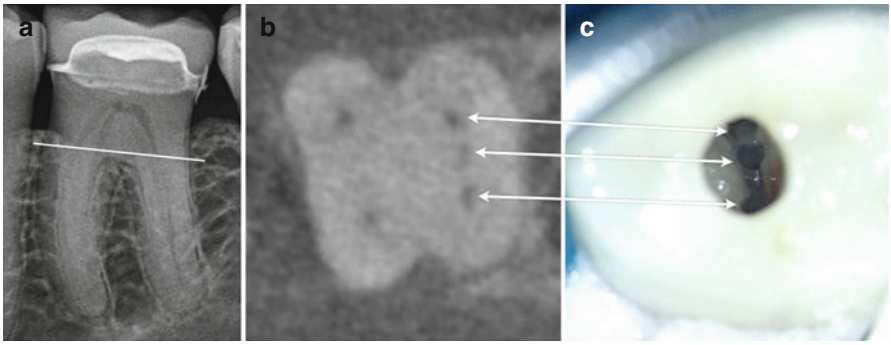

Fig. 4.14 Preoperative periapical radiograph of a mandibular first molar (*white line* represents level of axial CBCT slice) (**a**). Axial CBCT slice demonstrating three identifiable distal canals (**b**). Clinical photo demonstrating three instrumented distal canals through a conservative access design in the exact location shown in the preoperative axial CBCT slice (*arrows*) (**c**)

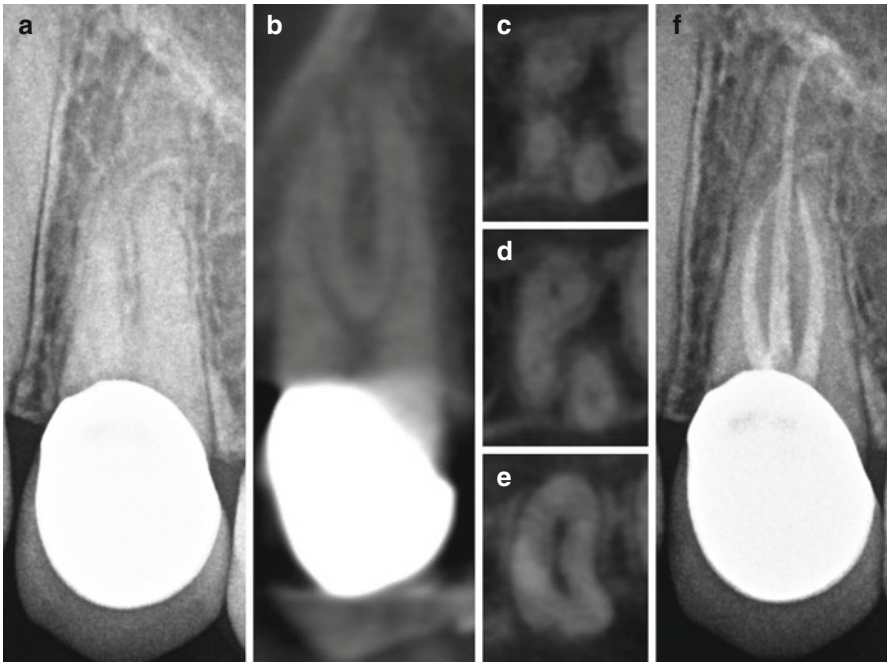

Fig. 4.15 Preoperative periapical radiograph of a maxillary left first premolar (**a**) with corresponding sagittal CBCT slice demonstrating a canal division of the buccal roots (**b**). Axial CBCT slices captured from the apical third (**c**), mid-root (**d**), and coronal third (**e**) demonstrate a trifurcation of the root canal system with three separate roots. Post-endodontic periapical radiograph demonstrates all identified root canal systems treated (**f**)

Fig. 4.16 Preoperative periapical radiograph of a left mandibular first premolar (**a**) with corresponding coronal CBCT slice demonstrating a mid-root division of the root canal system (**b**). Axial CBCT slices captured from the coronal third (**c**), mid-root (**d**), and apical third (**e**) demonstrate a single canal bifurcating into two separate canals within a single root. Post-endodontic periapical radiograph demonstrates all identified root canal systems treated (**f**)

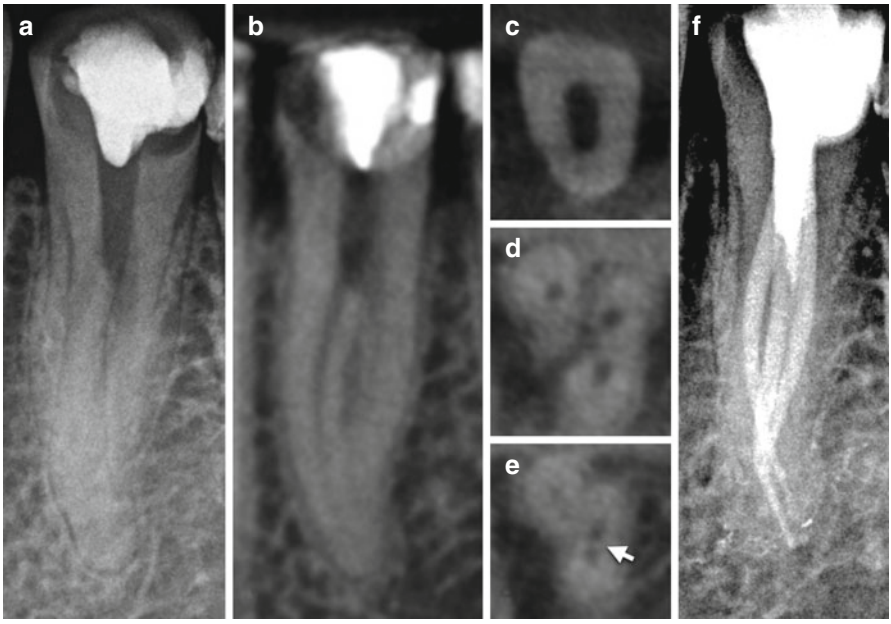

Fig. 4.17 Preoperative periapical radiograph of a previously accessed right mandibular second premolar demonstrating a classic "fast break" (**a**). The sagittal CBCT slice demonstrates a division of the buccal roots at the level of the "fast break." (**b**) The axial CBCT slice captured from the coronal third (**c**), mid-root (**d**), and apical third (**e**) demonstrates one root canal system trifurcating into three separate canals with confluence of the distobuccal and lingual canals in the apical third (*arrow*). Post-endodontic periapical radiograph demonstrates all identified root canal systems treated (**f**)

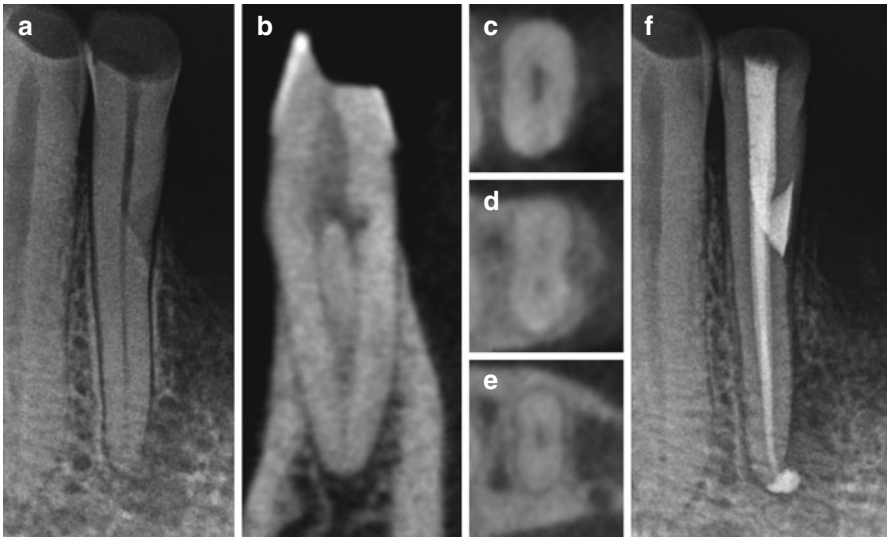

Fig. 4.18 Preoperative periapical radiograph of a left mandibular lateral incisor (note the mid-root resorptive defect) (**a**) with corresponding sagittal CBCT slice (**b**) and axial CBCT slices captured from the coronal third (**c**), mid-root (**d**), and apical third (**e**) demonstrating two root canal systems in the coronal third and mid-root, followed by canal confluence in the apical third. Post-endodontic periapical radiograph demonstrates proper management of the root canal system as well as the external repair of the resorptive defect (**f**)

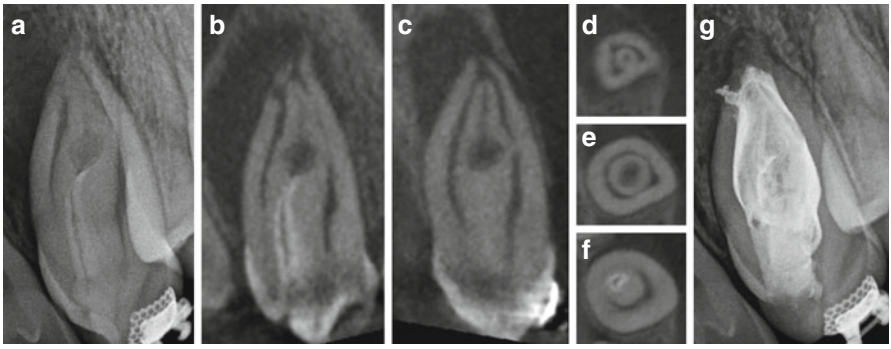

Fig. 4.19 Preoperative periapical radiograph of a maxillary left lateral incisor presenting with dens invaginatus (**a**). Coronal and sagittal CBCT slices (**b**, **c**) as well as axial CBCT slices captured from the apical third (**d**), mid-root (**e**), and coronal third (**f**) demonstrate the complex anatomical configuration of the developmental anomaly. Post-endodontic periapical radiograph demonstrates proper management of the root canal spaces (**g**) (Case courtesy of Dr. Hong Chon, Specialized Endodontic Solutions, Bloomingdale, IL)

accessory canals concentrated in the apical third of the root canal system [3]. Occasionally, accessory canals can be identified on a CBCT scan. The verifiable presence of these canals as well as the ability to determine their exact location can facilitate successful treatment of such intricate ancillary anatomy (Fig. 4.20).

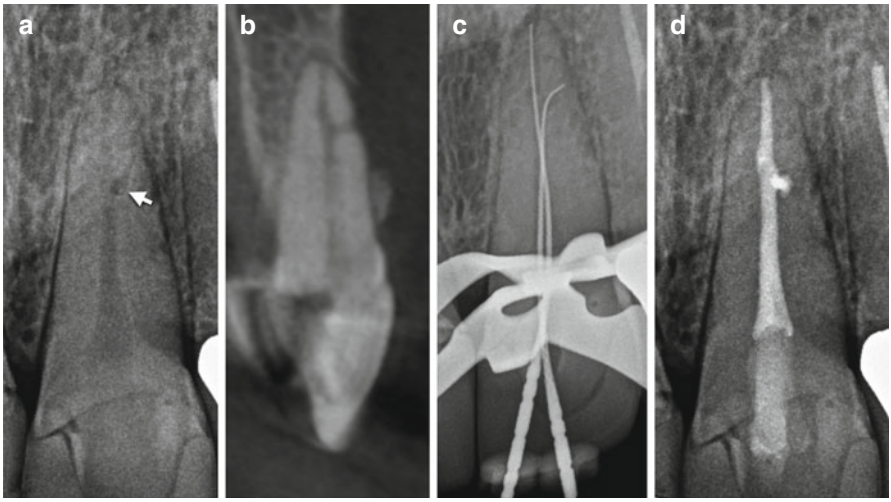

Fig. 4.20 Preoperative periapical radiograph of a maxillary left central incisor (note the radiolucent area superimposed on the root in the apical third [*white arrow*]) (**a**). The sagittal CBCT slice demonstrates the presence of an accessory canal with a buccal portal of exit (**b**). A mid-treatment periapical radiograph demonstrates an endodontic file placed in the main root canal system as well as the accessory canal (**c**). Post-endodontic periapical radiograph demonstrates proper management of both the main root canal system and the accessory canal (**d**)

4.9.3 Position of the Apical Foramen

The anatomical opening at the apex of the root through which nerves and blood vessels pass is often referred to as the apical foramen. This anatomic landmark represents the recommended apical termination of root canal instrumentation and obturation. The apical foramen can often present coronally in relation to the radiographic apex [32]. When the relationship between a coronally positioned apical foramen and the radiographic apex is exaggerated, two-dimensional endodontic radiographs create the illusion of clinically inadequate, incomplete, and/or inappropriate canal management. CBCT imaging can often confirm accurate management of these root canal systems by visually demonstrating the true position of the apical foramen as it relates to the anatomic root apex (Fig. 4.21).

4.9.4 Canal Confluence

When two canals leave the pulp chamber and merge to form a single canal short of the apical foramen, the canals are considered to be confluent. With the exception of severely rotated teeth, it is impossible to view canal confluence on a two-dimensional radiograph. Canal confluence can only be viewed in the coronal plane of posterior teeth or the sagittal plane of anterior teeth. Therefore, a CBCT scan may be the only opportunity to identify the presence of canal confluence as well as the level at which the canal confluence occurs (Fig. 4.22).

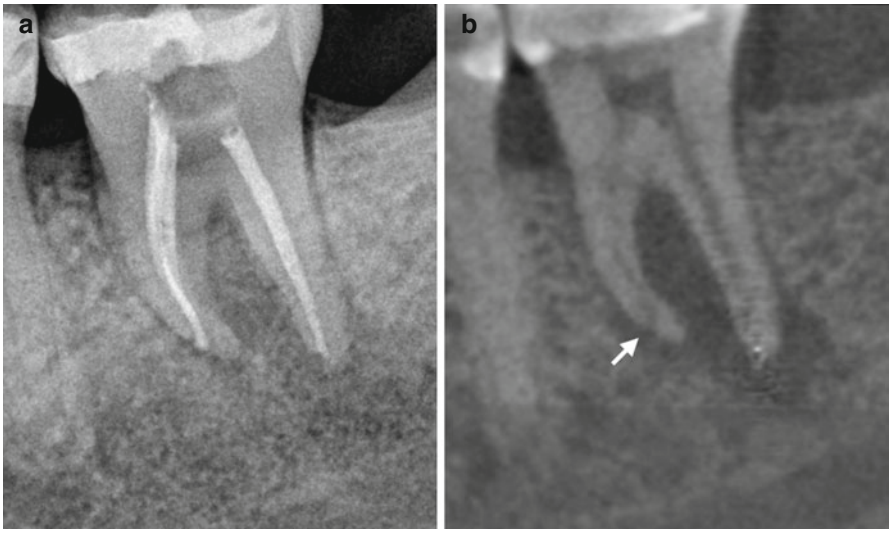

Fig. 4.21 Post-endodontic periapical radiograph of a left mandibular second molar demonstrating a coronally position apical foramen on the mesial root mimicking mismanaged canal instrumentation in the apical third (**a**). The preoperative sagittal CBCT slice demonstrates a coronally positioned apical foramen (*arrow*) in relation to the anatomic root apex verifying appropriate canal management (**b**)

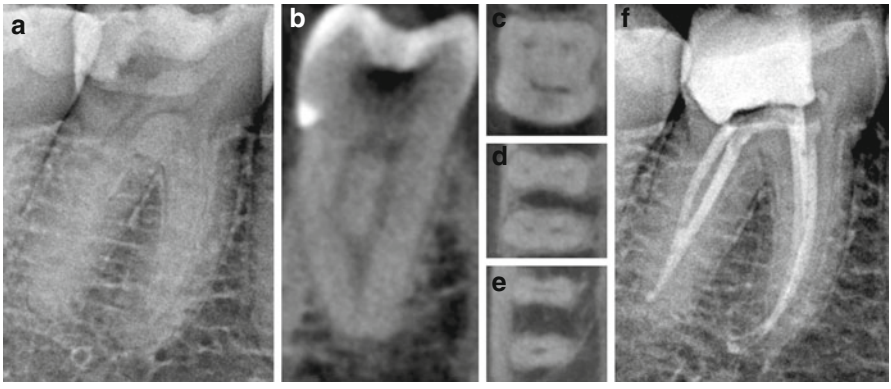

Fig. 4.22 Preoperative periapical radiograph of a right mandibular first molar (**a**) with corresponding coronal CBCT slice of the distal root (**b**) demonstrating canal confluence of the root canal system in the apical third. The axial CBCT slices captured from the coronal third (**c**), mid-root (**d**), and apical third (**e**) demonstrate canal confluence in the apical third of the root canal system in both the mesial and distal roots. Post-endodontic periapical radiograph demonstrates proper management of all identified root canal systems (**f**)

Conclusion

Different root shapes may appear at any level within a single root. Two-dimensional radiographs tend to make the root canal system appear uniform and consistent in shape, and aberrant canal configurations are not generally visible.

The more we view CBCTs, the more we realize that unconventional anatomy should be considered the norm rather than the exception.

Proper knowledge of root canal anatomy and morphology will cue the astute clinician to look for canal orifices in locations they are typically observed. However, canals are not always readily apparent or easily identified. Cone beam imaging has introduced an accurate, nondestructive, real-time method for clinical chairside evaluation of tooth anatomy and morphology, comparable to that of the histologic gold standard. The decision to incorporate CBCT imaging as a preoperative method to evaluate tooth anatomy can significantly enhance the clinical identification and endodontic management of complex root anatomy.

References

1. Walton WE, Vertucci FJ. Internal anatomy. In: Walton WE, Torabinejad M, editors. Principles and practice of endodontics. 3rd ed. Philadelphia: Saunders; 2002. p. 176–81.
2. Hess W. Formation of root canals in human teeth II. J Nat Dental Assoc. 1921;8:790–832.
3. Gutmann JL, Fan B. Tooth morphology, isolation, and access. In: Hargreaves KM, Berman LH, editors. Cohen's pathways of the pulp. 11th ed. St. Louis: Elsevier; 2016. p. 130–208.
4. Grover C, Shetty N. Methods to study root canal morphology: a review. In: Bonaccorso A, Chong BS, Schafer E, van der Sluis L, editors. ENDO – Endodontic practice today. 2012; 6(3):171–88.
5. Gomes BP, Rodrigues H, Tancredo N. The use of modelling technique to investigate the root canal morphology of mandibular incisors. Int Endod J. 1996;29:29–36.
6. Eder A, Kantor M, Moser T, Gahleitner A, Schedle A, Sperr W. Root canal system in the mesiobuccal root if the maxillary first molar: and in vitro comparison study of computer tomography and histology. Dentinomax Radiol. 2006;35:175–7.
7. Michetti J, Maret D, Mallet JP, Diemer F. Validation of come beam computed tomography as a tool to explore root canal anatomy. J Endod. 2010;36:1187–90.
8. Neelakantan P, Subbarao C, Subbarao CV. Comparative evaluation of modified canal clearing technique, cone beam computed tomography, peripheral quantitative computed tomography, spiral computed tomography, and plain and contrast medium-enhanced digital radiography in studying root canal morphology. J Endod. 2010;36:1547–51.
9. Blattner TC, George N, Lee CC, Kumar V, Yelton DJ. Efficacy of cone beam computed tomography as a modality to accurately identify the presence of second mesiobuccal canals in maxillary first and second molars: a pilot study. J Endod. 2010;36:867–79.
10. Weine FS, Healey HJ, Gerstein H, Evanson L. Canal configuration in the mesiobuccal root of the maxillary first molar and its endodontic significance. Oral Surg Oral Med Oral Pathol. 1969;28:419–25.
11. Gulabivala K, Aung TH, Ng YL. Root and canal morphology of Burmese mandibular molars. Int Endod J. 2001;34(5):359–70.
12. Sert S, Bayiril GS. Evaluation of root canal configurations of the mandibular and maxillary permanent teeth by gender in the Turkish population. J Endod. 2004;30:391–8.
13. Krasner P, Rankow HJ. Anatomy of the pulp chamber floor. J Endod. 2004;30:5–16.
14. Patel S, Dawood A, Whaites E, Pitt Ford T. New dimensions in endodontic imaging: part 1: conventional and alternative radiographic systems. Int Endod J. 2009;42:447–62.
15. Estrela C, Bueno MR, Sousa-Neto MD, Pecora JD. Method for determination of root curvature radius using cone-beam computed tomography images. Braz Dent J. 2008;19:114–8.
16. Scarfe WC, Farman AG, Sukovic P. Clinical applications if cone-beam computed tomography in dental practice. J Can Dent Assoc. 2006;72:75–80.

17. Ee J, Fayad MI, Johnson BR. Comparison of endodontic diagnosis and treatment planning decisions using cone-beam volumetric tomography versus periapical radiography. J Endod. 2014;40:910–6.
18. Mota de Almeida FJ, Knutsson K, Flygare L. The impact of cone beam computed tomography on the choice of endodontic diagnosis. Int Endod J. 2015;48:564–72.
19. Vizzotto MB, Silveira PF, Arus NA, Montagner F, Gomes BO, da Silveira HE. CBCT for the assessment of second mesiobuccal (MB2) canals in maxillary molar teeth: effect of voxel size and presence of root filling. Int Endod J. 2013;46:870–6.
20. Krishan R, Paque F, Ossareh A, Kishen A, Dao T, Friedman S. Impacts of conservative endodontic cavity on root canal instrumentation efficacy and resistance to fracture assessed in incisor, premolar and molars. J Endod. 2014;40:1160–6.
21. Kfir A, Telishevsky-Strauss Y, Leitner A, Metzger Z. The diagnosis and conservative treatment of a complex type 3 dens invaginatus using cone beam computed tomography (CBCT) and 3D plastic models. Int Endod J. 2013;46:275–88.
22. Kulild JC, Peters DD. Incidence and configuration of canal systems in the mesiobuccal root of maxillary first and second molars. J Endod. 1990;16:311.
23. Peikoff MD, Christie WH, Fogel HM. The maxillary second molar: variations in the number of roots and canals. Int Endod J. 1996;29:365–9.
24. De Moor R, Deroose C, Calberson F. The radix entomolaris in mandibular first molars: an endodontic challenge. Int Endod J. 2004;37:789–99.
25. Chai WL, Thong YL. Cross sectional morphology and minimum canal wall widths in c-shaped roots of mandibular molars. J Endod. 2004;30:509–12.
26. Ahmed HA, Abu-bakr NH, Yahia NA, Ibrahim YE. Root and canal morphology of permanent mandibular molars in a Sudanese population. Int Endod J. 2007;40:766–71.
27. La SH, Jung DH, Kim EC, Min KS. Identification of independent middle mesial canal in mandibular first molar using cone-beam computed tomography imaging. J Endod. 2010;237:1–4.
28. Vertucci FJ, Seelig A, Gillis R. Root canal morphology of the human maxillary second premolar. Oral Surg Oral Med Oral Pathol Oral Radiol Endod. 1974;38:456–64.
29. Vertucci FJ. Root canal morphology of mandibular premolars. J Am Dent Assoc. 1978;97(1):47–50.
30. Boruah LC, Bhuyan AC. Morphologic characteristics of root canal of mandibular incisors in North-East Indian population: an in vitro study. J Conserv Dent. 2011;14:346–50.
31. Hulsman M. Dens invaginatus. Aetiology, classification, prevalence, diagnosis and treatment considerations. Int Endod J. 1997;30:79.
32. Souza RA, Figueiredo JAP, Colombo S, Dantas JCP, Lago M, Pecora JD. Location of the apical foramen and its relationship with foramina file size. Dental Press Endod. 2011;1:64–8.

Nonsurgical Retreatment Utilizing Cone Beam Computed Tomography

5

Stephen P. Niemczyk

The primary tenet for conventional endodontic therapy is the negotiation, debridement, and disinfection of the affected and infected canal spaces [1, 2]. Advances in instrumentation notwithstanding, successful outcomes have been enhanced through the widespread utilization, at the specialist level, of the surgical operating microscope (SOM). It has proven itself indispensable in locating canals [3], identifying the location of MB_2 [4–6], removing separated instruments [7], perforation repair [8], and generally enhancing the delivery of quality care [9]. The mantra for its use, especially in the surgical environment, is "if you can see it better, you can do it better." While this holds true for structures readily apparent, what is our recourse for those anatomical variants that are not so easily disclosed or discovered? The corollary then becomes "you can only treat what you can see" especially when evaluating the patient in the pretreatment phase of the procedure. Clinicians have long relied on varied resources for the basis of their preoperative assessments. The classic India ink perfusions by Hess [10] provided insights into the variation and complexity of the canal spaces in extracted teeth but along with other observations in extracted teeth [5, 11] furnished only postmortem evidence about canal morphology. There are numerous reports of clinical observations employing radiographs [12, 13] or using various methods of magnification for canal discovery [14]. Empiricism also plays a significant role, but experience cannot be taught or contained in a textbook. An important element to consider with all these methodologies is that they are not patient specific and may not be an accurate representation of an anatomical variant that submits for clinical treatment.

It is in this regard that the cone beam computed tomography (CBCT) has proven invaluable and, in terms of its impact on the discipline of endodontics, could be regarded as the surgical operating microscope of the twenty-first century. The ability

S.P. Niemczyk
The Maxwell S. Fogel Department of Dental Medicine, Einstein Medical Center Philadelphia, 5501 Old York Road, Philadelphia 19141, PA, USA
e-mail: spndo@comcast.net

M. Fayad, B.R. Johnson (eds.), *3D Imaging in Endodontics*,
DOI 10.1007/978-3-319-31466-2_5

to view the selected field from an infinite number of angles, coupled with a 3D-rendered perspective of the jaw segment, enables the clinician to perform a "Virtual Surgery©" [15] in the selected field that is patient specific and nondestructive. The ability to discern the size, number, and location of canals using the CBCT is statistically superior when compared to conventional imaging [16–18]. It is especially advantageous when employing this technology as an inter-treatment survey for the location of undisclosed canals that may be atypically placed or dystrophically obscured [19]. A critical assessment as to the location and depth of the missing canal relative to known anatomical landmarks within the root is paramount to the successful acquisition in teeth that have been prosthetically altered. The margin for error can be miniscule when considering the available width and fragility of the root form undergoing treatment. An example of this challenge is presented in the first clinical case (Sect. 5.1, Case #1). An appreciation for the number and curvature of the roots is reinforced when surveying the cone beam scan that is absent in a two-dimensional assessment of the same tooth [20–23], especially in light of geographic diversity and variations. The presence of periapical disease can be masked in the uniplanar image because of the overlying structures; a scan of the same site often reveals obvious pathology coincident with the patient's signs and symptoms [24, 25]. Collectively, this expansion of available data expedites a focused and patient-centric treatment decision tree, where options and pitfalls can be disclosed with a greater degree of confidence and accomplished without subjecting the patient to unnecessary procedures or empirical guesswork. This is especially germane when a retreatment is being considered, where oftentimes the internal anatomy may be obliterated and the accompanying visual cues to certain structures are altered or nonexistent.

It is this arena of retreatment, or "revision" of an endodontically treated tooth that is failing, that has garnered the majority of attention and case reports in the literature involving CBCT. One retrospective study [26] reported that missed canal anatomy was responsible for 48 % of the unsuccessful initial therapies in molars, with the preponderance being the mesiobuccal root of maxillary first molars. The authors, in their concluding statements, made the following observation: "Given that failure to locate all canal systems of a tooth contributes significantly to unsuccessful endodontic treatment, all measures available to the clinician to maximize canal identification should be used." While it is not an outright endorsement of the technology, it presents a compelling argument for cone beam scanning of not only teeth requiring retreatment but also any tooth that demonstrates an "other than normal" initial radiographic appearance. Although not currently promoted for initial therapy, prudent scanning of selected cases can maximize the operator's understanding of the underlying morphology and allows them to confidently address the anatomy. Although not guaranteeing success, it is a significant step toward enhancing the outcome and reducing the likelihood of future treatment interventions.

An appropriate introduction to the nonsurgical use of CBCT would be with the simplest of all retreatments and one that is illustrative of the teeth in the above referenced study: missed canal anatomy in the mesiobuccal roots of maxillary molars (Sect. 5.2, Case #2). The patient had received treatment for both teeth within the previous 14 months and had remained symptomatic for much of that time. Conventional radiographs

failed to disclose any significant clues as to the etiology, and the patient was presenting for consultation. Unfortunately, this clinical scenario is not that unusual, and it is frustrating for the patient who is often told that "nothing is showing up in the X-rays."

CBCT of posterior segment revealed the presence of MB_2 in teeth #2 and #3, with slight edema at the respective apices. Axial sections demonstrated the typical asymmetrically located obturations, with evidence of the MB_2 either as a sealer streak (#3) or as a radiolucent dot. These features are even more evident when examining the coronal sections of the MB root. Especially interesting is the colorized coronal section of #3, with the MB_2 canal orifice clearly patent enough to accept the sealer.

A more subtle example of a missed canal is shown in the next case (Sect. 5.3, Case #3) involving tooth #18. The patient presented with similar signs and symptoms, with the past dental history of treatment and subsequent retreatment without resolution. The tooth was diagnosed as "fractured" and was presenting for consultation prior to extraction. The typical signs of fracture were not present in the preoperative exam or radiographs (deep isolated probing depths, vertical bone defects), but the multiple radiographic angles did accentuate the asymmetry of the obturation in the seemingly fused root form. A seasoned practitioner would observe this asymmetry and suspect an additional canal, but two principal questions remain: where would you commence the excavation, and in what direction? Careful examination of the axial sections, slice by slice, disclosed a minute sealer streak 4 mm from the floor of the chamber and inclined toward the mesiolingual line angle of the root. Coincidentally, the root is also slightly more bulbous in the same area, further evidence of an additional canal. Colorized versions of the axial and coronal sections illustrated the extent and angle of this streak, enhancing the three-dimensional comprehension preoperatively. Careful measurements and directional landmarks simplified the discovery of the mesiolingual canal after the filling materials were harvested, allowing for negotiation and debridement of the missing canal. The patient was asymptomatic after 1 week and has remained so since.

A variation of an extra canal is represented by Sect. 5.4, Case #4. The patient was asymptomatic, but presented with a sinus tract tracing to the mesial root apex. Multiple radiographic angles failed to disclose what the axial sections of the CBCT indicate with clarity: the presence of a middle mesial (MM) canal. A study in extracted teeth [27] correlated intercanal distances between the mesiobuccal and mesiolingual canals with the likelihood of these roots containing a middle mesial canal. Measurement of the isthmus in the axial section exceeding 3.0 mm was strongly indicative of a patent MM canal space. Conservative treatment of this canal and retreatment of all the remaining spaces effectively addressed the etiology, as evidenced by the resolution of the sinus tract within 1 week. Examination of the axial and coronal sections in a postoperative scan demonstrates a type VIII canal configuration of the mesial root according to Torres et al. [22].

Mandibular molars with distolingual supernumerary roots present a unique challenge to any practitioner. First coined *radix entomolaris* by Carabelli [28], they demonstrate great variability in anatomical presentations and ethnic predispositions [29–33]. While the presence of the additional root may be vaguely apparent

on conventional radiographs, the precise anatomical variant is readily displayed with the aid of the cone beam scan [34]. It proved an indispensable asset in the next case, the retreatment of tooth #30 (Sect. 5.5, Case #5). The existence of the radix is suggested by the radiographs, but the true nature of the roots position is revealed in the axial sections of the scan. The coronal and sagittal views disclose the extent of the periapical involvement preoperatively and the resolution 12 months later.

The variability of canal morphology in maxillary molars is not confined solely to the MB root, as the following case demonstrates (Sect. 5.6, Case #6). The initial radiographic exam was not encouraging, but despite the evidence to the contrary, the tooth's mobility was between a 1 and 2, with no depression into the socket. The lone region of deep periodontal probing depth was at the mesial aspect of the tooth, coincident with the vertical defect seen in the pretreatment radiographs. However, conservative reflection and examination with the SOM failed to disclose any crown-root fractures. The patient reported being told that the dentist had encountered some difficulties during the procedure, including an unexplained "obstruction" and possibly a separated instrument.

Initial analysis of the CBCT scan was even less encouraging; the bone loss appeared to be circumferential around the fused roots, with the only competent attachment at the palatal aspect. However, two observations were made during the slice-by-slice assessment: an asymmetrical root form at the DB portion of the root (suggestive of a missing canal) and the close proximity of the existing obturation to the mesial aspect of the root in the apical third of the tooth (consistent with a possible root perforation). These findings were presented to the patient, who desired to retain the tooth if at all possible. The retreatment was agreed to, after detailed informed consent and full disclosure of the poor prognosis.

Reentry into the chamber revealed an atypical C-shaped canal, coursing from the normal DB orifice location toward the palatal aspect of the chamber. Partial removal of the gutta-percha in the palatal canal confirmed that this C-shaped isthmus, containing small fragments of necrotic tissue, indeed joined the body of the palatal canal space. This anomaly is extremely rare in appearance, with a reported incidence in first molars of 0.091 % [35]. In second molars, this irregularity has only been associated clinically with the palatal root [36] or in the study of sectioned extracted teeth [37]. It also appears to be genetically determined, which could provide insights into the ethnic origins of those patients with this morphologic variation [38].

Complete removal of all the obturative material in the palatal canal uncovered the suspected perforation of the mesial aspect of the space in the coronal third of the root. Following gentle debridement and disinfection, the perforation was sealed with a bioceramic (ProRoot™ MTA, Dentsply Tulsa Dental), and the patient was appointed for the following day to complete the retreatment of the remaining canal space (MB) and placement of the inter-appointment medicament ($Ca(OH)_2$). The patients' treatment was completed 4 weeks later, and the 12 month recall examination displayed remarkable healing and normal mobility.

Occasionally, the discovery of unusual anatomy is serendipitous, often disclosed by the unintentional tracking of the root canal filling material. Such is the case with

the next clinical presentation (Sect. 5.7, Case #7). The patients' chief complaint referenced the MB root of tooth #14, which did demonstrate active disease secondary to a missed MB_2. However, the radiographic exam revealed the existence of a bifurcation in the palatal root. The existence of 2 canals in this root has multiple permutations: it can present as two orifices with two separate canals [39–41], two roots or orifices with a common apical foramen [42], or, the most uncommon of all, one orifice with a common canal that bifurcates or trifurcates [43–45]. As with other clinical situations regarding anatomy deep in the canal spaces, it is of paramount importance to have precise knowledge of how deep the anomaly is in the root and what direction(s) they are tracking toward. The CBCT permitted exact measurements in the palatal root to pinpoint the level of the bifurcation, facilitating exact and intentional instrumentation of both canals, with complete obturation of both prepared spaces in the palatal root.

Two canals in one root are also an uncommon occurrence in the tooth considered in the next example (Sect. 5.8, Case #8): the mandibular first premolar. A recent literature review [46] reported that two or more canals were found in 24.2 % of the teeth studied, with 21.1 % having two or more apical foramina. Higher incidences of teeth with additional canals and roots have been reported in Chinese, Australian, and sub-Sahara African populations, with the lowest incidence in Western Eurasian, Japanese, and American Arctic populations. As is the case with mandibular anterior teeth with two canals, the lingual canal of the pair is the most often misdiagnosed and missed. Careful pretreatment assessment using the CBCT assisted in the successful discovery and acquisition of this auxiliary canal.

The next two retreatment scenarios (Sects. 5.9 and 5.10, Cases #9 and #10) serve to reinforce the concept of appropriate instrumentation depths and extent. The conventional imaging fails to reveal the subtle dilacerations in the apical 2–3 mm of the distal root of both of these teeth. Failure to address the tissue contained in these apices resulted in tissue necrosis and development of periapical pathology (PAP). It is these small lesions that precipitate clinical symptoms and confound detection with standard periapical radiography, where overlying structures mask and conceal their presence. With the assistance of the scan, not only is their existence confirmed, but the morphology of root end is clearly displayed. Armed with that information, the clinician can better negotiate that difficult canal curvature with the appropriate armamentarium and technique.

The final clinical case (Sect. 5.11, Case #11) provides segue to both the surgical treatment planning section and a statement on the limitations of our nonsurgical interventions. The technology of three-dimensional imaging has exponentially expanded the realm of the possible, providing patients with the chance for better outcomes and resolution of their disease. However, it is just as impartial when it reveals that the situation cannot be resolved without extraordinary means, as with this separated instrument buried at the apical foramen of the DB root. Whichever way the decision rests, the patient is the ultimate benefactor: they either resolve their issue with a degree of confidence or are resolved in the fact that nothing else can be done. For the practitioner, they can take consolation in the fact that they can provide the most effective and appropriate service for their patients via the least invasive means possible.

5.1 Case #1

Description The patient presents for intentional treatment of #4/5 for prosthetic reasons.

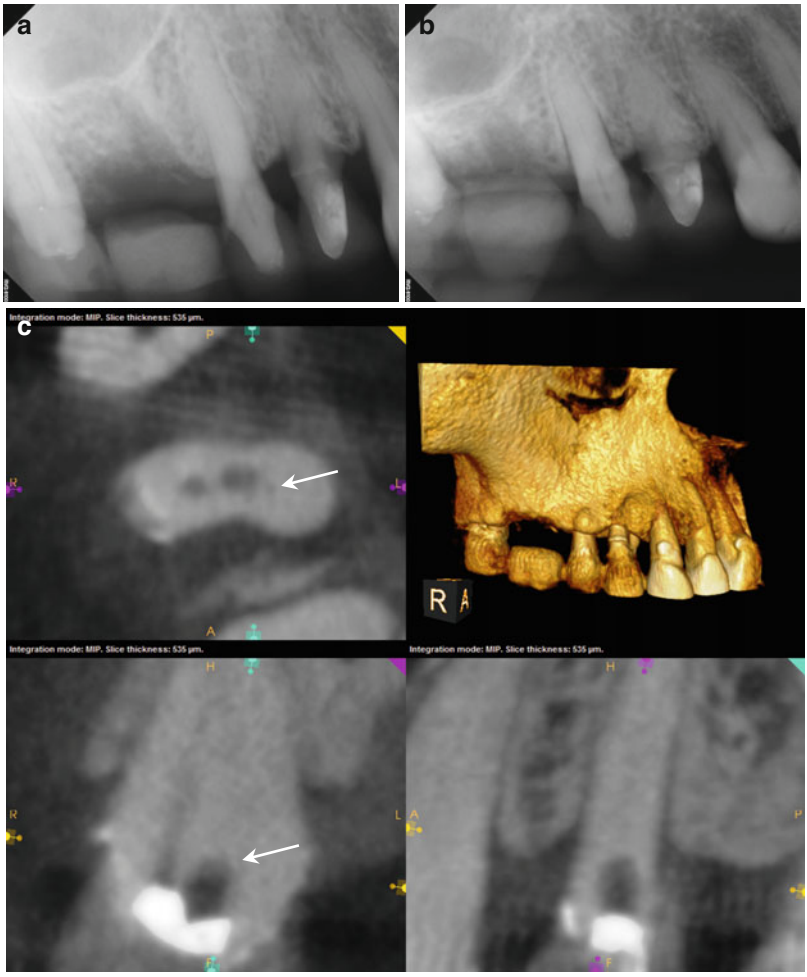

Fig. 5.1 (**a**, **b**) Preoperative radiographs reveal dystrophic obliteration of the canal spaces in tooth #5. Access and instrumentation was performed on #4, but only the buccal canal in #5 could be located. (**c**) An intra-treatment CBCT disclosed the location of the palatal canal 1 mm palatal and mesial to the area of ultrasonic excavation (*white arrow*). Note the kidney bean shape and mesial invagination of the root form not appreciated on the 2-D image. (**d**) A colorized axial section of the 3-D model demonstrates the instrumented canal diameters of #4 and the location of the palatal canal (*yellow arrow*) in #5. (**e**, **f**) Using a NiTi D11T spreader as an explorer, the palatal canal space is engaged and the orifice uncovered (*red arrow*). A small file will be inserted into the canal for verification and working length measurement. (**g**, **h**) Mid-obturation and final radiographs. Precise triangulation and accurate measurements guided the conservative excavation and location of this "calcified" canal in a critical abutment

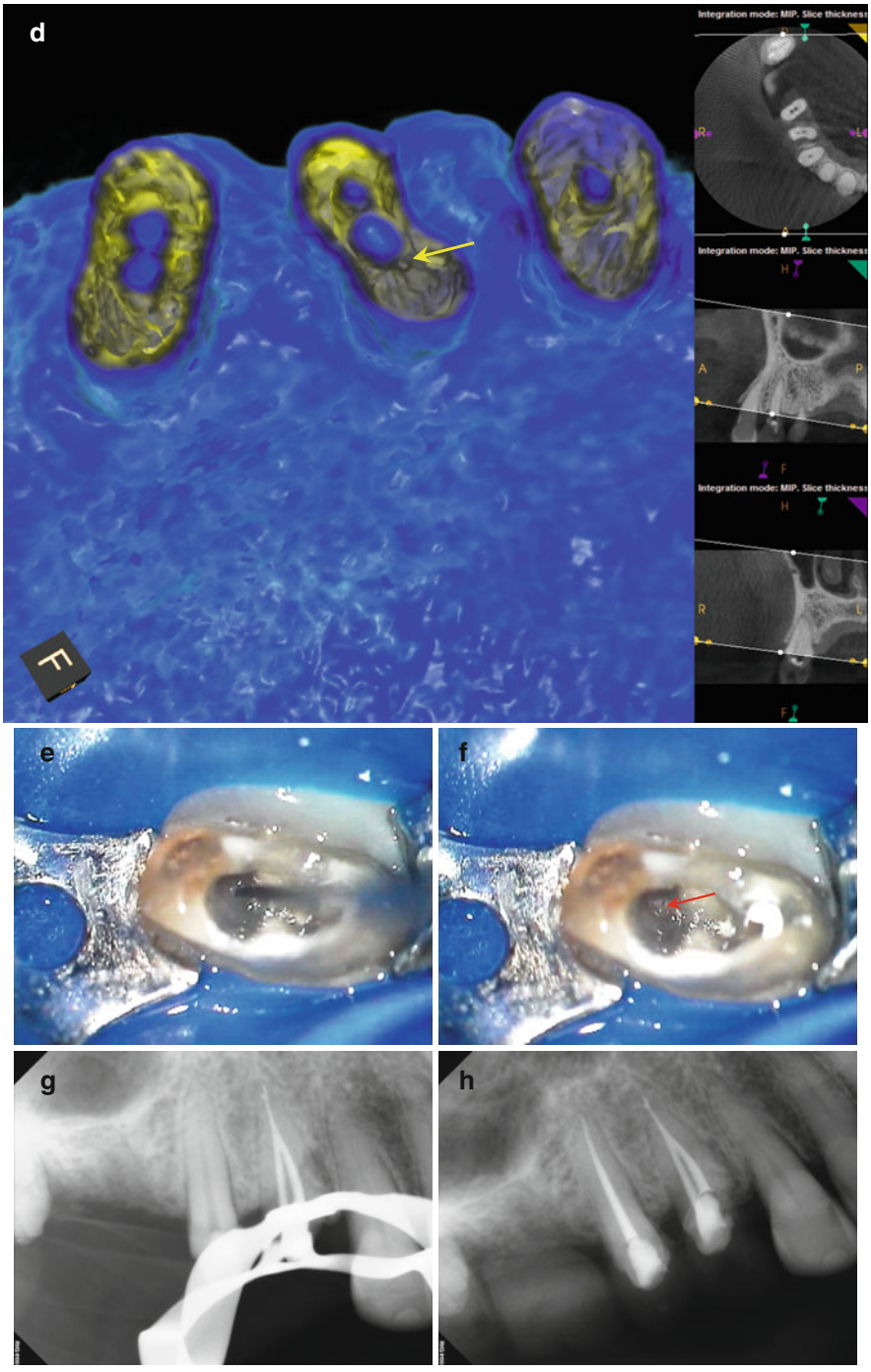

Fig. 5.1 (continued)

5.2 Case #2

Description The patient had RCT in teeth #2/3 approximately 14 months ago; both teeth have remained symptomatic. She is presenting for consultation.

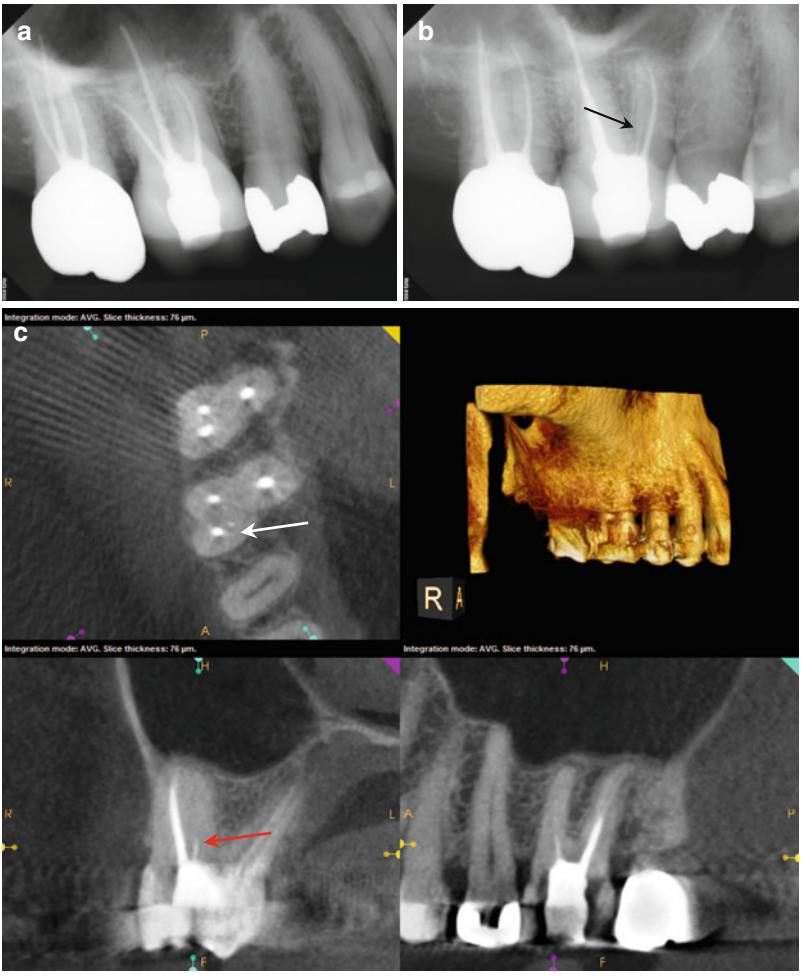

Fig. 5.2 (**a**, **b**) Preoperative radiographs disclose no obvious periapical pathology, but the obturation of the MB root in #3 appears to be off-center, and a thin radiopaque line is evident slightly distal to the filled MB canal (*black arrow*). (**c**) The axial section of #3 reveals a small high-density dot palatal to the MB_1 canal (The *white arrow* points to a sealer tract from the previous root canal filling in the MB root). The location, as well as the configuration relative to the MB_1 (*red arrow*), is suggestive of a sealer tract in the uninstrumented MB_2 canal. (**d**) The colorized 3-D coronal section highlights the presence of the sealer in MB_2, with a similar density to the root canal filling material (*yellow arrow*). (**e**) The axial section of #2 demonstrates a broad fusion of the MB and Palatal roots (*white arrow*), while the coronal section reveals a low-density line that is suggestive of MB_2 (*red arrow*). (**f**) The colorized 3-D axial section discloses the sealer tract in #3 and an area of dentin density in the MB root of #2 that may contain the MB_2 canal (*yellow arrows*)

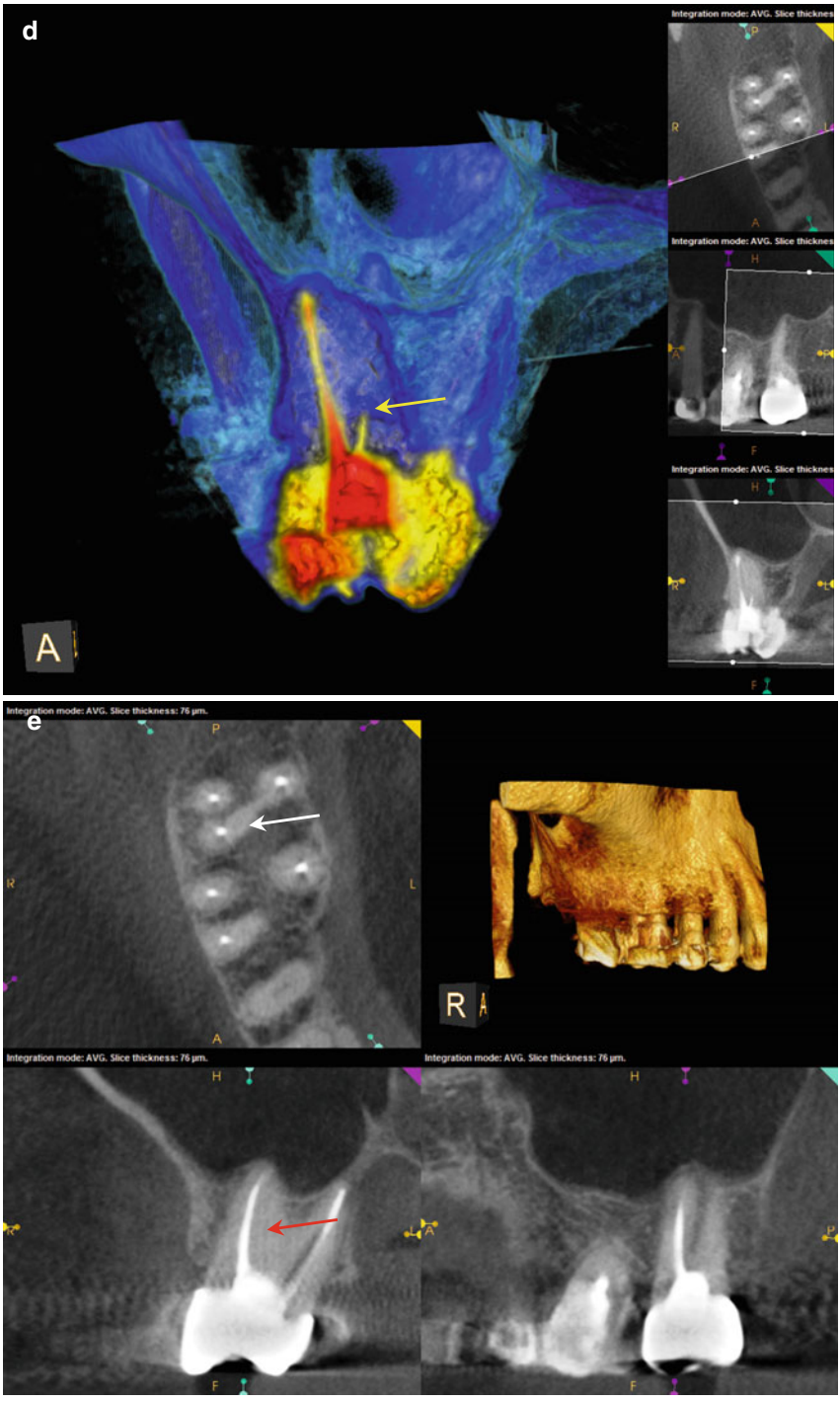

Fig. 5.2 (continued)

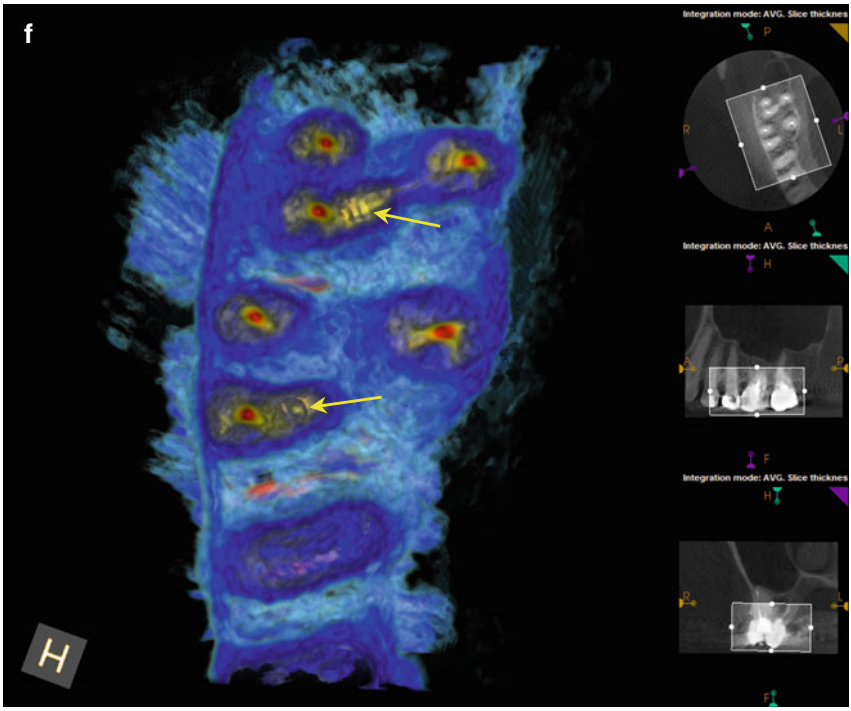

Fig. 5.2 (continued)

5.3 Case #3

Description The patient received RCT in tooth #18 approximately 3 years ago; the tooth was retreated 12 months prior to presentation. The patient has been symptomatic for the previous 2 years and recently reported a diagnosis of fractured tooth. The patient desires a second opinion.

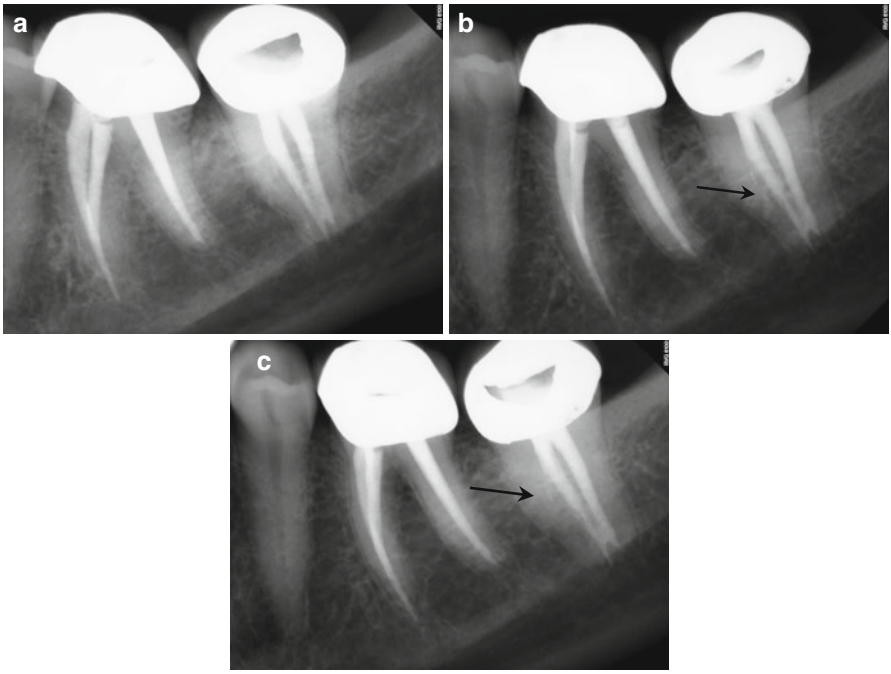

Fig. 5.3 (**a**–**c**) Preoperative radiographs from several different angulations fail to disclose a definitive diagnosis. However, closer examination of the magnified image suggests a thin radiopaque line from the mesial canal in two of the images (*black arrows*). The obturation is also off-center, again suggestive of additional canal spaces within the root. (**d**) The axial, coronal, and sagittal sections of the CBCT scan reveal a high-density dot or line, highly suggestive of sealer extruded into the uninstrumented ML canal space (*white arrows*). (**e**) The colorized 3-D axial section highlights the high-density object adjacent to the MB canal; the direction is on a line from the ML canal to the ML line angle of the root surface (*red arrow*). (**f**) The colorized 3-D coronal section reveals the bifurcation of the main canal, with sealer streaming into the lingual aspect of the bifurcation (*yellow arrow*). (**g**) A magnified view of the colorized coronal section with part of the sagittal aspect of the root removed. The detail of the bifurcation is displayed, and accurate measurements regarding depth can be obtained. It was ascertained from the scan that the depth from the floor of the chamber to the bifurcation entrance was 4 mm, on an angle toward the ML line angle of the mesial root. (**h**, **i**) The root canal filling (RCF) was harvested from the canal spaces, and the ML canal was located and negotiated (*black arrow*). A periapical radiograph was exposed to verify the complete removal of the RCF material. The canals were treated with $Ca(OH)_2$ for 3 weeks; the patients' symptoms subsided in 1 week and were absent at the completion appointment. (**j**, **k**) Right-angle and off-angle radiographs of the completed case, demonstrating the presence of three canals with multiple anastomoses between them

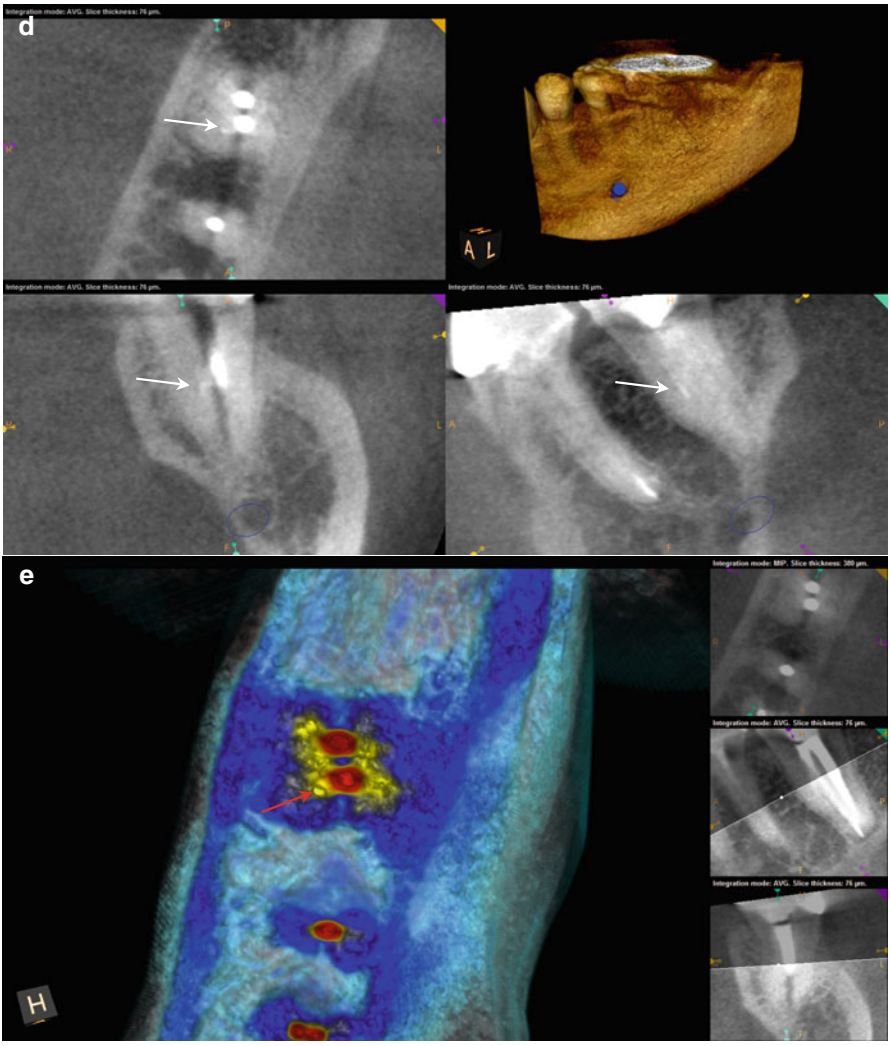

Fig. 5.3 (continued)

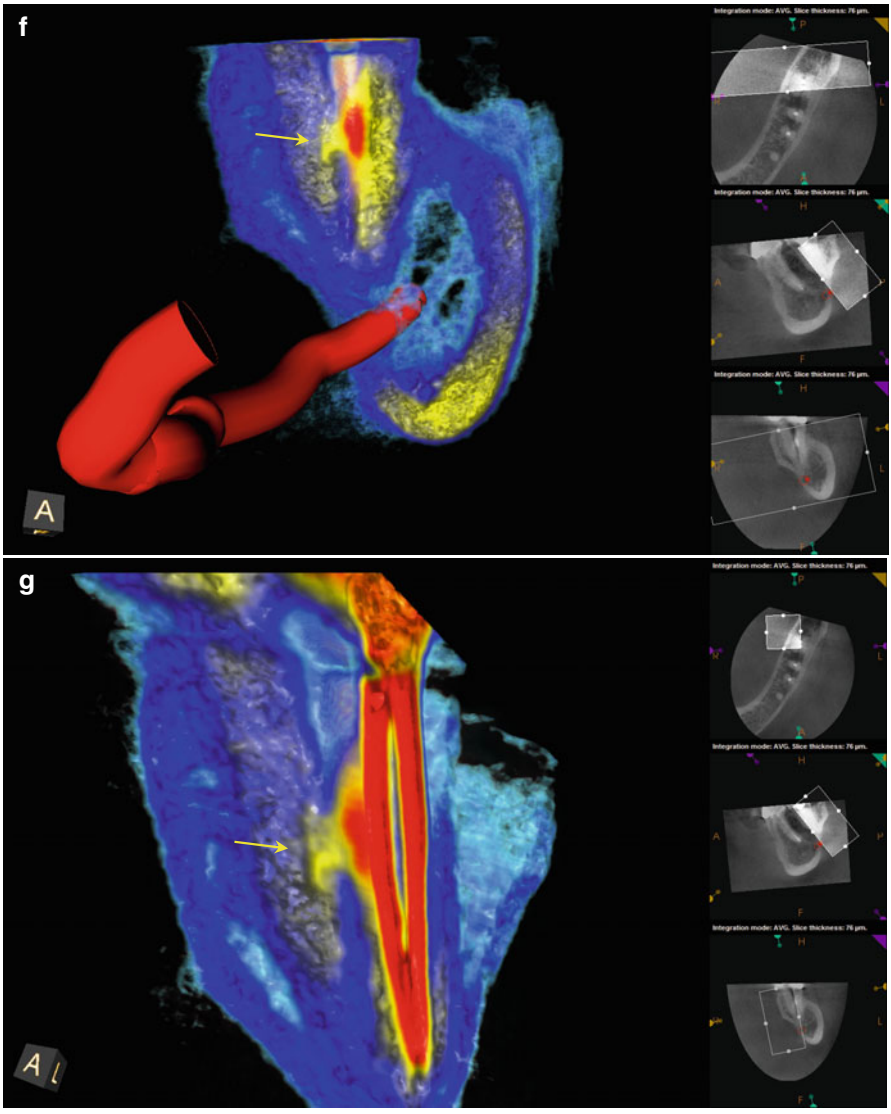

Fig. 5.3 (continued)

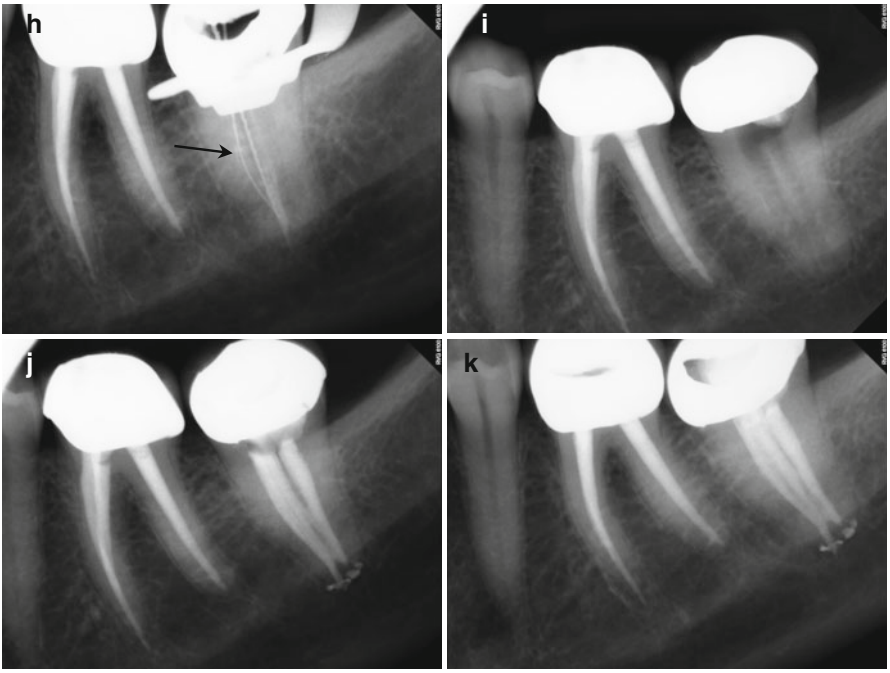

Fig. 5.3 (continued)

5.4 Case #4

Description The patient was asymptomatic, but presented for evaluation of a "pimple on his gum."

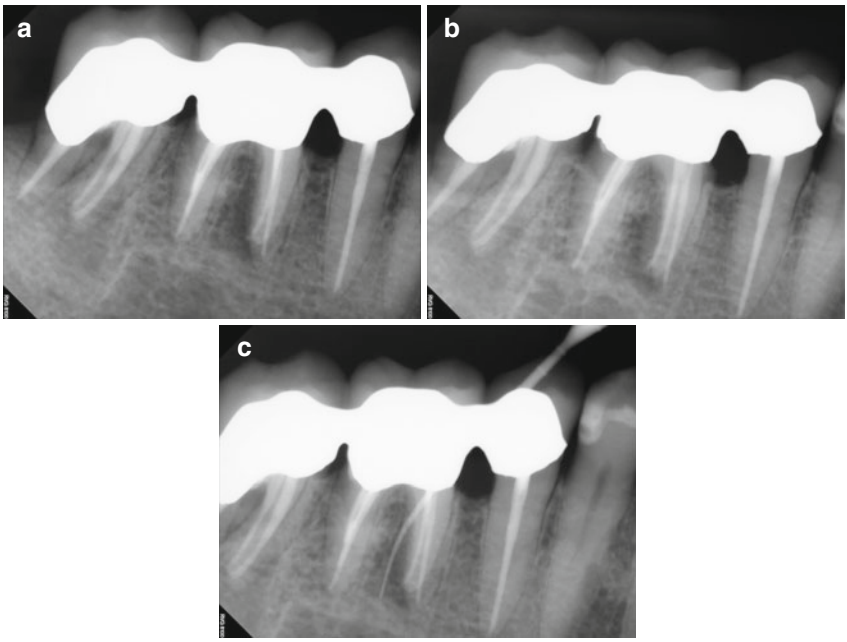

Fig. 5.4 (**a**, **b**) Right-angle and off-angle radiographs reveal PAP on the mesial root of tooth #30. There is also a suggestion of pathology on the mesial root of #31 as well. (**c**) Tracing the sinus tract revealed the source to be the apex of the mesial root of #30. Periodontal probing of the tooth was within normal limits, discounting a vertical root fracture as an etiology. (**d**) The axial and coronal sections of the CBCT scan were suggestive of a middle mesial canal: the distance between the MB and ML canals in the axial section measured 4.3 mm, exceeding the reported minimum span for a third negotiable space. Note also the PAP on the mesial root of #31, with the high probability of the same etiology. (**e**–**g**) Right-angle and off-angle radiographs reveal 3 separate canals and apical foramen in the completed mesial root. The retreated distal root also had 3 canals, but the final instrumentation created one large, scalloped ribbon canal configuration. (**h**) The axial and coronal sections demonstrate the span of the obturation in the mesial root and the confluence of the canals in the distal (The *white arrow* is pointing to the obturation of the Middle Mesial canal space in the axial section of the post-operative CBCT scan). (**i**) The colorized 3-D model highlights the comparative sizes between the retreated MB and ML canals and the primary instrumentation of the MM canal, terminating in 3 separate apical foramina

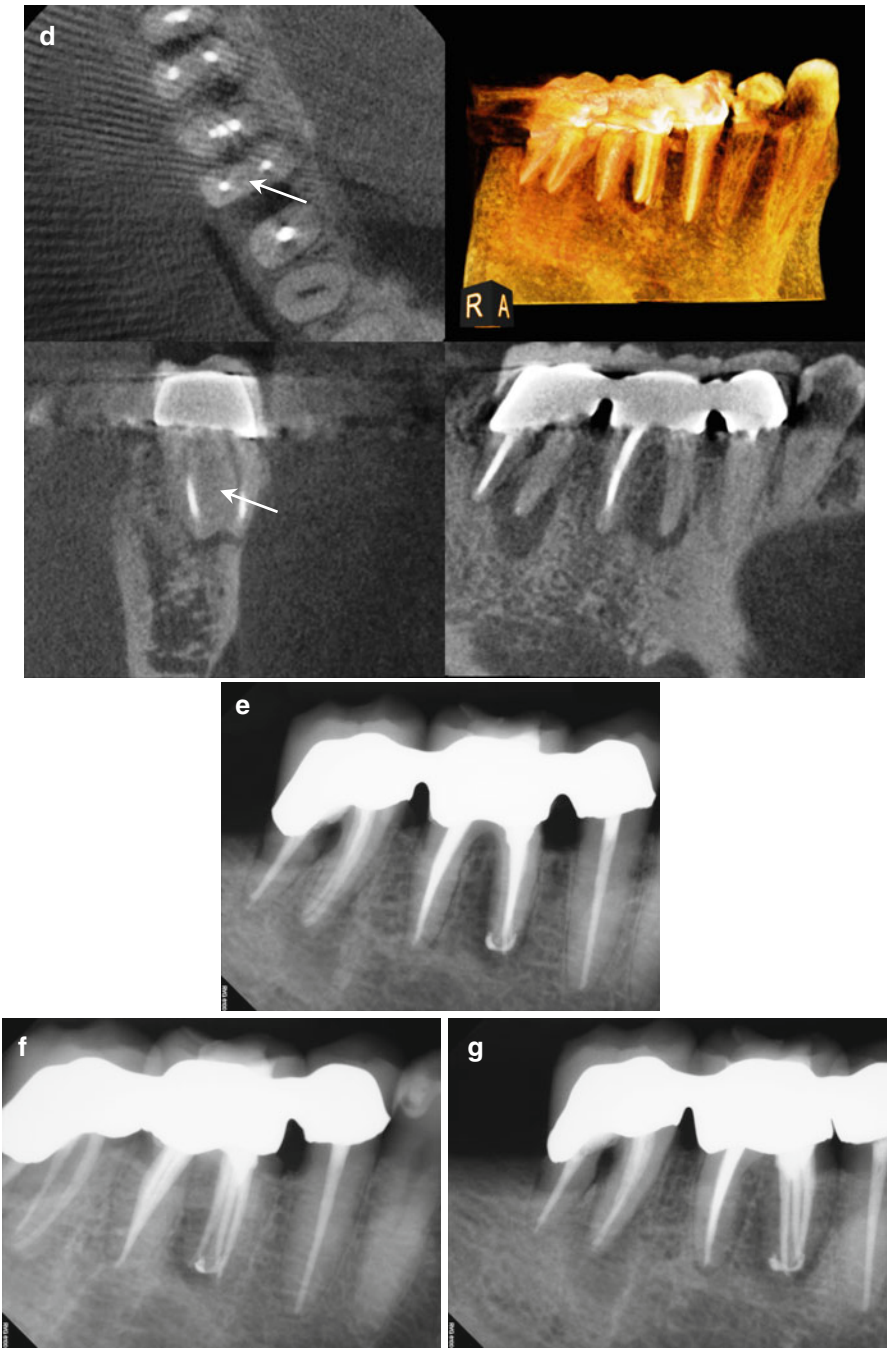

Fig. 5.4 (continued)

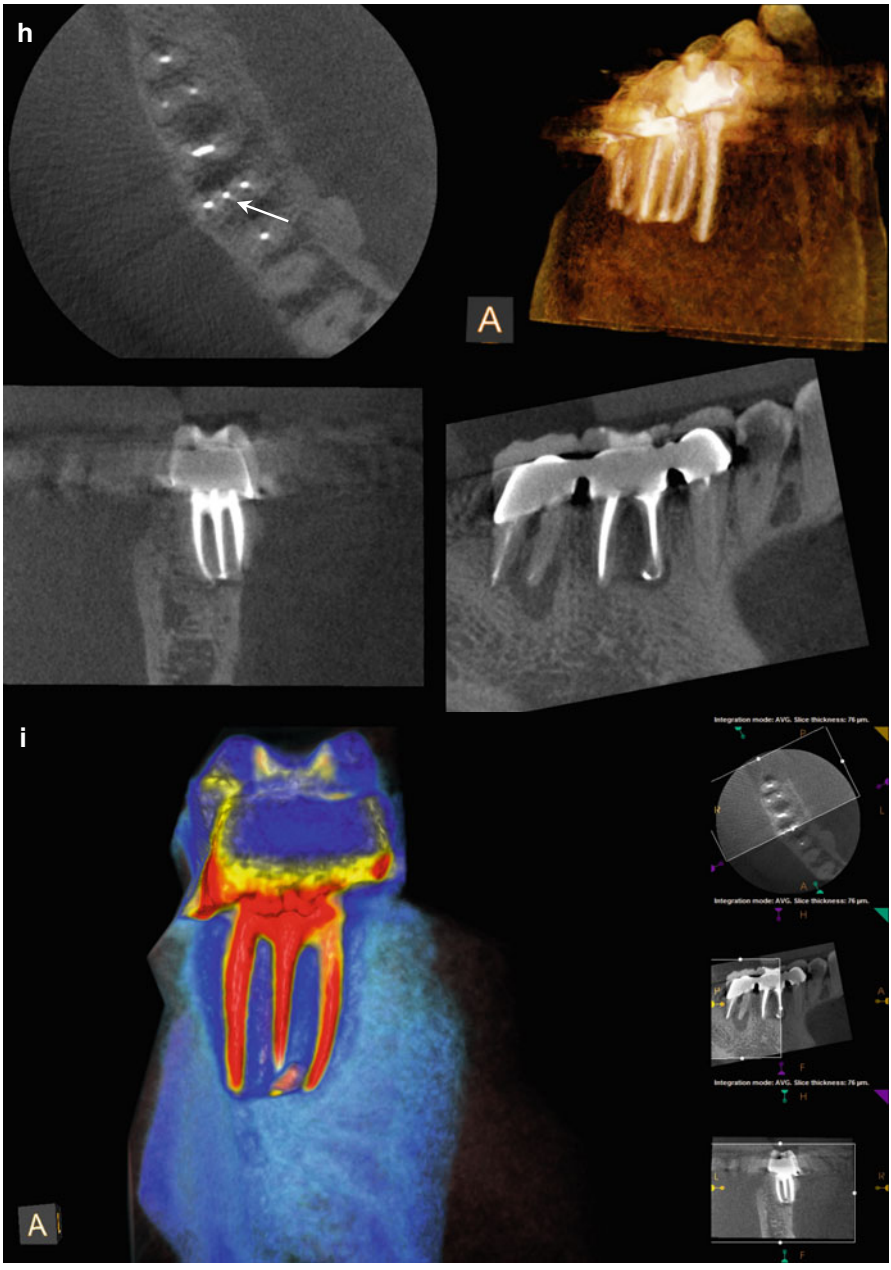

Fig. 5.4 (continued)

5.5 Case #5

Description The patient presented with a diagnosis of symptomatic apical periodontitis, localized to a tooth that was endodontically treated 3 years previously.

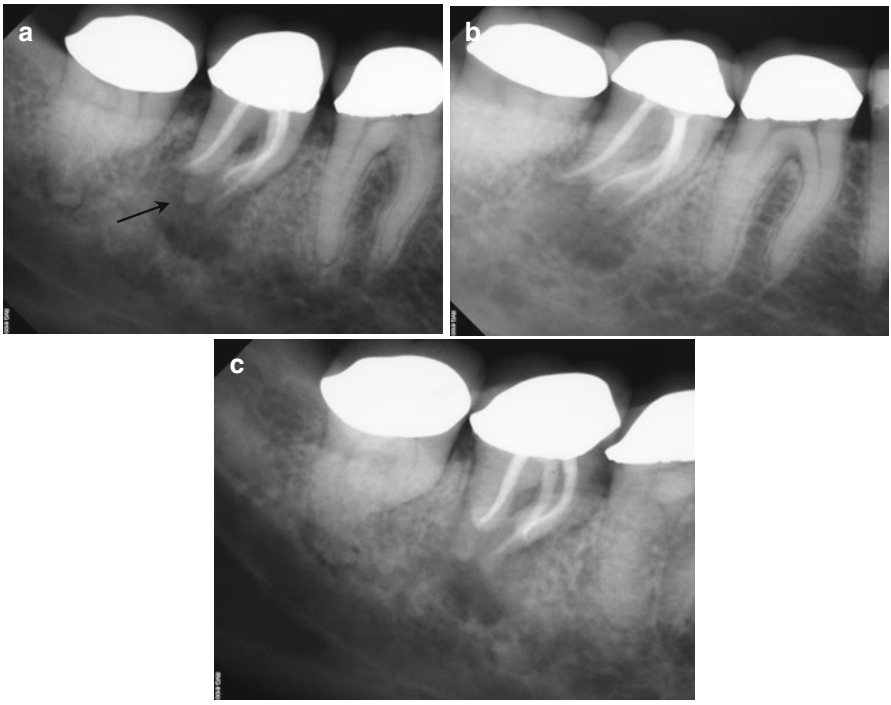

Fig. 5.5 (**a**–**c**) Right-angle and off-angle radiographs reveal a large PAA at the apices of tooth #30. There is a suggestion of an auxiliary root in (**a**) (*black arrow*), but its origin within the chamber and buccal-lingual position is not disclosed in any of the conventional images. (**d**) The axial view in the scan 2 mm apical to the CEJ confirms the presence of a second canal in the distal root, 2 mm lingual to the DB (*white arrow*). The coronal section reveals a sharp dilacerations of this root toward the buccal as it nears its terminus (*red arrow*); this change in direction will be explained in the next. (**e**) The axial view 2 mm from the terminus shows the DL root fusing with the ML root (*white arrow*), but their respective canal spaces do not join. At this level, the canal assumes a more linear path (*red arrow*). (**f**) The colorized 3-D coronal section highlights the juxtaposition of the DB and DL roots (*red arrow*) as well as the extent of the PA lesion and the thinning of the lingual cortical plate (*white arrows*). (**g**) Working length radiograph with files in the DB and DL canals. The gutta-percha is yet to be removed from the mesial canals (the radiopaque pin in the image is a 5 mm reference in the film holder). (**h**) Final radiographs of the completed retreatment. Note the overlapping of the mesial roots and the DL root. (**i**) 12-month recall radiographs; the lesion appears to be resolved, but overlying structures can mask underlying spaces. (**j**) 12-month CBCT scan demonstrates complete resolution after a thorough review of all the slices in all planes. This slice level corresponds to the location of the largest dimension of the lesion preoperatively. (**k**) A comparison of the preoperative (*top*) and 12-month postoperative (*bottom*) coronal and sagittal slices at almost identical levels, exhibiting complete resolution of the lesion

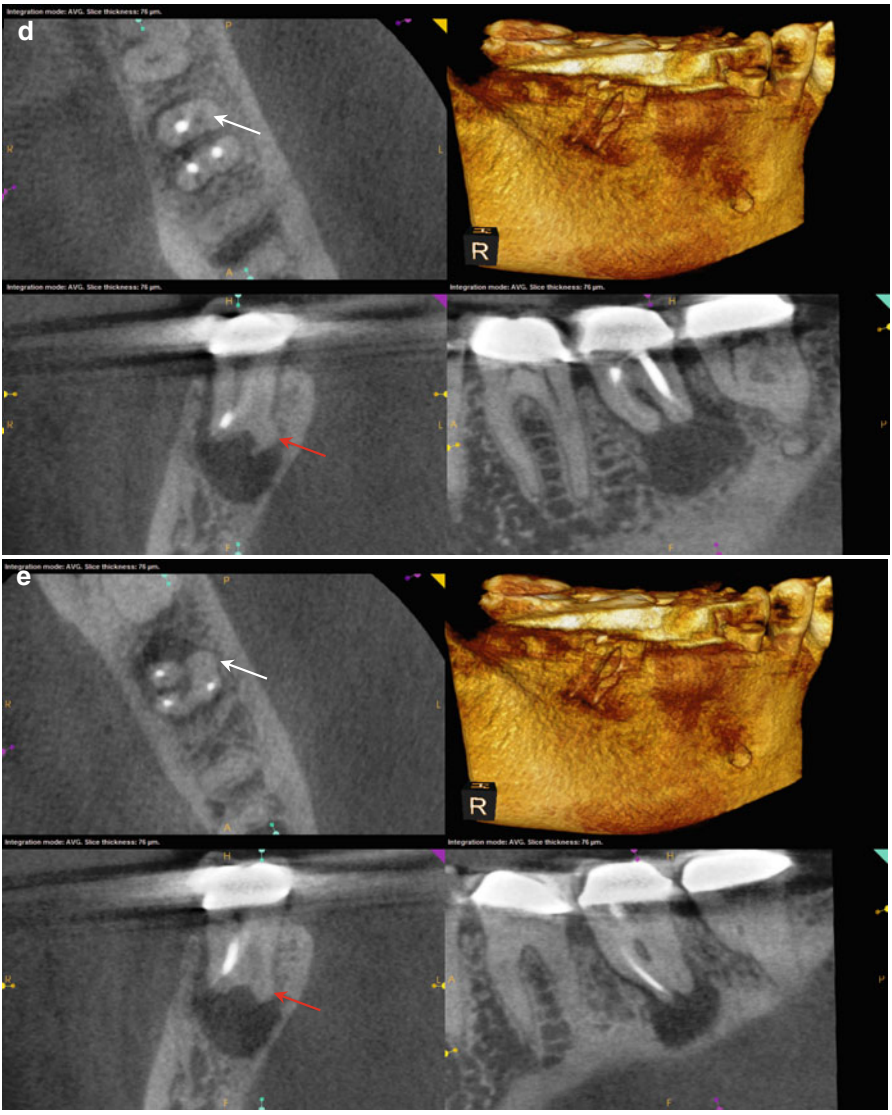

Fig. 5.5 (continued)

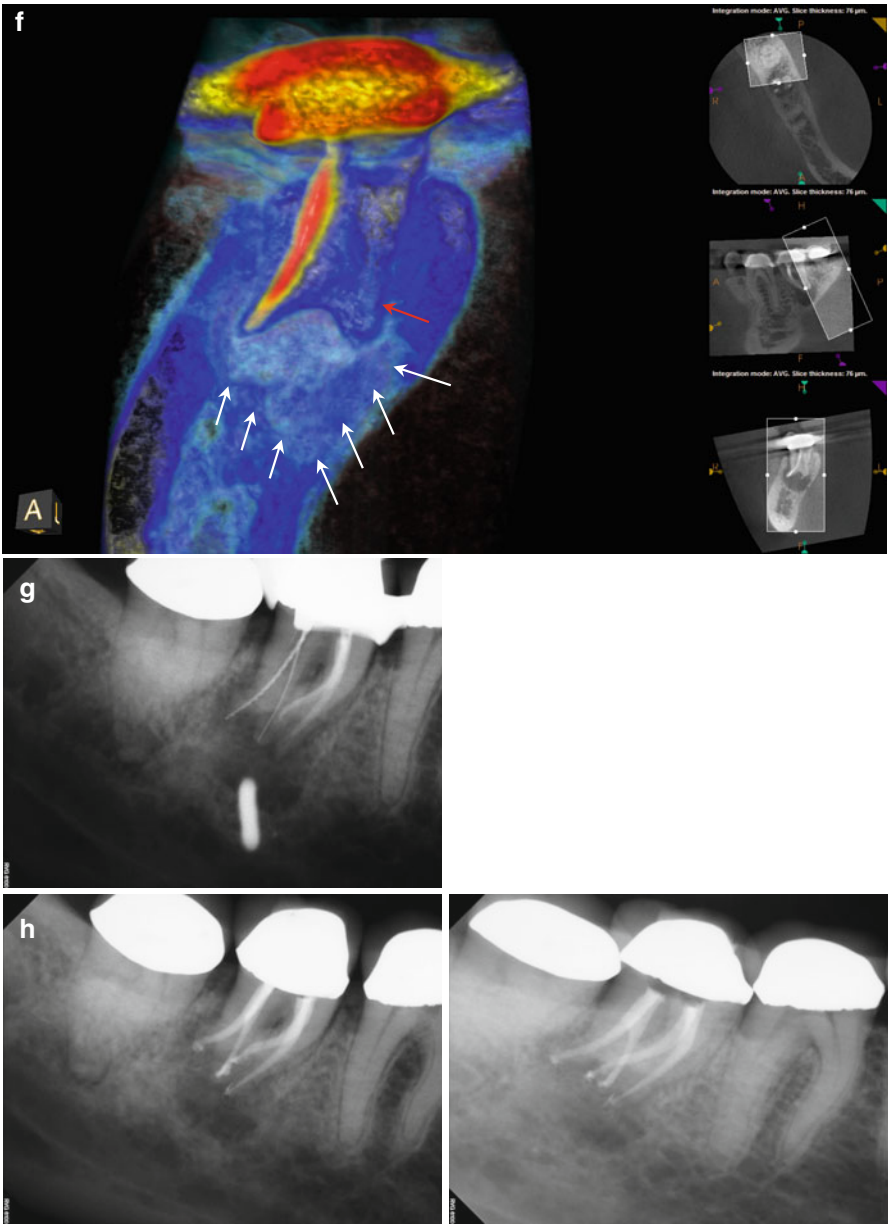

Fig. 5.5 (continued)

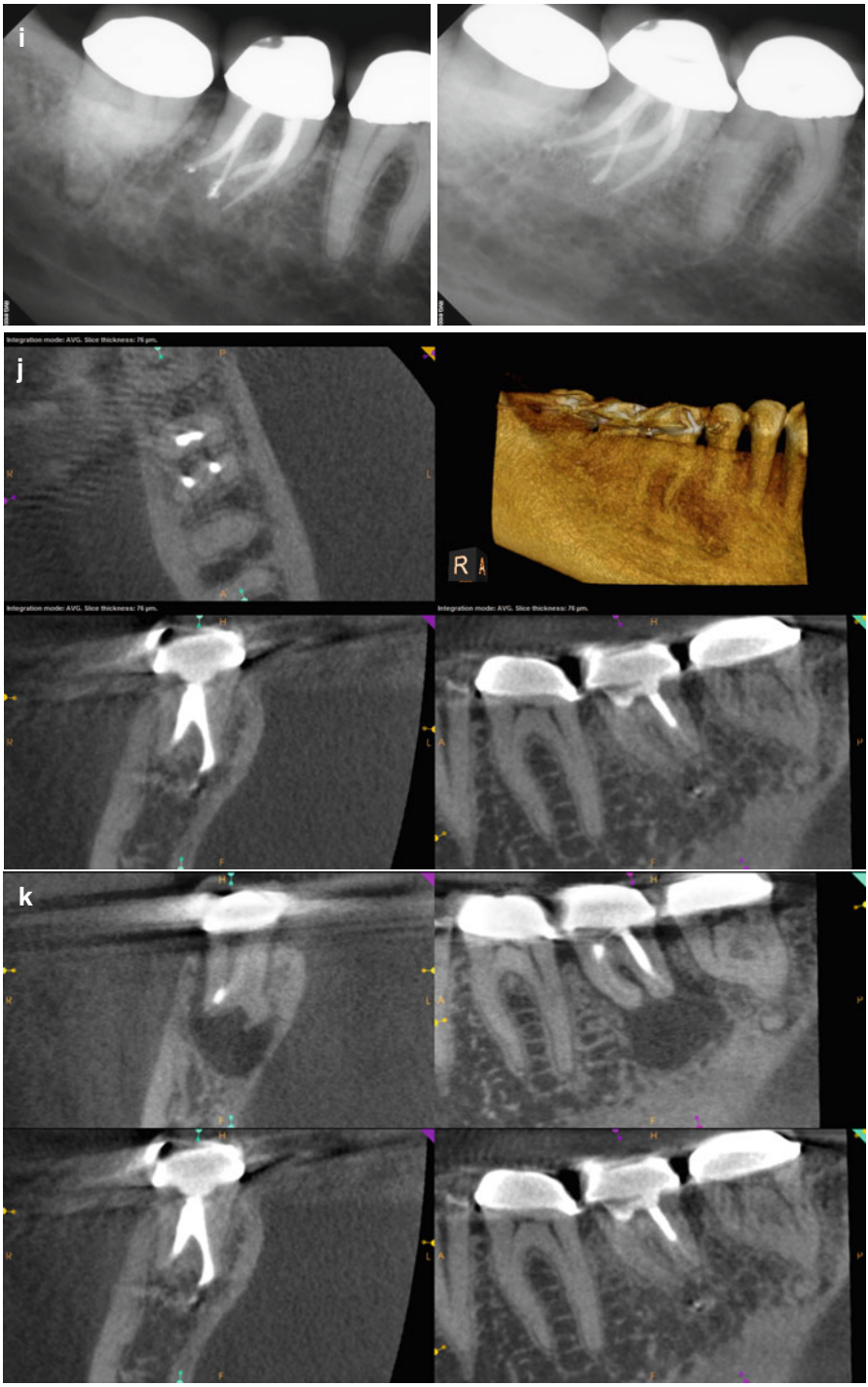

Fig. 5.5 (continued)

5.6 Case #6

Description The patient presents for evaluation of tooth #2. It has been treated within the previous 9 months and has developed deep periodontal probing at the mesial aspect of the root. The tooth is mobile but not depressible in the socket. Initial micro-reflection of the area and inspection with the SOM did not disclose any vertical fracture.

Fig. 5.6 (**a**, **b**) Preoperative radiographs demonstrating the extent of the bone loss at the mesial aspect of the root and the appearance of a 3-walled defect (*black arrow*). (**c**, **d**) The axial view reveals the extent of the bone loss at the mesial and distal aspects, with only the palatal wall intact (*white arrows*). The bulbous portion of the root at the distal suggests the location of the DB canal (*red arrow*). The coronal view shows the approximate location of the suspected perforation (*red-dashed arrows*); the invagination of the root form and the proximity of the obturative material were suggestive of this iatrogenic event. Reaccess of the canal spaces confirmed the presence of the DB canal and the perforation in the palatal canal. (**e**) Final posttreatment radiograph; note the multiple apical foramina in the mesial and distal aspects of the apical third of the root and the dramatic change in the width of the obturation. (**f**, **g**) Recall radiographs 6 months after initial treatment. The probing depth was reduced dramatically, and the tooth became more stable in the alveolus. Multiple apical foramina can be seen in the mesial and distal aspects of the apical third of the root. (**h**, **i**) 12-month recall radiographs reveal resolution of the mesial defect, although the PDL is widened and indicates possible occlusal trauma. The periodontal probing depths are within normal limits. (**j**) 12-month recall CBCT scan demonstrates approximately 80% resolution of the presenting lesion, with a reestablishment of the buccal cortical plates and periapical bone matrix (*white arrows*)

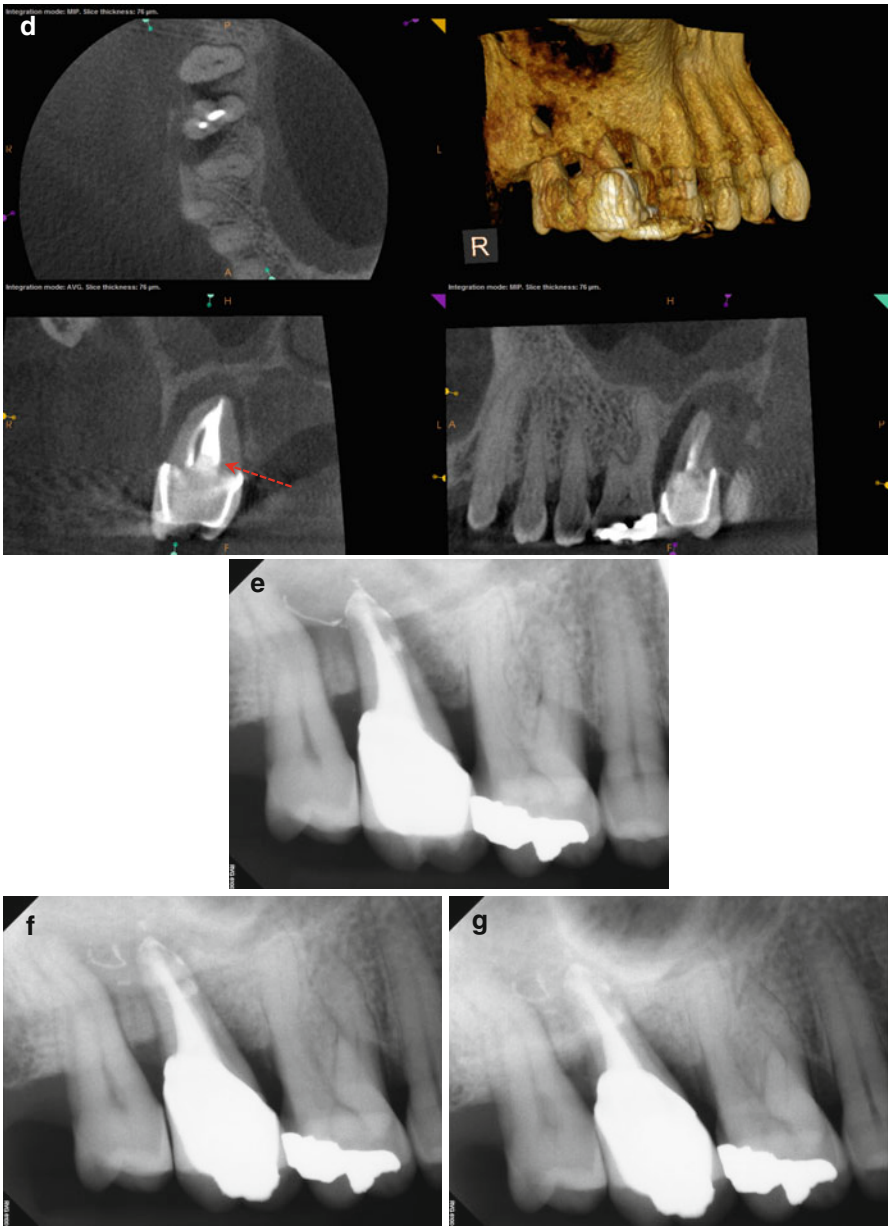

Fig. 5.6 (continued)

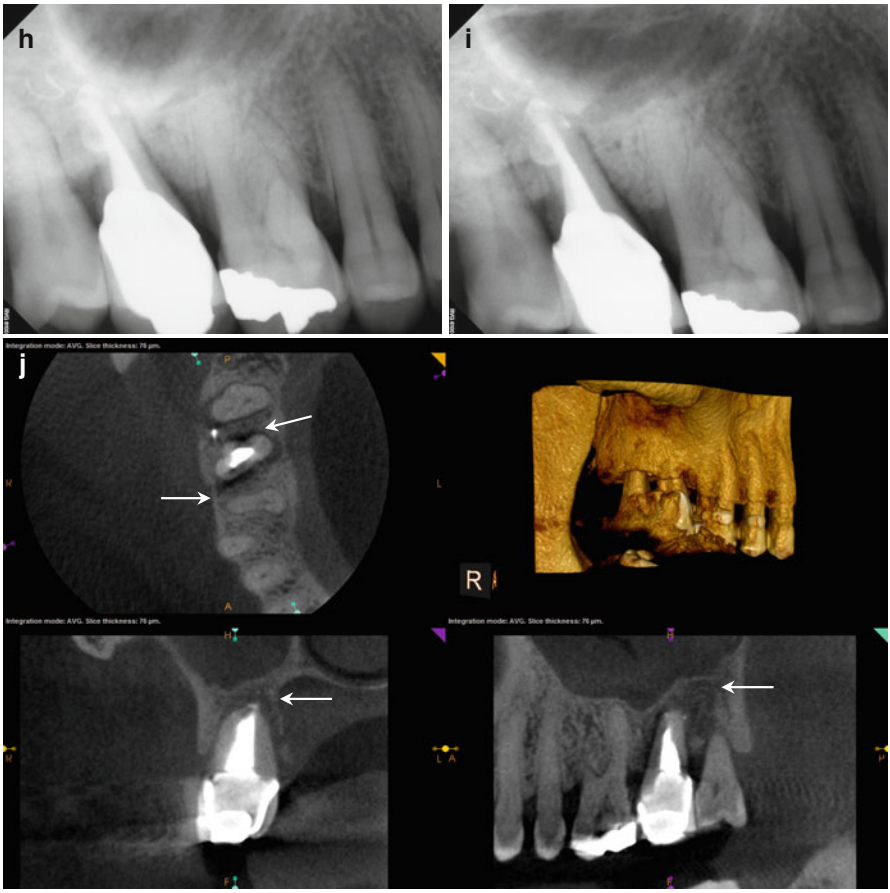

Fig. 5.6 (continued)

5.7 Case #7

Description The patient presents in pain in a tooth that has been previously treated 1 year ago. Her preliminary diagnosis is symptomatic apical periodontitis.

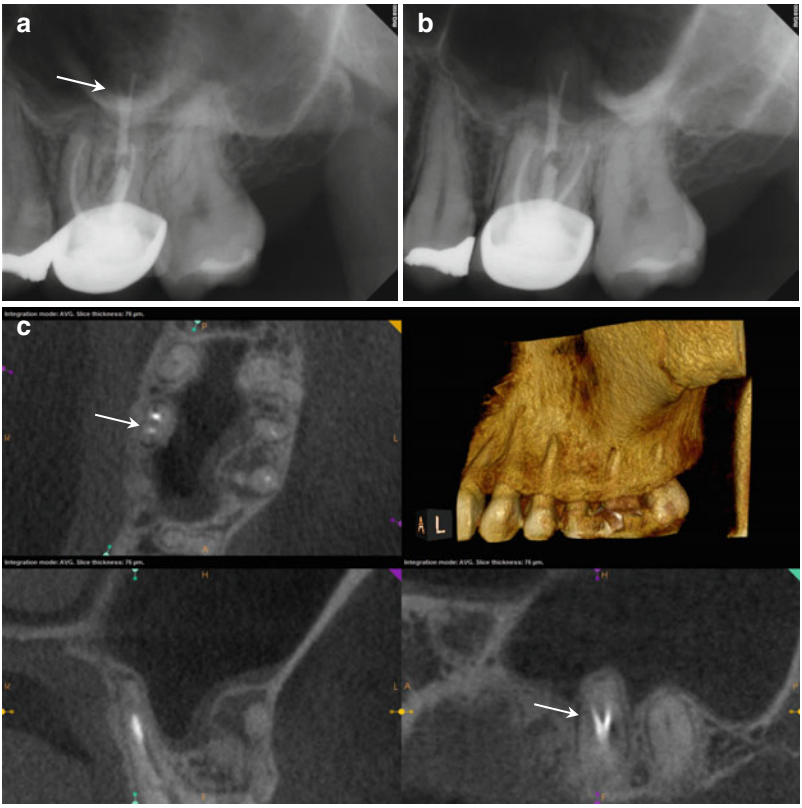

Fig. 5.7 (**a**, **b**) Preoperative radiographs from different angles reveal PAP on the MB root apex, as well as the suggestion of a bifurcation of the palatal canal (*white arrow*). The distal part of the split appears more dense than the mesial, implying that the mesial radiopacity is a sealer tract. (**c**) The CBCT scan shows definitively two separate canals in the palatal root. Accurate measurements place the level of the bifurcation 4.3 mm from the terminus of the distopalatal canal. The higher density spot in the axial and sagittal sections of the palatal root is the gutta-percha; the lower density object is the sealer tract (*white arrows*). (**d**) This colorized sagittal section has been magnified to ascertain the angle of the bifurcation; the deviation is less than 40°, so an appropriately angled instrument should be able to engage the orifice without difficulty (*white arrow*). When the angle of bifurcation is 60° or more, the dilaceration may be too abrupt to allow easy insertion of the file without additional coronal modification of the common canal space. (**e**) The axial section of the MB root demonstrates the eccentric placement of the MB root canal filling, indicative of the presence of an MB_2 canal (*white arrow*). The coronal view of the same root suggests that the MB_2 may, in fact, be a separate root fused to the MB_1 (*red arrow*). (**f**) The colorized coronal section highlights the MB_2 root and the distension/expansion of the floor of the maxillary sinus from the developing apical lesion (*yellow arrows*). (**g**, **h**) Final treatment radiographs presenting the obturation of the separate MB1/MB2 canals as well as the mesiopalatal and distopalatal canals. (**i**) 12-month recall radiograph: the lesion at the MB root appears healed, and the patient is asymptomatic

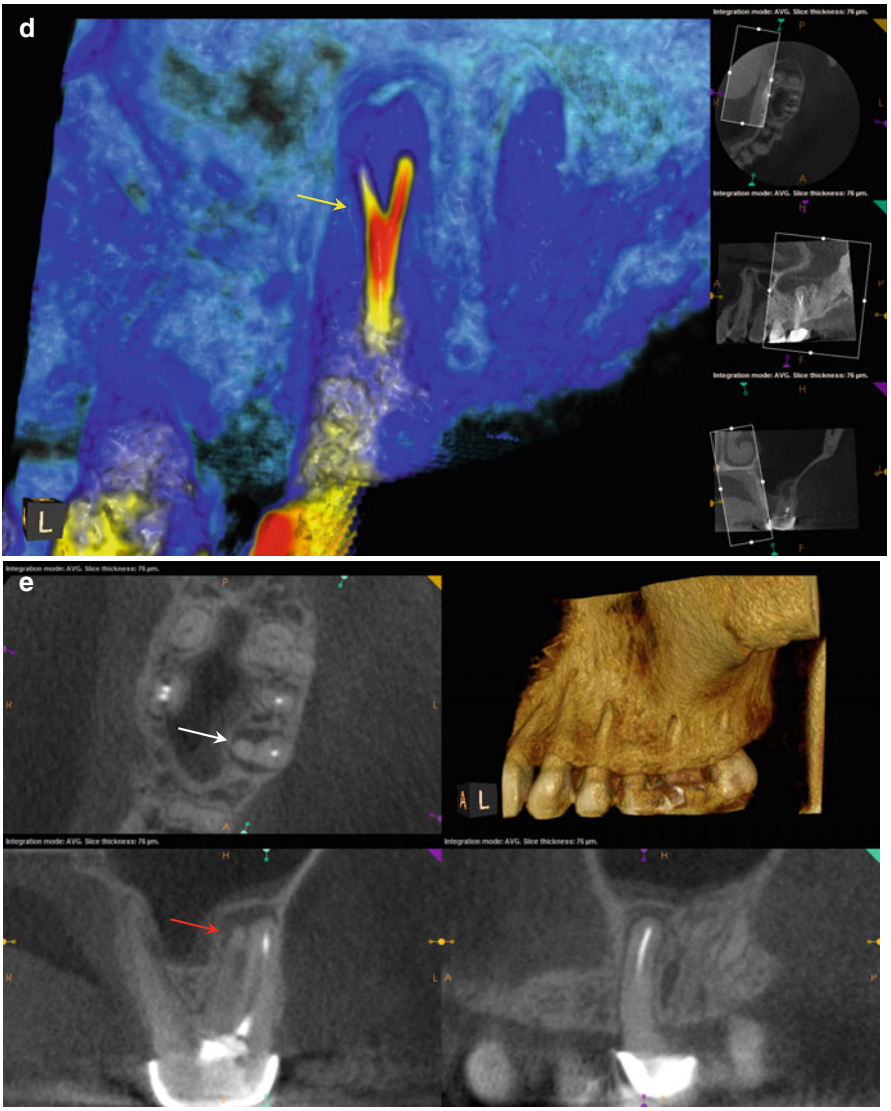

Fig. 5.7 (continued)

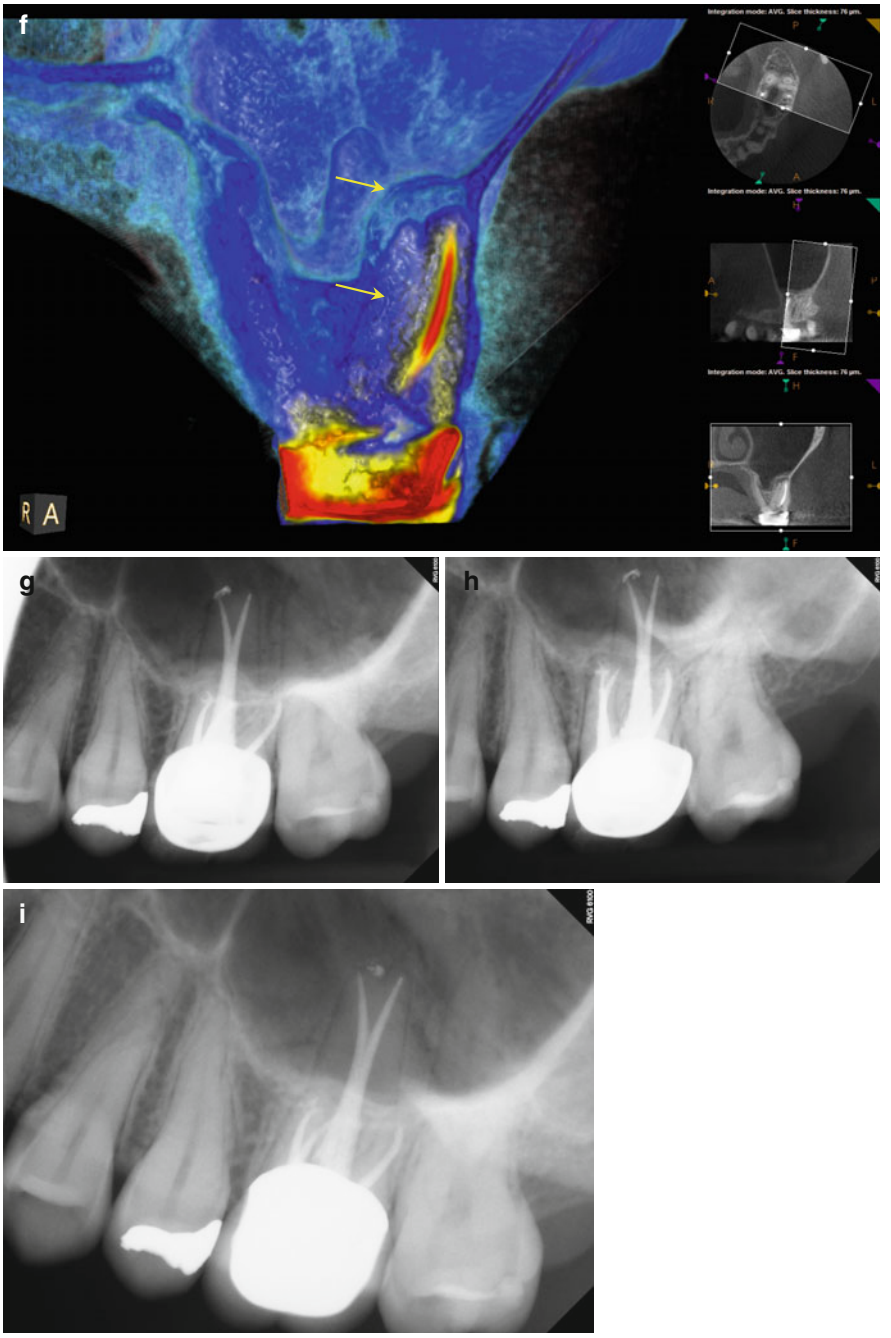

Fig. 5.7 (continued)

5.8 Case #8

Description The patient presents with the chief complaint of biting sensitivity. The tooth was endodontically treated the previous year and was referred for evaluation of vertical fracture.

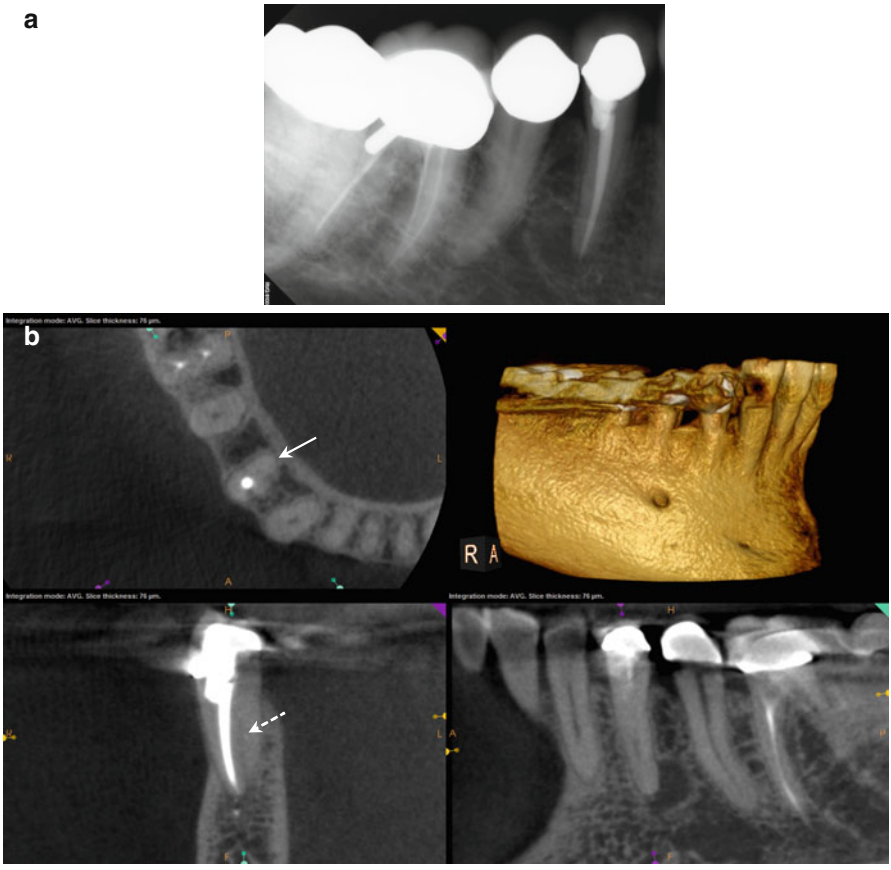

Fig. 5.8 (**a**) Preoperative radiograph of tooth #28. The tooth has been restored with a full coverage crown, and there is a periapical area at the apex of the tooth. Periodontal probing is minimal, with no deep probing evident circumferentially. The tooth is, however, sensitive to percussion and biting. (**b**) Survey of the axial sections in the CBCT reveals the asymmetry of the existing root canal filling, highly suggestive of an additional canal space (*white arrow*). A faint low-density line can be seen in the coronal section (*broken white arrows*) bifurcating from the buccal canal at the junction of the coronal and middle thirds of the root. This most likely represents the lingual canal space. (**c**) The colorized coronal section demonstrates the buccal displacement of the existing obturation; the *yellow arrow* points to the area of the suspected canal location. (**d**, **e**) Posttreatment radiographs from different angles, displaying the deep point of the bifurcation (middle third of the root) and sealer extrusions into the periapical area

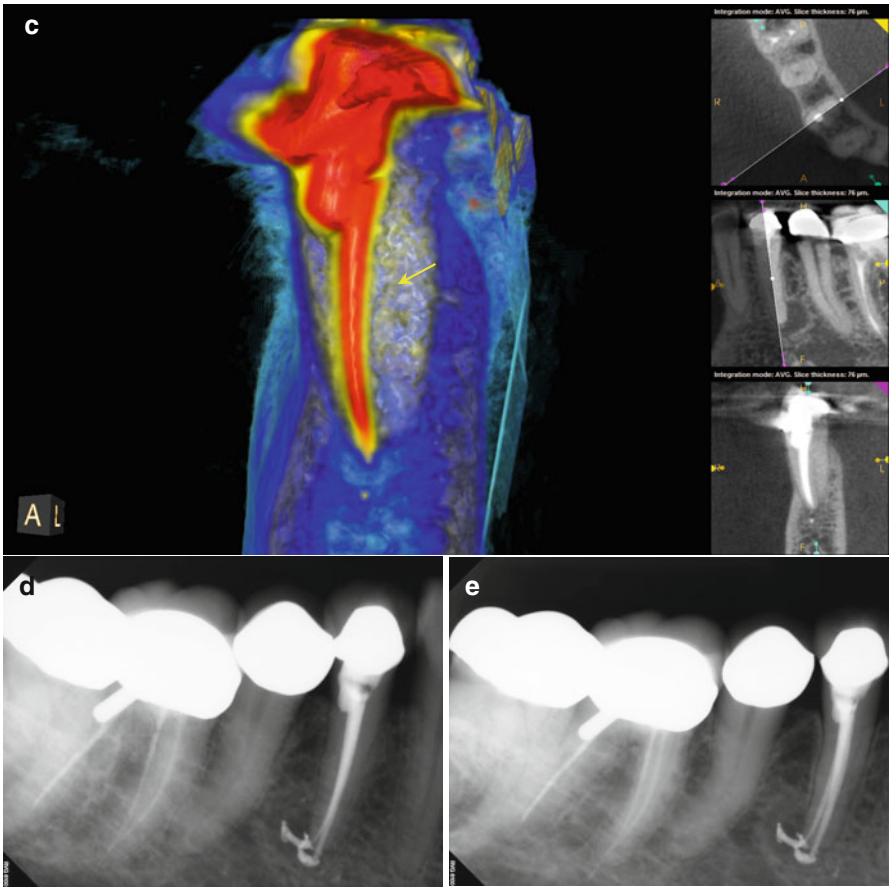

Fig. 5.8 (continued)

5.9 Case #9

Description The patient had tooth #19 initially treated 2 years ago; persistence of symptoms prompted the retreatment of the same tooth 18 months later. The patient remains symptomatic to biting and chewing and was advised that the tooth is fractured and requires extraction. He is seeking a second opinion.

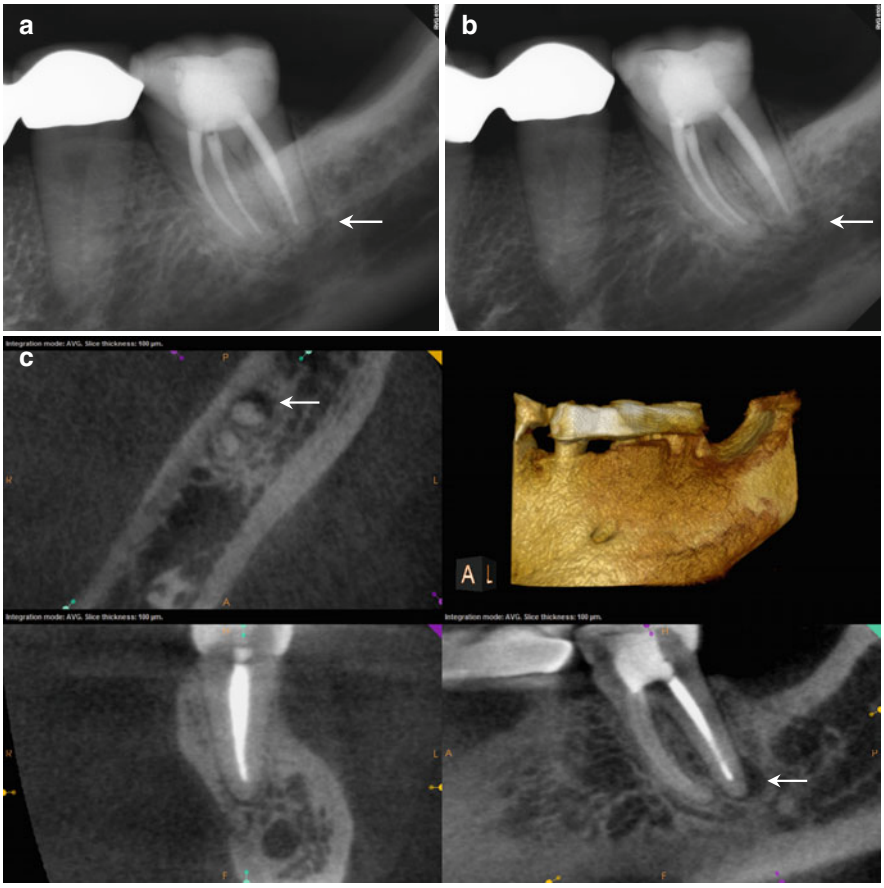

Fig. 5.9 (**a**, **b**) Preoperative radiographs reveal adequate root canal fillings, but a faint area at the distal aspect of the distal root apex is evident in both images (*white arrows*). (**c**) The axial and sagittal sections demonstrate a small area of low density at the distal aspect of the distal root apex; this most likely is the result of tissue remaining in the dilacerated portion of the canal that has not been negotiated and debrided (*white arrows*). Slice-by-slice examination of the sagittal sections discloses the angle and direction of this short canal segment. The mesial canals appear underextended as well. (**d**) The colorized version of the sagittal section has been magnified to highlight the periapical area (*yellow arrows*) as well as the dilacerated canal path (*red arrow*). (**e**) Working length radiograph after harvesting the gutta-percha in the distal canal, confirming the negotiation of the file to the minor constriction. The remaining root canal filling materials were removed, and the canals re-instrumented as well. (**f**, **g**) Final radiographs showing the extension of the filling material into the distal dilacerations and the extended mesial canals. (**h**) 12-month recall scan showing resolution of the distal low-density area. The patient remains asymptomatic. (**i**) The colorized sagittal section at the 12-month recall: note the resolution of the distal area as compared to (**d**)

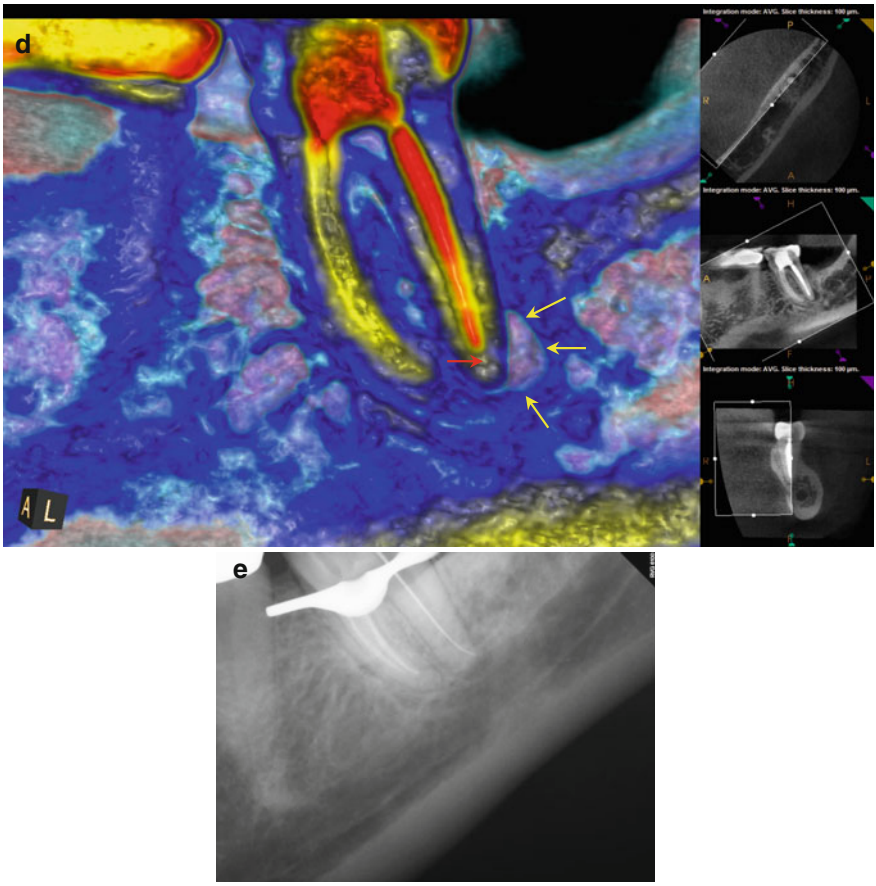

Fig. 5.9 (continued)

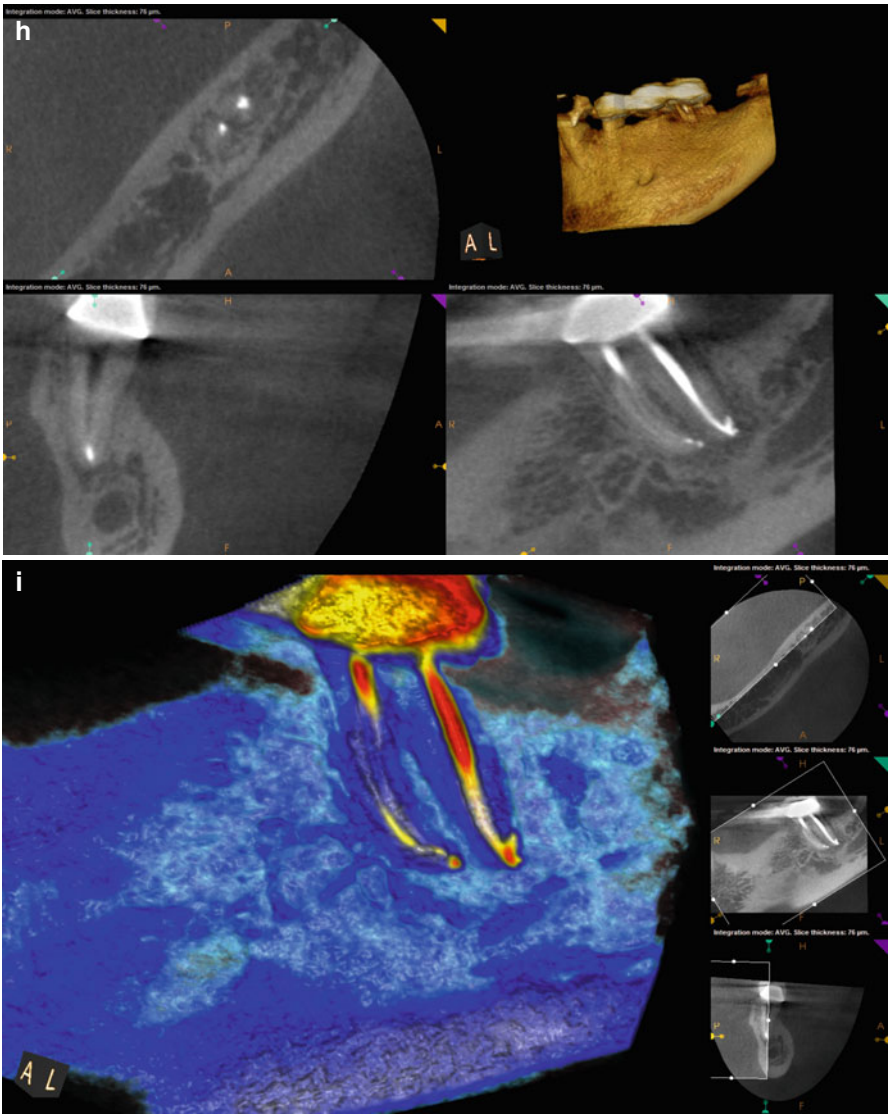

Fig. 5.9 (continued)

5.10 Case #10

Description The patient is referred for retreatment of tooth #31 prior to the placement of a new crown. The restorative dentist noticed an area on the distal root on a routine radiograph.

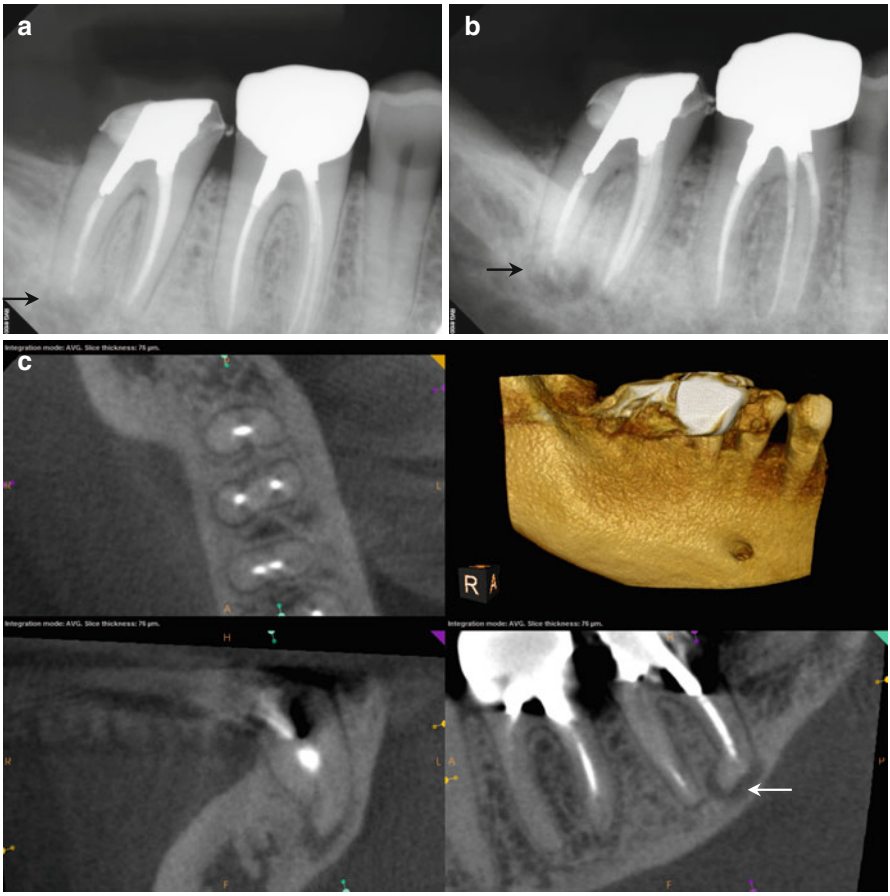

Fig. 5.10 (**a**, **b**) Preoperative radiographs confirm the presence of a periapical area on the distal root apex of #31 (*black arrows*). There is also a cast post/core cemented in the distal canal and must be removed prior to retreatment. (**c**) Preoperative CBCT scan discloses a sharp dilacerations of the distal root apex toward the mesial (*white arrow*). There is also a low-density area associated with this dilaceration, most likely the result of residual tissue in this root segment. (**d**) The colorized sagittal section has been magnified to highlight the dilacerated root segment and associated area (*yellow arrows*). This segment is too sharply bent and too abrupt for conventional rotary instruments; after harvesting the root canal filling materials, this section of the distal root canal will be negotiated and instrumented using conventional hand files. This should minimize the chance of a separation event. (**e**, **f**) Final posttreatment radiographs demonstrating the extrusion of softened gutta-percha into the sharp dilacerations (*black arrows*). Prior knowledge of the angle and direction of this small dilaceration enabled the successful negotiation and cleaning of this small, but crucial, space

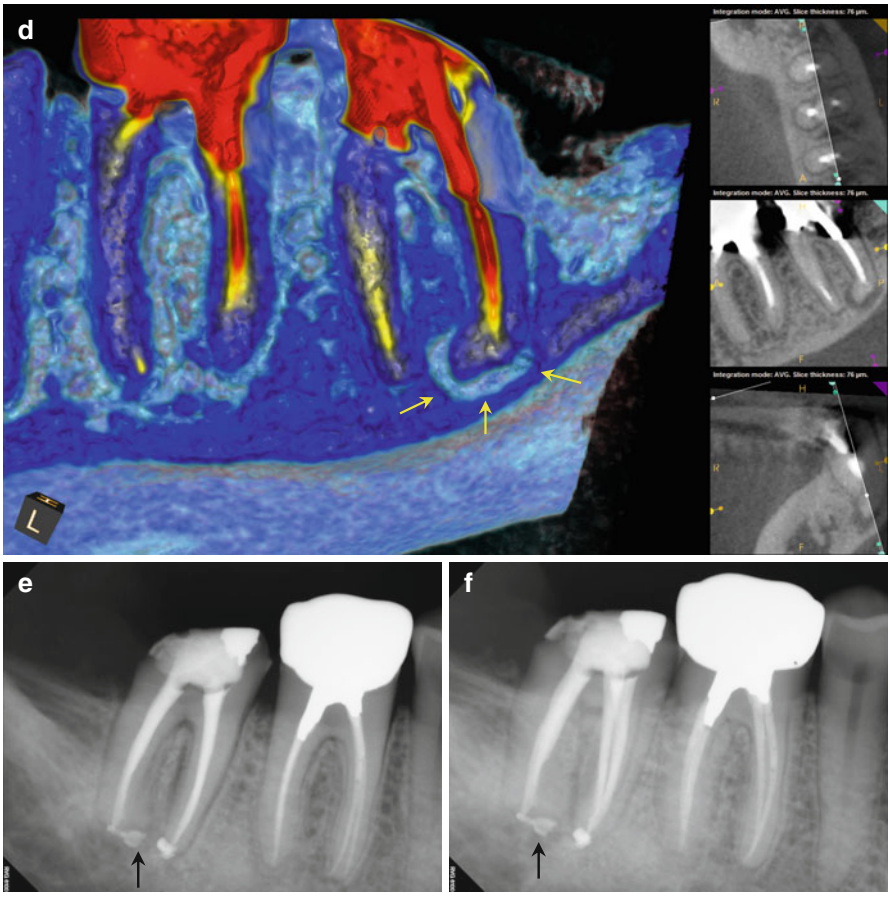

Fig. 5.10 (continued)

5.11 Case #11

Description The patient was referred for completion of tooth #15. The root canal treatment had been initiated by the general dentist, but then remarked to the patient that one of the canals was "blocked" and would require more specialized treatment. The patient is asymptomatic.

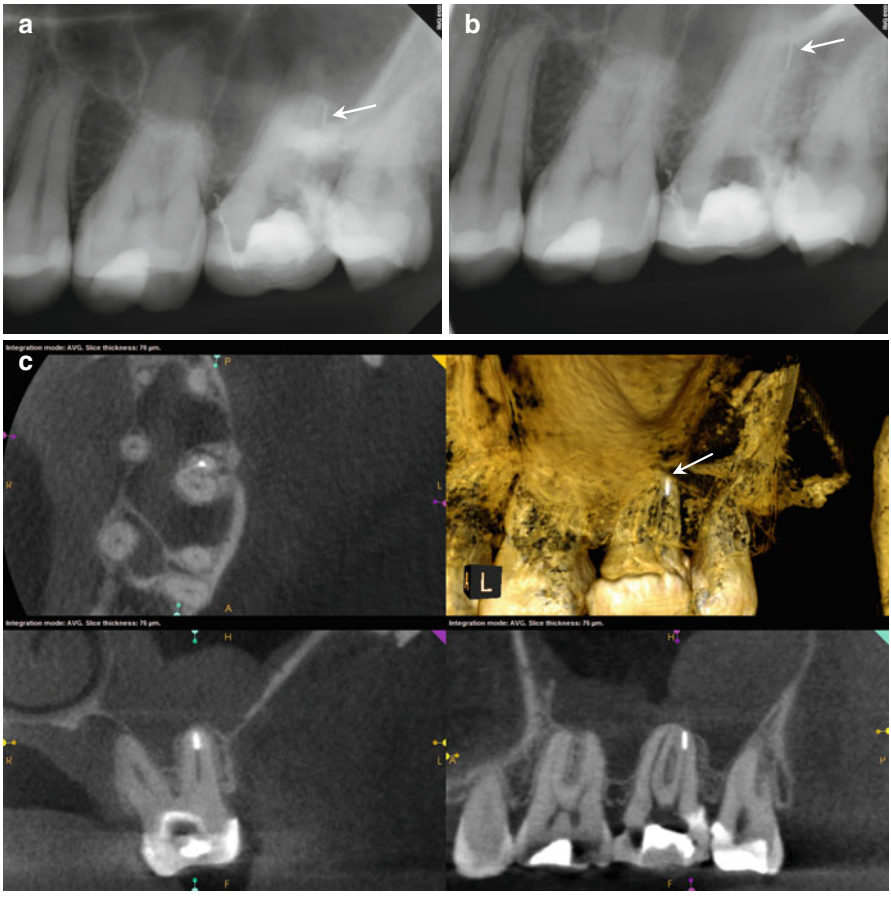

Fig. 5.11 (**a**, **b**) Preoperative radiographs reveal a small, radiopaque object in the region of the DB root. (**c**) Preoperative CBCT scan reveals the presence of a high-density object, 2.5 × 0.3 mm at the apical terminus of the DB canal of tooth #15 (*white arrow*). This is most likely a separated instrument. There is also a marked thickening of the Schneiderian membrane evident in the coronal and sagittal views, but the patient denies any sinus symptoms. (**d**) The colorized sagittal section highlights the object in the DB canal, as well as insights into its possible density. Consultation with the referring office confirmed that they were unaware of the separation. The patient was informed of the object and attempts were made (unsuccessfully) to retrieve it. (**e**, **f**) Final treatment radiographs displaying the root canal obturations in the other three canal spaces and the obturation of the DB canal to the object. The patient will be recalled at appropriate intervals, and surgical revision of the DB apex will be performed as needed

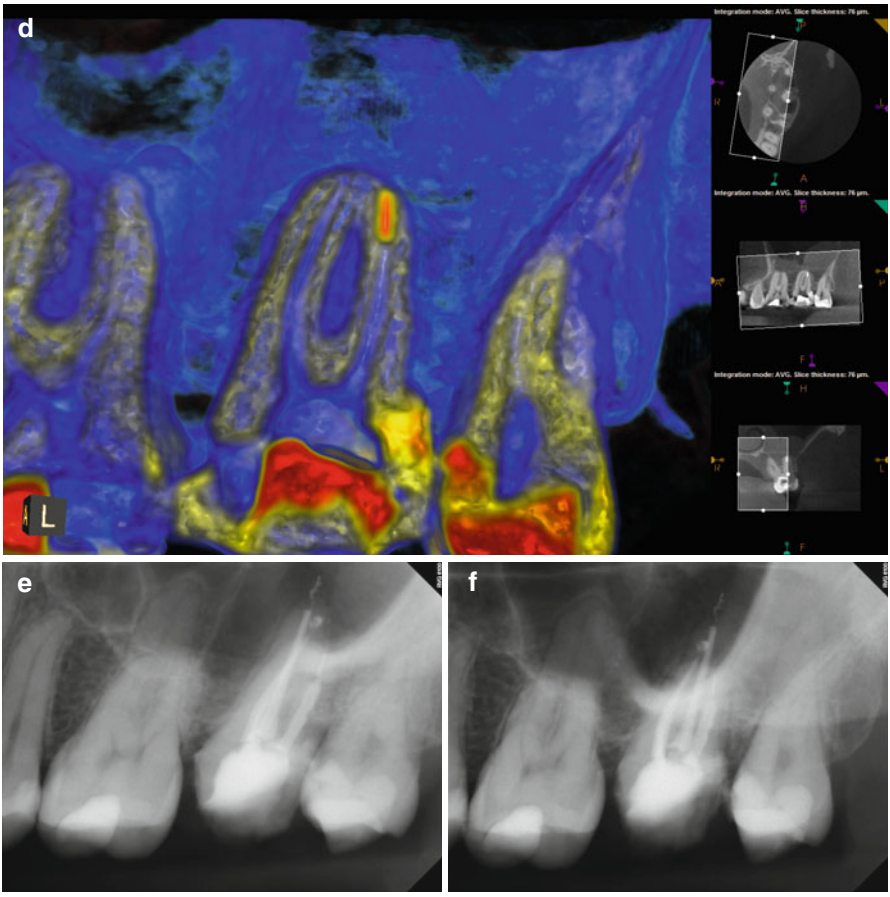

Fig. 5.11 (continued)

References

1. Grossman LI, Oliet S, Del Rio CE. Endodontic practice. 11th ed. Philadelphia: Lea & Febiger; 1988.
2. Weine F. Endodontic therapy. Saint Louis: The C.V.Mosby Company; 1972.
3. Krasner P, Rankow HJ. Anatomy of the pulp-chamber floor. J Endod. 2004;30(1):5–16.
4. Schwarze T, Baethge C, Stecher T, Geurtsen W. Identification of second canals in the mesiobuccal root of maxillary first and second molars using magnifying loupes or an operating microscope. Aust Endod J. 2002;28(2):57–60.
5. Kulild JC, Peters DD. Incidence and configuration of canal systems in the mesiobuccal root of maxillary first and second molars. J Endod. 1990;16(7):311–7.
6. Stropko JJ. Canal morphology of maxillary molars: clinical observations of canal configurations. J Endod. 1999;25(6):446–50.
7. Suter B, Lussi A, Sequeira P. Probability of removing fractured instruments from root canals. Int Endod J. 2005;38(2):112–23.
8. Roda RS. Root perforation repair: surgical and nonsurgical management. Pract Proced Aesthet Dent. 2001;13(6):467–72; quiz 474.
9. Koch K. The microscope. Its effect on your practice. Dent Clin N Am. 1997;41(3):619–26.
10. Hess W. The anatomy of the root canals of the teeth of the permanent dentition. London: John Bale, Sons & Danielsson Ltd; 1925.
11. Fj V. Root canal anatomy of the mandibular anterior teeth. J Am Dent Assoc. 1974;89(2):369–71.
12. Neaverth EJ, Kotler LM, Kaltenbach RF. Clinical investigation (in vivo) of endodontically treated maxillary first molars. J Endod. 1987;13(10):506–12.
13. Bellizzi R, Hartwell G. Radiographic evaluation of root canal anatomy of in vivo endodontically treated maxillary premolars. J Endod. 1985;11(1):37–9.
14. Fogel HM, Peikoff MD, Christie WH. Canal configuration in the mesiobuccal root of the maxillary first molar: a clinical study. J Endod. 1994;20(3):135–7.
15. Niemczyk S. CBCT: the virtual surgery© in endodontic diagnosis. Dent Econ Oral Hygiene. 2012;102(2):80–81.
16. Michetti J, Maret D, Mallet JP, Diemer F. Validation of cone beam computed tomography as a tool to explore root canal anatomy. J Endod. 2010;36(7):1187–90.
17. Baratto Filho F, Zaitter S, Haragushiku GA, de Campos EA, Abuabara A, Correr GM. Analysis of the internal anatomy of maxillary first molars by using different methods. J Endod. 2009;35(3):337–42.
18. Matherne RP, Angelopoulos C, Kulild JC, Tira D. Use of cone-beam computed tomography to identify root canal systems in vitro. J Endod. 2008;34(1):87–9.
19. Badole GP, Warhadpande MM, Shenoi PR, Lachure C, Badole SG. A rare root canal configuration of bilateral maxillary first molar with 7 root canals diagnosed using cone-beam computed tomographic scanning: a case report. J Endod. 2014;40(2):296–301.
20. Llena C, Fernandez J, Ortolani PS, Forner L. Cone-beam computed tomography analysis of root and canal morphology of mandibular premolars in a Spanish population. Imaging Sci Dent. 2014;44(3):221–7.
21. Silva EJ, Nejaim Y, Silva AI, Haiter-Neto F, Zaia AA, Cohenca N. Evaluation of root canal configuration of maxillary molars in a Brazilian population using cone-beam computed tomographic imaging: an in vivo study. J Endod. 2014;40(2):173–6.
22. Torres A, Jacobs R, Lambrechts P, et al. Characterization of mandibular molar root and canal morphology using cone beam computed tomography and its variability in Belgian and Chilean population samples. Imaging Sci Dent. 2015;45(2):95–101.
23. Mahendra M, Verma A, Tyagi S, Singh S, Malviya K, Chaddha R. Management of complex root canal curvature of bilateral radix entomolaris: three-dimensional analysis with cone beam computed tomography. Case Rep Dent. 2013;2013:697323.

24. Low KM, Dula K, Burgin W, von Arx T. Comparison of periapical radiography and limited cone-beam tomography in posterior maxillary teeth referred for apical surgery. J Endod. 2008;34(5):557–62.
25. Bornstein MM, Lauber R, Sendi P, von Arx T. Comparison of periapical radiography and limited cone-beam computed tomography in mandibular molars for analysis of anatomical landmarks before apical surgery. J Endod. 2011;37(2):151–7.
26. Witherspoon DE, Small JC, Regan JD. Missed canal systems are the most likely basis for endodontic retreatment of molars. Tex Dent J. 2013;130(2):127–39.
27. Karapinar-Kazandag M, Basrani BR, Friedman S. The operating microscope enhances detection and negotiation of accessory mesial canals in mandibular molars. J Endod. 2010;36(8):1289–94.
28. Carabelli G. Systematiches Handbuch Der Zahnheikunde. 2nd ed. Vienna: Braumuller and Seidel; 1844.
29. Steelman R. Incidence of an accessory distal root on mandibular first permanent molars in Hispanic children. ASDC J Dent Child. 1986;53(2):122–3.
30. de Souza-Freitas JA, Lopes ES, Casati-Alvares L. Anatomic variations of lower first permanent molar roots in two ethnic groups. Oral Surg Oral Med Oral Pathol. 1971;31(2):274–8.
31. Garg AK, Tewari RK, Kumar A, Hashmi SH, Agrawal N, Mishra SK. Prevalence of three-rooted mandibular permanent first molars among the Indian Population. J Endod. 2010;36(8):1302–6.
32. Schafer E, Breuer D, Janzen S. The prevalence of three-rooted mandibular permanent first molars in a German population. J Endod. 2009;35(2):202–5.
33. De Moor RJ, Deroose CA, Calberson FL. The radix entomolaris in mandibular first molars: an endodontic challenge. Int Endod J. 2004;37(11):789–99.
34. Hannah R, Kandaswamy D, Jayaprakash N. Endodontic management of a mandibular second molar with radix entomolaris: a case report. Restor Dent Endod. 2014;39(2):132–6.
35. De Moor RJ. C-shaped root canal configuration in maxillary first molars. Int Endod J. 2002;35(2):200–8.
36. Singla M, Aggarwal V. C-Shaped palatal canal in maxillary second molar mimicking two palatal canals diagnosed with the aid of spiral computerized tomography. Oral Surg Oral Med Oral Pathol Oral Radiol Endod. 2010;109(6):e92–5.
37. Carlsen O, Alexandersen V, Heitmann T, Jakobsen P. Root canals in one-rooted maxillary second molars. Scand J Dent Res. 1992;100(5):249–56.
38. Alavi AM, Opasanon A, Ng YL, Gulabivala K. Root and canal morphology of Thai maxillary molars. Int Endod J. 2002;35(5):478–85.
39. Harris WE. Unusual root canal anatomy in a maxillary molar. J Endod. 1980;6(5):573–5.
40. Benenati FW. Maxillary second molar with two palatal canals and a palatogingival groove. J Endod. 1985;11(7):308–10.
41. Bond JL, Hartwell G, Portell FR. Maxillary first molar with six canals. J Endod. 1988;14(5):258–60.
42. Thews ME, Kemp WB, Jones CR. Aberrations in palatal root and root canal morphology of two maxillary first molars. J Endod. 1979;5(3):94–6.
43. Stone LH, Stroner WF. Maxillary molars demonstrating more than one palatal root canal. Oral Surg Oral Med Oral Pathol. 1981;51(6):649–52.
44. Cecic P, Hartwell G, Bellizzi R. The multiple root canal system in the maxillary first molar: a case report. J Endod. 1982;8(3):113–5.
45. Wong M. Maxillary first molar with three palatal canals. J Endod. 1991;17(6):298–9.
46. Cleghorn BM, Christie WH, Dong CC. The root and root canal morphology of the human mandibular first premolar: a literature review. J Endod. 2007;33(5):509–16.

Surgical Treatment Utilizing Cone Beam Computed Tomography

6

Mohamed I. Fayad and Bradford R. Johnson

Abstract

Cone beam computed tomography (CBCT) is a diagnostic imaging modality that provides a high-quality, dimensionally accurate three-dimensional (3D) representation of the osseous elements of the maxillofacial skeleton. CBCT has the potential to transform the practice of endodontic microsurgery, much in the same way that other new technologies introduced over the past two decades – such as microscopes, ultrasonic devices, and new root-end filling materials – have led to enhanced safety and treatment outcomes. The different applications of CBCT in diagnosis, treatment planning, and long-term outcome evaluation of periapical surgery will be reviewed. In this chapter cases will be presented to demonstrate the value of CBCT information in presurgical assessment, case selection, and treatment planning in endodontic microsurgery. The use of CBCT to identify and manage cases involving close proximity to important anatomical structures (e.g., maxillary sinus, the inferior alveolar, mental, and nasopalatine neurovascular bundles) and to evaluate the outcome of periapical microsurgery will be presented and discussed.

6.1 Potential Applications of CBCT in Treatment Planning of Endodontic Microsurgery

Cone beam computed tomography (CBCT) is a radiographic method which allows the clinician to visualize an individual tooth or teeth in relation to the surrounding structures and to create a three-dimensional (3D) image of the area. Traditional radiographic examinations are usually limited to two-dimensional views captured using radiographic film or digital sensors. Two-dimensional methods reproduce the

M.I. Fayad, DDS, MS, PhD (✉) • B.R. Johnson, DDS, MHPE
Department of Endodontics, University of Illinois at Chicago, Chicago, IL, USA
e-mail: mfayad1@uic.edu; bjohnson@uic.edu

M. Fayad, B.R. Johnson (eds.), *3D Imaging in Endodontics*,
DOI 10.1007/978-3-319-31466-2_6

three-dimensional anatomy as a 2D image. Crucially, essential information of the three-dimensional anatomy of the tooth/teeth and adjacent structures is obscured, and even with paralleling techniques, distortion and superimposition of dental structures in periapical views are unavoidable.

The role of CBCT in planning for periapical microsurgery has been well documented [1–4]. A major advantage of CBCT is the three-dimensional geometric accuracy compared with conventional radiographs. Comparing CBCT with periapical films, the CBCT has been reported to be a more sensitive means to detect changes in density of the bony structures [5] and the presence of periapical rarefaction. Three-dimensional visualization of the location of any lesions and the increased accuracy for the diagnosis of the periapical status have been reported [6, 7]. The different spatial views of CBCT images eliminate the superimposition of anatomical structures. Periapical microsurgery involving maxillary and mandibular molars is often challenging. Difficulties include the close proximity of the apices or periapical lesions to vital structures. In the posterior maxillary region, the roots of maxillary teeth overlap with anatomic structures such as the maxillary sinus and the zygomatic process. The roots of maxillary posterior teeth and their periapical tissues can be visualized separately and in all three orthogonal planes without superimposition of the overlying zygomatic process, alveolar bone, and adjacent roots. In the posterior mandibular region, the roots of the mandibular premolars and molars are associated with close proximity of the apices or periapical pathology to the mental foramen and mandibular canal.

Both medical CT and CBCT have been used for planning endodontic microsurgery [8, 9]. Three-dimensional imaging allows for a more precise preoperative analysis of the anatomical relationship of the root apices to important neighboring structures such as the mandibular canal, mental foramen, and maxillary sinus. Velvart et al. [8] found that the relationship of the mandibular canal to the root apices could be determined in every case when using medical CT, but in less than 40 % of cases when using conventional radiography. It is likely that similar results could be achieved with CBCT using considerably less radiation. Rigolone et al. [9] concluded that CBCT may play an important role in periapical microsurgery of palatal roots of maxillary first molars. The distance between the cortical plate and the palatal root apex can be measured, and the presence or absence of the maxillary sinus between the roots could be assessed. In addition, the thickness of the cortical plate, the cancellous bone pattern, fenestrations, the shape of the maxilla and mandible, and the inclination of the roots of teeth planned for periapical surgery can be determined before starting surgery. Root morphology can be visualized in three dimensions, as can the number of root canals and whether they converge or diverge from each other. Missed (and untreated) root canals in root-filled teeth may be identified using axial slices, allowing for a level of diagnostic precision that is usually not possible, even with several angled 2D radiographs. The true size, location, and extent of periapical disease can be appreciated using CBCT, and the actual root, or roots, associated with a periapical lesion can be identified with confidence.

In two recent studies, the thickness and the anatomic characteristics of the Schneiderian membrane and cortical bone were evaluated using CBCT in patients' treatment planned for periapical surgery in the maxillary molar region [10, 11]. The Schneiderian membrane in the vicinity of roots with apical lesions tends to be significantly thicker when compared to the roots of teeth without apical pathosis [10].

Close proximity and even contact of the root apices of mandibular posterior teeth and the mandibular canal are not rare and must be taken into consideration when planning apical microsurgery to decrease the risk of iatrogenic nerve damages [12]. The mean distance between the mandibular canal and the apices of the adjacent teeth was evaluated in a recent study [13]. A total of 821 s mandibular premolars and 597 first, 508 s, and 48 third mandibular molars were included in this study. The mean distances were 4.2, 4.9, 3.1, and 2.6 mm, respectively. The occurrence of a direct relationship between the root tips and the mandibular canal was noted in 3.2, 2.9, 15.2, and 31.3 % of the teeth. Women were almost twice as often affected as men. No significant differences were found concerning the location (right/left) of the teeth ($P > .05$). Significantly shorter distances from the mandibular canal to the root apices were found in patients younger than 35 years old compared with older patients.

CBCT enables periapical disease at the root apex to be detected earlier than on conventional radiographs [14]. CBCT scans resulted in 62 % more periapical radiolucent areas being detected on individual roots of posterior mandibular and maxillary teeth when compared with two angled periapical radiographs. In situations where patients have poorly localized symptoms associated with an untreated or previously root-filled tooth, and clinical and periapical radiographic examination shows no evidence of disease, CBCT may be indicated to detect the presence of previously undiagnosed periapical disease. Simon et al. [15] compared the ability of CBCT and biopsy with histological examination to differentiate between periapical cysts and granulomas in teeth with large periapical lesions. It was found that gray-scale value measurements of periapical lesions on CBCT images were able to differentiate solid (granulomas) from cystic- or cavity (cyst)-type lesions. If confirmed, these findings could influence the decision-making process when considering a non-surgical or surgical approach to endodontic retreatment.

A recent study evaluated the concordance of 2- and 3-dimensional radiography with histopathology in the diagnosis of periapical lesions [16]. The final histologic diagnosis of the periapical lesions included 55 granulomas (94.8 %) and 3 cysts (5.2 %). Radiographic assessment overestimated cysts by 28.4 % (CBCT imaging) and 20.7 % (periapical radiography), respectively. In contrast to Simon et al. [15], it was concluded that in order to establish a definitive diagnosis of an apical lesion, the tissue specimen should be evaluated histologically. Analysis of 2-dimensional and 3-dimensional radiographic images results only in a tentative diagnosis that should be confirmed with biopsy.

One of the more interesting areas in which CBCT may be applied in endodontics is evaluating the outcome of treatment [17, 18]. CBCT scans should result in a more objective and therefore more accurate determination of the outcome of endodontic treatment. The CBCT images are geometrically accurate, and there is no distortion of the teeth being assessed or superimposition of overlying anatomy as often seen with conventional film and digitally captured periapical radiographs. Recently, clinical studies have compared the diagnostic value of 2D and 3D radiography for the post-surgical assessment of periapical healing following periapical microsurgery [19–21]. There was higher agreement when evaluating healing using CBCT compared to the 2D imaging. The results of these studies demonstrated that the percentage of repair was different for both methods. More remaining osseous defects were detected after periapical microsurgery on CBCT images than on periapical radiographs. The lower

rate of healing observed on CBCT could be attributed to the type of the bony defect that might require regenerative procedures, or longer observation periods of healing assessment are necessary. There is a need to define the criteria for radiographic healing when using CBCT for microsurgical outcomes assessment.

Future research may show that root-filled teeth that appear to have "healed" using conventional radiographs may still have signs of periapical disease (e.g., widened periodontal ligament space, periapical radiolucency) when imaged using CBCT. This in turn may have implications for restorative treatment planning, in situations where evidence of healing using 2D radiographs is one of the criteria to move forward with a new restoration. It is worth remembering that CBCT still uses ionizing radiation and is not without risk. It is essential that patient radiation exposure is kept as low as reasonably practicable (ALARA) and that evidence-based selection criteria for CBCT are developed. Endodontic cases should be judged individually, and until further evidence is available, CBCT should only be considered when it has been determined that conventional radiographs are yielding insufficient information for diagnosis and treatment planning.

Figures 6.1, 6.2, 6.3, 6.4, 6.5, 6.6, 6.7, 6.8, 6.9, 6.10, 6.11, 6.12, 6.13, 6.14, 6.15, 6.16, 6.17, 6.18, 6.19, 6.20, 6.21, 6.22, and 6.23 demonstrate a series of surgical cases where CBCT was a valuable aid in accurate diagnosis and treatment planning prior to surgical treatment.

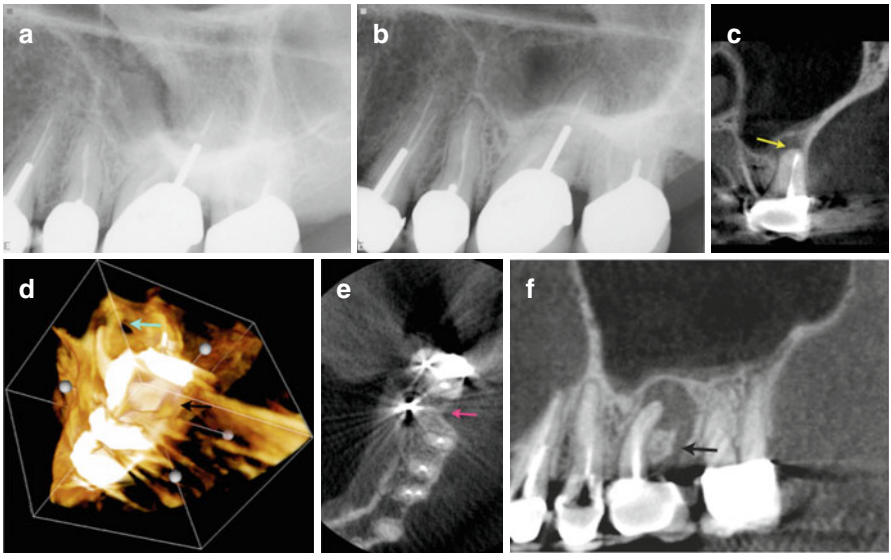

Fig. 6.1 Periapical radiographs of tooth #14, mesial and distal angles, respectively (**a**, **b**). Coronal view of the mesiobuccal root showing a missed mesiobuccal canal and periapical pathology not detected on the 2D radiograph (*yellow arrow*) (**c**). 3D reconstruction showing a crestal bony defect (*blue arrow*) (**d**). Axial view showing a previous distobuccal root amputation site (*pink arrow*) that was not detected on the periapical radiographs (**e**). (**f**) Sagittal view showing the crestal defect (*black arrow*) communicating with the periapical lesion and elevating the floor of the maxillary sinus, with no evidence of sinus perforation (**f**)

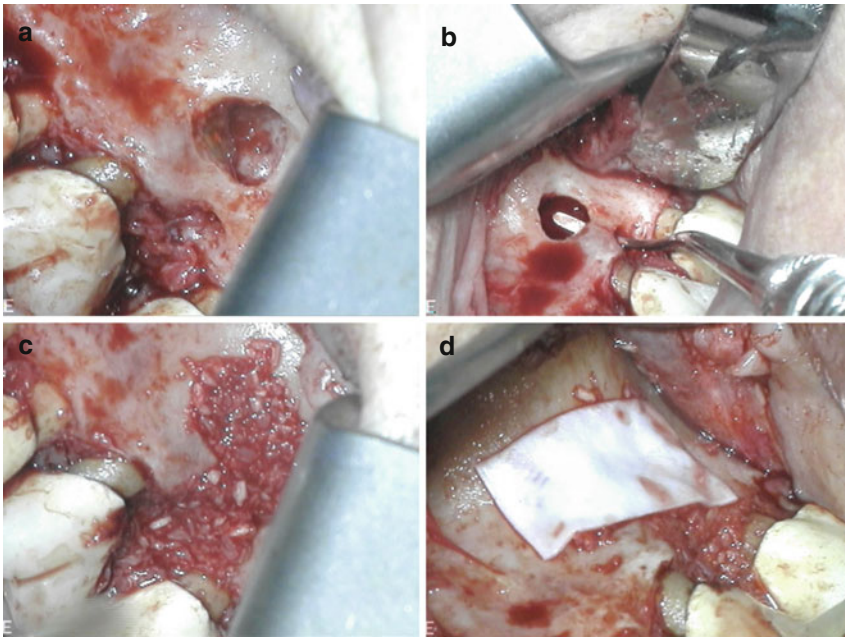

Fig. 6.2 Continuation of case presented in Fig. 6.1: clinical picture after flap reflection showing both crestal and periapical lesions (**a**). Communication between both defects (**b**). Both defects grafted with enCore™ combination allograft (Osteogenics Biomedical, Lubbock, TX) (**c**). CopiOs™ pericardium membrane (Zimmer, Warsaw, IN) (**d**)

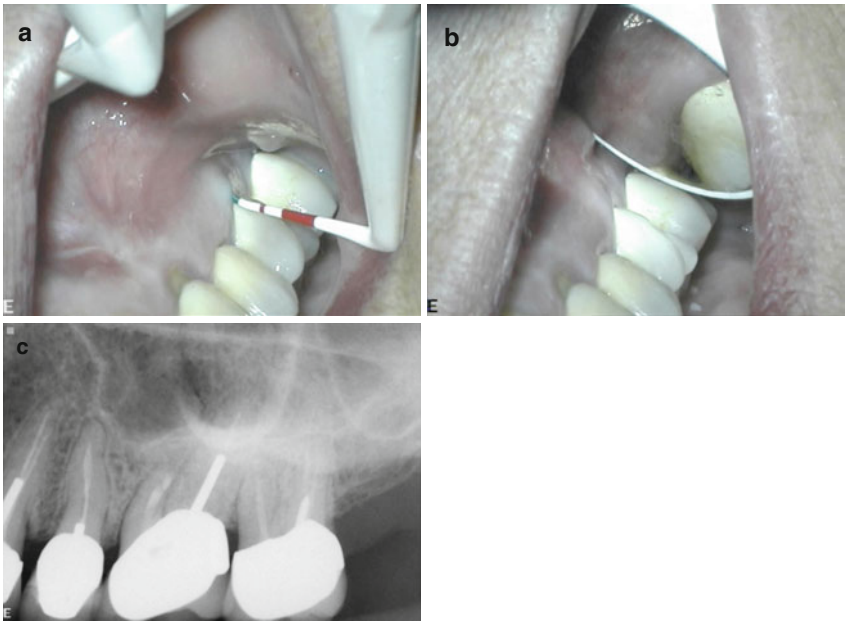

Fig. 6.3 Continuation of case presented in Figs. 6.1 and 6.2: clinical soft tissue healing one year postoperative (**a**, **b**). One-year postoperative recall radiograph (**c**)

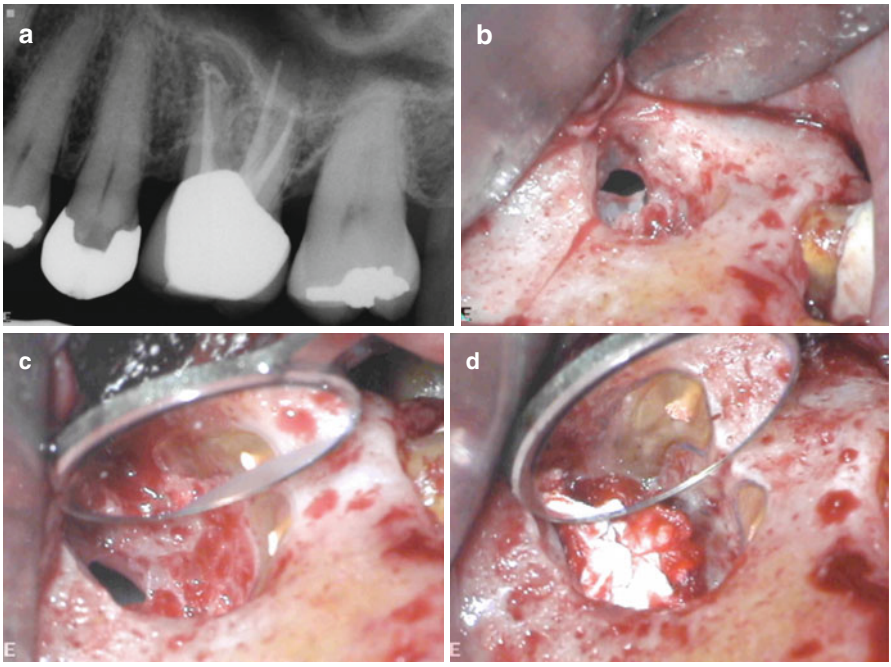

Fig. 6.4 Periapical radiograph of tooth #14 referred for periapical surgery (**a**). Clinical picture demonstrating sinus communication after degranulation of the defect (**b**, **c**). Clinical picture demonstrating the protection of the sinus communication with CollaCote™ and methyle ne blue staining of the MB root resection to confirm complete resection and locate the untreated mesio-palatal canal prior to ultrasonic root-end preparation (**d**)

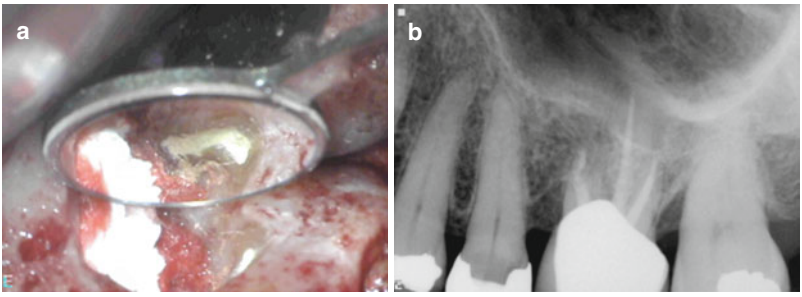

Fig. 6.5 Continuation of case presented in Fig. 6.4: root-end filling with MTA (**a**). Postoperative radiograph (**b**). 8-year recall CBCT demonstrating the coronal (**c**), sagittal (**e**), axial (**d**), and 3D rendering (**f**). Complete bone regeneration of the buccal plate as well as the floor of the sinus can be visualized

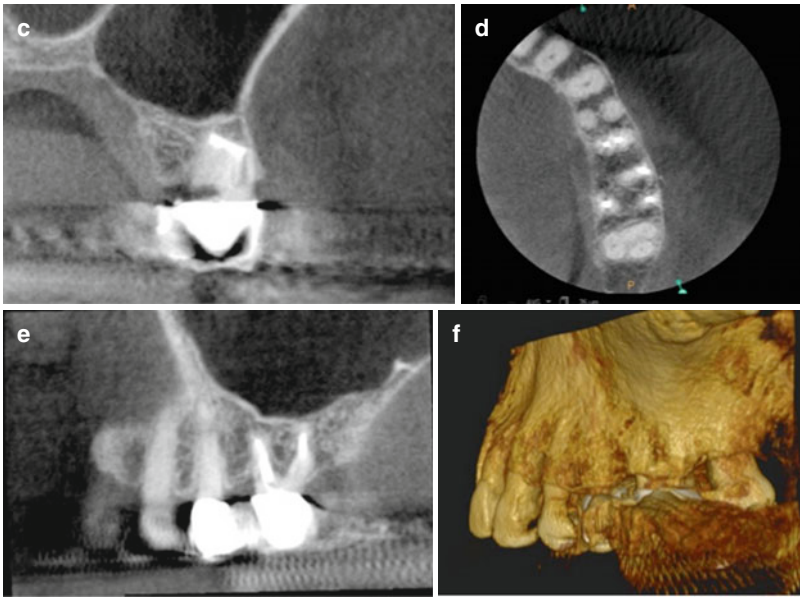

Fig. 6.5 (continued)

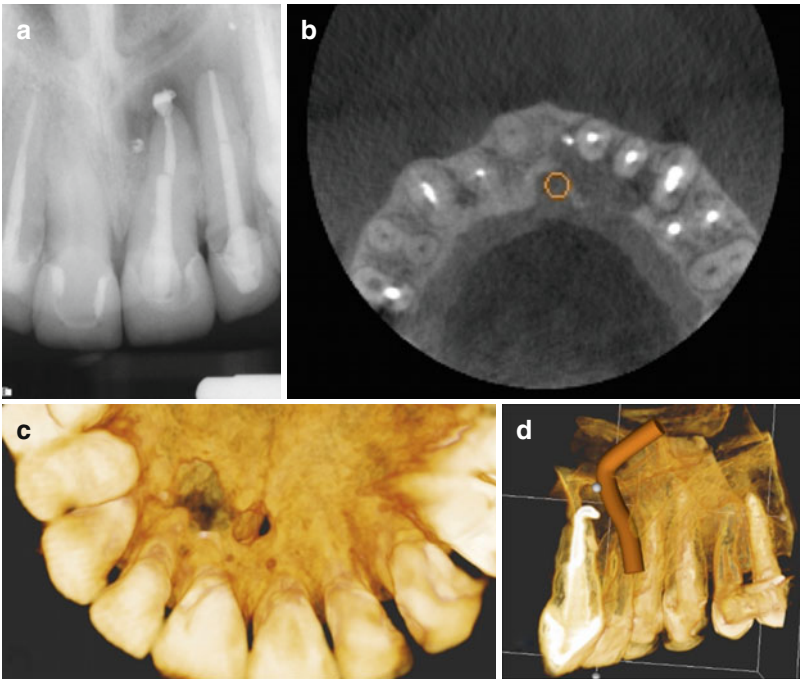

Fig. 6.6 Periapical radiograph of the maxillary anterior region showing a periapical lesion associated with tooth #9 (**a**). (**b**) Axial view showing the extent of the lesion, palatal plate perforation, and relationship of the nasopalatine neurovascular bundle to the periapical lesion (**b**). Palatal view of the 3D reconstruction showing perforation of the palatal plate (**c**). 3D reconstruction showing the nasopalatine bundle (**d**)

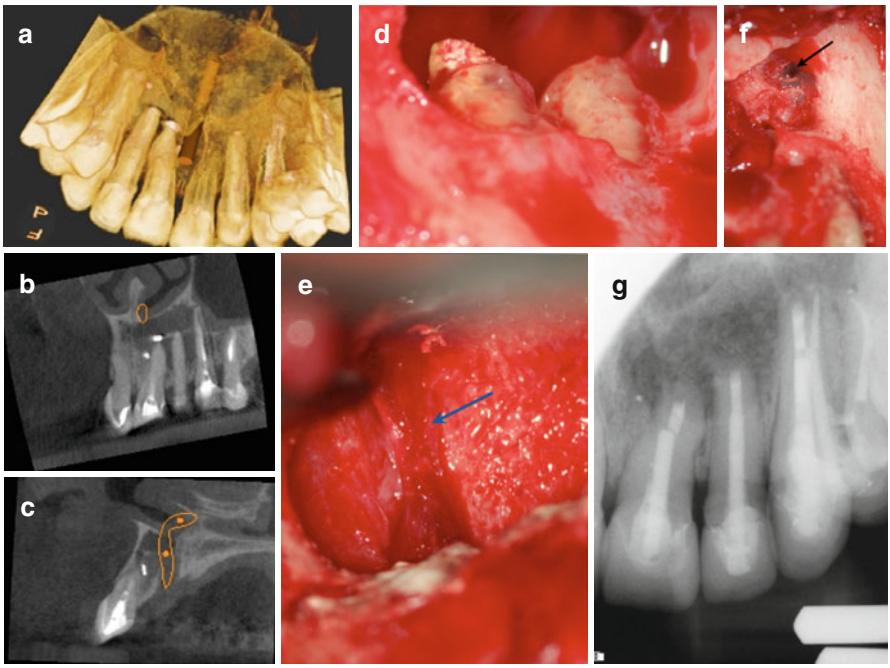

Fig. 6.7 Continuation of case presented in Fig. 6.6: palatal view CBCT reconstruction showing the exit of the nasopalatine bundle from the incisive canal (**a**). Coronal view showing periapical radiolucency involving teeth #9, #10, and #11 (**b**). Sagittal view of the exit of the nasopalatine bundle from the incisive canal (**c**). Periapical defect after degranulation showing the apices of teeth #9 and #10 before resection (**d**). (**e**) A clinical picture of the intact nasopalatine neurovascular bundle (*blue arrow*) after degranulation (**e**). Lateral wall of the maxillary sinus distal to tooth #11 (*black arrow*) (**f**). Immediate postoperative radiograph (**g**) after grafting the through-and-through defect with Puros allograft™ (Zimmer Dental, Warsaw, IN) material and CopiOs™ membrane

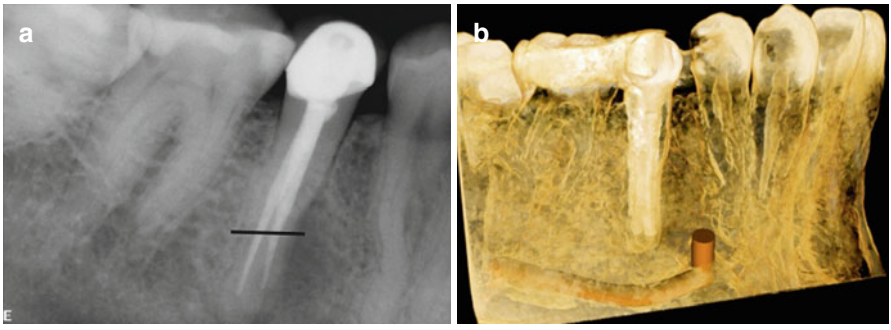

Fig. 6.8 Periapical radiograph of tooth #29 that was referred for apical microsurgery (**a**). The line corresponds to the level of the axial view in (**c**). Note the C-type-shaped canal (*black arrow*). 3D rendering demonstrating the relationship and proximity of the inferior alveolar nerve (IAN) and mental foramen to the apex of tooth #29 (**b**). Axial view of the apical 1/3 demonstrating the extent of the periapical defect (**c**). Coronal view demonstrating the relationship and the proximity of the IAN canal (**d**). 3D rendering demonstrating the relationship and the proximity of the IAN to the periapical defect as well the apex of tooth #29 (**e**)

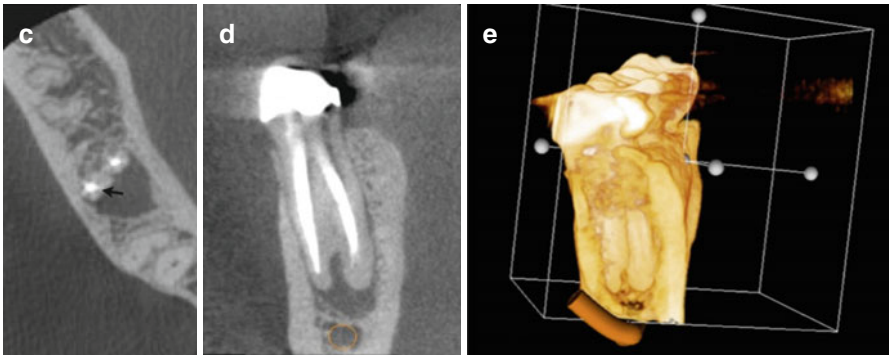

Fig. 6.8 (continued)

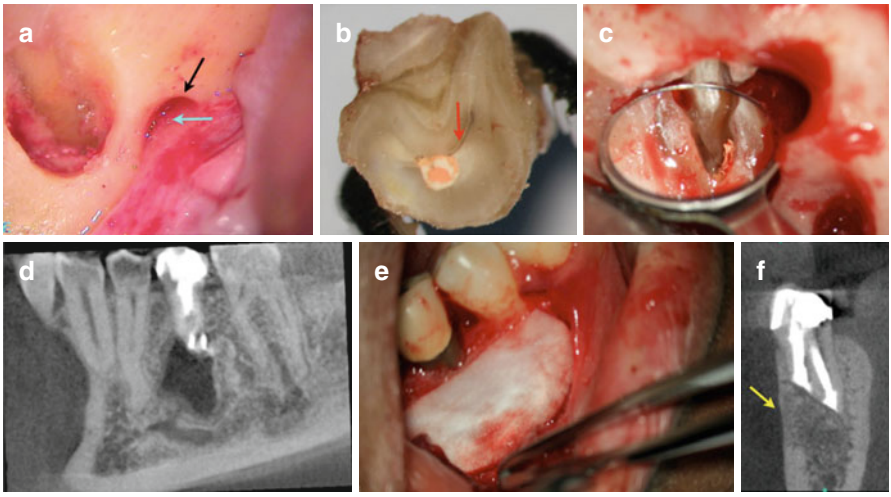

Fig. 6.9 Continuation of case presented in Fig. 6.8: clinical picture of the mental foramen (*black arrow*) and the neurovascular bundle (*blue arrow*) being identified (**a**). Clinical picture of the resected apex of tooth #29 after extraction and root-end resection, in preparation for root-end preparation, filling, and intentional replantation (**b**). Note the C-shaped anatomy which is similar to the axial view in the axial view (**c**). Replanted tooth after ultrasonic apical preparation of the C-shaped canal and MTA root-end filling of the apical preparation (**d**). Bony defect grafted with Puros™ allograft (Zimmer Dental, Warsaw, IN) and CopiOs™ membrane (**e**). One-year coronal view CBCT recall demonstrating complete remodeling of the defect including the buccal cortical plate (*yellow arrow*) (**f**)

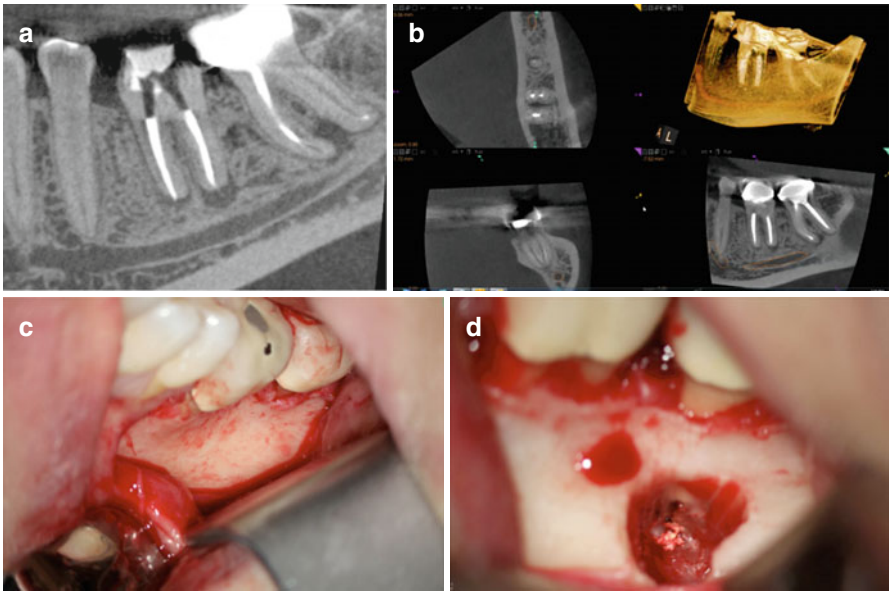

Fig. 6.10 CBCT sagittal view of tooth #18 that was referred for periapical microsurgery (**a**). CBCT of the axial, coronal, sagittal views, and 3D rendering demonstrating the proximity of the IAN to the mesial root of tooth #18 (**b**). Clinical picture after surgical flap reflection showing the buccal cortical plate (**c**). Osteotomy and resection of the mesial root (**d**)

Fig. 6.11 Continuation of case presented in Fig. 6.10: clinical picture demonstrating the MTA root-end filling (**a**). Periapical defect grafted with Puros™ allograft (Zimmer Dental, Warsaw, IN) material and before placing CopiOs™ membrane (**b**). Immediate postsurgical radiograph (**c**)

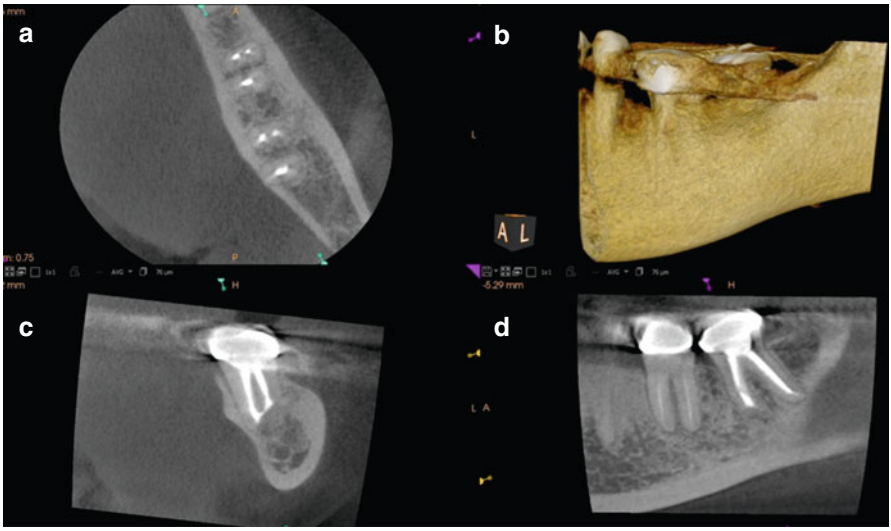

Fig. 6.12 Continuation of case presented in Figs. 6.10 and 6.11: 18-month postoperative CBCT scan demonstrating complete remodeling of the defect and the buccal plates (**a**–**d**)

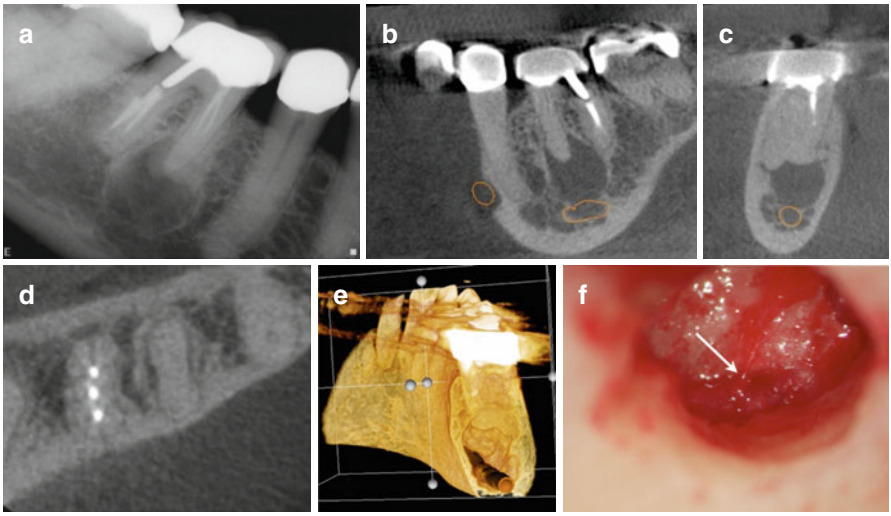

Fig. 6.13 Periapical radiograph of tooth #30 that was referred for periapical surgery (**a**). CBCT of the sagittal, coronal, and axial views and 3D rendering demonstrating the proximity and communication of the defect and IAN to the mesial root of tooth #18 (**b**–**e**). Clinical picture after surgical flap reflection, mesial root resection, and degranulation of the defect (**f**). The IAN was detected (*white arrow*) at the base of the defect

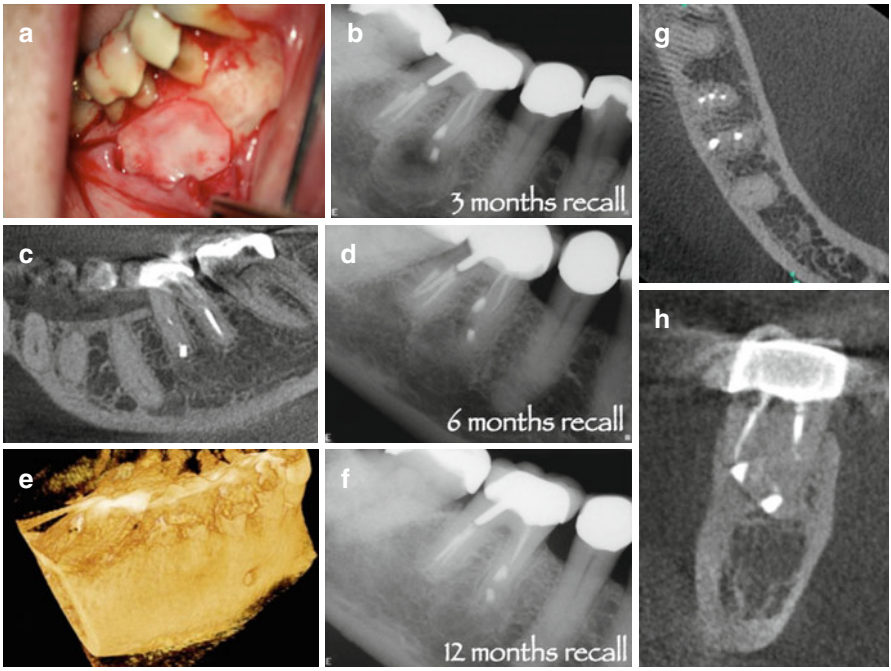

Fig. 6.14 Continuation of case presented in Fig. 6.13: clinical picture of CopiOs™ membrane without graft material (**a**). Periapical radiograph of 3-month recall (**b**). CBCT sagittal view, periapical radiograph, and 3D rendering at 6-month recall (**c**–**e**). Periapical radiograph, axial and coronal views of tooth #30 at 12-month recall demonstrating complete remodeling of the defect including the buccal cortical plate (**f**–**h**)

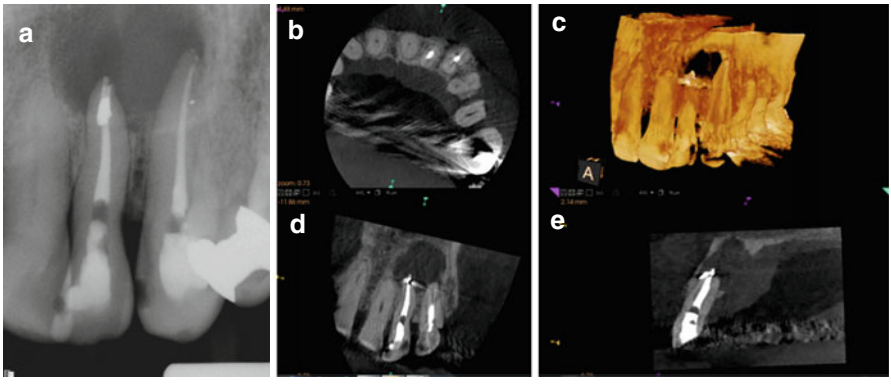

Fig. 6.15 Periapical radiograph of teeth # 10 and #11 (**a**). The 2D radiograph does not allow for appreciation of the true size and extent of the defect. CBCT scan demonstrating the actual size of the defect (**b**–**e**). Perforation and loss of palatal bone can be clearly seen in the sagittal view (**e**)

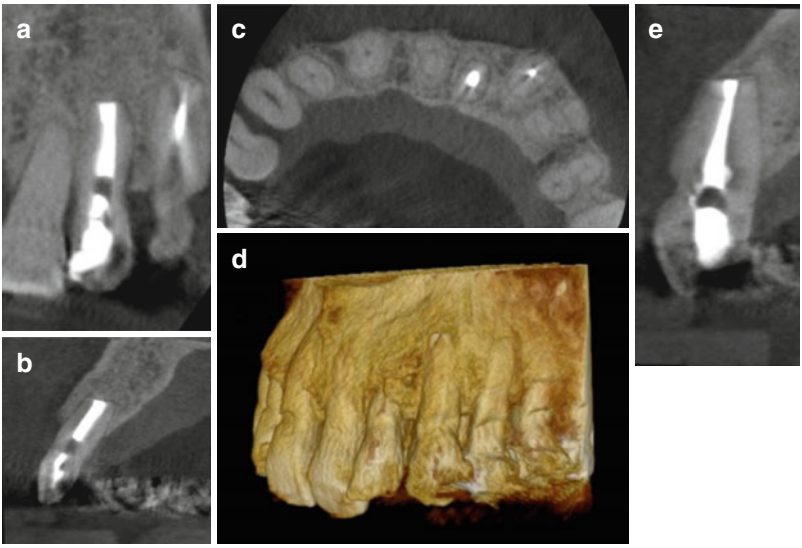

Fig. 6.16 Continuation of case presented in Fig. 6.15: 2-year recall CBCT scan of teeth #10 and #11 demonstrating complete remodeling of the defect including the buccal and palatal cortical plates (**a**–**e**)

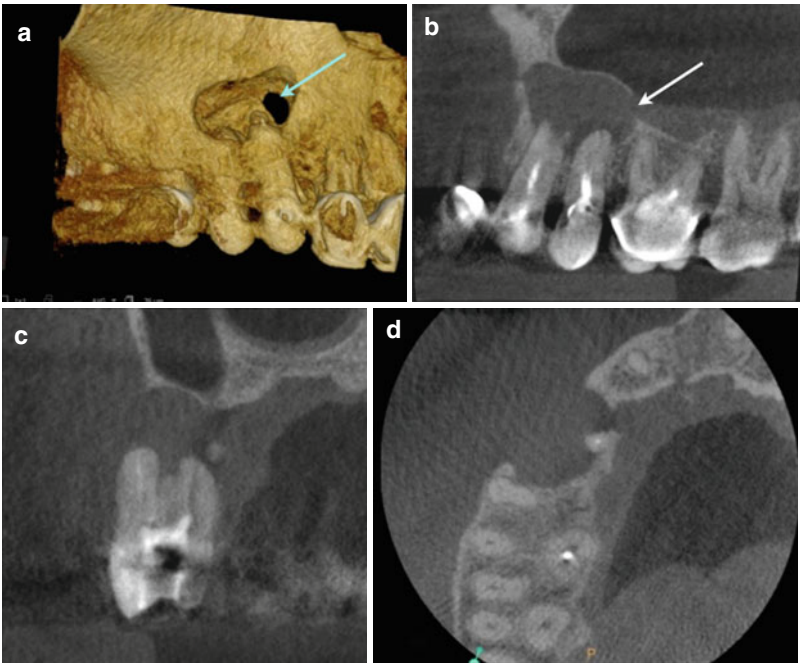

Fig. 6.17 CBCT 3D rendering of teeth #12 and #13 referred for periapical surgery (**a**). Peroration of the maxillary sinus can be visualized (*blue arrow*). Sagittal view of teeth #12 and #13 (**b**). Perforation of the maxillary sinus noted (*white arrow*). Coronal view of tooth #12 demonstrating the through-and-through nature of the periapical defect (**c**). Axial view demonstrating the mesio-distal extent of the periapical defect (**d**)

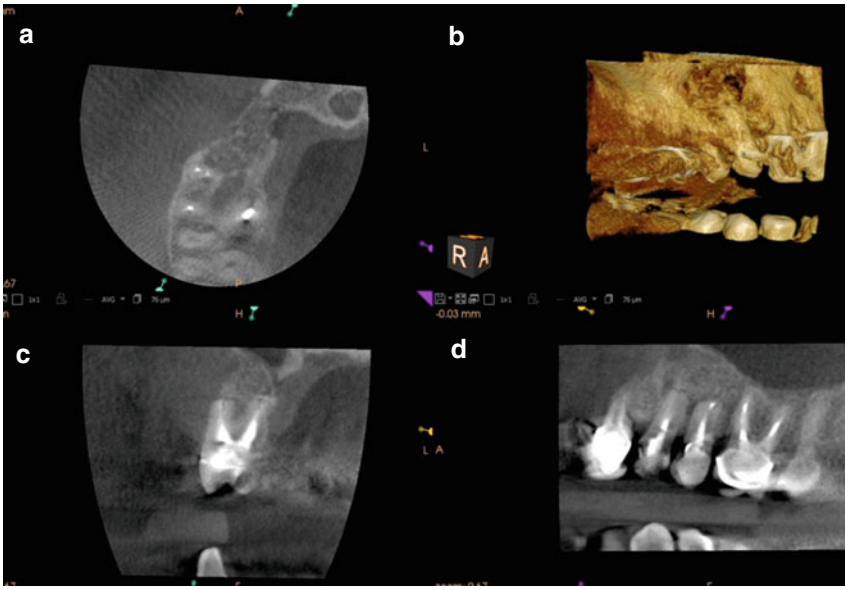

Fig. 6.18 Continuation of case presented in Fig. 6.17: 12-month postoperative CBCT scan of teeth #12 and #13 demonstrating bone remodeling observed in axial (**a**), 3D rendering (**b**), coronal (**c**), and sagittal (**d**)

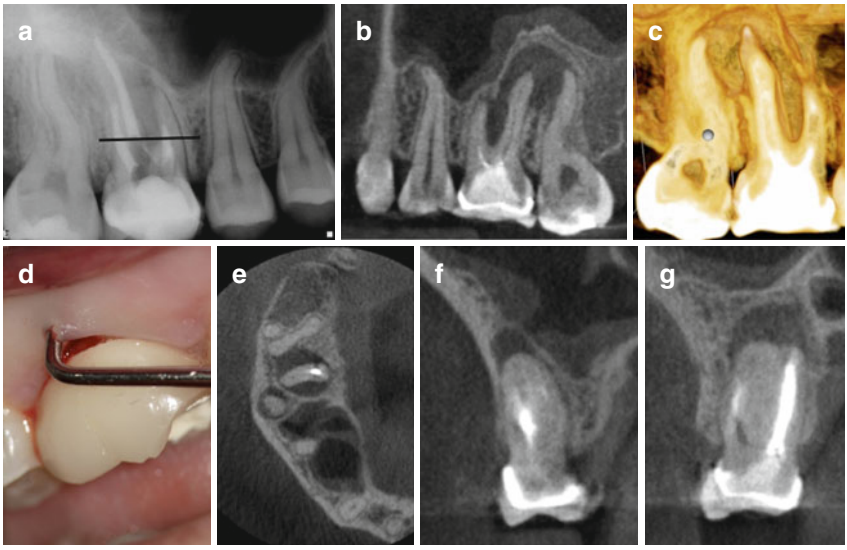

Fig. 6.19 Periapical radiograph of tooth #3 that was referred for periapical surgery (**a**). A nonsurgical retreatment attempt was performed prior to periapical microsurgery. The mesiobuccal canal was blocked. The *black line* in (**a**) corresponds to the level of the axial view in (**e**). Sagittal view demonstrating the extent of the periapical defect (**b**). 3D rendering of the periapical defect (**c**). Clinical picture demonstrating the endodontic/periodontal communication (**d**). Axial view of the mesiobuccal, distobuccal, and palatal roots (**e**). Note the fused distal and palatal roots. Coronal view of the mesiobuccal root and the fused distal-palatal roots (**f**, **g**)

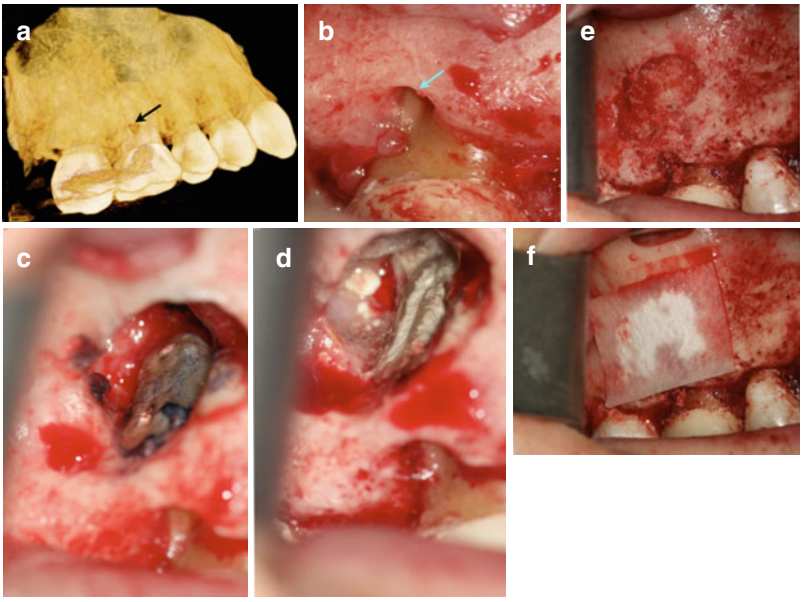

Fig. 6.20 Continuation of case presented in Fig. 6.19: 3D rendering demonstrating the periodontal defect (*black arrow*) (**a**). After full-thickness flap reflection, the periodontal defect was determined to communicate with the periapical defect (*blue arrow*) (b). Root resection of the fused distal and palatal roots prior to ultrasonic preparation (**c**). (**d**) MTA root-end filling of the ultrasonically prepared distal and palatal preparation (**d**). Periodontal and periapical defects grafted with Puros™ allograft (Zimmer Dental, Warsaw, IN) material (**e**). Grafted defect covered with CopiOs™ membrane (Zimmer Dental, Warsaw, IN) (**f**)

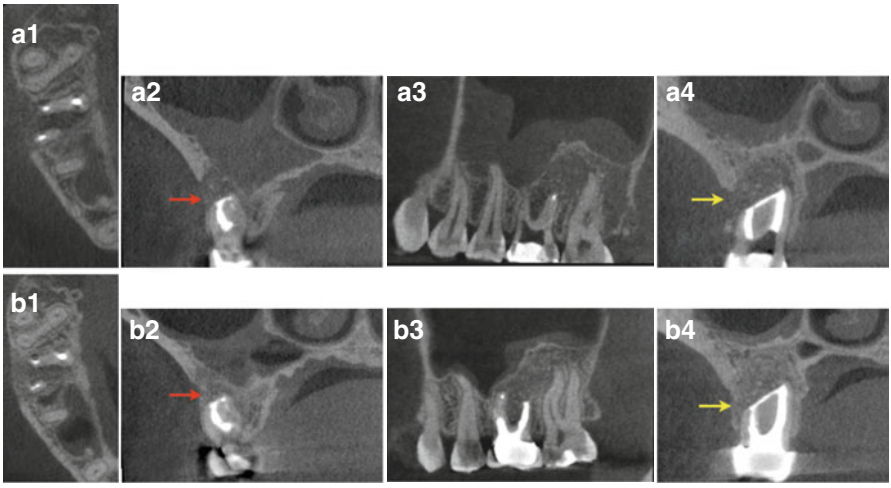

Fig. 6.21 Continuation of case presented in Figs. 6.19 and 6.20: immediate postsurgical CBCT scan (**a.1**–**a.4**). Note buccal defect (*red and yellow arrows*). (**b1**–**b4**) 6-month recall CBCT scan (**b.1**–**b.4**). Note the initial regeneration of the defect including the buccal cortical plate. One-year recall CBCT scan demonstrating complete remodeling of the defect and the buccal plate (*red and yellow arrows*) (**c.2**–**c.4**)

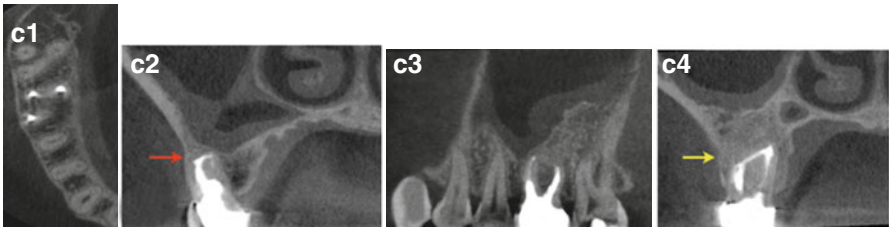

Fig. 6.21 (continued)

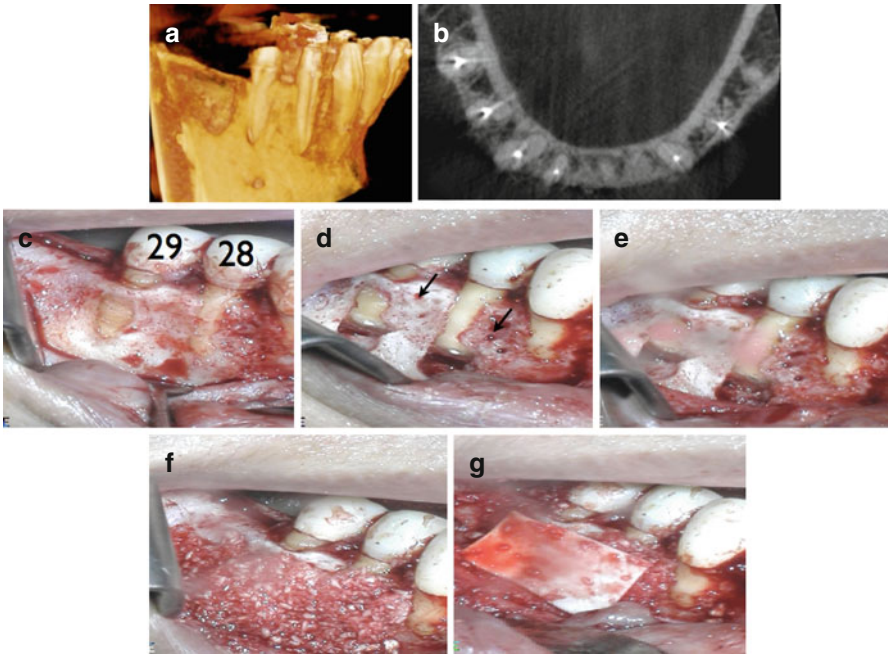

Fig. 6.22 3D CBCT rendering and axial view of teeth #28 and #29 that were referred for apical surgery (**a**, **b**). Complete dehiscence of the root of tooth #28 and fenestration of tooth #29 was observed. Clinical picture after surgical flap reflection confirming the CBCT findings (**c**). Root-end resection, conditioning, and root-end filling with MTA. Size #2 round bur cortical holes were placed (*black arrow*) for the rapid acceleration phenomenon (RAP) to ensure blood supply to the bone graft (**d**, **e**). Periodontal and periapical defect grafted with enCore™ combination (70 % cortical and 30 % cancellous) from Osteogenics Biomedical Lubbock, TX. CopiOs™ membrane (Zimmer Dental, Warsaw, IN) was placed over the grafting material (**f**, **g**)

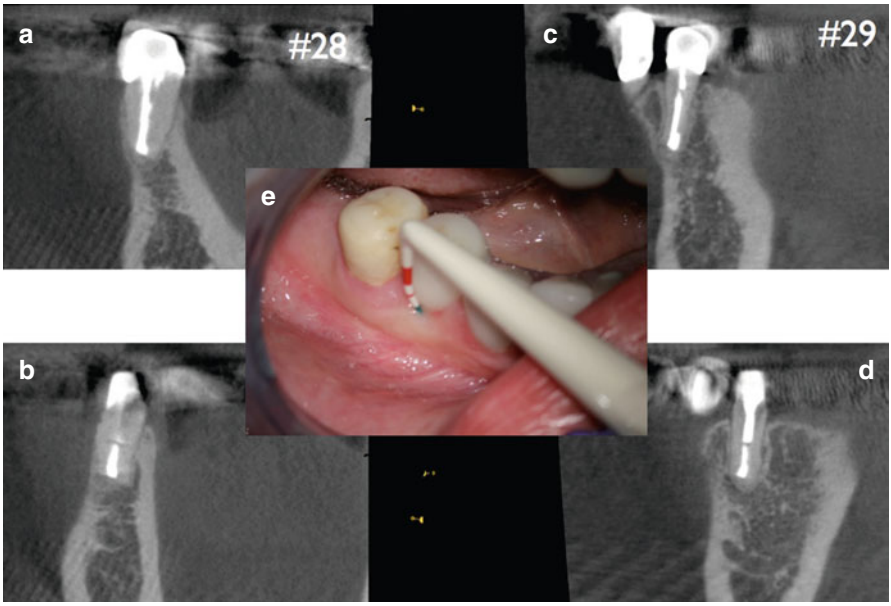

Fig. 6.23 Continuation of case presented in Fig. 6.22: 18-month CBCT coronal and sagittal views demonstrating complete remodeling of the defect and the buccal plates (**a**–**d**). Clinical picture of 18-month recall demonstrating normal color, texture, and periodontal attachment (**e**)

References

1. Cheung GS, Wei WL, McGrath C. Agreement between periapical radiographs and cone-beam computed tomography for assessment of periapical status of root filled molar teeth. Int Endod J. 2013;46:889–95.
2. Esposito S, Huybrechts B, Slagmolen P, Cotti E, Coucke W, Pauwels R, Lambrechts P, Jacobs R. A novel method to estimate the volume of bone defects using Cone-Beam Computed Tomography: An In Vitro Study. J Endod. 2013;39(9):1111–5.
3. Bornstein MM, Lauber R, Sendi P, von Arx T. Comparison of periapical radiography and limited cone-beam computed tomography in mandibular molars for analysis of anatomical landmarks before apical surgery. J Endod. 2011;37(2):151–7.
4. Low MTL, Dula KD, B€urgin W, von Arx T. Comparison of periapical radiography and limited cone-beam tomography in posterior maxillary teeth referred for apical surgery. J Endod. 2008;34:557–62.
5. Tsai P, Torabinejad M, Rice D, Azevedo B. Accuracy of cone-beam computed tomography and periapical radiography in detecting small periapical lesions. J Endod. 2012;38:965–70.
6. Tyndall DA, Rathore S. Cone-beam diagnostic applications: caries, periodontal bone assessment, and endodontic applications. Dental Clin North Am. 2008;52:825–41.
7. Cotton TP, Geisler TM, Holden DT, Schwartz SA, Schindler WG. Endodontic applications of cone-beam volumetric tomography. J Endodont. 2007;33:1121–32.
8. Velvart P, Hecker H, Tillinger G. Detection of the apical lesion and the mandibular canal in conventional radiography and computed tomography. Oral Surg Oral Med Oral Pathol Oral Radiol Endod. 2001;92(6):682–8.

9. Rigolone M, Pasqualini D, Bianchi L, Berutti E, Bianchi SD. Vestibular surgical access to the palatine root of the superior first molar: "low-dose cone-beam" CT analysis of the pathway and its anatomic variations. J Endod. 2003;29:773–5.
10. Maillet M, Bowles WR, McClanahan SL, John MT, Ahmad M. Cone-beam computed tomography evaluation of maxillary sinusitis. J Endod. 2011;37(6):753–7.
11. Bornstein MM, Wasmer J, Sendi P, Janner SF, Buser D, von Arx T. Characteristics and dimensions of the Schneiderian membrane and apical bone in maxillary molars referred for apical surgery: a comparative radiographic analysis using limited cone beam computed tomography. J Endod. 2012;38(1):51–7.
12. Kovisto T, Mansur Ahmad M, Bowles W. Proximity of the mandibular canal to the tooth apex. J Endod. 2011;37(3):311–5.
13. Bürklein S, Carolin Grund C, Schäfer E. Relationship between root apices and the mandibular canal: a cone-beam computed tomographic analysis in a German population. J Endod. 2015;41(10):1696–700.
14. Lofthag-Hansen S, Huumonen S, Grondahl K, Grondahl H-G. Limited cone-beam CT and intraoral radiography for the diagnosis of periapical pathology. Oral Surg Oral Med Oral Pathol Oral Radiol Endod. 2007;103:114–9.
15. Simon JH, Enciso R, Malfaz J-M, Roges R, Bailey-Perry M, Patel A. Differential diagnosis of large periapical lesions using cone-beam computed tomography measurements and biopsy. J Endod. 2006;32(9):833–7.
16. Bornstein MM, Bingisser AC, Reichart PA, Sendi P, Bosshardt DD, von Arx T. Comparison between radiographic (2-dimensional and 3-dimensional) and histologic findings of periapical lesions treated with apical surgery. J Endod. 2015;41(6):804–11.
17. De Paula-Silva FW, Junior MS, Leonardo MR, Consolaro A, daSilva LA. Cone-beam computerized tomographic, radiographic, and histologic evaluation of periapical repair in dogs' post-endodontic treatment. Oral Surg Oral Med Oral Pathol Oral Radiol Endod. 2009;5:796–805.
18. Kourkouta S, Bailey G. Periradicular regenerative surgery in a maxillary central incisor: 7-year results including cone-beam computed tomography. J Endod. 2014;40(7):1013–9.
19. Christiansen R, Kirkevang LL, Gotfredsen E, Wenzel A. Periapical radiography and cone beam computed tomography for assessment of the periapical bone defect 1 week and 12 months after root-end resection. Dentomaxillofac Radiol. 2009;38(8):531–6.
20. Von Arx T, Janner SF, Hänni S, Bornstein MM. Agreement between 2D and 3D radiographic outcome assessment one year after periapical surgery. Int Endod J. 2015:1–11.
21. Tanomaru-Filho M, Jorge EG, Guerreiro-Tanomaru JM, Reis JM, Spin-Neto R, Goncalves M. Two- and tridimensional analysis of periapical repair after endodontic surgery. Clin Oral Investig. 2015;19:17–25.

The Use of CBCT in the Diagnosis and Management of Root Resorption

7

Martin D. Levin and George Jong

Abstract

Root resorption results in the loss of dentin, cementum, or bone by the action of clastic cells. Root resorption in permanent teeth is a pathologic process in response to inflammation that can be caused by numerous factors, such as infection, orthodontic treatment, traumatic injury, cysts, neoplasia, systemic disease, or chemical injury. Root resorption may be classified into external or internal root resorption, based on the location of the lesion. Accurate assessment is essential as the pathogenesis of external and internal root resorption is different and treatment protocols vary. Although periapical and panoramic imaging modalities may be helpful in identifying root resorption, early detection with periapical radiography is not considered reliable because of the difficulty in identifying lesions on the buccal or lingual/palatal surfaces. In contrast, CBCT makes it possible to examine the region of interest in any plane, determine accurate measurements, and eliminate tissue compression. CBCT has been used in the detection of small lesions, classification of the lesion, localizing and differentiation of the resorptive defect from other lesions, and directing treatment. CBCT aids in surgical planning by showing the relationship of the teeth and associated pathoses to important anatomic landmarks. The use of CBCT to show the true nature of external and internal resorption relies on the ability to examine the region of interest in any plane without distortion and eliminate artifacts associated with conventional radiography. Careful use of CBCT is advocated.

M.D. Levin, DMD (✉)
Adjunct Professor of Endodontics, University of Pennsylvania, Philadelphia, Pennsylvania, USA
e-mail: mdlevin@upenn.edu

G. Jong, DDS
Private Practice, Bethesda-Chevy Chase Root Canal Specialists, Chevy Chase, Maryland, USA

M. Fayad, B.R. Johnson (eds.), *3D Imaging in Endodontics*,
DOI 10.1007/978-3-319-31466-2_7

7.1 Introduction

Root resorption results in the loss of dentin, cementum, or bone by the action of clastic cells [1]. In the primary dentition, root resorption is a normal physiologic process that allows for the eruption of the secondary dentition, except when resorption is premature. Root resorption in permanent teeth is a pathologic process in response to inflammation that can be caused by numerous factors, such as infection, orthodontic treatment, traumatic injury, cysts, neoplasia, systemic disease, or chemical injury [2]. The loss of tooth structure due to clastic activity may result from chronic inflammation and in some cases is a self-limiting process [3]. Root resorption may be classified into external or internal root resorption, based on the location of the lesion [4]. External root resorption affects the outer surface of the root and internal resorption affects the walls of the root canal. Accurate assessment is essential as the pathogenesis of external and internal root resorption is different and treatment protocols vary.

Root resorption may be inconsequential or cause the premature loss of the teeth affected [5]. The successful management of root resorption requires early clinical and radiographic detection and accurate diagnosis [6]. Although periapical and panoramic imaging modalities may be helpful in identifying root resorption, early detection with periapical radiography is not considered reliable [7] because of the difficulty in identifying lesions on the buccal or lingual/palatal surfaces [8].

A review of the current literature shows a number of case reports, case series, and laboratory studies of limited sample sizes, with few high-level reports on the efficacy of CBCT to guide clinical decisions. Additional studies with strong evidence grades are needed.

7.2 CBCT: Serial Cross-Sectional Imaging

Therapeutic interventions are aided by the use of serial cross-sectional imaging in a wide range of endodontic tasks. Conventional radiographic techniques are limited by the superimposition and misrepresentation of structures, geometric distortion, and magnification. In contrast, CBCT makes it possible to examine the region of interest in any plane, determine accurate measurements, and eliminate tissue compression. CBCT aids in surgical planning by showing the relationship of the teeth and associated pathoses to important anatomic landmarks. CBCT has been used in the detection of small lesions, classification of the lesion, localizing and differentiation of the resorptive defect from other lesions, and directing treatment [9].

According to the joint position statement of the American Association of Endodontists and the American Academy of Oral and Maxillofacial Radiology on the use of cone beam computed tomography in endodontics, 2015 Update (Appendix A and available online at http://www.aae.org or http://www.aaomr.org), "Limited field of view CBCT is the imaging modality of choice in the localization and differentiation of external and internal resorptive defects and the determination of appropriate treatment and prognosis."

CBCT may provide information leading to improved treatment planning. In a study by Mota de Almeida et al., to determine the diagnostic impact of CBCT in endodontic interventions using the European Commission Guidelines (2012), 80 teeth in 52 patients were evaluated, resulting in a changed diagnosis in 37 % of the cases [10]. In another comparison of endodontic diagnosis and treatment planning with periapical radiography and CBCT in 30 completed cases by Ee et al., CBCT provided additional information that led to treatment plan modifications in approximately 62 % of the cases [11].

7.3 CBCT: Volume Size, Spatial Resolution, and Radiation Dose

In endodontics, CBCT units capable of producing limited scan volumes should be employed whenever possible to take advantage of their inherent increased spatial resolution and to minimize radiation dose. Laboratory studies of simulated resorptive lesions have demonstrated improved accuracy with the use of smaller voxel sizes [12, 13]. When high-resolution CBCT scans were compared to low-resolution scans and periapical radiography in an ex vivo study by Ponder et al. [14], improved visualization was demonstrated. This finding was in agreement with studies conducted by Dalili et al. and others [15]. Although voxel size is important, processing algorithms and technique factors to improve contrast and spatial resolution may also affect probability of lesion detection.

Radiation dose is an important consideration when selecting the appropriate imaging protocol for the task at hand. Although the effective radiation dose of CBCT is significantly less than conventional CT, CBCT requires a higher radiation dose than periapical or panoramic imaging. In keeping with the ALARA (an acronym for "as low as reasonably achievable") principle, selection of the most appropriate imaging protocol must be determined on a case-by-case basis, with the benefits and risks explained to the patient. Additional consideration must be applied to the imaging of children because they are up to three times more susceptible to the effects of ionizing radiation than that of young adults aged 20–25 years and as much as an order of magnitude more than mature adults, aged 60 [16].

7.4 External Root Resorption

External root resorption can be divided into five main types: external surface resorption, external inflammatory resorption, external replacement resorption, external cervical resorption, and transient apical breakdown [17]. Local factors can promote extensive external resorption, such as impacted teeth, orthodontic treatment, apical periodontitis, tumors, cysts, and luxated or autotransplanted teeth. External resorption can also be related to systemic diseases, such as thyroid disorders, calcinosis, and Gaucher's and Paget's disease.

Fig. 7.1 Periapical radiographs can be suboptimal in representing complex anatomy compared with CBCT. A 71-year-old male presented with discomfort in the maxillary right quadrant. (**a**) Periapical radiograph shows an area of low density in the middle third of the palatal root (*arrow*) and an impacted third molar. Clinical testing revealed pulp necrosis. CBCT images of the (**b**) cross-sectional reformation, (**c**) axial reformation, and (**d**) sagittal reformation show features consistent with external inflammatory resorption of the palatal root (*arrows*) and a periradicular periodontitis, which could not be localized in the periapical radiograph. The excessive pressure from the impacted third molar may have caused the resorptive defect. The maxillary sinus within the CBCT image has features consistent with chronic sinusitis. The tooth was non-restorable and extraction was recommended. The CBCT image data was used to assess the position of the maxillary right third molar for surgical planning

External surface resorption may occur after chronic injury to the periodontal ligament. It is usually associated with orthodontic treatment, occlusal trauma, pressure from cysts or apical granulomas, and ectopically erupting teeth (Fig. 7.1). In laboratory studies, the use of CBCT in the detection of surface resorption has been shown to be superior to conventional imaging, with improved visualization as the defect increases in size [18].

External inflammatory root resorption is a common complication of dental trauma, affecting up to 18 % of patients after luxation injuries of all types [19] and up to 30 % of replanted avulsed teeth. External inflammatory resorption after trauma is a well-known complication after intrusive luxation injuries and replantation of avulsed teeth, progresses quickly, and is radiographically distinguished by cavitation-like areas of low density along the root surface and surrounding alveolar bone.

CBCT provides improved assessment of the presence and type of root resorption, especially in the apical third of the root [20] (Fig. 7.2). Simulated external resorption in 131 cavities using single-slice CT scans showed higher sensitivity and excellent specificity in the detection of resorption in small cavities in the apical 1/3 of extracted human incisors [21]. Laboratory studies using extracted teeth with simulated resorptive lesions [12, 22] suggest that CBCT provides high sensitivity and specificity in the detection of simulated resorptive lesions on mandibular incisors. However, these ex vivo studies do not exactly replicate the clinical situation, where changes in the supporting structures such as the periodontal ligament and surrounding bone may have influenced the result. In addition, the synthetic resorption cavities in the teeth studied were created with round burs that may not have accurately replicated the irregular nature of some resorptive lesions, which may have influenced detection.

The advantages of serial cross-sectional imaging have been well documented in the orthodontic and endodontic literature [23]. Several ex vivo studies in the orthodontic literature have demonstrated the advantages of CBCT in the detection of root resorption in maxillary teeth in close proximity to impacted canines [24]. External apical root resorption in orthodontics is estimated to affect at least one root in 94 % of patients investigated [25].

Diagnosis and management of external cervical resorption (Fig. 7.3) is challenging to diagnose and manage and is most commonly associated with orthodontic treatment, dental trauma, cervical restorations, and/or bleaching [26]. This type of resorption is characterized by a circular lesion that progresses in a coronal and apical direction (Fig. 7.4). The root canal is not invaded in the early phases. External cervical resorption may be distinguished from caries by a “non-sticky” feel upon exploration. A pink area may be noticed by the patient or clinician, a result of vascular granulation tissue visible through the resorbed dentin. Two-dimensional radiographs may not show the full extent of the lesion nor the portal of entry, complicating treatment. CBCT shows the extension of the lesion and assists with the determination of the expected outcome and location of important anatomic structures to facilitate a surgical approach, if indicated. According to Heithersay, orthodontic treatment was potentially related to 24.1 % of external cervical resorption cases studied, with a time to diagnosis of between 1.5 years and 33 years and predilection for maxillary canines, maxillary incisors, and mandibular molars. External cervical resorption was also associated with trauma and bleaching, with 15.1 % and 7.4 % of teeth involved, respectively [26]. Many case reports of multiple idiopathic external cervical resorption have been published, with the number of teeth involved ranging from 5 to 24 per patient. While there was no unique region of the mouth that was affected, 13 of the 18 patients were female [27].

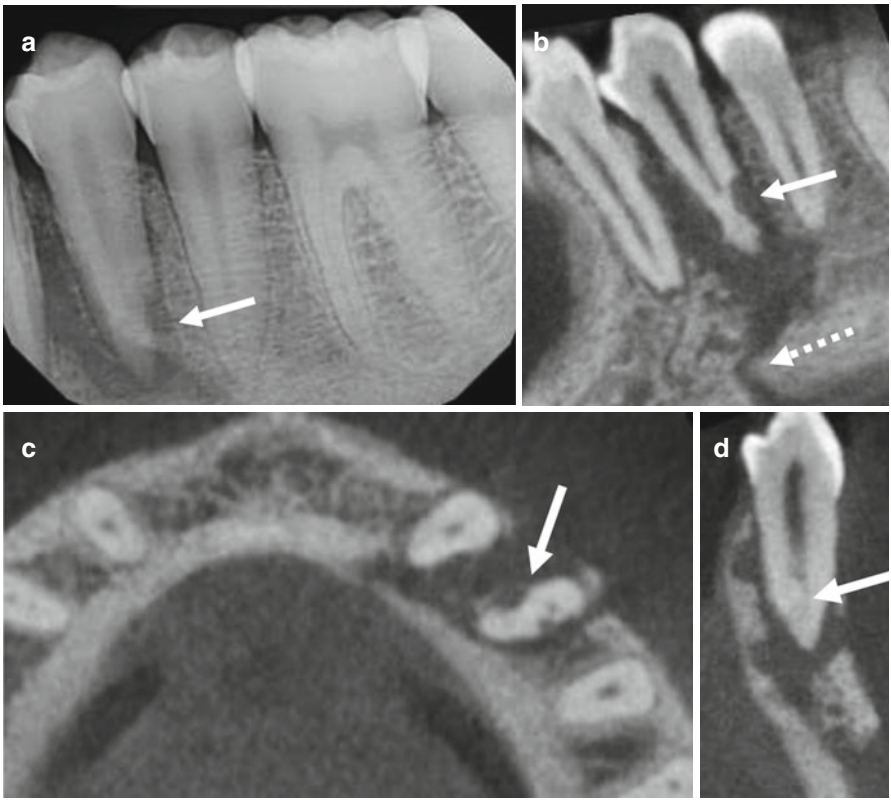

Fig. 7.2 A 21-year-old male presented for evaluation and possible treatment with a history of trauma to the mandibular left quadrant. The left mandibular body fracture was directly fixated for 6 weeks prior to endodontic evaluation. (**a**) Periapical image shows an area of low density associated with the mandibular left first premolar. This feature extends laterally and apically. There is a well-defined area of low density on the distal aspect of the apical third of the root (*arrow*); a feature consistent with external inflammatory resorption. CBCT images of the (**b**) sagittal reformation demonstrates the full extent of the lesion, which is contiguous with the fracture line (*dashed arrow*). (**c**) A separate area of low density (*arrow*) shows on the mesial aspect in the axial reformation. (**d**)There is an apical split of the canals visible in the cross-sectional reformation

7.5 Internal Root Resorption

Intraradicular internal root resorption is inflammatory in nature, relatively rare when compared with external root resorption, asymptomatic in its early stages, slowly progressing, and usually detected on routine radiographic examinations. Diagnosis using two-dimensional radiographic modalities is difficult; however, internal root resorption has clearly defined borders, usually round or oval shaped [28], with no canal radiographically visible in the defect (Figs. 7.5 and 7.6). In

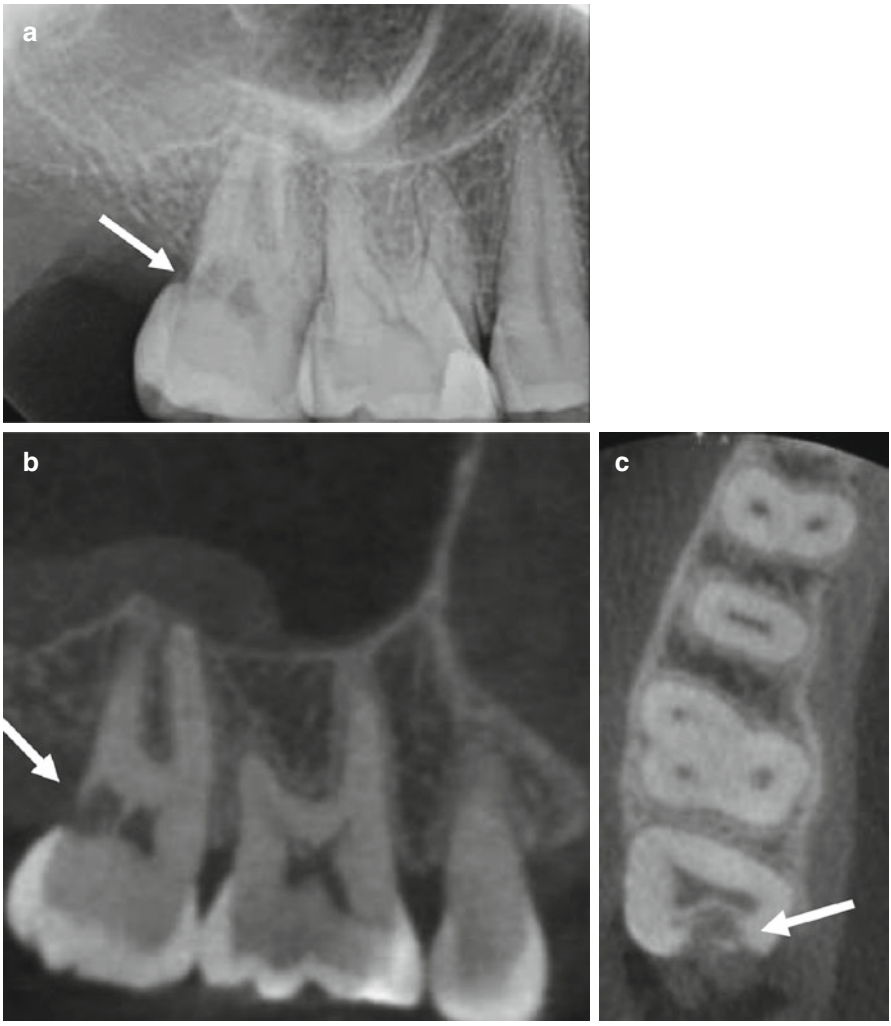

Fig. 7.3 CBCT has been shown to be more accurate than periapical radiography in the detection of invasive cervical resorption. A 41-year-old female patient presented with a history of orthodontic treatment during childhood. (**a**) Periapical radiograph of the maxillary right second molar shows an irregular area of low density in the coronal third, with ill-defined margins and penetration into the dentin (*arrow*). CBCT images of the (**b**) sagittal reformation, and (**c**) axial reformation demonstrate the full extent of the resorptive defect including the portal of entry (*arrows*). The pulp space was preserved by the peritubular dentin and there is a moderate mucositis superior to the second molar. The tooth was deemed non-restorable and extraction was recommended. The acquired CBCT scan was used for implant site assessment

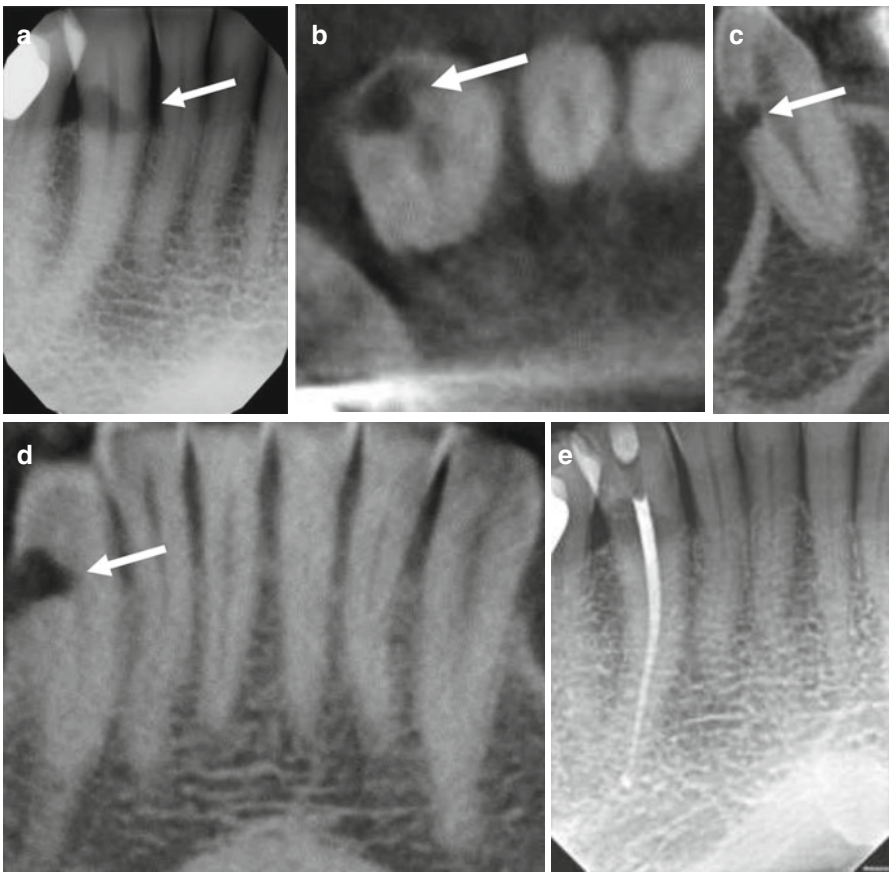

Fig. 7.4 External resorption may be inconsequential or cause significant damage to the tooth and supporting structures if the resorptive process continues. (**a**) Periapical radiograph shows an irregular, well-defined area of low density (*arrow*) in the CEJ area of the mandibular right canine; features consistent with external cervical resorption. The canal space appears to be unaffected. CBCT images of the (**b**) axial reformation, (**c**) cross-sectional reformation, and (**d**) cropped panoramic reformation, and (**d**) sagittal reformation demonstrate the full extent of this feature (*arrows*) affecting the facial dentin. The lamina dura appears intact. Orthograde endodontic treatment was performed (**e**) and restored after crown lengthening using an apically positioned flap and ostectomy

Fig. 7.5 A 39-year-old male presented with a history of trauma to the maxillary anterior region. (**a**) Periapical radiograph of the maxillary right central incisor reveals an approximately 3–4 mm long, 1 mm diameter, oval, well-defined area of low density centered mesiodistally, with calcification of the remaining pulp space (*arrow*); features consistent with internal resorption and canal calcification. CBCT images of the (**b**) sagittal reformation, (**c**) axial reformation, and (**d**) cross-sectional reformation show the location of the resorptive lesion (*arrows*) and its relationship to the calcified canal. The resorptive lesion was non-perforating, positioned facially, and separate from the pulp space. An area of low density extending facially to the junction of the middle and apical thirds was appreciated. Conventional nonsurgical endodontic treatment was performed (**e**) and the resorptive defect was incorporated into the three dimensional obturation

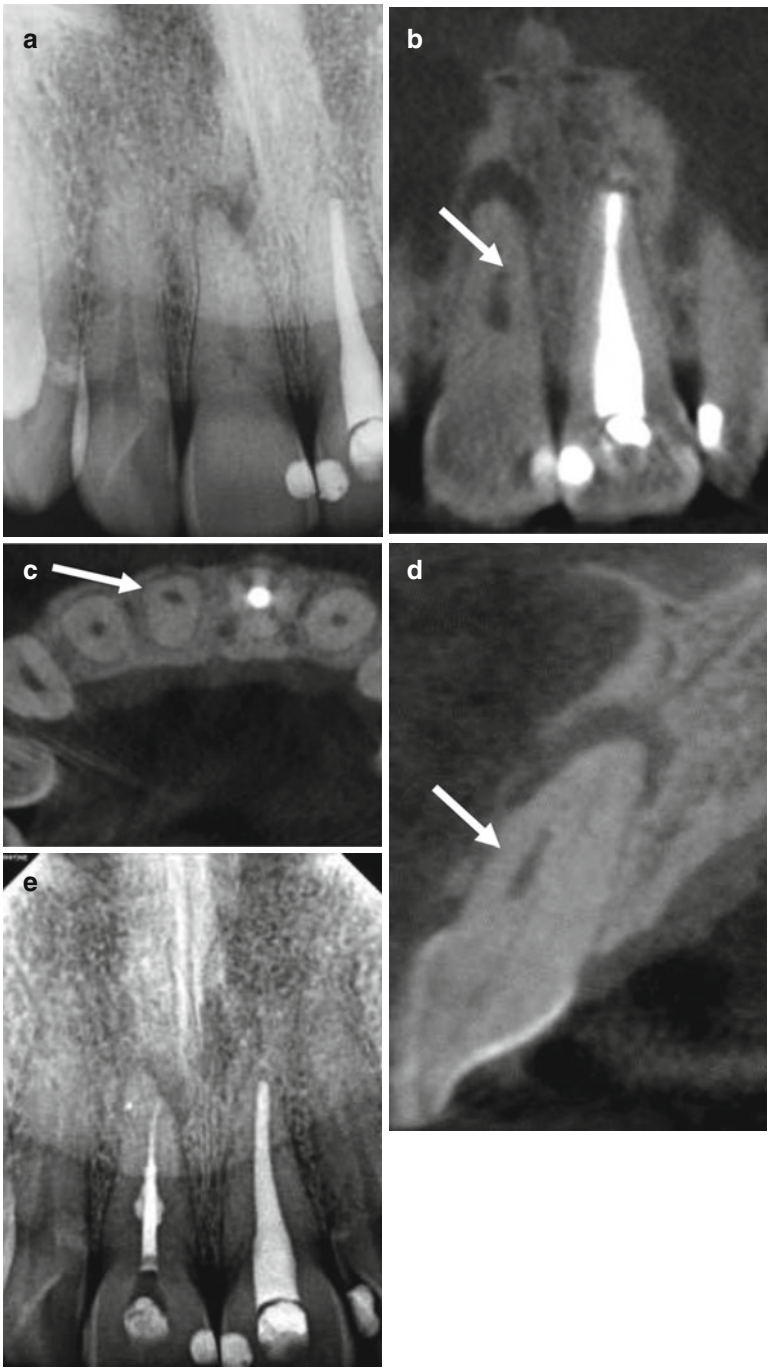

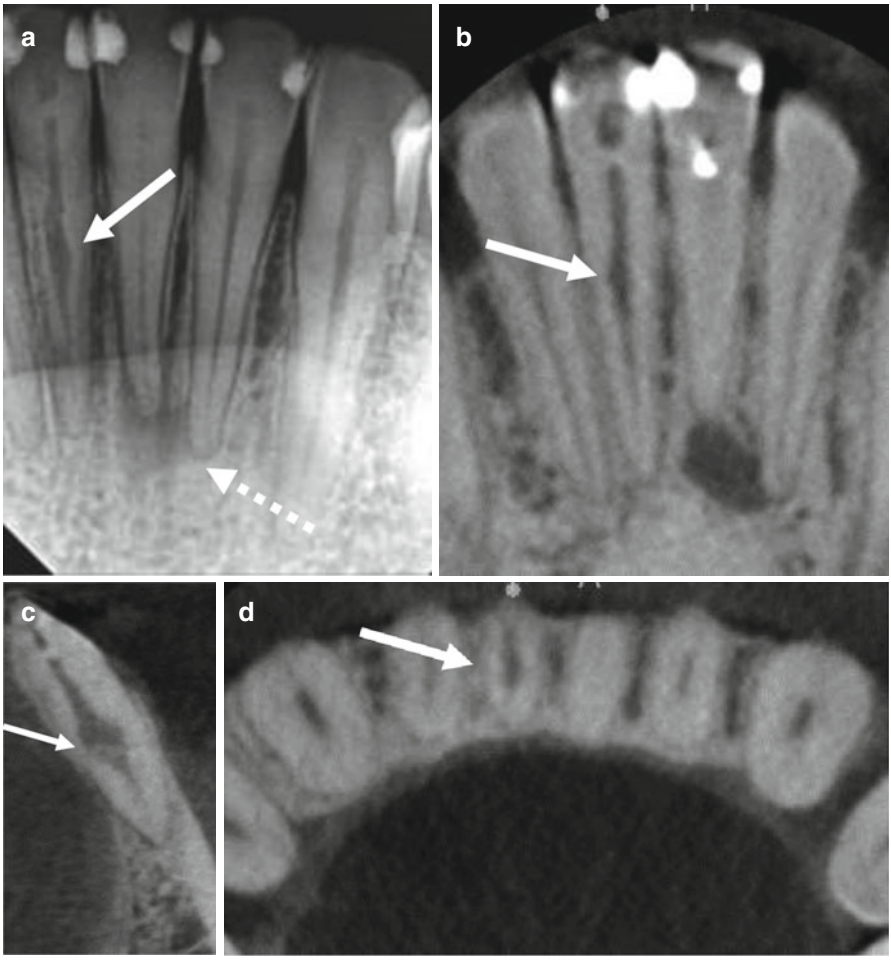

Fig. 7.6 Clinically detectible internal root resorption is considered a rare occurrence. A 33-year-old female presented for evaluation and possible treatment with a history of trauma to the mandibular anterior region. (**a**) Periapical radiograph shows a centrally located, well-defined, irregular area of low density (*arrow*) in the mandibular right central incisor; features consistent with internal resorption. The mandibular left central incisor shows a well-defined, uniformly radiolucent area of low density centered over a point at the apex; features consistent with pulp necrosis and calcification of the canal. CBCT images of the (**b**) coronal reformation (**c**) cross-sectional reformation, and (**d**) axial reformation demonstrate the same low-density area (*arrows*) of the mandibular right central incisor with greater dentinal penetration in the faciolingual dimension. Note the severe calcification of the mandibular left central incisor. Orthograde endodontic treatment was recommended for both teeth. The CBCT scan provided useful guidance to localize the calcified canal

contrast, external resorption usually presents with an irregular radiolucency and intact root canal [29]. Internal root resorption has been described as either apical or intraradicular based on the location of the lesion [30].

The prevalence of apical inflammatory root resorption associated with periapical lesions has been reported to range from 61.4 to 100 % [31, 32]. In 88 roots

examined by Estrela et al. in 14 patients, apical inflammatory root resorption associated with periapical lesions was visible using CBCT (0.20 mm voxel size) in at least half of the cases evaluated [31]. After extraction, SEM assessment of the same roots showed resorptive features in 61.4 % of the cases examined. In other studies, periapical images showed poor results. In a study to determine the reliability of single periapical radiographs in the diagnosis of apical inflammatory root resorption using histology as ground truth, only 19 % of the cases examined showed radiographic lesions [33].

Resorption in the crown portion of the tooth may result in a pink-colored area. In the presence of mild inflammation, irregular dentin enlargement of the pulp space may be replaced with metaplastic hard tissue. Internal root resorption may be confused with other forms of root resorption, possibly resulting in treatment errors [34]. Intraradicular internal root resorption is characterized by mild inflammation accompanied by replacement with metaplastic hard tissue similar to the bone. These teeth show radiographic evidence of irregular enlargement of the pulp space, with features consistent with the deposition of bone-like tissue. Nonsurgical root canal treatment is considered the treatment of choice for internal resorption without an external component [35].

In simulated internal root resorption conducted under laboratory conditions, Kamburoglu and Kursun [13] found some limitations on the sensitivity and specificity for the CBCT systems tested. CBCT assessments can provide the true location and extent of the lesion [36].

Conclusion

The use of CBCT to show the true nature of external and internal resorption relies on the ability to examine the region of interest in any plane without distortion and eliminate artifacts associated with conventional radiography. Careful use of CBCT is advocated.

Note: CBCT data for all figures were acquired on a CS 9000 3D at 0.076 mm resolution and reformatted using Carestream Dental Imaging Software v.3.5.7 (Carestream Dental, Atlanta, GA, USA).

References

1. Bakland LK. Root resorption. Dent Clin N Am. 1992;36:491–507.
2. Estrela C, Bueno MR, Gonc AH, et al. Method to evaluate inflammatory root resorption by using cone beam computed tomography. J Endod. 2009;35:1491–7.
3. Hülsmann M, Schäfer E. Problems in endodontics; etiology, diagnosis and treatment. London: Quintessence; 2009. p. 421–34.
4. Tronstad L. Root resorption: etiology, terminology and clinical manifestations. Endod Dent Traumatol. 1988;4:241–52.
5. Fuss Z, Tsesis I, Lin S. Root resorption – diagnosis, classification and treatment choices based on stimulation factors. Dent Traumatol. 2003;19(4):175–82.
6. Patel S, Kanagasingam S, Pitt Ford T. External cervical resorption: a review. J Endod. 2009;35:616.
7. Chapnick L. External root resorption: an experimental radiographic evaluation. Oral Surg Oral Med Oral Pathol. 1989;67:578–82.

8. Nance RS, Tyndall D, Levin LG, Trope M. Diagnosis of external root resorption using TACT (tuned-aperture computed tomography). Endod Dent Traumatol. 2000;16:24–8.
9. Patel S, Dawood A. The use of cone beam computed tomography in the management of external cervical resorption lesions. Int Endod J. 2007;40:730–7.
10. Mota de Almeida FJ, Knutsson K, Flygare L. The impact of cone beam computed tomography on the choice of endodontic diagnosis. Int Endod J. 2015;48:564–72.
11. Ee J, Fayad MI, Johnson BR. Comparison of endodontic diagnosis and treatment planning decisions using cone-beam volumetric tomography versus periapical radiography. J Endod. 2014;40:910–6.
12. Liedke GS, da Silveira HE, da Silveira HL, Dutra V, de Figueiredo JA. Influence of voxel size in the diagnostic ability of cone beam tomography to evaluate simulated external root resorption. J Endod. 2009;35:233–5.
13. Kamburoğlu K, Kursun S. A comparison of the diagnostic accuracy of CBCT images of different voxel resolutions used to detect simulated small internal resorption cavities. Int Endod J. 2010;43:798—807.
14. Ponder SN, Benavides E, Kapila S, Hatch NE. Quantification of external root resorption by low- vs high-resolution cone-beam computed tomography and periapical radiography: a volumetric and linear analysis. Am J Orthod Dentofacial Orthop. 2013;143(1):77–91.
15. Daalili A, Taramsari M, Mehr SZ, Salamat F. Diagnostic value of two modes of cone-beam computed tomography in evaluation of simulated external root resorption: an in vitro study. Imaging Sci Dent. 2012;42:19–24.
16. 1990 Recommendations of the International Commission on Radiological Protection. Ann ICRP. 1991;21(1–3):1–201.
17. Patel S, Pitt FT. Is the resorption external or internal? Dent Update. 2007;34:218–29.
18. Hahn W, Fricke-Zech S, Fricke J, et al. Detection and size differentiation of simulated tooth root defects using flat-panel volume computerized tomography (fpVCT). Oral Surg Oral Med Oral Path Oral Radiol Endod. 2009;107:272–8.
19. Crona-Larsson G, Bjarnasan S, Norén JG. Effect of luxation injuries on permanent teeth. Endod Dent Traumatol. 1991;7:199–206.
20. Shokri A, Mortazavi H, Salemi F, et al. Diagnosis of simulated external root resorption using conventional intraoral film radiography, CCD, PSP and CBCT: a comparison study. Biomed J. 2013;36:18–22.
21. Silveira HLD, Silveira HED, Liedke GS, Lermen CA, Santos RB, Figueiredo JAP. Diagnostic ability of computed tomography to evaluate external root resorption in vitro. Dentomaxillofac Radiol. 2007;36:393–6.
22. Durack C, Patel S, Davies J, Wilson R, Mannocci F. Diagnostic accuracy of small volume cone beam computed tomography and intraoral periapical radiography for the detection of simulated external inflammatory root resorption. Int Endod J. 2011;44:136–47.
23. Kim E, Kim KD, Roh BD, Cho YS, Lee SJ. Computed tomography as a diagnostic aid for extracanal invasive resorption. J Endod. 2003;29(7):463–5.
24. Walker L, Enciso R, Mah J. Three-dimensional localization of maxillary canines with cone-beam computed tomography. Am J Orthod Dentofacial Orthop. 2005;128(4):418–23.
25. Lund H, Grondahl K, Hansen K, Grondahl HG. Apical root resorption during orthodontic treatment. Angle Orthod. 2012;82:480–7.
26. Heithersay GS. Clinical, radiologic and histopathologic features of invasive cervical resorption. Quintessence Int. 1999;30:27–37.
27. Liang H, Burkes EJ, Frederiksen NL. Multiple idiopathic cervical root resorption: systematic review and report of four cases. Dentomaxillofac Radiol. 2003;32:150–5.
28. Haapasalo M, Endal U. Internal inflammatory root resorption: the unknown resorption of the tooth. Endod Topics. 2006;14:60–79.
29. Cohenca N, Simon JH, Mathur A, Malfaz JM. Clinical indications for digital imaging in dento-alveolar trauma—part 2: root resorption. Dent Traumatol. 2007;23:105–13.
30. Levin L, Trope M. Root resorption. In: Hargreaves KM, Goodis HE, editors. Seltzer and Bender's dental pulp. Chicago: Quintessence Publishing Co Inc; 2002. p. 425–48.

31. Estrela C, Guedes OA, Rabelo LE, et al. Detection of inflammatory root resorption associated with periapical lesion using different methods. Braz Dent J. 2014;25:404–8.
32. Delzangles B. Apical periodontitis and resorption of the root canal wall. Endod Dent Traumatol. 1988;4:273–7.
33. Laux M, Abbott PV, Pajarola G, Nair PNR. Apical inflammatory root resorption: a correlative radiographic and histological assessment. Int Endod J. 2000;33:483–93.
34. Frank AL. External-internal progressive resorption and its nonsurgical correction. J Endod. 1981;7:473–6.
35. Ne RF, Witherspoon DE, Gutmann JL. Tooth resorption. Quintessence Int. 1999;30:9–25.
36. Patel S, Dawood A, Wilson R, et al. The detection and management of root resorption lesions using intraoral radiography and cone beam computed tomography – an in vivo investigation. Int Endod J. 2009;42:831–8.

AAE and AAOMR Joint Position Statement

M. Fayad, B.R. Johnson (eds.), *3D Imaging in Endodontics*,
DOI 10.1007/978-3-319-31466-2

AAE and AAOMR Joint Position Statement

The following statement was prepared by the Special Committee to Revise the Joint American Association of Endodontists/American Academy of Oral and Maxillofacial Radiology Position on Cone Beam-Computed Tomography, and approved by the AAE Board of Directors and AAOMR Executive Council in May 2015. AAE members may photocopy this position statement for distribution to patients or referring dentists.

Use of Cone Beam-Computed Tomography in Endodontics 2015 Update

INTRODUCTION

This updated joint position statement of the American Association of Endodontists and the American Academy of Oral and Maxillofacial Radiology is intended to provide scientifically based guidance to clinicians regarding the use of cone beam-computed tomography in endodontic treatment and reflects new developments since the 2010 statement (1). The guidance in this statement is not intended to substitute for a clinician's independent judgment in light of the conditions and needs of a specific patient.

Endodontic disease adversely affects quality of life and can produce significant morbidity in afflicted patients. Radiography is essential for the successful diagnosis of odontogenic and nonodontogenic pathoses, treatment of the root canal systems of a compromised tooth, biomechanical instrumentation, evaluation of final canal obturation and assessment of healing.

Until recently, radiographic assessments in endodontic treatment were limited to intraoral and panoramic radiography. These radiographic technologies provide two-dimensional representations of three-dimensional anatomic structures. If any element of the geometric configuration is compromised, the image may demonstrate errors (2). In more complex cases, radiographic projections with different beam angulations can allow parallax localization. However, complex anatomy and surrounding structures can render interpretation of planar images difficult.

The advent of CBCT has made it possible to visualize the dentition, the maxillofacial skeleton, and the relationship of anatomic structures in three dimensions (3). CBCT, as with any technology, has known limitations, including a possible higher radiation dose to the patient. Other limitations include potential for artifact generation, high levels of scatter and noise and variations in dose distribution within a volume of interest (4).

CBCT should be used only when the patient's history and a clinical examination demonstrate that the benefits to the patient outweigh the potential risks. CBCT should not be used routinely for endodontic diagnosis or for screening purposes in the absence of clinical signs and symptoms. Clinicians should use CBCT only when the need for imaging cannot be met by lower-dose two-dimensional radiography.

Volume Size(s)/Field of View

There are numerous CBCT equipment manufacturers, and several models are available. In general, CBCT is categorized into large, medium and limited-volume units based on the size of their "field of view." The size of the FOV describes the scan volume of CBCT machines. That volume determines the extent of anatomy included. It is dependent on the detector size and shape, beam projection geometry and the ability to collimate the beam. To the extent practical, FOV should only slightly exceed the dimensions of the anatomy of interest.

Generally, the smaller the FOV, the lower the dose associated with the study. Beam collimation limits the radiation exposure to the region of interest and helps ensure that an optimal FOV can be selected based on disease presentation.

Smaller scan volumes generally produce higher-resolution images. Because endodontics relies on detecting small alterations such as disruptions in the periodontal ligament space, optimal resolution should be sought (5).

The principal limitations of large FOV CBCT imaging are the size of the field irradiated and the reduced resolution compared to intraoral radiographs and limited-volume CBCT units with inherent small voxel sizes (5). The smaller the voxel size, the higher the spatial resolution. Moreover, the overall scatter generated is reduced due to the limited size of the FOV. Optimization of the exposure protocols keeps doses to a minimum without compromising image quality. If a low-dose protocol can be used for a diagnostic task that requires lower resolution, it should be employed, absent strong indications to the contrary.

In endodontics, the area of interest is limited and determined prior to imaging. For most endodontic applications, limited FOV CBCT is preferred to medium or large FOV CBCT because there is less radiation dose to the patient, higher spatial resolution and shorter volumes to be interpreted.

Dose Considerations

Selection of the most appropriate imaging protocol for the diagnostic task must be consistent with the ALARA principles that every effort should be made to reduce the effective radiation dose to the patient "as low as reasonably achievable." Because radiation dose for a CBCT study is higher than that for an intraoral radiograph, clinicians must consider overall radiation dose over time. For example, will acquiring a CBCT study now eliminate the need for additional imaging procedures in the future? It is recommended to use the smallest possible FOV, the smallest voxel size, the lowest mA setting (depending on the patient's size) and the shortest exposure time in conjunction with a pulsed exposure-mode of acquisition.

If extension of pathoses beyond the area surrounding the tooth apices or a multifocal lesion with possible systemic etiology is suspected, and/or a nonendodontic cause for devitalization of the tooth is established clinically, appropriate larger field of view protocols may be employed on a case-by-case basis.

There is a special concern with overexposure of children (up to and including 18 years of age) to radiation, especially with the increased use of CT scans in medicine. The AAE and the AAOMR support the Image Gently Campaign led by the Alliance for Radiation Safety in Pediatric Imaging. The goal of the campaign is "to change practice; to raise awareness of the opportunities to lower radiation dose in the imaging of children." Information on use of CT is available at www.imagegently.org/Procedures/ComputedTomography.aspx.

Interpretation

If a clinician has a question regarding image interpretation, it should be referred to an oral and maxillofacial radiologist (6).

RECOMMENDATIONS

The following recommendations are for limited FOV CBCT scans.

Diagnosis

Endodontic diagnosis is dependent upon thorough evaluation of the patient's chief complaint, history and clinical and radiographic examination. Preoperative radiographs are an essential part of the diagnostic phase of endodontic therapy. Accurate diagnostic imaging supports the clinical diagnosis.

Recommendation 1: Intraoral radiographs should be considered the imaging modality of choice in the evaluation of the endodontic patient.

Recommendation 2: Limited FOV CBCT should be considered the imaging modality of choice for diagnosis in patients who present with contradictory or nonspecific clinical signs and symptoms associated with untreated or previously endodontically treated teeth.

Rationale:

- In some cases, the clinical and planar radiographic examinations are inconclusive. Inability to confidently determine the etiology of endodontic pathosis may be attributed to limitations in both clinical vitality testing and intraoral radiographs to detect odontogenic pathoses. CBCT imaging has the ability to detect periapical pathosis before it is apparent on 2-D radiographs (7).
- Preoperative factors such as the presence and true size of a periapical lesion play an important role in endodontic treatment outcome. Success, when measured by radiographic criteria, is higher when teeth are endodontically treated before radiographic signs of periapical disease are detected (8).
- Previous findings have been validated in clinical studies in which primary endodontic disease detected with intraoral radiographs and CBCT was 20% and 48%, respectively. Several clinical studies had similar findings, although with slightly different percentages (9,10). *Ex vivo* experiments in which simulated periapical lesions were created yielded similar results (11,12). Results of *in vivo* animal studies, using histologic assessments as the gold standard, also showed similar results observed in human clinical and *ex vivo* studies (13).
- Persistent intraoral pain following root canal therapy often presents a diagnostic challenge. An example is persistent dentoalveolar pain also known as atypical odontalgia (14). The diagnostic yield of conventional intraoral radiographs and CBCT scans was evaluated in the differentiation between patients presenting with suspected atypical odontalgia versus symptomatic apical periodontitis, without radiographic evidence of periapical bone destruction (15). CBCT imaging detected 17% more teeth with periapical bone loss than conventional radiography.

Initial Treatment

Preoperative

Recommendation 3: Limited FOV CBCT should be considered the imaging modality of choice for initial treatment of teeth with the potential for extra canals and suspected complex morphology, such as mandibular anterior teeth, and maxillary and mandibular premolars and molars, and dental anomalies.

Intraoperative

Recommendation 4: If a preoperative CBCT has not been taken, limited FOV CBCT should be considered as the imaging modality of choice for intra-appointment identification and localization of calcified canals.

Postoperative

Recommendation 5: Intraoral radiographs should be considered the imaging modality of choice for immediate postoperative imaging.

Rationale:

- Anatomical variations exist among different types of teeth. The success of nonsurgical root canal therapy depends on identification of canals, cleaning, shaping and obturation of root canal systems, as well as quality of the final restoration.
- 2-D imaging does not consistently reveal the actual number of roots and canals. In studies, data acquired by CBCT showed a very strong correlation between sectioning and histologic examination (16,17).
- In a 2013 study, CBCT showed higher mean values of specificity and sensitivity when compared to intraoral radiographic assessments in the detection of the MB2 canal (18).

Nonsurgical Retreatment

Recommendation 6: Limited FOV CBCT should be considered the imaging modality of choice if clinical examination and 2-D intraoral radiography are inconclusive in the detection of vertical root fracture.

Rationale:

- In nonsurgical retreatment, the presence of a vertical root fracture significantly decreases prognosis. In the majority of cases, the indication of a vertical root fracture is more often due to the specific pattern of bone loss and periodontal ligament space enlargement than direct visualization of the fracture. CBCT may be recommended for the diagnosis of vertical root fracture in unrestored teeth when clinical signs and symptoms exist.
- Higher sensitivity and specificity were observed in a clinical study where the definitive diagnosis of vertical root fracture was confirmed at the time of surgery to validate CBCT findings, with sensitivity being 88% and specificity 75% (19). Several case series studies have concluded that CBCT is a useful tool for the diagnosis of vertical root fractures. *In vivo* and laboratory studies (20, 21) evaluating CBCT in the detection of vertical root fractures agreed that sensitivity, specificity, and accuracy of CBCT were generally higher and reproducible. The detection of fractures was significantly higher for all CBCT systems when compared to intraoral radiographs. However, these results should be interpreted with caution because detection of vertical root fracture is dependent on the size of the fracture, presence of artifacts caused by obturation materials and posts and the spatial resolution of the CBCT.

Recommendation 7: Limited FOV CBCT should be the imaging modality of choice when evaluating the nonhealing of previous endodontic treatment to help determine the need for further treatment, such as nonsurgical, surgical or extraction.

Recommendation 8: Limited FOV CBCT should be the imaging modality of choice for nonsurgical retreatment to assess endodontic treatment complications, such as overextended root canal obturation material, separated endodontic instruments, and localization of perforations.

Rationale:

- It is important to evaluate the factors that impact the outcome of root canal treatment. The outcome predictors identified with periapical radiographs and CBCT were evaluated by Liang et al. (22) The results showed that periapical radiographs detected periapical lesions in 18 roots (12%) as compared to 37 on CBCT scans (25%). Eighty percent of apparently short root fillings based on intraoral radiographs images appeared flush on CBCT. Treatment outcome, length and density of root fillings and outcome predictors determined by CBCT showed different values when compared with intraoral radiographs.
- Accurate treatment planning is an essential part of endodontic retreatment. Incorrect, delayed or inadequate endodontic diagnosis and treatment planning places the patient at risk and may result in unnecessary treatment. Treatment planning decisions using CBCT versus intraoral radiographs were compared to the gold standard diagnosis (23). An accurate diagnosis was reached in 36%-40% of the cases with intraoral radiographs compared to 76%-83% with CBCT. A high level of misdiagnosis was noted in invasive cervical resorption and vertical root fracture. In this study, the examiners altered their treatment plan after reviewing the CBCT in 56%-62.2% of the cases, thus indicating the significant influence of CBCT.

Surgical Retreatment

Recommendation 9: Limited FOV CBCT should be considered as the imaging modality of choice for presurgical treatment planning to localize root apex/apices and to evaluate the proximity to adjacent anatomical structures.

Rationale:

The use of CBCT has been recommended for treatment planning of endodontic surgery (24, 25). CBCT visualization of the true extent of periapical lesions and their proximity to important vital structures and anatomical landmarks is superior to that of periapical radiographs.

Special Conditions

Implant placement

Recommendation 10: Limited FOV CBCT should be considered as the imaging modality of choice for surgical placement of implants (26).

Traumatic injuries

Recommendation 11: Limited FOV CBCT should be considered the imaging modality of choice for diagnosis and management of limited dento-alveolar trauma, root fractures, luxation, and/or displacement of teeth and localized alveolar fractures, in the absence of other maxillofacial or soft tissue injury that may require other advanced imaging modalities (27).

Resorptive defects

Recommendation 12: Limited FOV CBCT is the imaging modality of choice in the localization and differentiation of external and internal resorptive defects and the determination of appropriate treatment and prognosis (28, 29).

REFERENCES

1. American Association of Endodontists;American Academy of Oral and Maxillofacial Radiology. Use of cone-beam computed tomography in endodontics Joint Position Statement of the American Association of Endodontists and the American Academy of Oral and Maxillofacial Radiology. Oral Surg Oral Med Oral Pathol Oral Radiol Endod. 2011;111(2):234-7.
2. Grondahl HG, Huumonen S. Radiographic manifestations of periapical inflammatory lesions. Endodontic Topics. 2004;8:55-67.
3. Patel S, Durack C, Abella F, Shemesh H, Roig M, Lemberg K. Cone beam computed tomography in Endodontics — a review. Int Endod J 2015;48:3-15.
4. Suomalainen A, Pakbaznejad Esmaeili E, Robinson S. Dentomaxillofacial imaging with panoramic views and cone beam CT. Insights imaging 2015;6:1-16.
5. Venskutonis T, Plotino G, Juodzbalys G, Mickevicienè L. The importance of cone-beam computed tomography in the management of endodontic problems: a review of the literature. J Endod 2014;40(12):1895-901.
6. Carter L, Farman AG, Geist J, Scarfe WC, Angelopoulos C, Nair MK, Hildebolt CF, Tyndall D, Shrout M. American Academy of Oral and Maxillofacial Radiology executive opinion statement on performing and interpreting diagnostic cone beam computed tomography. Oral Surg Oral Med Oral Pathol Oral Radiol Endod 2008;106(4):561-2.
7. De Paula-Silva FW, Wu MK, Leonardo MR, da Silva LA, Wesselink PR. Accuracy of periapical radiography and cone-beam computed tomography scans in diagnosing apical periodontitis using histopathological findings as a gold standard. J Endod 2009;35(7):1009-12.
8. Friedman S. Prognosis of initial endodontic therapy. Endodontic Topics 2002;2:59-98.
9. Patel S, Wilson R, Dawood A, Mannocci F. The Detection of periapical pathosis using periapical radiography and cone beam computed tomography — part 1: preoperative status. Int Endod J 2012;8:702-10.
10. Abella F, Patel S, Duran-Sindreu F, Mercad M, Bueno R, Roig M. (2012a) Evaluating the periapical status of teeth with irreversible pulpitis by using cone-beam computed tomography scanning and periapical radiographs. J Endod 2012;38(12):1588-91.
11. Cheung G, Wei L, MvGrath C. (2013) Agreement between periapical radiographs and cone-beam computed tomography for assessment of periapical status of root filled molar teeth. Int Endod J 2013;46(10):889-95.
12. Sogur E, Grondahl H, Bakst G, Mert A. Does a combination of two radiographs increase accuracy in detecting acid-induced periapical lesions and does it approach the accuracy of cone-beam computed tomography scanning. J Endod 2012;38(2):131-6.
13. Patel S, Dawood A, Mannocci F, Wilson R, Pitt Ford T. (2009a) Detection of periapical bone defects in human jaws using cone beam computed tomography and intraoral radiography. Int Endod J 2009;42(6):507-15.
14. Nixdorf D, Moana-Filho E, Persistent dento-alveolar pain disorder (PDAP): Working towards a better understanding. Rev Pain. 2011;5(4):18-27.
15. Pigg M, List T, Petersson K, Lindh C, Petersson A. (2011) Diagnostic yield of conventional radiographic and cone-beam computed tomographic images in patients with atypical odontalgia. Int Endod J 2011;44(12):1365-2591.
16. Blattner TC, Goerge N, Lee CC, Kumar V, Yelton CGJ. (2010) Efficacy of CBCT as a modality to accurately identify the presence of second mesiobuccal canals in maxillary first and second molars: a pilot study. J Endod 2012;36(5):867-70.
17. Michetti J, Maret D, Mallet J-P, Diemer F. Validation of cone beam computed tomography as a tool to explore root canal anatomy. J Endod 2010;36(7):1187-90.
18. Vizzotto MB, Silveira PF, Arús NA, Montagner F, Gomes BP, Da Silveira HE. (2013) CBCT for the assessment of second mesiobuccal (MB2) canals in maxillary molar teeth: effect of voxel size and presence of root filling. Int Endod J 2013;46(9):870-6.
19. Edlund M, Nair MK, Nair UP. Detection of vertical root fractures by using cone-beam computed tomography: a clinical study. J Endod 2011;37(6):768–72.
20. Metska ME, Aartman IH, Wesselink PR, Özok AR. (2012) Detection of vertical root fracture in vivo in endodontically treated teeth by cone-beam computed tomography scans. J Endod 2012;38(10):1344-7.
21. Brady E, Mannocci F, Wilson R, Brown J, Patel S. (2014) A comparison of CBCT and periapical radiography for the detection of vertical root fractures in non-endodontically treated teeth. Int Endod J 2014;47(8):735-46.

22. Liang H, Li Gang, Wesselink P, WuM. Endodontic outcome predictors identified with periapical radiographs and cone-beam computed tomography scans. J Endod 2011;37(3):326-31.
23. Ee J, Fayad I M, Johnson B. Comparison of endodontic diagnosis and treatment planning decisions using cone-beam volumetric tomography versus periapical radiography. J Endod 2014;40(7):910-6.
24. Venskutonis T, Plotino G, Tocci L, Gambarini G, Maminskas J, Juodzbalys G. Periapical and Endodontic status scale based on periapical bone lesions and endodontic treatment quality evaluation using cone-beam computed tomography. J Endod 2015;41(2):190-6.
25. Low KM, Dula K, Bürgin W, Arx T. Comparison of periapical radiography and limited cone-beam tomography in posterior maxillary teeth referred for apical surgery. J Endod 2008;34(5):557-62.
26. Tyndall D, Price J, Tetradis S, Ganz S, Hildebolt C, Scarfe W. Position statement of the American Academy of Oral and Maxillofacial Radiology on selection criteria for the use of radiology in dental implantology with emphasis on cone beam computed tomography. Oral Surg Oral Med Oral Pathol Oral Radiol 2012June;113(6):817-26.
27. May JJ, Cohenca N, Peters OA. Contemporary management of horizontal root fractures to the permanent dentition: diagnosis, radiologic assessment to include cone-beam computed tomography. Pediatric Dentistry 2013;35:120–4.
28. Estrela C, Bueno MR, De Alencar AH, Mattar R, Valladares Neto J, Azevedo BC, De Araújo Estrela CR. Method to evaluate Inflammatory Root Resorption by using Cone Beam computed tomography. J Endod 2009;35(11):1491-7.
29. Durack C, Patel S, Davies J, Wilson R, Mannocci F. Diagnostic accuracy of small volume cone beam computed tomography and intraoral periapical radiography for the detection of simulated external inflammatory root resorption. Int Endod J.2011Feb;44(2):136-47.

Thank you to the Special Committee to Revise the Joint AAE/AAOMR Position Statement on Cone Beam-Computed Tomography:

Mohamed I. Fayad, Co-Chair, AAE
Martin D. Levin, AAE
Richard A. Rubinstein, AAE
Craig S. Hirschberg, AAE Board Liaison
Madhu K. Nair, Co-Chair, AAOMR
Erika Benavides, AAOMR
Sevin Barghan, AAOMR
Axel Ruprecht, AAOMR